

**Transport of Microplastics in Shore Substrates: Roles of Polymer  
Characteristics and Environmental Processes**

Qi Feng

A Thesis  
In the Department  
of  
Building, Civil, and Environmental Engineering

Presented in Partial Fulfillment of the Requirements  
For the Degree of  
Doctor of Philosophy (Civil Engineering) at  
Concordia University  
Montréal, Québec, Canada

May 2023

©Qi Feng, 2023

**CONCORDIA UNIVERSITY**  
**SCHOOL OF GRADUATE STUDIES**

This is to certify that the thesis

prepared By: Qi Feng

Entitled: Transport of microplastics in shore substrates: roles of polymer characteristics and environmental processes

and submitted in partial fulfillment of the requirements for the degree of

DOCTOR OF PHILOSOPHY (Civil Engineering)

complies with the regulations of the University and meets the accepted standards with respect to originality and quality.

Signed by the final examining committee:

\_\_\_\_\_ Chair  
Dr. Rabin Raut

\_\_\_\_\_ External Examiner  
Dr. Miriam Diamond

\_\_\_\_\_ Examiner  
Dr. S. Samuel Li

\_\_\_\_\_ Examiner  
Dr. Catherine Mulligan

\_\_\_\_\_ Examiner  
Dr. Xia Li

\_\_\_\_\_ Thesis Co-supervisor  
Dr. Zhi Chen

\_\_\_\_\_ Thesis Supervisor  
Dr. Chunjiang An

Approved by \_\_\_\_\_  
Dr. Chunjiang An, Graduate Program Director

July 21, 2023 \_\_\_\_\_  
Dr. Mourad Debbabi, Dean

Gina Cody School of Engineering and Computer Science

## **Abstract**

### **Transport of microplastics in shore substrates: roles of polymer characteristics and environmental processes**

**Qi Feng, Ph.D.**

**Concordia University, 2023**

The presence of plastic fragments in the environment is a growing global concern. The coast is particularly vulnerable to microplastic (MP) pollution. However, field experiments are less capable of disentangling the complex interplay of various factors. Therefore, this study aims to investigate the transport of MPs in porous media combined with typical coastal processes. Firstly, a weathering experiment was conducted to comprehensively reveal the changes in MPs in the environment. The results indicated that seawater aging mainly affected the physical properties of MPs, increasing its surface pores and hydrophilicity. Ultraviolet (UV) aging significantly increased its hydrophilicity and crystallinity and introduced oxygen-containing functional groups onto MPs.

Then, the detachment of MPs from porous media under various water content conditions combined with flow patterns was studied. For both the wet and dry conditions, the increase in flow rates decreased the detachment of hydrophobic polyethylene (PE) of two sizes and hydrophilic polymethylmethacrylate (PMMA). Transient flows with varied flow rates and ionic strength led to flow peaks and more MP detachment compared to steady flow. Furthermore, substrate drying significantly impeded the detachment of MPs compared to wet conditions irrespective of the flow regimes. The release of MPs decreased pronouncedly with prolonged air

drying duration of the column since drying heightens the energy barrier for MPs to detach.

Tide is a typical coastal process that has profound influence on many biological and abiotic processes. In the following study, the effects of tidal cycles on transport of MPs (4–6  $\mu\text{m}$  PE1; 125  $\mu\text{m}$  PE2; and 5–6  $\mu\text{m}$  polytetrafluoroethylene, PFTE) in porous media were systemically investigated. Smaller substrate sizes exhibited higher retention percentages compared to those of larger substrate sizes under different tidal cycles. In terms of the size of MPs, a larger size (same density) was found to result in enhanced retention of MPs in the column. As the number of tidal cycles increased, although the transport of MPs from the substrate to the water phase was enhanced, less hydrophobic MPs was washed out more with the change in water level. The results implied that MPs with size far smaller than the substrate tend to end up in the open ocean.

To expand our understanding of MP mobilization by tidal movement, the influence of dynamic fluctuations of capillary fringe on the transport of MPs was explored. An increase in the cycles of water table fluctuations enhanced the MPs transport from substrate to the water below. More MPs with larger size were retained in substrate compared to the smaller one. The retention percentages of both PE1 and PTFE in column increased with the elevated ionic strength and the decrease of fluctuation velocity. The results highlight that capillary fringe fluctuation can serve as a pathway to relocate MPs to the tidal aquifer.

Finally, a mesoscale tank experiment was conducted to simulate the infiltration and resuspension of MPs in a slope substrate under the influence of repeated tidal forces. The results imply that large, high-density, and less flat particles tend to be distributed in the lower tidal zone and deeper substrate layers. The obtained observation contributes valuable insights into the behavior, transport, and redistribution of MPs in complex environmental systems. The findings enhance our understanding of MP fate and distribution, assisting in the development of strategies for mitigating MP pollution and managing its impact in coastal areas.

## Acknowledgements

Nearly four years ago, I embarked my doctoral journey and joined Dr. An' group. Back then, the year 2023 seemed so distant, but now it is approaching to the end. It has been an incredible and unforgettable journey because I was lucky to collaborate with a group of inspirational people and work on interesting scientific questions. As this remarkable chapter comes to a close, I would like to express my sincere gratitude for people who have inspired me, helped me, and warm me.

First of all, I would like to extend my heartfelt gratitude to my supervisor, Chunjiang An, for giving me the opportunity to join his group and for his belief in my abilities. He is always supportive in the plan I proposed with tireless efforts. He always respects my ideas and efforts. During these four year, beyond the realm of knowledge and research methodologies, observing his manners and attitudes towards his work, colleagues, and students has left an indelible mark on me. More importantly, I learned from him for how he faces difficulties and how he helps me to transform challenges into opportunities. These lessons have not only shaped my academic journey but have also become invaluable treasures that will guide me throughout my life.

I also want to express my heartily gratitude to my supervisor, Zhi Chen. Throughout my doctoral journey, his unwavering support and encouragement have been instrumental in my growth and development. He is always open for discussion and support me to explore many interesting areas. His dedication to imparting knowledge and developing a passion for learning has left a profound impact on me. I have learned invaluable lessons from observing his approach to teaching and his enthusiasm for sharing knowledge with his students.

Also many big thanks to my talented groupmates and lab mates, Mengfan Cai, Zhikun Chen, Xuelin Tian, Huifang Bi, Liuqing Yang, Rezvan Iravani, Azar Vahabisani, Zheng Wang, Zhaonian Qu, Xinya Chen, Shuyan Wan, Xiaohan Yang, Siyuan Zhou, Linxiang Lyu, He Peng, Jiyao Sui, Xinyu Xu who always inspire me and help me to improve my experiment and design. Their support and friendship have kept me motivated and energized. I would never complete my work without your generous help. I would also like to thank our great technician Guan Hong, Mazen Samara, Luc Demers, and Dmytro Kevorkov who are so patient, curious, and generous.

Furthermore, I would like to thank my thesis committee members, Dr. Miriam Diamond, Dr. Catherine Mulligan, Dr. Xia Li, Dr. S. Samuel Li, Dr. Zhi Chen, Dr. Chunjiang An for their time, valuable suggestions, and constructive comments.

Finally, I would like to express my heartfelt gratitude to my dearest partner, Zheng Wang. Your love and understanding are truly unconditional, and your unwavering understanding and encouragement have meant the world to me. I feel the world becomes serene and complete when I hold your hands. I would also like to sincerely thank my parent and my grandparents, who always support me without any reservations. Your belief in me has been a constant source of strength and motivation. I also want to thank my little family member Bella. Through you, I have come to appreciate the uniqueness of every living creature and the inherent beauty of life itself. Looking into your big round eyes and feeling you in my embrace has taught me that every individual seeks love, understanding, and respect.

I am grateful to have encountered Su Shi's essay, which beautifully captures the essence of seeking profound experiences in nature, translated as “the ancients, through their contemplation of the universe, found insight in the majestic mountains, winding rivers, vibrant vegetation, diverse species of insects, fish, birds, and beasts. Their quest for depth of thought and breadth of exploration led them to remote and perilous places, where they discovered the most extraordinary, awe-inspiring views, which remained hidden to ordinary travelers.” As I reflect on my own journey, I can do so without any regrets, since I have wholeheartedly devoted myself to exploring the world around me. I consider myself fortunate to have witnessed the sheer beauty and magnificence of the sceneries that unfolded before my eyes. I would like to thank again all the individuals who give me the power and energy to get there. Now, the new journey is about to sail.

# Table of Contents

<b>List of Figures .....</b>	<b>xi</b>
<b>List of Tables.....</b>	<b>xvi</b>
<b>List of Abbreviations.....</b>	<b>xvii</b>
<b>Chapter 1. Introduction .....</b>	<b>1</b>
1.1 Problem statement .....	1
1.2 Research objectives .....	11
<b>Chapter 2 Literature Review.....</b>	<b>13</b>
2.1 Methods .....	16
2.1.1 Data Sources .....	16
2.1.2 Data Analysis .....	17
2.2 Results .....	19
2.2.1 General dataset description.....	19
2.2.2 Global distribution of MPs in estuaries .....	23
2.2.3 Patterns of MP abundance affected by sampling, extraction, and environment.....	31
2.2.4 Characteristics of MP morphology in global estuaries .....	34
2.2.5 Driving factors of MP abundance in global estuaries .....	40
2.2.6 Risk assessment of MPs in global estuaries.....	44
2.3 Discussion.....	55
2.3.1 The impact of environmental and anthropogenic factors on MP abundance in estuaries .....	55
2.3.2 The impact of MP sampling and processing on MP abundance in estuaries .....	60
2.3.3 The impact of morphological characteristics on MP behaviors.....	62
2.3.4 Potential risks of MPs in global estuaries.....	65
<b>Chapter 3 Characterization of aged MPs.....</b>	<b>67</b>
3.1 Methods .....	67
3.2 Results and discussion.....	68
<b>Chapter 4 The effects of water content and flow patterns on MP mobilization .....</b>	<b>79</b>
4.1 Background.....	79
4.2 Methods .....	82

4.2.1 Chemicals and materials .....	82
4.2.2 Simulated MP release with column test.....	83
4.2.3 Theoretical considerations .....	86
4.2.4 Detachment modeling.....	87
4.3 Results and discussion.....	88
4.3.1 The effect of flow rate on MP detachment under steady flow .....	88
4.3.2 The effect of MP properties on detachment.....	92
4.3.3 MP detachment during intermittent flow .....	94
4.3.4 MP detachment during flow transient in ionic strength.....	97
4.3.5 MP detachment during temporal variation in flow rate .....	99
4.3.6 The effect of prolonged drying .....	101
4.3.7 Environmental implications.....	105
<b>Chapter 5 Transport of microplastics in shore substrates over tidal cycles: roles of polymer characteristics and environmental factors.....</b>	<b>107</b>
5.1 Background.....	107
5.2 Methods .....	111
5.2.1 Chemicals and materials .....	111
5.2.2 Preparation of aged MPs.....	111
5.2.3 MPs characterization.....	112
5.2.4 Simulated tidal cycles with column test.....	112
5.2.5 Statistic Analysis.....	119
5.3. Results and discussion.....	120
5.3.1 Characterization of pristine and aged MPs .....	120
5.3.2 Effects of substrate size on MPs transport.....	124
5.3.3 Effects of size and density of MPs on transport in tide-influenced substrates .....	127
5.3.4. Effects of aging on MPs transport in tide-influenced substrates .....	129
5.3.5 Effects of salinity on MPs transport in tide-influenced substrates .....	130
5.3.6 Effects of tidal velocity on MPs transport in tide-influenced substrates .....	132
5.3.7 Insights from correlation analysis and environmental implications .....	134
<b>Chapter 6 A new perspective on the mobilization of MPs through capillary fringe fluctuation in a tidal aquifer environment.....</b>	<b>138</b>

6.1. Background.....	138
6.2 Methods .....	141
6.2.1 Chemicals and materials .....	141
6.2.2 Simulated capillary fringe fluctuation with column test.....	142
6.2.3 Characterization of capillary fringe fluctuation .....	147
6.3 Results and discussion .....	147
6.3.1 Rise of capillary in substrate under the influence of water table fluctuations .....	147
6.3.2 Effects of substrate size on MPs transport in substrate under fluctuating capillary fringe .....	149
6.3.3 Effects of MPs properties on transport in substrates under fluctuating capillary fringe .....	152
6.3.4 Effects of aging on MPs transport in substrates under fluctuating capillary fringe.....	153
6.3.5 Effects of fluctuating velocity on MPs transport in substrates under fluctuating capillary fringe .....	154
6.3.6 Effects of groundwater salinity on MPs transport in substrates under fluctuating capillary fringe .....	156
6.3.7 Environmental implications of MPs being influenced by the capillary fringe .....	158
<b>Chapter 7 Tide-induced infiltration and resuspension of MPs in shorelines: insights from tidal tank experiments .....</b>	<b>161</b>
7.1 Background.....	161
7.2 Methods .....	164
7.2.1 Particle characteristics .....	164
7.2.2 Experiment setup .....	168
7.2.3 MP quantification and distribution analysis.....	170
7.3 Results and discussion .....	170
7.3.1 The infiltration of MPs under the influence of tidal cycles .....	170
7.3.2 The resuspension of MPs under the influence of tidal cycles.....	178
7.3.3 The significance of surface tension in determining the transport of MPs .....	183
7.3.4 Implications for field sampling and data interpretation.....	185
<b>Chapter 8 Contributions and significance of thesis research, and suggestions for future work .....</b>	<b>189</b>

8.1 Contributions and significance of thesis research ..... 189

8.2 Suggestions for future work ..... 190

**Journal publications..... 192**

**References ..... 195**

**Appendices ..... 222**

## List of Figures

<b>Figure 2.1</b> The sampling, extraction, and identification techniques used to analyze MPs in water and sediment.....	22
<b>Figure 2.2</b> Global distribution of MP abundance in water (a) and sediment (b), and latitudinal distribution of MP abundance in water (c) and sediment (d).....	24
<b>Figure 2.3</b> MP abundances in various environmental, sampling, and extraction categories in water (a) and sediment (b).....	33
<b>Figure 2.4</b> (a–d) Fractions of color, shape, type, and size of MPs in water and sediment. (e–j) RDA of the color (e, h), shape (f, i), and type (g, j) of MPs in water (e–g) and sediment (h–j) explained by explanatory factors. PPEO denotes the probability of plastic being emitted to ocean and SGMPW denotes the share of global mismanaged plastic waste. ....	39
<b>Figure 2.5</b> Relationship between explanatory factors and MP abundance in water (a–e) and sediment (f–h). Geodetector result for water (i) and sediment (j). The values on the diagonal line are q-value of individual explanatory factors, and * denotes 5% significance. ....	43
<b>Figure 2.6</b> Pollution load index (PLI) and potential ecological risk index (ERI) in water (a, c) and sediment (b, d).....	46
<b>Figure 2.7</b> MP abundance in water versus salinity. ....	59
<b>Figure 3.1</b> SEM images of the pristine (a, b, c), SW60 (d, e, f), and UV60 (g, h, i) MPs. ....	69
<b>Figure 3.2</b> XRD spectra of pristine and aged MPs.....	71
<b>Figure 3.3</b> XPS survey scan of seawater-aged MPs (a) and UV-aged MPs (b).....	73
<b>Figure 3.4</b> FTIR spectra of the pristine and aged MPs under (a) seawater and (b) UV aging conditions. ....	73
<b>Figure 3.5</b> Changes of mean particle size (a), contact angle (b), CI index (c), and O/C ratio (d) of seawater aged and UV aged MPs with different aging durations. ....	74
<b>Figure 3.6</b> Synchronous (a, c) and asynchronous (b, d) 2D COS maps drawn based on time-dependent FTIR spectra of MPs under seawater (a, b) and UV (c, d) aging. Red color and blue color symbolize positive and negative correlation, respectively. Darker color demotes a stronger positive or negative correlation. ....	76
<b>Figure 4.1</b> Calibration curves of PE1, PE2, and PMMA.....	84

<b>Figure 4.2</b> Detachment curves of PE1, PE2, and PMMA at different flow velocities under wet and air-dried conditions (a–i). Detachment percentages of MPs at different flow velocities under wet and air-dried conditions (j). .....	91
<b>Figure 4.3</b> Detachment curves for aged PE1 and PMMA under wet and air-dried conditions. For display purpose, only the first 10 PVs are presented. ....	94
<b>Figure 4.4</b> Detachment curves for PE1, PE2, and PMMA under intermittent flow (a-f). Detachment percentages of PE1, PE2, and PMMA under intermittent flow (g).....	96
<b>Figure 4.5</b> Detachment curves for PE1, PE2, and PMMA under transients in solution ionic strength (a-f). Detachment percentages of PE1, PE2, and PMMA under transients in solution ionic strength (g). ....	98
<b>Figure 4.6</b> Detachment curves for PE1, PE2, and PMMA under transients in flow rates (a-f). Detachment percentages of PE1, PE2, and PMMA under transients in flow rates (g). ....	100
<b>Figure 4.7</b> Detachment percentages of PE1, PE2 and PMMA under wet and various air-dry durations. ....	102
<b>Figure 4.8</b> Experimental (dot) and simulated (line) detachment curves of PE1, PE2 and PMMA under wet and various air-dry durations. ....	103
<b>Figure 5.1</b> Sketch of column test setup. ....	115
<b>Figure 5.2</b> SEM images of the pristine and aged PE1 (a–f) and PTFE (g–l) particles. ....	122
<b>Figure 5.3</b> CI index, contact angle, mean particle size, and zeta potential of various aged PE1 and PTFE.....	123
<b>Figure 5.4</b> The FTIR spectra of pristine and various aged MPs.....	124
<b>Figure 5.5</b> Effects of substrate size on MPs distribution and retention. (a–d) PE1 distribution in columns with 1, 2, 3+5, and 4 mm GB under different tidal cycles; (e–h) PTFE distribution in columns with 1, 2, 3+5, and 4 mm GB under different tidal cycles. (i–j) PE1 and PTFE retention in the whole columns with 1, 2, 3+5, and 4 mm GB under different tidal cycles.....	126
<b>Figure 5.6</b> Effects of MPs properties on their distribution and retention. (a) PE2 distribution in column with 1 mm GB under different tidal cycles. (b) Retention of PE1, PE2, and PTFE in the whole column with 1, 2, 3+5, 4 mm GB under different tidal cycles. ....	128
<b>Figure 5.7</b> Effects of aging on MPs distribution and retention. (a) PE1-pristine, PE1-SW30, PE1-SW60 distributions in the columns with 10 tidal cycles. (b) PE1-pristine, PE1-UV30, PE1-UV60 distributions in the columns with 10 tidal cycles. (c) PTFE-pristine, PTFE-SW30, PTFE-SW60	

distributions in the columns with 10 tidal cycles. (d) PTFE-pristine, PTFE-UV30, PTFE-UV60 distributions in the columns with 10 tidal cycles. (e–f) Retention of PE1 and PTFE with various aging conditions in the whole column with 10 tidal cycles. .... 130

**Figure 5.8** Effects of salinity on MPs transport and the calculated interaction energy. (a–b) PE1 and PTFE distribution in columns at various ionic strengths with 10 tidal cycles. (c) Retention of PE1 and PTFE in the whole columns at various ionic strengths with 10 tidal cycles. (d–e) Interaction energy versus surface-to-surface separation distance for PE1/PTFE and GB at various ionic strengths. .... 132

**Figure 5.9** Effects of flow velocities on MPs distribution and retention. PE1 (a) and PTFE (b) distribution in column under various flow velocities with 5 tidal cycles. (c) Retention of PE1 and PTFE in the whole column under various flow velocities with 5 tidal cycles. .... 133

**Figure 5.10** Relationship between MPs retention and stratification in the column with various MPs and environmental properties. (a) Correlation of MPs (PE1, PE2, PTFE) retention and stratification with various MPs and environmental properties. (b, c, d) RDA plot for MPs (PE1, PE2, PTFE), PE1, PTFE retention and stratification with various MPs and environmental properties. .... 135

**Figure 6.1** Sketch of the column test setup..... 144

**Figure 6.2** Capillary rise in experiment and simulation by Hydrus-2D under the influence of water table fluctuation. (a) Capillary rise in 1 mm GBs. (b) Capillary rise in 2 mm GBs. (c) Hydrus-2D simulation results..... 148

**Figure 6.3** Effects of substrate size on MPs mobilization under the influence of water table fluctuation. (a–c) PE1 distribution in 0.5, 1, and 2 mm GBs packed column under different fluctuation cycles; (d–f) PTFE distribution in 0.5, 1, and 2 mm GBs packed column under different fluctuation cycles. (g–h) Retention percentages of PE1 and PTFE in the 0.5, 1, and 2 mm GBs packed columns under different fluctuation cycles. The size of the bubble denotes the MP retention percentages. .... 151

**Figure 6.4** Effects of MPs properties on their mobilization under the influence of water table fluctuation. (a) PE2 distribution in 1 mm GBs packed column under the influence of water table fluctuation. (b) Retention percentages of PE1, PE2, and PTFE in 0.5, 1, and 2 mm GBs packed columns under the influence of water table fluctuation. The size of the bubble denotes the MP retention percentages. .... 153

**Figure 6.5** Effects of aging and water table fluctuation velocity on MPs mobilization. (a) Pristine PE1, UV60 PE1, and SW60 PE1 distributions in substrate under 5 cycles of water table fluctuation. (b) Pristine PTFE, UV60 PTFE, and SW30 PTFE distributions in substrate under 5 cycles of water table fluctuation. (c) Retention percentages of aged PE1 and PTFE in substrate under 5 cycles of water table fluctuation. PE1 (d) and PTFE (e) distribution in substrate under 5 cycles of water table fluctuation at various velocities. (f) Retention percentages of PE1 and PTFE in substrate under 5 cycles of water table fluctuation at various velocities. The size of the bubble denotes the MP retention percentages. .... 155

**Figure 6.6** Effects of salinity on MPs mobilization under the influence of water table fluctuation. (a–b) PE1 and PTFE distribution in substrate at various ionic strengths under 5 cycles of water table fluctuation. (c) Retention percentages of PE1 and PTFE in substrate at various ionic strengths under 5 cycles of water table fluctuation. (d–e) Ratios of detachment force to attachment force (DLVO force), shear force, and force difference between gravity and buoyancy force for PE1 and PTFE. The size of the bubble denotes the MP retention percentages. .... 157

**Figure 6.7** Interaction energy versus surface-to-surface separation distance for PE1/PTFE and GB at various ionic strengths. .... 158

**Figure 7.1** Shape of the selected MPs. (a) Relation between axis ratio and particle shape/sphericity classification (Krumbein, 1941; Corey, 1949). (B)Sphericity-form diagram (Sneed and Folk, 1958). C= Compact, CP = Compact platy, CB = Compact bladed, CE = Compact elongated, P = Platy, B = Bladed, E = Elongated, VP = Very platy, VB = Very bladed, VE = Very elongated. .... 167

**Figure 7.2** The schematic diagram of the tidal tank simulator. .... 169

**Figure 7.3** The floating percentages of MPs after each water level increase at the rates of tidal level change of 0.25, 0.50, and 0.75 cm/min. .... 173

**Figure 7.4** Spearman correlation analysis between floating percentages of MPs and various indicators considering all the MP types (a), only the low-density MPs (b), and only the high-density MPs (c). ( $p < 0.05$ ). .... 174

**Figure 7.5** The distribution of various MPs in substrate under the rates of tidal level change of 0.25 cm/min (a–c), 0.50 cm/min (d–f), and 0.75 cm/min (g–i). The distribution of various MPs in the top 1 cm layer under the rates of tidal level change of 0.25 cm/min (j), 0.50 cm/min. (k), and 0.75 cm/min (l). .... 176

<b>Figure 7.6</b> Spearman correlation analysis between MP horizontal/vertical position and various indicators for the scenario that MP placed on the substrate surface (n=1139) (a) and MPs placed in the bottom of substrate (n=1128) (b). ( $p < 0.05$ ).....	177
<b>Figure 7.7</b> The floating percentages of MP at the rates of tidal level change of 0.25, 0.50, and 0.75 cm/min.....	180
<b>Figure 7.8</b> Spearman correlation analysis between floating percentages of MPs and various indicators considering all the MP types (a), only the low-density MPs (b), and only the high-density MPs (c). ( $p < 0.05$ ).....	181
<b>Figure 7.9</b> The distribution of various MPs in substrate under the rates of tidal level change of 0.25 cm/min (a–c), 0.50 cm/min (d–f), and 0.75 cm/min (g–i). The distribution of various MPs in the top 1 cm layer under the rates of tidal level change of 0.25 cm/min (j), 0.50 cm/min (k), and 0.75 cm/min (l).....	182
<b>Figure 7.10</b> Gravity force and surface tension force for sphere particles, adapted from (Stolte et al., 2015) (a). The aggregates of MPs on water surface (b). .....	184

## List of Tables

Table 1.1 Summary of articles regarding the interaction between MPs and tidal dynamics <sup>a</sup> .....	5
Table 2.1 MP abundance in estuarine water. ....	25
Table 2.2 MP abundance in estuarine sediment. ....	28
Table 2.3 PLI in estuarine water. ....	47
Table 2.4 PLI in estuarine sediment. ....	50
Table 2.5 ERI in estuarine water. ....	53
Table 2.6 ERI in estuarine sediment. ....	54
Table 3.1 Synchronous and asynchronous (in the brackets) 2D COS results on the bond assignment and sign of each cross-peak with increasing seawater or UV aging duration (signs were obtained from the upper-left corner of the maps). ....	78
Table 4.1 Fitted parameters by Hydrus-1D. ....	104
Table 5.1 Experimental design .....	116
Table 6.1 Experiment design. ....	145
Table 7.1 MP types and properties used in tank experiment. ....	166

## List of Abbreviations

MPs	Microplastics
2D COS	Two-dimensional correlation spectroscopy
CF	Contamination factor
DLVO	Derjaguin-Landau-Verwey-Overbeek
ERI	Ecological risk index
FTIR	Fourier-transform infrared spectroscopy
HDI	Human Development Index
$k_{att}$	Rate coefficients of attachment
kB	Boltzmann's constant
$k_{det}$	Rate coefficients of detachment
LISST	Laser In-Situ Scattering and Transmissometry
PA	Polyamide
PE	Polyethylene
PES	Polyester
PET	Polyethylene terephthalate
PFTE	Polytetrafluoroethylene
PLI	Pollution load index
PMMA	Polymethylmethacrylate
PP	Polypropylene
PS	Polystyrene
PV	Pore volume
PVC	Polyvinyl chloride
Py-GC-MS	Pyrolysis-gas chromatography-mass spectrometry
SEM	Scanning electron microscope
SR-XRF	Synchrotron X-ray fluorescence
SW	Seawater
T	Absolute temperature
UV	Ultraviolet
XPS	X-ray photoelectron spectroscopy

XRD	X-ray Diffraction
$V_{VDW}$	van der Waals interaction
$V_{EDL}$	electrostatic double layer interaction
GB	Glass beads
M	Mass of MPs obtained in each flask
$M_0$	Original MPs mass
CI	Carbonyl index
PLA	Polylactic acid
CSF	Corey shape factor
$F_{cap}$	Capillary force
$\gamma$	Surface tension
$\theta$	Indentation angle
C	Compact
CP	Compact platy
CB	Compact bladed
CE	Compact elongated
P	Platy
B	Bladed
E	Elongated
VP	Very platy
VB	Very bladed
VE	Very elongated
$a$	Longest particle side length
$b$	Medium particle side length
$c$	Shortest particle side length

# Chapter 1. Introduction

## 1.1 Problem statement

Microplastics (MPs) have been uncovered ubiquitously in environments. Around 94% of plastics settle in landfills or are released into the environment, whereas only 6–26% are recycled (Alimi et al., 2018). MPs are either primary or secondary according to their origin. Primary MPs are small particles produced for commercial usage. Secondary MPs are originated from the fragmentation of large pieces weathered through mechanical abrasion, UV radiation, fluctuating temperatures, and biodegradation (Eerkes-Medrano et al., 2015). Due to the increasing demand of humans for plastics and the on-going fragmentation of plastics into tiny pieces, the amount of MPs is predicted to reach around 10 million tons by 2040 (Lau et al., 2020). MPs have been documented extensively in the ocean (Pabortsava and Lampitt, 2020), coast (Nor and Obbard, 2014), lagoon (Quesadas-Rojas et al., 2021), estuary (Liu et al., 2021), sediment (Corcoran et al., 2020), vegetation, and organisms (Cole et al., 2013). The pervasive existence of MPs poses long-lasting influence on ecosystem and human health. However, compared to MPs in water, information respecting the fate of MPs in sediment is still limited.

Sediments are of critical importance due to their interaction with contaminants. With porosity and large chemically reactive surface areas, sediments absorb and concentrate many pollutants from the water column, and as a result, act as a major sink for pollutants (Wang et al., 2021). The existence of plastics in sediment has been reported frequently in field study (Alomar et al., 2016; Bosker et al., 2019; Bridson et al., 2020). Studying the distribution of MPs and the determining

factors provide vital information required for managing MPs pollution and estimating its ecological risks. The MPs distribution patterns in sediment vary significantly in both temporal and spatial aspects, which depends on a number of entangled factors, such as substrate and MPs characteristics, geographic factors, climate and hydrodynamic forces. Hydrological processes are critical important physical processes in the aquatic system, playing a key role in the retention and transportation of inorganic substances (Wang et al., 2018). Floating plastics could be flushed onto shores by currents and waves. Stranded plastics can be flushed back to the open water. Turbulent mixing with sediment could accelerate the broken of plastics, burying them into the sediment (Turra et al., 2014). The infiltration depth, retention time, and remobilization of MPs in sediment are of great ecotoxicological significance influencing its exposure to organisms. Many aquatic vertebrate and invertebrate communities depend on habitable substrate and groundwater–surface-water interaction (Hunt et al., 2006). The nutrient uptake also is sensitive to substrate composition and hyporheic exchange (Roche et al., 2019). Therefore, the existence of MPs in sediment may have fundamental impacts on the adjacent environment and organisms.

Tidal zones, such as estuarine and coastal ecosystem, providing habitat for an array of plants, birds, and benthic species, are particularly vulnerable to MPs pollution (French, 1996). Estuaries at the terrestrial-ocean interface render the MPs transport complex. Tramoy et al. (2020) suggested that up to 70% of MPs were “old” plastics possibly correlated to the meandering dynamic of the river over large space and time scales, and hydrodynamics at smaller scales, contributing to increasing the residence time of plastics into the estuary with interminable deposit and remobilization cycles. Physical processes of MPs transport in tidal sediment are complex and are affected by a number of hydrodynamic and sedimentological aspects over large temporal and spatial scales (Wang, 2012). The majority of the existing research on the distribution of MPs in

tidal zone concentrated on large spatial distribution. There is a lack of validated information for more precise analysis of the sediment transport under the influence of tidal cycles.

A review of the literature published in peer-reviewed journals up to December 2021 was conducted. Publications were searched from Web of Science using keywords of “tid\*” and “microplastic\*”. Articles that explored the relationships between tidal dynamics and MPs were summarized (Table 1.1). Tidal range (spring/neap), flood/ebb, tidal zones, tidal cycles, flow velocity were the major influencing factors that were investigated through field sampling or modeling methods. Inconsistent results are suggested in studies concerning the impacts of spring/neap tide and flood/ebb tide on MPs concentration in water or sediment phase. For instance, Sukhsangchan et al. (2020) claimed that neap tide had higher MPs abundance compared to spring tide in surface water near a river mouth, whereas Sadri and Thompson (2014) found that more MPs were observed during spring tides in the surface water. Wu et al. (2020) revealed that MPs were more abundant in surface sediment layer in the neap tide compared to spring tide, and the numbers of MPs demonstrated a negative correlation with hydrological forces in an estuary. Zhang et al. (2020) observed linear relationships between MPs growth rates and the tidal current velocity, but not with the tidal range. Studies regarding tidal zone revealed that the abundance of MPs is higher than that in low tide (Piehl et al., 2019; Sathish et al., 2019). Few articles explored the effects of tidal cycles on MPs, which all concluded that MPs concentration could vary greatly within or between tidal cycles, resulting in considerable uncertainty in interpreting data from field sampling (Moreira et al., 2016; Cohen et al., 2019; Balthazar-Silva et al., 2020). No concrete trend of MPs concentration can be observed with the change of tidal cycles. Evidence from field experiments could not detangle the intricate factors between each other. In addition, density separation is generally used in sample extraction processing. According to a review by

Harris (2020), the fluid used for floating the MPs was around  $1.60 \text{ g/cm}^3$  and the highest fluid density is  $1.80 \text{ g/cm}^3$ . Polypropylene (PP), polyethylene terephthalate (PET), polyethylene (PE), polystyrene (PS), expanded polystyrene (EPS), polyamide (PA), polycarbonate (PC), and polyvinylchloride (PVC) are the most commonly detected MPs in the environment, whose densities are 0.92, 1.38, 0.97, 1.05, 0.02, 1.15, 1.20, and  $1.31 \text{ g/m}^3$ , respectively (Waldschlager et al., 2020; Guo et al., 2021). In consequence, MPs with densities higher than  $1.80 \text{ g/cm}^3$  received far less attention.

Table 1.1 Summary of articles regarding the interaction between MPs and tidal dynamics<sup>a</sup>

Factor	Region	Location	Type	Focus phase	Methods	Main finding	References
Spring/neap tide	Thailand	Chao Phraya River	Estuary	Surface water	Sampling	MPs abundance: neap > spring	(Sukhsangchan et al., 2020)
Spring/neap tide	China	Yangtze Estuary	Estuary	Sediment	Sampling	MPs abundance: neap (surface 0–2 cm) > spring	(Wu et al., 2020)
Spring/neap tide	Brazil	Goiana Estuary	Estuary	Water	Sampling	MPs density varied within tidal cycles	(Lima et al., 2016)
Spring/neap tide	United Kingdom	River Tamar	Estuary	Surface water	Sampling	MPs abundance: spring > neap, more fragments of larger size observed during spring tides	(Sadri and Thompson, 2014)
Flood/ebb	Thailand	Phraya River Estuary	Estuary	Surface water	Sampling	MPs abundance in water: flood > ebb	(Oo et al., 2021)
Flood/ebb	Iberian Peninsula	Ria de Vigo	Estuary	Water	Model	MPs abundance in water: ebb > flood.	(Sousa et al., 2021)
Flood/ebb	India	Mumbai coast	River mouth	Water	Sampling	MPs abundance in water: flood > ebb	(Manickavasagam et al., 2020)

Factor	Region	Location	Type	Focus phase	Methods	Main finding	References
Flood/ebb	Mexico	Rio Lagartos coastal lagoon	lagoon	Sediment, water	Sampling	MPs abundance in water: ebb > flood	(Quesadas-Rojas et al., 2021)
Flood/ebb	United States	Hudson River	Estuary	Surface water	Sampling	No significant difference in MPs collected during ebb and flood tides	(Polanco et al., 2020)
Flood/ebb	United Kingdom	London	River	Water column	Sampling	MPs abundance: ebb > flood	(Rowley et al., 2020)
Flood/ebb	United Kingdom	Southampton Water	Salt marsh	Surface water	Sampling	MPs abundance: flood > ebb.	(Stead et al., 2020)
Flood/ebb	Thailand	Bandon Bay	Coast	Water, sediment, shellfish	Sampling	MPs abundance in water: ebb > flood. The load from river to bay during low tide was higher than that during high tide	(Chinfak et al., 2021)
Discharge	France	Bay of Biscay	Estuary	Surface, subsurface, bottom	Model and sampling	Neutrally-buoyant MPs are easily flushed out, heavier MPs are prone to entrapment	(Defontaine et al., 2020)

Factor	Region	Location	Type	Focus phase	Methods	Main finding	References
				water		in the estuary, in particular under low discharge conditions.	
Flow velocity	Taiwan	Fengshan River	River system	Sediment	Sampling	MPs in sediment were negatively correlated with flow velocity	(Tien et al., 2020)
River discharge, tidal straining	Spain	Guadalquivir estuary	Estuary	Water	Model and sampling	River flow-induced circulation dominates the upper and middle parts of the estuary, tidal straining dominates the lower stretches.	(Bermudez et al., 2021)
Tidal zone	Italy	Po River Delta	Estuary	Sediment	Sampling	The accumulation of MPs among drift lines showed no consistent pattern.	(Piehl et al., 2019)
Tidal zone	India	Tamil Nadu	Coast	Sediment	Sampling	MPs abundance: High tide > low tide	(Sathish et al., 2019)
Tidal zone	Iran	Persian Gulf	Gulf	Sediment	Sampling	MPs abundance: High tide > low tide, except for mangrove	(Naji et al., 2017)

Factor	Region	Location	Type	Focus phase	Methods	Main finding	References
						sampling sites	
Spatial	Mexico	Gulf of Mexico	Estuary	Sediment	Sampling	There was a gradient in MPs abundance with locations more exposed to currents and tides having higher abundance and diversity, as well as a higher contribution by denser polymers.	(Wessel et al., 2016)
Cycles	Brazil	Santos region	Coastline	Sediment	Sampling	No interaction between MPs concentration, season, zones or cycles	(Balthazar-Silva et al., 2020)
Cycles	United States	Delaware Bay	Estuary	Water	Model and sampling	MP concentrations could vary significantly within a tidal cycle	(Cohen et al., 2019)
Cycles	Brazil	Pontal do Sul Balneary	Estuary	Sediment	Sampling	Beach dynamic processes such as the overlap of strandlines might increase the variability in data	(Moreira et al., 2016)

Factor	Region	Location	Type	Focus phase	Methods	Main finding	References
Location	Argentina	Río de la Plata	Estuary	Subsurface water (1m depth)	Sampling	Correlation between MPs concentration and measured environmental variables were not found.	(Pazos et al., 2018)
Tidal zone	Spain	Canary Island	Coastline	Surface water, sediment	Sampling	MPs abundance: high tide sediment > water samples > sediment from submerged zones	(Reinold et al., 2021)
Tidal zone	Portugal	Ria Formosa	Lagoon	Sediment, canopy of coastal vegetation	Sampling	Trapping capacity of MPs in the sediment and on the canopy was higher for subtidal than for intertidal area	(Cozzolino et al., 2020)
Location	China	Xiamen Bay	Mangrove	Surface water, Sediment	Sampling	MPs abundance can be affected by tides and sampling locations	(Liu et al., 2021)
Tidal range; velocity	China	Beibu Gulf	Mangrove	Sediment	Sampling	MPs growth rates showed linear correlation with the tidal current velocity, no	(Zhang et al., 2020)

Factor	Region	Location	Type	Focus phase	Methods	Main finding	References
						relationships with the tidal range	
Wind speed, wave height and river discharges	France	Arcachon	Bay	Sediment	Sampling	Highest MPs concentrations in beached took place during energetic hydrodynamic conditions	(Lefebvre et al., 2021)

Many laboratory studies have been conducted to uncover the detailed mechanisms regarding the MPs transport in sediment. The mobility of MPs in sediments is greatly associated with porewater chemistry, such as ionic strength, organic carbon content, and the properties of MPs such as size, shape, density, surface charge, surface chemical composition, and the properties of substrates (size distribution, shape). Waldschlager and Schuttrumpf (2020) considered the properties of MPs and substrate, which suggested that the infiltration depth of MPs increased with the decreasing diameter of MPs and with a larger diameter of the substrate. Additionally, MPs in sediment experience a series of transformations, influencing their aggregation, transportation, and deposition. According to Derjaguin–Landau–Verwey–Overbeek (DLVO) theory, increasing ionic strength compresses the electrical double layer reduces repulsive forces, leading to higher aggregation or deposition efficiency (Li et al., 2021). Alimi et al. (2021) concluded that exposure to 10 freeze-thaw cycles consistently led to significant aggregation and mobility reduction of nanoplastics compared to that held at 10 °C, especially at high ionic strengths in the absence of natural organic matter. Nevertheless, due to the determination restriction of MPs concentration, previous transport studies mostly focused on nanoplastics, that is to say PS was commonly selected due to the size control (Hou et al., 2020). There has been limited research on micro-scale MPs and other types of MPs. Moreover, information in terms of the hydrodynamic forces, such as tidal cycles, flow velocity, submerging time on MPs transport is still scarce.

## **1.2 Research objectives**

The study aims to in-depth investigate the mobilization of MPs under the influence of typical coastal processes, combining key environmental and polymer properties. By conducting lab

control experiments, complicated environmental factors can be differentiated. To achieve these objectives, this study designed novel experiment design and methodologies. The detailed research objectives are listed as following:

- Unveil the intricate aging mechanism of microplastics (MPs) in typical coastal settings, focusing on changes in physical and chemical properties induced by environmental weathering processes;
- Investigate how the flow regimes and water content affect the detachment of MPs from porous media;
- Explore how the oscillation of air-water interface affect the transport of MPs in combination with MP properties and environmental factors (e.g., substrate size, flow rate, and salinity);
- Investigate how the capillary fringe fluctuation affect the mobilization of MPs in association with MP characteristics and environmental factors;
- Explore the infiltration and resuspension behaviors of MPs under the influence of tidal cycles combined with the rates of tidal level change and MP characteristics using a tidal tank.

## Chapter 2 Literature Review\*

The presence of plastic debris in the environment rises considerable public concern. Globally, plastic consumption and production have increased exponentially since the 1940s, reaching 390 million tonnes per year (PlasticsEurope, 2022). Only 6–26% of plastic products are recycled, while up to 94% end up in landfills or the environment (Alimi et al., 2018). Eriksen et al. (2023) estimated over 170 trillion plastic particles floating in the ocean. Estuaries are one of the primary pathways transferring MPs from the land to the ocean. Based on the Human Development Index (HDI), an estimate predicted that 57,000–265,000 metric tons of plastic would flow into the ocean from rivers in 2018 (Mai et al., 2020). Understanding the distribution and patterns of MPs along the major pathway is crucial for identifying local plastic sources in order to inform the management and mitigation of MPs transferred from the land to the ocean.

Coastal estuaries are among the most valuable ecosystems on the planet, providing a diverse array of habitats, services, and goods (Costanza et al., 1997). Estuarine ecosystems consist of biologically heterogeneous subsystems, such as water columns, mudflats, bivalve beds, and seagrass flats (Pihl et al., 2002). It is a critical interface for the exchange of matter, energy, and information between the land and marine, and the internal subsystems (Telesh, 2004). Estuaries are habitats for numerous fishes, birds, mammals, and other wildlife species. Economically, estuaries provide tourism, aquaculture, fisheries, and recreational activities, public infrastructure, shipping and transportation ports for humans (Feng et al., 2021). Moreover, estuaries carry other valuable services, such as coastal erosion control, storm surges protection, climate regulation,

---

\* This work has been published as Feng, Q., An, C., Chen, Z., Lee, K., Wang, Z., 2023. Identification of the driving factors of microplastic load and morphology in estuaries for improving monitoring and management strategies: A global meta-analysis. 333: 122014.

pollution purification, etc. (Luisetti et al., 2014). Therefore, plastics could endanger human well-being, the economy, and ecosystem health (Eerkes-Medrano et al., 2015). However, the distribution and transport of MPs in estuaries are subjected to interplayed hydrodynamic forces and anthropogenic activities, which complicates the assessment of MPs in estuaries (Wang et al., 2022).

Estuaries are typical tidal zones and tidal dynamics add uncertainties in sampling and data interpretation. A few field studies have examined the association between tidal dynamics and MP abundance (Balthazar-Silva et al., 2020; Defontaine et al., 2020). Flood and ebb, tidal range (spring/neap), tidal cycles, tidal zones, and flow velocity were the primary influencing factors investigated (Feng et al., 2022). Nevertheless, previous studies did not yield consistent results. For instance, a simulation study revealed that a tidal cycle can cause MP concentrations to differ by 1000-fold (Cohen et al., 2019). Balthazar-Silva et al. (2020) found no interaction between MP concentration, season, zones, or cycles on a coastline. Moreira et al. (2016) sampled the pellets in the intertidal zone on a small temporal and spatial scale, suggesting that strandline overlap could increase data variability. Regarding the tidal bulge, some studies found greater MP abundance at the surface during spring tides (Sadri and Thompson, 2014), while others suggested that neap tides had greater MP abundance at the surface (Sukhsangchan et al., 2020). To better understand the regime of MPs in estuaries, it is imperative to assess the MP abundance across larger temporal and spatial scales.

As a connection between the ocean and rivers, estuaries are subject to unique hydrodynamic forces and have traditionally been considered either a sink or a source of pollutants and plastic waste (Vermeiren et al., 2016; Chen et al., 2022). Estuaries are intermediate zones of brackish

water between riverine habitats and the ocean. Freshwater with a lower density usually remains in the surface layer of the estuary. Due to the shallow depth of the estuary, advection and diffusion processes dynamically interact to maintain two layers of gravity circulation (Sanford and Chen, 2009). These bidirectional freshwater-seawater flow boundary systems can accumulate plastics due to their heterogeneous nature. Zhang et al. (2020) reported that MP abundance in the surface water of the Qin river increased from upstream to downstream and reached a peak in the estuary. In addition, numerous human activities, such as port development, urban and industrial development, sewage systems, recreational areas, and farming, have been conducted in estuaries (Pye and Blott, 2014). A large number of MPs enter the environment by means of wastewater effluent (Murphy et al., 2016), urban runoff (Grbic et al., 2020), agricultural runoff (Liu et al., 2021) and industrial land use (Mallow et al., 2020). MPs accumulate in estuaries worldwide due to high population density, intensive plastic inputs, and high fragmentation and storage potential of plastic (Yonkos et al., 2014). Understanding the transport of MPs in estuaries can therefore aid in the development of mitigation strategies. Although the existence and distribution of MPs in estuaries have been documented, studies revealing the global patterns of MP abundance are scarce.

The present study conducted a systematic quantitative meta-analysis to uncover the MP abundance and related driving factors on the basis of data extracted from peer-reviewed papers globally. The knowledge gaps to fill are (1) the global load and morphology of MPs in estuarine water and sediment, (2) the patterns of MP abundance in different environmental and processing categories, (3) the driving factors of MP abundance and morphological fraction in estuaries, (4) the potential risk of MPs in global estuaries. The results obtained from this systematic review provide useful information for MP risks and management in estuaries.

## 2.1 Methods

### 2.1.1 Data Sources

Searches were conducted using Web of Science for peer-reviewed articles up to June 2022. The following key terms were used: “(estuary\* OR river mouth\*) AND microplastic\*”. In total, 716 articles were found. The articles were screened by the following criteria: (1) studies sampled MPs in estuaries and river mouths along the coast. Articles concerning MPs in lake estuaries are excluded; (2) articles presented MP concentration as per area unit were excluded; (3) articles explored MP concentration in water or sediment; (4) the studied MPs are smaller than 5 mm in size. After screening, 138 articles have been included in our dataset. For each observation, information regarding MP abundance, MP shape, MP color, MP composition, MP size, geographic locations (estuary name, longitude, latitude), season, sampling information (sampling method, sampling depth, mesh/filter size, density of the density separation fluid), extraction, and identification were obtained from articles or extracted from graphs by GetData Graph Digitizer ([www.getdata-graph-digitizer.com](http://www.getdata-graph-digitizer.com)). The CSI-CGIAR Global-Aridity geodataset was utilized to extract the aridity index for each observation, which is the ratio of mean annual precipitation to mean annual potential evapotranspiration (Trabucco and Zomer, 2019). The population density was collected from GPW version 4 with a resolution of 1 km (CIESIN, 2018). Data on the share of global mismanaged plastic waste, per capita plastic waste (kg/person/day), and probability of plastic being emitted to ocean was collected from Ritchie and Roser (2018). The probability of plastic being emitted to the ocean is computed from the probability of intersection of plastic mobilization on land, transport from land to rivers, and transport from rivers to the ocean (Meijer et al., 2021). The mean population density was calculated using 10-kilometer buffer zones

surrounding each observation point. The HDI was obtained from United Nations Development Programme (2019).

## 2.1.2 Data Analysis

### 2.2.1 Distinguishing the drivers for MP abundance

The Geodetector was employed to quantify the degree to which the explanatory variables (X) affect the dependent variable (Y), MPs concentration (Wang et al., 2010). The Geodetector hypothesizes that if an independent variable significantly influences a dependent variable, the spatial distribution of both variables is likely to be similar. The main advantage over other methods is the ability to detect relationships between drivers and dependent variables without assuming linear relationships, thus collinearities of multiple variables will not affect calculation processes. The following equation is used to calculate the power of the determinant q:

$$q = 1 - \frac{\sum_{h=1}^L N_h \sigma_h^2}{N \sigma^2} \quad (2.1)$$

where  $N_h$  and  $N$  are the classification number of the explanatory variable in class  $h$  ( $h = 1, \dots, L$ ) and in total.  $\sigma_h^2$  and  $\sigma^2$  are the variances of MP abundance in  $h$  class and in total. A greater  $q$ -value indicates a greater capacity to explain MP abundance. The interactive detector is used to identify whether two explanatory factors enhance or weaken the explanatory power or if they are independent. The interaction effects of two explanatory factors on MP abundance were determined using the relationship between the  $q$ -values of two explanatory factors and their interaction ( $X_1 \cap X_2$ ). The interaction categories can be found in Wang et al. (2010).

To identify explanatory factors driving MP morphological characteristics, redundancy analysis (RDA) was used to extract and summarize the variation in a set of response variables including MP colors, MP shapes, and MP composition, which can be explained by a set of explanatory

variables including longitude, latitude, aridity index, year, season, sampling depth, mesh/filter size, density of density separation fluid, extraction, identification, mean population, share of global mismanaged plastic waste, per capita plastic waste (kg/person/day), probability of plastic being emitted to ocean, and HDI.

### 2.2.2 Risk assessment for MPs

Pollution load index (PLI) can effectively assess the regional environmental risk posed by MPs.

PLI can be determined by:

$$CF_i = C_i/C_0 \quad (2.2)$$

$$PLI = \sqrt{CF_i} \quad (2.3)$$

$$PLI_e = \sqrt[n]{PLI_1 \times PLI_2 \times \dots \times PLI_n} \quad (2.4)$$

where  $CF_i$  is the contamination factor of MPs at sampling point  $i$  in an estuary, which is the ratio of measured concentration ( $C_i$ ) to background ( $C_0$ ).  $N$  is the sampling number in an estuary. Here, the safe concentration of MPs in the surface water body, 6.65 items/L, estimated by a mathematical model was used as  $C_0$  for water samples (Everaert et al., 2018). The lowest measured mean MP abundance in sediment of an estuary in the current dataset was used as the  $C_0$  for sediment, which is 14.07 items/kg.  $PLI_e$  is the PLI in an estuary, which is categorized into four classes: < 10, 10–20, 20–30, and > 30 corresponding to low, medium, high, and extremely high levels of pollution, respectively.

The potential ecological risk index (ERI) considers MP toxicology (Peng et al., 2018), which is calculated as follows:

$$T_i = \sum_{n=1}^n \frac{P_n}{C_i} \times S_n \quad (2.5)$$

$$ERI = T_i \times C_f \quad (2.6)$$

where  $P_n$  is the proportion of each polymer type in each sample and  $S_n$  is the hazard score of a specific polymer composition. The hazard values of polyethylene (PE), polyethylene terephthalate (PET), polypropylene (PP), polystyrene (PS), polyvinyl chloride (PVC), polyamide (PA), polyester (PES), and acrylic are 11, 4, 1, 30, 5001, 47, 1414, and 230, respectively (Lithner et al., 2011). The score indicates that this polymer is synthesized from hazardous substances. The production and usage of this polymer may release hazardous substances or degradation products. ERI was classified into five categories, < 150, 150–300, 300–600, 600–1200, and > 1200, which are corresponding to pollution levels I, II, III, IV, and V, respectively. Data analysis and visualization were conducted by Origin (OriginLab Corporation, USA) and ArcMap 10.5 (ESRI Ltd, USA). RDA was conducted using Canoco 5 (Lepš and Šmilauer, 2003).

## 2.2 Results

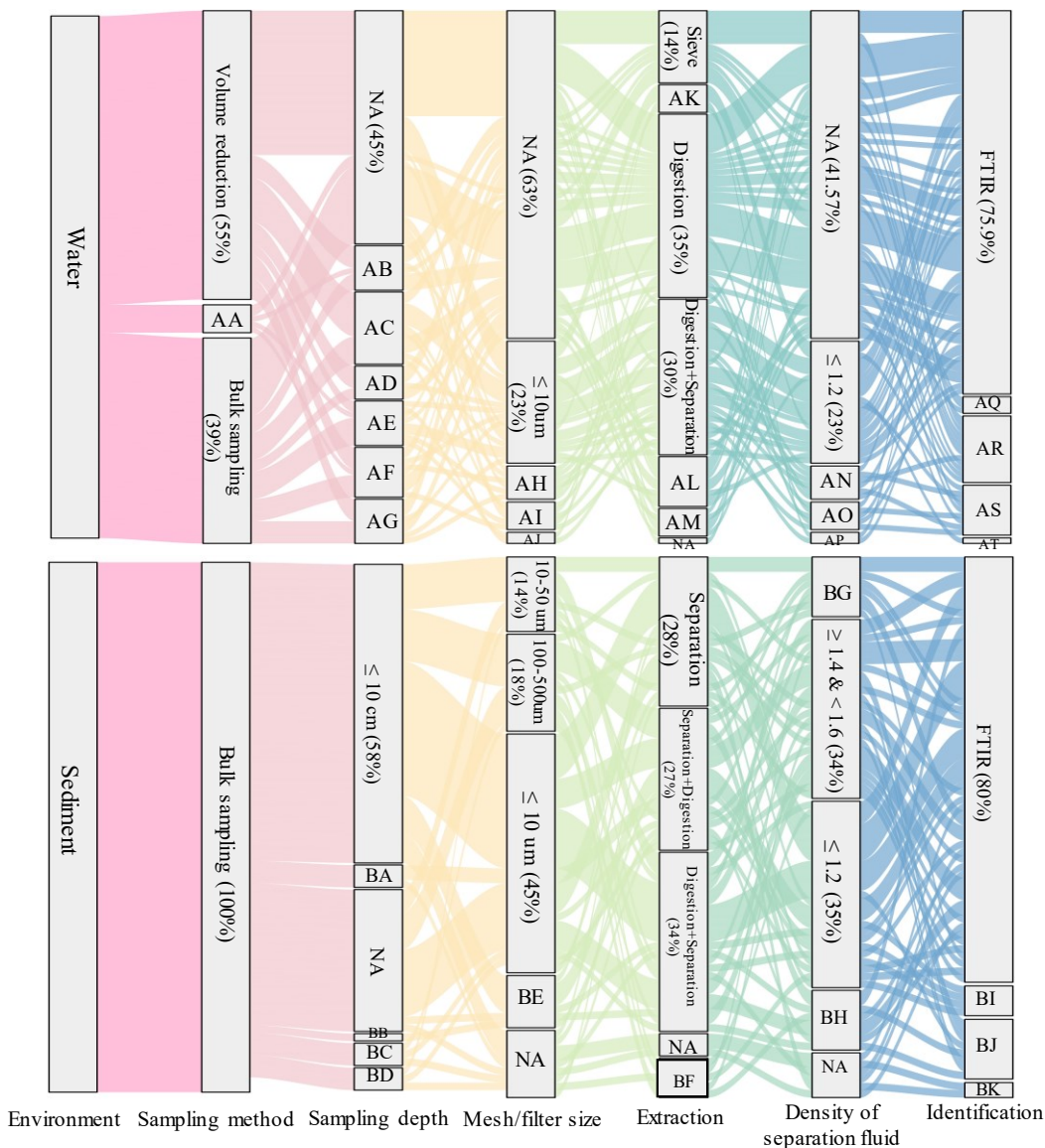
### 2.2.1 General dataset description

Following the screening of articles, a total of 135 publications (Appendix, Text S1) containing 1477 observations spanning the continents of Asia, Africa, North America, South America, Europe, and Oceania, and covering 124 estuarine areas were included. The longitude spanned from  $-123.64^\circ$  to  $153.56^\circ$  and the latitude spanned from  $-48.00^\circ$  to  $54.18^\circ$ . Sampling years ranged from 2004 to 2022. Spring, summer, autumn, and winter sampling accounted for 22%, 26%, 30%, and 22% of the total, respectively. Figure 2.1 summarized the sampling and extraction of MPs from water and sediment. For water samples, 55% of the studies utilized the volume reduction method, 39% utilized the bulk sampling method, and the remaining studies (6%) involved both volume reduction and bulk sampling methods. Studies sampled water depths

of  $\leq 10$ ,  $>10 \ \& \ \leq 20$ ,  $>20 \ \& \ \leq 30$ ,  $>30 \ \& \ \leq 50$ ,  $>50 \ \& \ \leq 100$ , and  $> 100$  cm, which represented 9%, 9%, 9%, 13%, 10%, and 6%, respectively. The mesh/filter sizes of  $< 10$ ,  $> 10 \ \& \ \leq 50$ ,  $> 50 \ \& \ \leq 100$ ,  $> 100 \ \& \ \leq 500$ , and  $> 500$   $\mu\text{m}$  represented 13%, 24%, 4%, 48%, and 2% of the studies, respectively. Mesh size of around 300  $\mu\text{m}$  is the most commonly used size for water sampling, accounting for 45% of the studies. 7 studies used not only one mesh/filter size. In terms of the extraction of MPs from water samples, 24% of the studies utilized only filtration or sieving, 34% utilized only digestion with filtration or sieving, 5% utilized only density separation with filtration or sieving, 30% utilized digestion followed by density separation with filtration or sieving, and 5% utilized density separation with filtration or sieving followed by digestion. For studies that applied density separation to collect MPs in water samples, fluids with a density of 1.2  $\text{g}/\text{cm}^3$  were most often used, accounting for 66% of the studies, and those with a density greater than 1.2  $\text{g}/\text{cm}^3$  accounted for 34%.

All the studies employed bulk sampling to collect MPs in sediment. The studies sampled sediment depths of  $\leq 10$ ,  $> 10 \ \& \ \leq 20$ ,  $> 20 \ \& \ \leq 30$ ,  $> 50 \ \& \ \leq 100$ , and  $> 100$  cm accounted for 58%, 1%, 4%, 4%, and 4%, respectively. For MP sampling in sediment, mesh or filter size of  $< 10$ ,  $> 10 \ \& \ \leq 50$ ,  $> 50 \ \& \ \leq 100$ , and  $> 100 \ \& \ \leq 500$   $\mu\text{m}$  accounted for 45%, 14%, 10%, and 18% of the studies, respectively. In the remaining studies, neither the mesh size nor the filter size was specified for sediment collection. Among these studies, 28% of the studies used only density separation with filtration or sieving to extract MPs from sediment, 34% of the studies used digestion followed by density separation with filtration or sieving, and 27% of the studies used density separation followed by digestion with filtration or sieving. Two studies employed density separation, digestion, and density separation steps, and one study employed digestion, density separation, and digestion steps. Furthermore, two studies used dispersant as part of the extraction

step, and three studies did not detail the extraction process. For the density of separation fluid used to collect MPs in sediment samples, 35% studies used a fluid density  $\leq 1.2 \text{ g/cm}^3$ , 45% used a fluid density  $> 1.2 \text{ \& } \leq 1.6 \text{ g/cm}^3$ , 11% used a fluid density  $> 1.6 \text{ g/cm}^3$ . FTIR, Raman, visual identification, and stereomicroscope accounted for 77%, 10%, 3%, and 9%, respectively, of the identification techniques used to determine the MPs. In addition, one study identified MPs using Pyrolysis–gas chromatography–mass spectrometry (Py-GC-MS).



- AA Volume reduction + Bulk sampling (6%)
- AB  $\leq 10$  cm (9%)
- AC  $> 30$  &  $\leq 50$  cm (14%)
- AD  $> 100$  cm (6%)
- AE  $> 20$  &  $\leq 30$  cm (9%)
- AF  $> 50$  &  $\leq 100$  cm (10%)
- AG  $> 10$  &  $\leq 20$  cm (9%)
- AH 100 - 500  $\mu\text{m}$  (6%)
- AI 50 - 100  $\mu\text{m}$  (5%)
- AJ 10 - 50  $\mu\text{m}$  (2%)
- AK Separation + Digestion (5.32%)
- AL Filtration (10%)
- AM Separation (5%)
- AN  $> 1.6$  (6%)
- AO  $> 1.4$  &  $\leq 1.6$  (5%)
- AP  $> 1.2$  &  $\leq 1.4$  (2%)
- AQ Vision (3%)
- AR Microscopy (12%)
- AS Raman (10%)
- AT GC MASS (1%)
- NA Not available
- BA  $> 100$  cm (4%)
- BB  $> 10$  &  $\leq 20$  cm (1%)
- BC  $> 50$  &  $\leq 100$  cm (4%)
- BD  $> 20$  &  $\leq 30$  cm (4%)
- BE Digestion (10%)
- BF Other (7%)
- BG  $\geq 1.2$  &  $< 1.4$  (11%)
- BH  $> 1.6$  (11%)
- BI Microscopy (6%)
- BJ Raman (11%)
- BK Vision (3%)

**Figure 2.1** The sampling, extraction, and identification techniques used to analyze MPs in water and sediment.

### 2.2.2 Global distribution of MPs in estuaries

MPs varied considerably in water and sediment. MP abundance in water ranged from  $2.00 \times 10^{-4}$  to  $1.39 \times 10^6$  items/m<sup>3</sup> with a mean of  $2.13 \times 10^4 \pm 1.23 \times 10^5$  items/m<sup>3</sup> and from 0.90 to  $1.16 \times 10^5$  items/kg with a mean of  $1.31 \times 10^3 \pm 6.30 \times 10^3$  items/kg in sediment (Figure 2.2, Table 2.1). The highest MP abundance in water was detected in the north subtropics (30–40°N), followed by the north tropics (0–30°N), south subtropics (30–40°S), north temperate zone (40–60°N), south tropics (0–30°S), and south temperate zone (40–60°S), with abundances of  $5.86 \times 10^4 \pm 2.10 \times 10^5$ ,  $1.70 \times 10^4 \pm 6.18 \times 10^4$ ,  $8.30 \times 10^2 \pm 1.48 \times 10^3$ ,  $5.38 \times 10^2 \pm 1.42 \times 10^3$ ,  $3.49 \times 10^2 \pm 7.80 \times 10^2$ , and  $8.10 \times 10^{-1}$  items/m<sup>3</sup>, respectively (Figure 2.2b, Table 2.2). The north temperate zone has the highest MP abundance in sediment, followed by the south temperate zone, north tropics, north subtropics, south subtropics, and south tropics, with respective values of  $6.41 \times 10^3 \pm 2.65 \times 10^4$ , 3315,  $2274.49 \pm 7250.77$ , and  $606.54 \pm 945.01$ ,  $251.83 \pm 244.27$ ,  $241.84 \pm 206.48$  items/kg (Figure 2.2d).

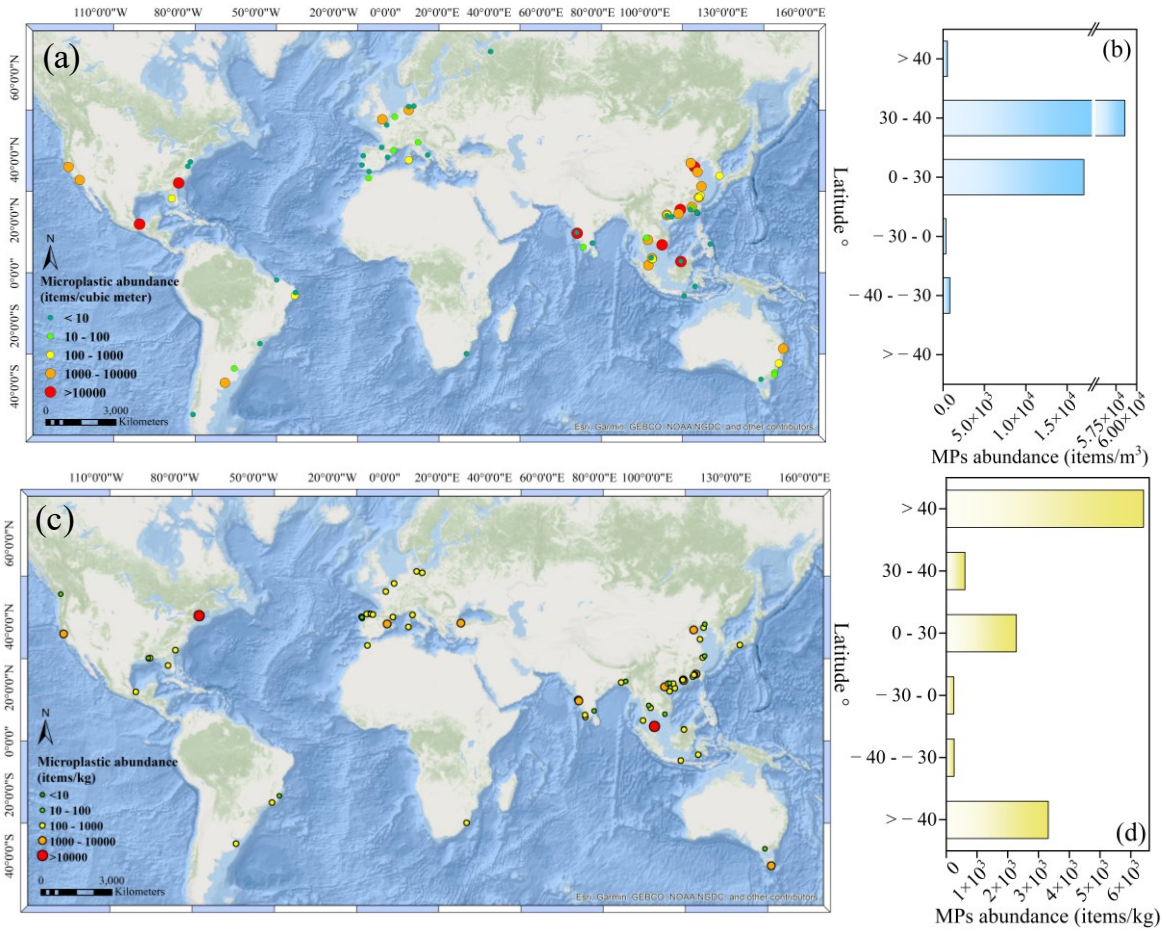


**Figure 2.2** Global distribution of MP abundance in water (a) and sediment (b), and latitudinal distribution of MP abundance in water (c) and sediment (d)

Table 2.1 MP abundance in estuarine water.

Number	Estuary name	Longitude	Latitude	Abundance (items/m <sup>3</sup> )
1	KwaZulu-Natal Estuary	31.13	-29.63	1.64
2	Charleston Harbor Estuary	-79.89	32.79	11103.25
3	Adour Estuary	-1.52	43.53	0.96
4	Pearl River Estuary	113.07	22.28	2648.80
5	Terengganu Estuary	103.12	5.32	421.37
6	Jiaojiang Estuary	121.53	28.66	951.22
7	Oujiang Estuary	120.94	27.98	682.93
8	Minjiang Estuary	120.95	27.98	722.28
9	Yangtze Estuary	121.84	31.68	5387.04
10	Goiana Estuary	-34.83	-7.50	0.00
11	Xiamen Bay Estuary	118.19	24.64	4084.44
12	Chao Phraya River Estuary	100.65	13.48	10.68
13	Baram River Estuary	113.97	4.59	0.01
14	Mandovi-Zuari Estuary	73.79	15.43	0.10
15	Weser Estuary	8.87	53.06	1488.48
16	Tweed River Estuary	153.42	-27.97	2215.65
17	Maozhou River Estuary	113.78	23.75	66500.00
18	North Setiu Wetland	102.80	5.67	2312.50
19	Guadalquivir Estuary	-6.38	36.38	0.04
20	Gulf of Mexico Estuary	-95.00	18.50	151000.00
21	Miri River Estuary	113.98	4.40	12300.00
22	Rio Formoso Estuary	-35.09	-8.69	568.48
23	Río de la Plata Estuary	-58.44	-34.48	96.28
24	Lawaan River Estuary	125.30	11.14	0.96
25	Tallo River Estuary	119.45	-5.10	2.67
26	Sebou Estuary	-6.55	34.34	72.75
27	Sal Estuary	73.95	15.16	48000.00
28	Dongshan Bay Estuary	117.61	23.73	1.66

Number	Estuary name	Longitude	Latitude	Abundance (items/m <sup>3</sup> )
29	Maowei Sea Estuary	108.56	21.84	3551.45
30	Klang River Estuary	101.39	3.00	2476.41
31	Badung River Estuary	115.22	-8.73	0.59
32	Sado Estuary	-9.15	38.43	0.44
33	Martinez-Baker Estuary	-74.36	-47.77	0.81
34	Erren River Estuary	120.17	22.91	0.24
35	Agongdian River Estuary	120.20	22.80	0.34
36	Dianbao River Estuary	120.25	22.72	0.32
37	Houjin River Estuary	120.26	22.71	0.22
38	Love River Estuary	120.29	22.62	0.36
39	Canon River Estuary	120.30	22.60	0.90
40	Chienchen River Estuary	120.30	22.58	0.66
41	Salt River Estuary	120.34	22.54	0.23
42	Gaoping River Estuary	120.42	22.47	0.40
43	Jiaozhou Bay Estuary	120.32	36.26	1348.15
44	Jiulong River Estuary	118.11	24.26	85.43
45	Chesapeake Bay Estuary	-76.35	37.99	0.16
46	Po Delta	12.51	44.96	14.84
47	Elbe Estuary	8.95	53.87	1.56
48	Trave Estuary	10.89	53.96	0.30
49	Qin River Estuary	108.58	21.83	160.76
50	Cherating River estuary	102.49	5.87	0.01
51	Cochin Estuary	76.27	10.01	75.17
52	Acaraí Lagoon	-48.52	-26.25	0.01
53	Linkun Island	120.94	27.94	3470.00
54	Port Phillip Bay Estuary	144.90	-37.84	0.00
55	Bahía Blanca Estuary	-62.05	-38.93	3767.63
56	Ebro River Delta	0.72	40.71	3.10
57	Tampa Bay	-82.57	27.61	572.57

Number	Estuary name	Longitude	Latitude	Abundance (items/m <sup>3</sup> )
58	Hunter Estuary	151.74	-32.85	951.56
59	Bage Estuary	150.07	-36.42	78.82
60	Clyde Estuary	150.21	-35.70	84.03
61	Dagu Estuary	117.72	38.96	1194.71
62	Douro Estuary	-8.66	41.14	0.16
63	Maowei Sea Estuary	108.55	21.89	7100.00
64	Long Beach	-118.11	33.74	8637.67
65	Saigon River Estuary	106.72	10.76	355910.35
66	Seine River Estuary	0.41	49.45	9.98
67	Scheldt River Estuary	3.50	51.49	21.64
68	Parnaíba and Jaguaribe River Estuary	-42.12	-2.67	0.16
69	Northern Dvina River Estuary	40.49	64.61	0.01
70	Yellow River Estuary	119.24	37.79	789357.62
71	Delaware Bay Estuary	-75.38	39.33	0.93
72	Hamble Estuary and Beaulieu Estuary	-1.31	50.85	4833.33
73	Nakdong River Estuary	128.92	35.05	936.92
74	Ofanto River Estuary	16.20	41.36	6.00
75	Têt River Estuary	3.04	42.71	78.36
76	San Francisco Bay Estuary	-122.47	37.81	1860.69
77	Vellar Estuary	79.77	11.50	2.07
78	Dafeng River Estuary	108.57	21.59	0.50
79	Lis River Mouth	8.96	39.88	233.76
80	Zhanjiang Bay Estuary	110.43	21.18	0.39
81	Rayong River Estuary	101.28	12.66	1174.00

Table 2.2 MP abundance in estuarine sediment.

Number	Estuary name	Longitude	Latitude	Abundance (items/kg)
1	KwaZulu-Natal Estuary	31.13	-29.63	159.67
2	Bay Champagne Estuary	-90.18	30.17	77.90
3	Little Lake Estuary	-90.08	30.10	640.87
4	Golden Horn Estuary	28.96	40.99	1960.00
5	Bang Yai Canal Mouth	98.39	7.87	324.13
6	Kayamkulam Estuary	76.46	9.16	460.10
7	Pearl River Estuary	113.60	22.77	716.30
8	Mississippi Gulf Coast Marshes	-89.52	30.18	125.83
9	Atlantic Argentinean Estuaries	-56.77	-36.32	424.55
10	Ria de vigo Estuary	-8.68	42.28	74.63
11	Ría de Pontevedra Estuary	-8.70	42.42	86.90
12	Ría de Arousa Estuary	-8.78	42.64	36.10
13	Ría de Muros Estuary	-8.93	42.79	130.00
14	Jinjiang Estuary	118.63	24.79	2033.33
15	Yunxiao Mangrove	117.40	23.88	477.61
16	Futian Mangrove	113.93	22.50	2985.07
17	Zhanjiang Mangrove	109.91	21.45	298.51
18	Fangchenggang Mangrove	107.95	21.47	179.10
19	Dongzhaigang Mangrove	110.53	19.85	447.76
20	Dongfang Mangrove	108.60	18.72	686.57
21	Yangtze Estuary	121.93	30.87	71.39
22	Osaka Bay estuary	135.34	34.44	506.33
23	Jagir Estuary	112.82	-7.31	345.20
24	Qiantang River Esturay	121.17	30.38	259.90
25	Mekong River Estuary	106.76	10.27	42.50
26	Warnow Estuary	12.09	54.18	112.18
27	Eo Estuary	-7.00	43.55	295.00
28	Avilés Estuary	-5.93	43.60	308.50

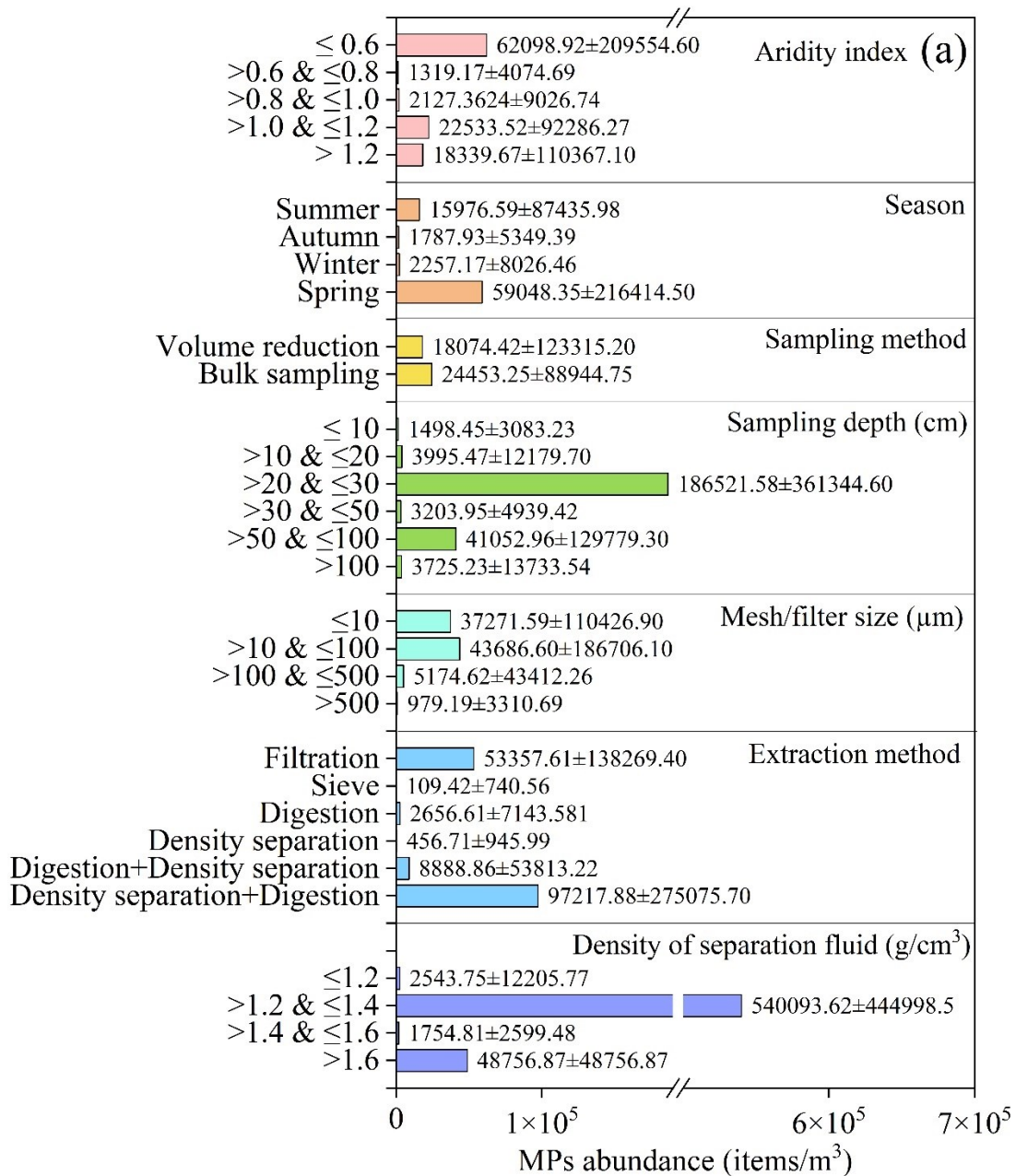
Number	Estuary name	Longitude	Latitude	Abundance (items/kg)
29	Villaviciosa Estuary	-5.38	43.53	291.50
30	Llanes Estuary	-4.61	43.40	210.00
31	Guanabara Bay Estuary	-43.04	-22.70	551.48
32	Vitoria Bay Estuary	-40.29	-20.32	41.17
33	Cecina River Estuary	10.49	43.30	105.50
34	Maowei Sea Estuary	113.78	22.76	820.68
35	Derwent Estuary	147.29	-42.79	3315.00
36	Oder/Peene Estuary	14.22	53.87	425.00
37	Têt River Estuary	3.04	42.72	163.89
38	Cowichan-Koksilah Estuary	-123.62	48.76	14.64
39	Liaohe Estuary	121.97	40.67	97.07
40	Changjiang Estuary	121.84	31.68	121.00
41	Fuzhou River Estuary	121.51	39.67	320.00
42	Great Bay Estuary	-70.87	43.07	116000.00
43	Xiamen Bay Estuary	118.20	24.65	235.50
44	Baram River Estuary	114.03	4.57	680.26
45	Mandovi-Zuari Estuary	73.77	15.48	5632.70
46	North Setiu wetland	102.81	5.67	40261.43
47	Estuary in Gulf of Mexico	-95.00	18.50	121.00
48	Miri River Estuary	114.01	4.47	356.22
49	Tallo River Estuary	119.45	-5.10	111.67
50	Sebou Estuary	-6.67	34.27	122.63
51	Sal Estuary	73.96	15.22	3727.25
52	Cochin Estuary	76.28	9.96	134.00
53	Port Phillip Bay Estuary	144.90	-37.84	79.10
54	Ebro River Delta	0.86	40.74	1023.12
55	Tampa Bay Estuary	-82.70	27.73	278.89
56	Dagu Estuary	117.72	38.98	1220.55

Number	Estuary name	Longitude	Latitude	Abundance (items/kg)
57	Charleston Harbor Estuary	-79.89	32.79	433.59
58	Jiulong River Estuary	117.81	24.46	156.67
59	Seine River Estuary	0.31	49.43	300.00
60	Scheldt River Estuary	3.52	51.41	210.96
61	Jiaozhou Bay Estuary	120.14	36.18	334.00
62	Maozhou River Estuary	113.78	22.76	7279.50
63	Chao Phraya River Estuary	100.58	13.55	39.38
64	Red River Delta	106.60	20.27	1157.76
65	San Francisco Bay Estuary	-122.50	37.79	3577.80
66	Rayong River Estuary	101.28	12.66	227.00
67	Vellar Estuary	79.77	11.50	31.18
68	Galachipa and Andharmanik River Estuary	90.09	21.85	231.25
69	Dafeng River Estuary	108.55	21.59	14.07
70	Lis River Mouth	8.96	39.88	416.67
71	Karnaphuli River Estuary	91.82	22.23	39.76

### 2.2.3 Patterns of MP abundance affected by sampling, extraction, and environment

Figure 2.3 depicts the categorization of MP abundance into various environments, sampling, and extraction. In terms of the aridity index, the MP abundance for aridity index  $\leq 0.6$ ,  $> 0.6 \& \leq 0.8$ ,  $> 0.8 \& \leq 1.0$ ,  $> 1.0 \& \leq 1.2$ , and  $> 1.2$  are  $6.21 \times 10^4 \pm 2.10 \times 10^5$ ,  $1.32 \times 10^3 \pm 4.07 \times 10^3$ ,  $2.13 \times 10^3 \pm 9.03 \times 10^3$ ,  $2.25 \times 10^4 \pm 9.23 \times 10^4$ ,  $1.83 \times 10^4 \pm 1.10 \times 10^5$  items/m<sup>3</sup>, respectively, in water samples, and are  $3.93 \times 10^2 \pm 6.98 \times 10^2$ ,  $4.15 \times 10^2 \pm 1.23 \times 10^3$ ,  $1.33 \times 10^3 \pm 1.12 \times 10^4$ ,  $2.41 \times 10^2 \pm 5.74 \times 10^2$ ,  $2.56 \times 10^3 \pm 7.00 \times 10^3$  items/kg in sediment samples. For different sampling seasons, the summer, autumn, winter, and spring have respective MP abundances of  $1.60 \times 10^4 \pm 8.74 \times 10^4$ ,  $1.79 \times 10^3 \pm 5.35 \times 10^3$ ,  $2.26 \times 10^3 \pm 8.03 \times 10^3$ ,  $5.90 \times 10^4 \pm 2.16 \times 10^5$  items/m<sup>3</sup> in water samples, and  $3.51 \times 10^2 \pm 1.09 \times 10^3$ ,  $2.20 \times 10^3 \pm 7.47 \times 10^3$ ,  $4.96 \times 10^2 \pm 1.02 \times 10^3$ , and  $1.16 \times 10^3 \pm 2.24 \times 10^3$  items/kg in sediment samples. The volume reduction method for sampling MPs in water yielded  $1.81 \times 10^4 \pm 1.23 \times 10^5$  items/m<sup>3</sup>, whereas the bulk sampling method yielded  $2.45 \times 10^4 \pm 8.89 \times 10^4$  items/m<sup>3</sup>, indicating that bulk sampling yields a greater MP abundance. Even at depths greater than 1 m, a significant number of MPs were detected. MPs were found to be more abundant in the 0–30 cm sediment layers than in the sediment layers below. Regarding the size of the mesh or filter used to collect MPs, a decreasing trend in MP abundance toward an increasing mesh or filter size was observed. The mesh or filter sizes of  $\leq 10$ ,  $>10 \& \leq 100$ ,  $>100 \& \leq 500$ , and  $>500 \mu\text{m}$  have MP abundances of  $3.73 \times 10^3 \pm 1.10 \times 10^5$ ,  $4.37 \times 10^4 \pm 1.87 \times 10^5$ ,  $5.17 \times 10^3 \pm 4.34 \times 10^4$ ,  $9.79 \times 10^2 \pm 3.31 \times 10^3$  items/m<sup>3</sup> in water, and  $2.24 \times 10^3 \pm 8.90 \times 10^3$ ,  $1.54 \times 10^3 \pm 7.14 \times 10^4$ ,  $5.64 \times 10^2 \pm 8.76 \times 10^2$  items/kg in sediment. For the extraction of MPs from water samples, studies that only employed filtration demonstrated a higher MP abundance than those that only employed sieving. Chemical digestion, density separation, chemical digestion followed by density separation, and density separation followed by chemical digestion had respective MP abundances of  $2.66 \times 10^3 \pm 7.14 \times 10^3$ ,  $4.57 \times 10^2 \pm$

$9.46 \times 10^2$ ,  $8.89 \times 10^3 \pm 5.38 \times 10^4$ , and  $9.72 \times 10^4 \pm 2.75 \times 10^5$  items/m<sup>3</sup>. To extract MPs from sediment samples, processing only involved density separation exhibited higher MP abundance than chemical digestion followed by density separation or density separation followed by chemical digestion. Regarding the density of the flotation fluid, there is no discernible pattern among the various density groups.



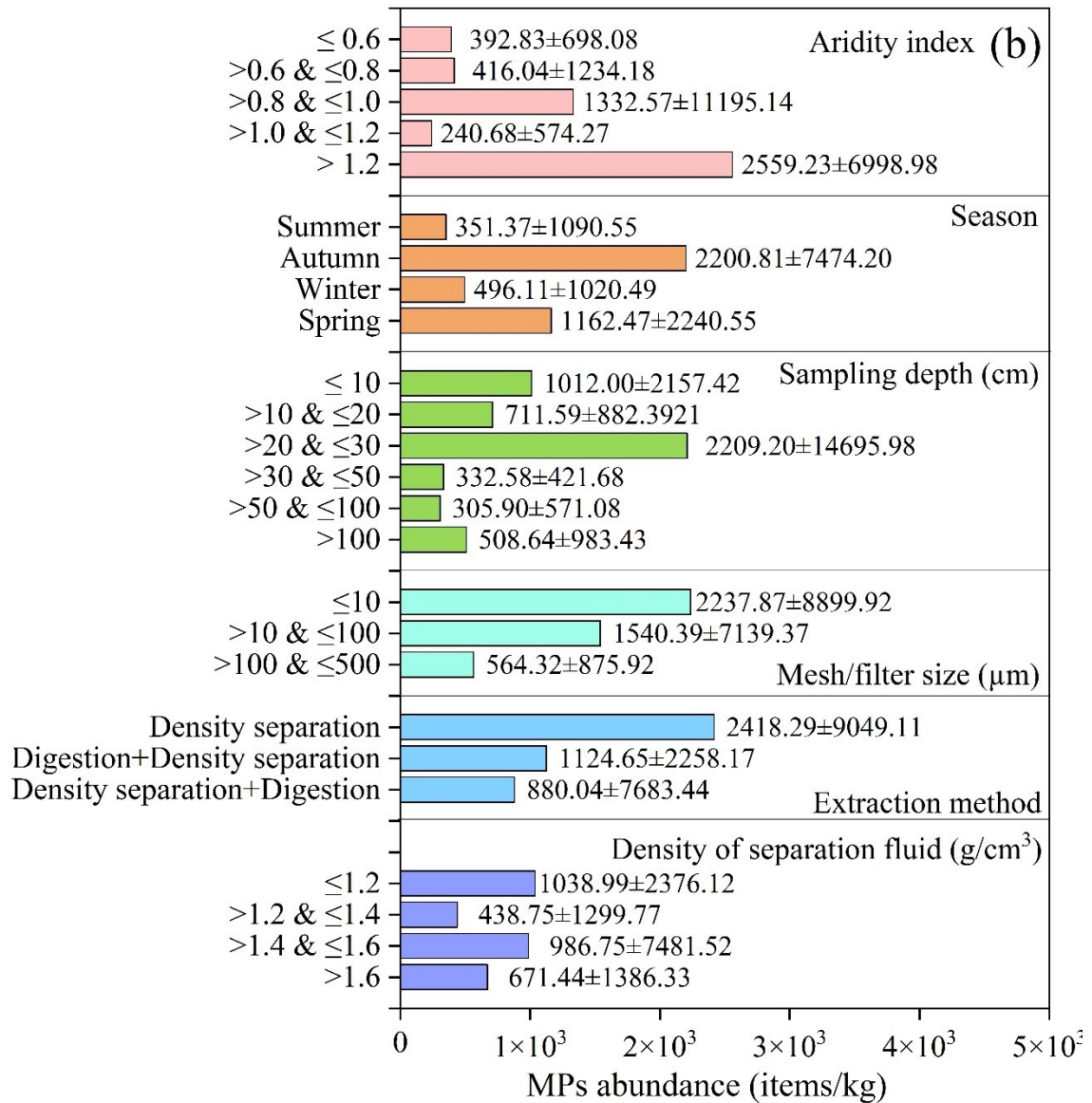


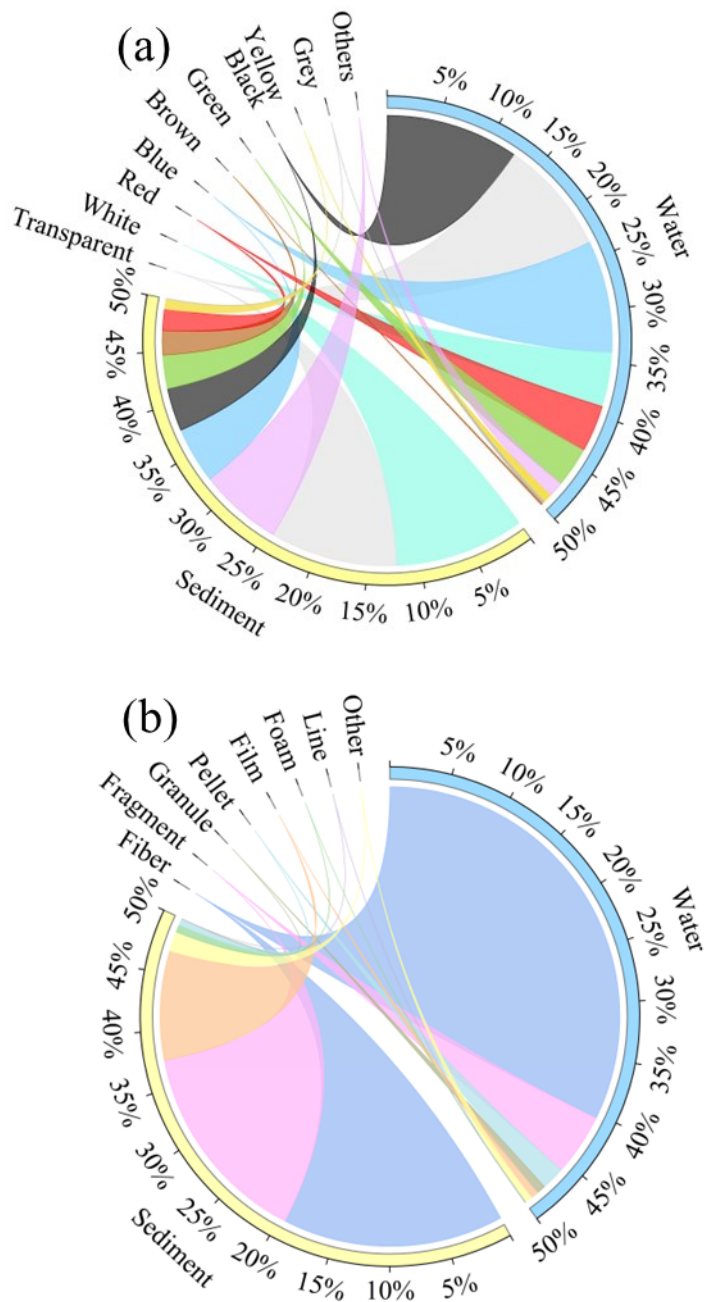
**Figure 2.3** MP abundances in various environmental, sampling, and extraction categories in water (a) and sediment (b).

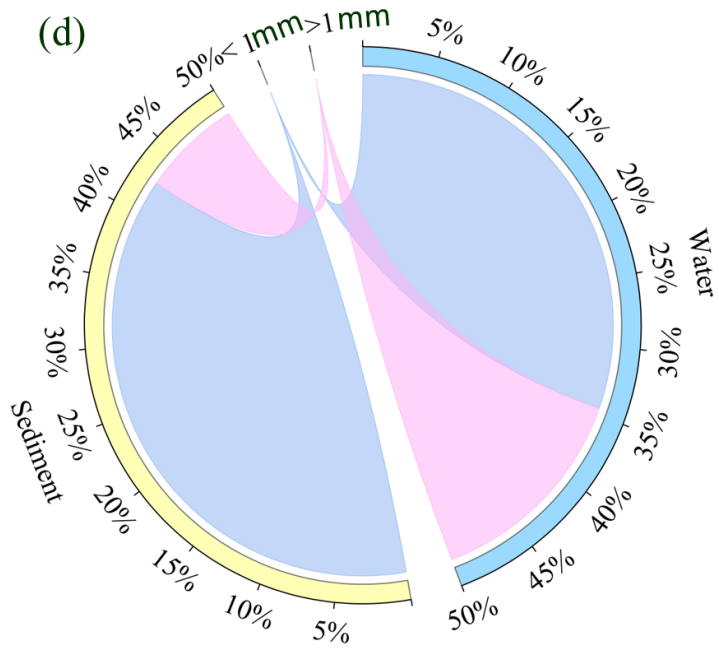
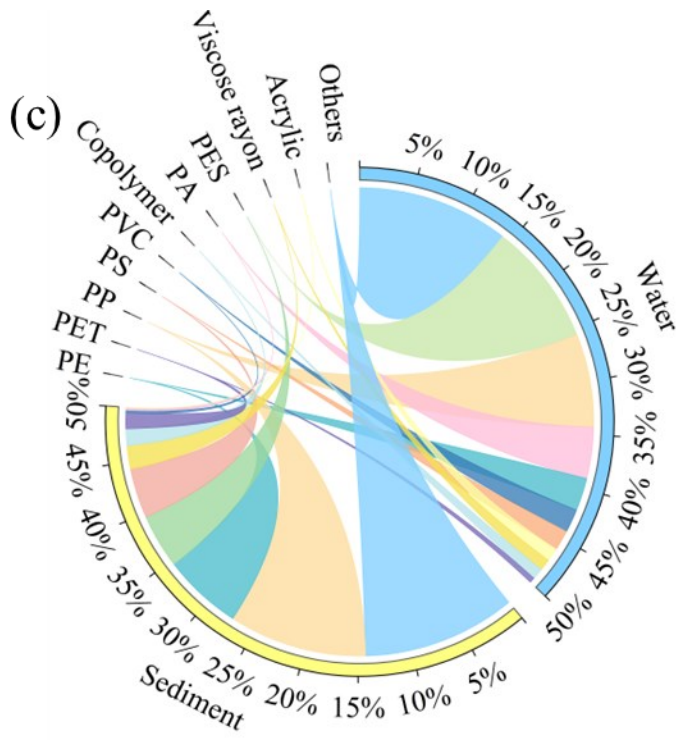
#### 2.2.4 Characteristics of MP morphology in global estuaries

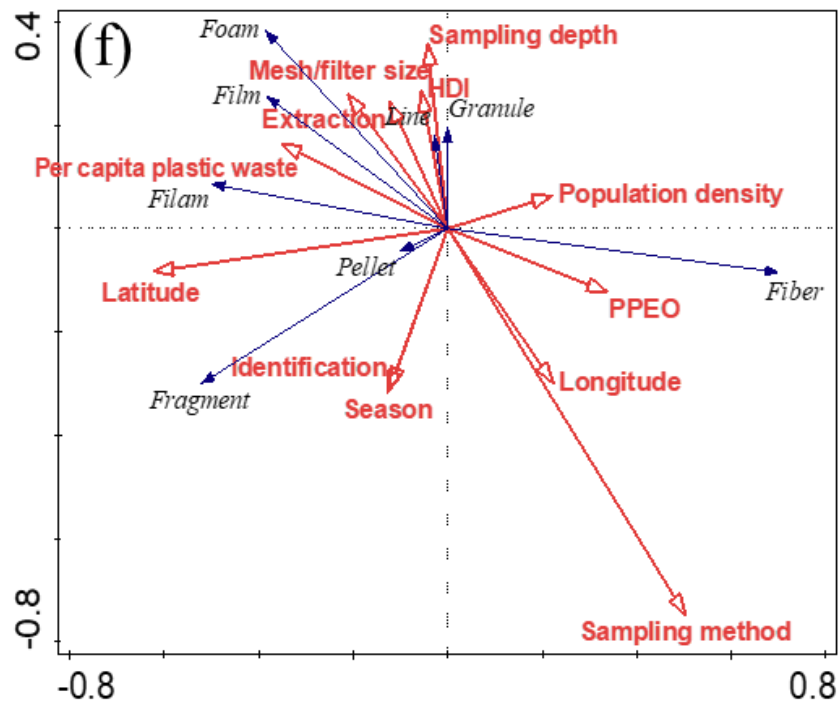
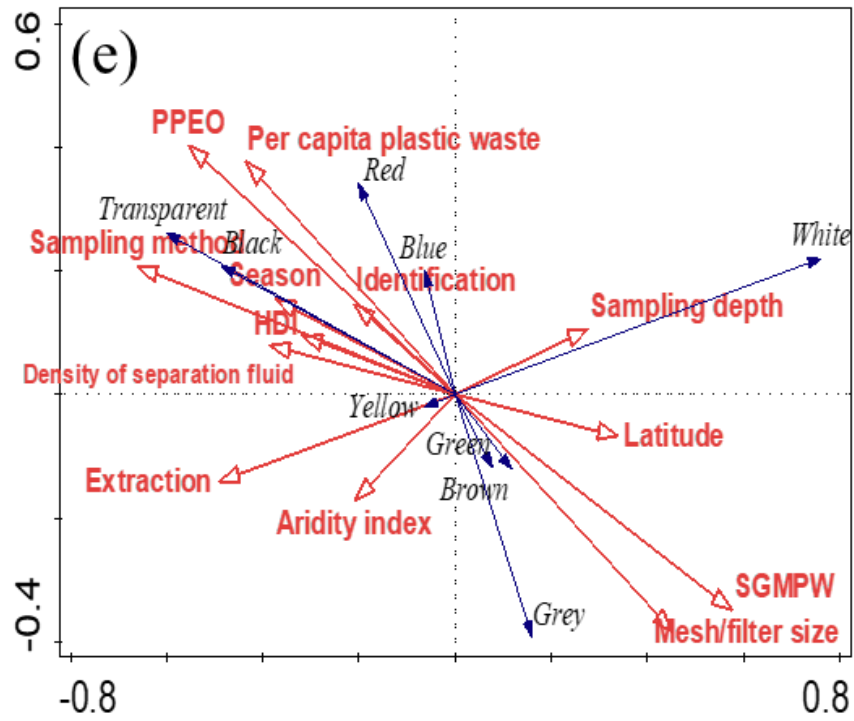
The fractions of color, shape, polymer composition, and size of MPs in estuaries are shown in Figure 2.4a–d. The most abundant MPs colors in water were black, transparent, and blue, taking a proportion of 25.16%, 21.68%, and 21.24%, respectively. Colors of white, red, green, and yellow accounted for 10.15%, 8.90%, 7.51%, and 1.66%, respectively. 24.53% and 24.04% of sediment's MPs were white and transparent, respectively, followed by blue (10.62%), black (8.12%), green (6.29%), brown (4.61), red (4.03%), and yellow (1.93%). The most prevalent MP shape in water was fiber, accounting for 80.72%, followed by fragment (10.88%) and pellet (4.07%). In sediment, fiber and fragment are also the most frequently detected MPs, comprising 38.87 and 36.01%, respectively, followed by film (19.17%), foam (1.28%), and pellet (1.16%). PES and PP are the two most frequently detected MPs in water (22.88% and 17.40%, respectively), followed by PA, PE, PVC, and PS (9.44%, 6.11%, 4.34%, and 3.76%, respectively). In sediment, the proportions of PP, PE, PES, and PS are 25.75%, 14.79%, 10.12%, and 9.24%, respectively. In addition, 68.73% and 85.51% of the MPs detected in water and sediment are smaller than 1 mm.

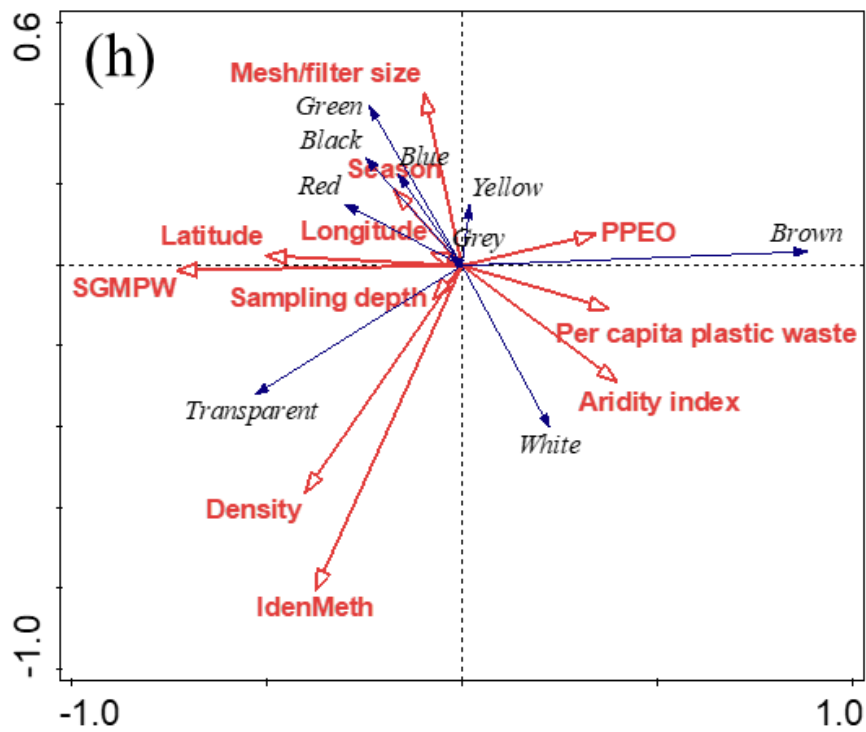
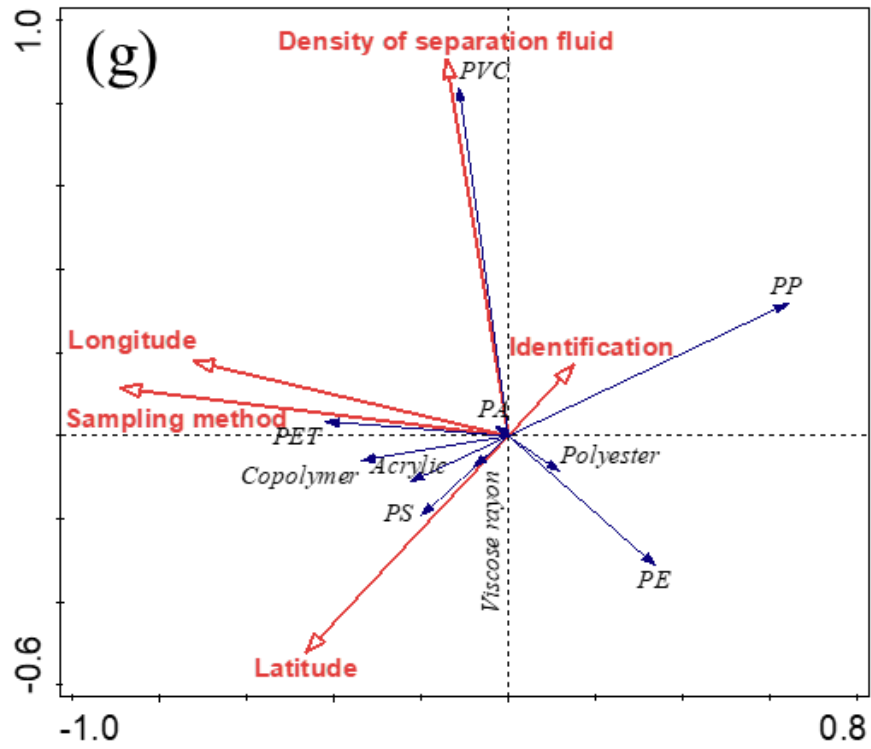
RDA indicates that the effects of a set of explanatory factors on the fractions of MP morphological characteristics varied between water and sediment. In Figure 2.4e–j, only significant factors are displayed. More than 10% of the variance in MP color in water can be attributed to the sampling and extraction methods, respectively. While share of global mismanaged plastic waste was the most important factor in explaining the variation in sediment (14.9%). Latitude explained 13.8% of the variance in the shapes of MPs detected in water. However, plastic waste per capita accounted for 27.8% of the variation in sediment. The

sampling method explained 17.9% of the variation in the MP composition in water, while the identification method and latitude explained most of the variation in sediment (14.4% and 11.9%).









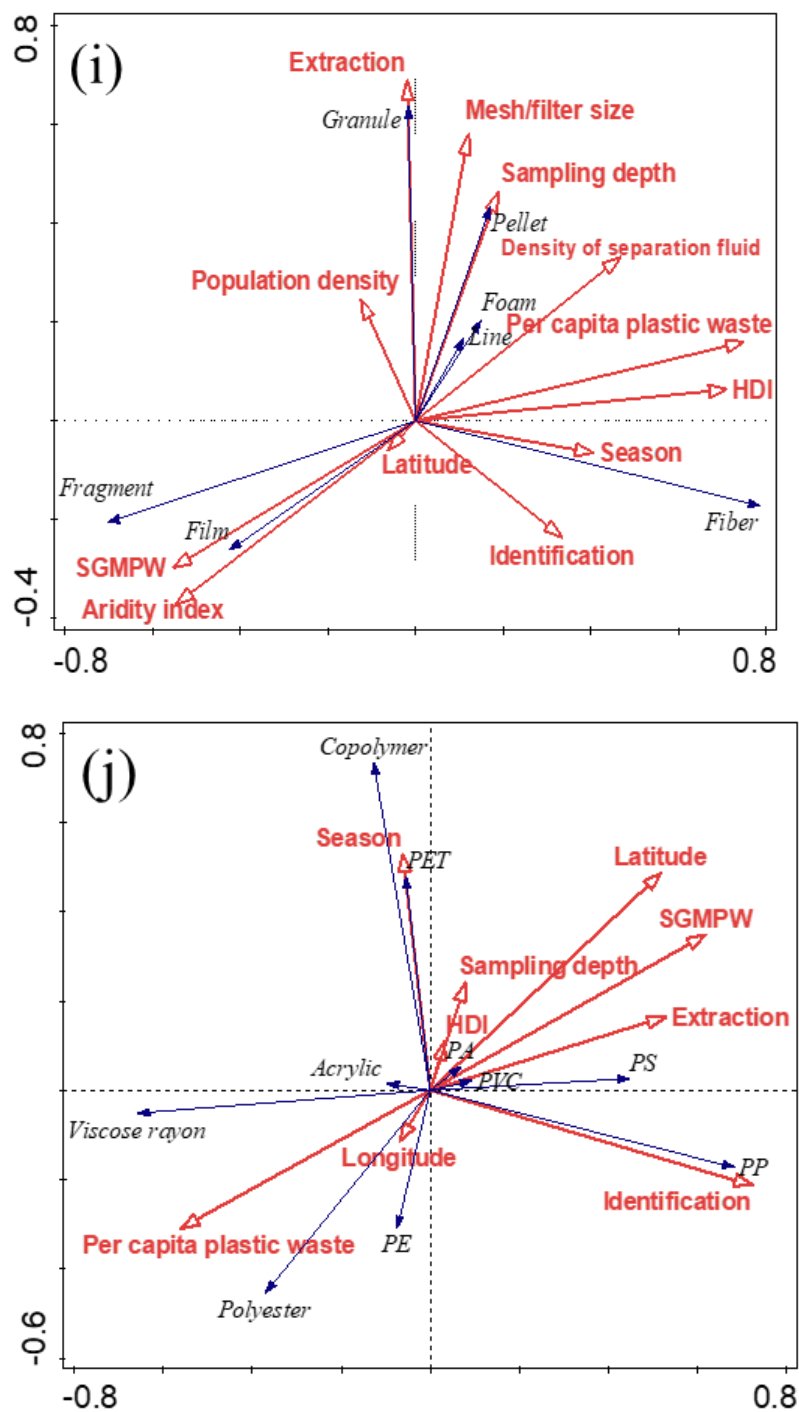


**Figure 2.4** (a-d) Fractions of color, shape, type, and size of MPs in water and sediment. (e-j) RDA of the color (e, h), shape (f, i), and type (g, j) of MPs in water (e-g) and sediment (h-j) explained by explanatory factors. PPEO denotes the probability of plastic being emitted to ocean and SGMPW denotes the share of global mismanaged plastic waste.

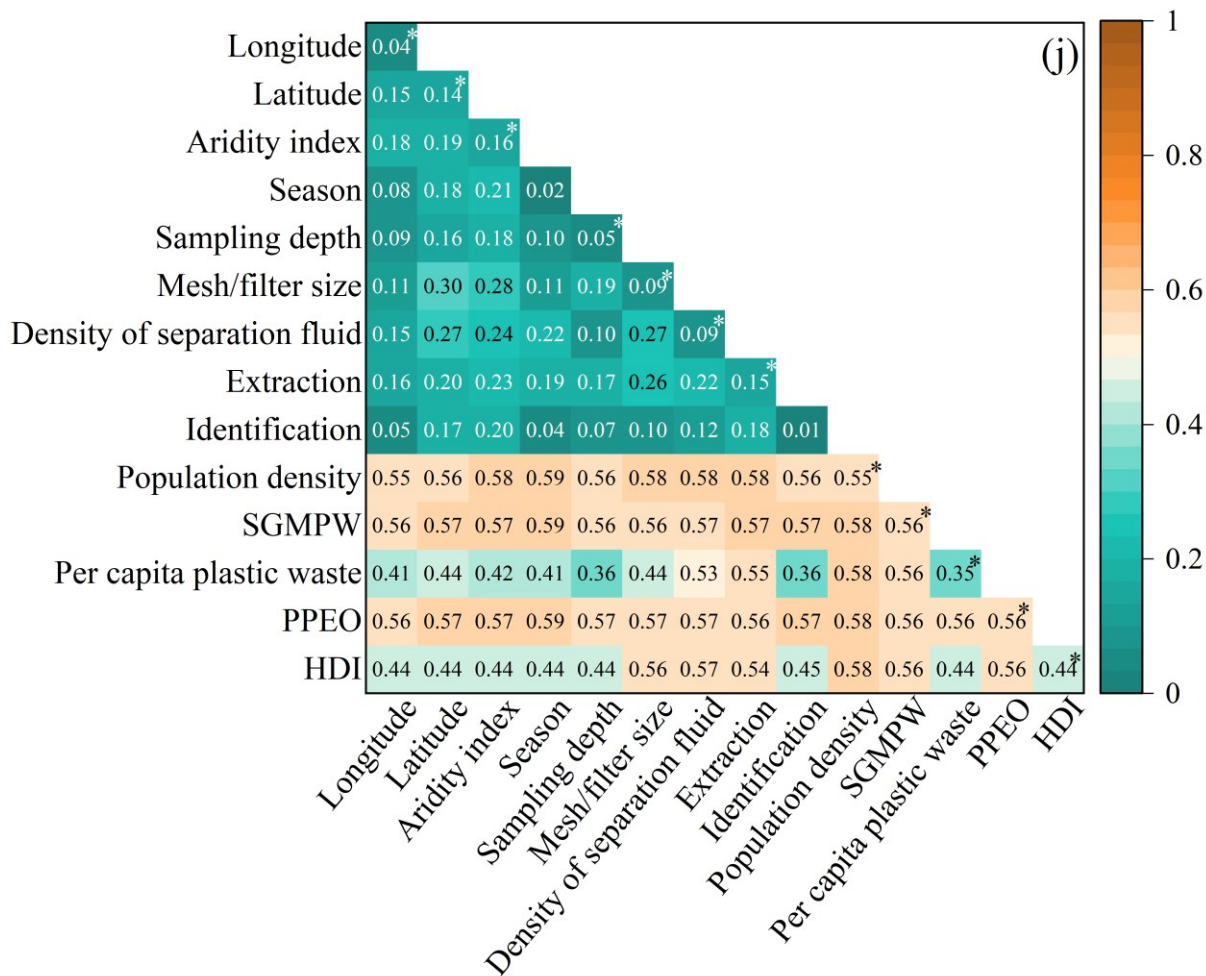
### 2.2.5 Driving factors of MP abundance in global estuaries

The regression analysis between MP abundance and various numerical factors, including aridity index, mesh/filter size, density of separation fluid, sampling depth, population, share of global mismanaged plastic waste, per capita plastic waste (kg/person/day), and probability of plastic being emitted to ocean, was performed to unveil their potential interactions. Figure 2.5a-h illustrate significant linear interactions between MP abundance and a variety of variables (insignificant regression is not presented). It should be noted that the purpose of the regression is only to reveal the general relationship between the variables and the mathematical predictions should be interpreted with caution. Significantly negative correlations are found between MP abundance in water and mesh/filter size, per capita plastic waste (kg/person/day), and HDI. Nonetheless, the correlation between MP abundance in water and population, as well as share of global mismanaged plastic waste, is significantly positive. Both the aridity index and probability of plastic being emitted to ocean are significantly positively correlated with MP abundance in sediment. However, the correlation between MP abundance in sediment and mesh/filter size is significantly negative.

Figure 2.5i-j depict the Geodetector's findings. The greater the q-value, the greater the explanatory variables' influence on the dependent variables. The effects of longitude, latitude, aridity index, season, sampling depth, mesh/filter size, density of flotation fluid, extraction method, population density, share of global mismanaged plastic waste, probability of plastic being emitted to ocean, and HDI on MP abundance are significant ( $p < 0.05$ ). Thereinto, the three highest q values are extraction method, flotation fluid density, and sampling depth (0.88, 0.58, and 0.30). Longitude, latitude, aridity index, sampling depth, mesh/filter size, density, extraction method, population density, share of global mismanaged plastic waste, per capita plastic waste,

probability of plastic being emitted to ocean, and HDI have significant effects on MP abundance in sediment ( $p < 0.05$ ). The highest  $q$  values are associated with the share of global mismanaged plastic waste, probability of plastic being emitted to ocean, and population density (0.56, 0.56, 0.55). The interaction of these explanatory factors enhances the explanatory power on MP abundance in both water and sediment. Thereinto, the interactions of the density of separation fluid and extraction method with other factors maximized the  $q$  value greatly for water samples (Figure 2.5i). For sediment, the interactions of population density, share of global mismanaged plastic waste, and probability of plastic being emitted to ocean with other explanatory factors enlarge the  $q$  value greatly (Figure 2.5j).

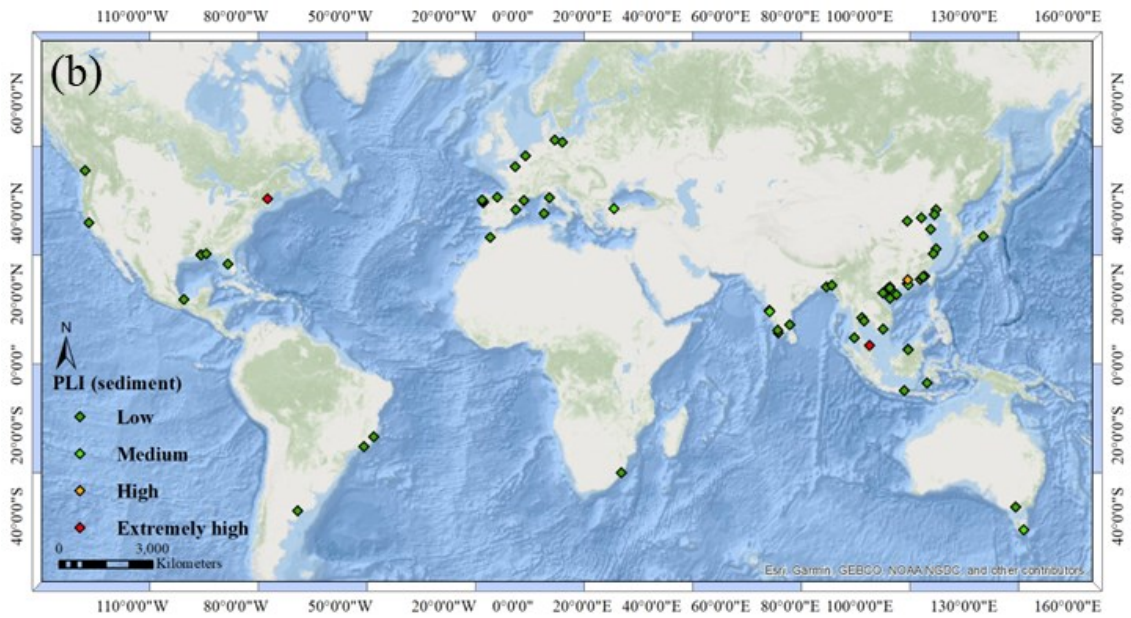
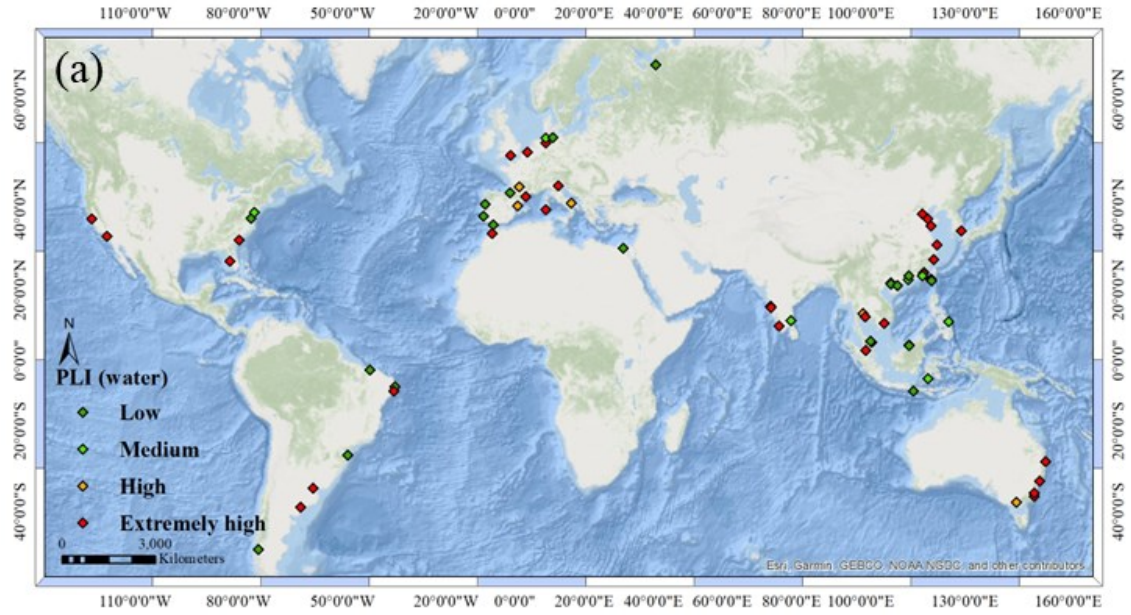




**Figure 2.5** Relationship between explanatory factors and MP abundance in water (a-e) and sediment (f-h). Geodector result for water (i) and sediment (j). The values on the diagonal line are q-value of individual explanatory factors, and \* denotes 5% significance.

### 2.2.6 Risk assessment of MPs in global estuaries

According to the PLI in water, 36%, 10%, 6 %, and 47% of estuaries were categorized into low, moderate, high, or extremely high levels of pollution, respectively (Figure 2.6a, Table 2.3). Regarding the PLI in sediment, 86%, 10%, 1 %, and 3% of estuaries, respectively, had low, moderate, high, and extremely high levels (Figure 2.6b, Table 2.4). 73 % of estuaries exhibited a risk level of V with respect to ERI in water, while 4% and 23% exhibited risk levels of III and IV, respectively (Figure 2.6c, Table 2.5). For the sediment phase, the proportion of risk level V was the highest (43%), followed by risk levels I, II, IV, and III, which accounted for 22%, 13%, 13%, and 9%, respectively (Figure 2.6d, Table 2.6). In general, the risk levels of MPs in water were higher than those in sediment at a given site.



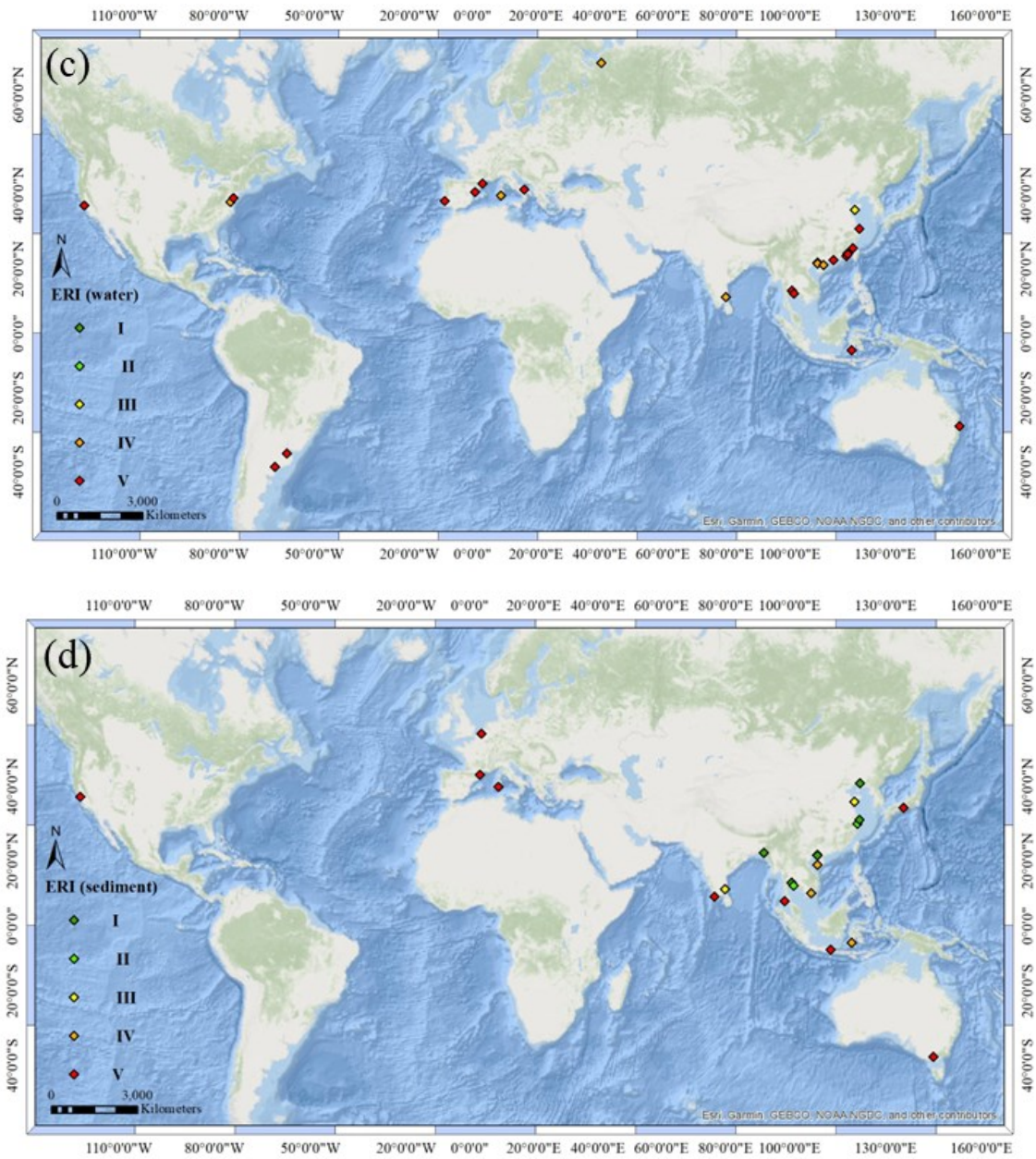


**Figure 2.6** Pollution load index (PLI) and potential ecological risk index (ERI) in water (a, c) and sediment (b, d).

Table 2.3 PLI in estuarine water.

Estuary name	Longitude	Latitude	PLI
Goiana Estuary	-34.83	-7.50	Low
North Setiu Wetland	102.80	5.67	Low
KwaZulu-Natal Estuary	31.12	30.85	Low
Northern Dvina River Delta	40.49	64.61	Low
Acará Lagoon Estuary	-48.52	-26.25	Low
Miri River Estuary	113.98	4.40	Low
Baram River Estuary	113.97	4.59	Low
Guadalquivir Estuary	-6.38	36.38	Low
Chesapeake Bay	-76.35	37.99	Low
Maozhou River Estuary	113.78	23.75	Low
Mandovi-Zuari Estuary	73.79	15.43	Low
Douro Estuary	-8.66	41.14	Low
Parnaíba and Jaguaribe River Estuary	-42.12	-2.67	Low
Houjin River Estuary	120.26	22.71	Low
Salt River Estuary	120.34	22.54	Low
Erren River Estuary	120.17	22.91	Low
Sado Estuary	-9.15	38.43	Low
Dafeng River Estuary	108.57	21.59	Low
Trave Estuary	10.89	53.96	Low
Dianbao River Estuary	120.25	22.72	Low
Agongdian River Estuary	120.20	22.80	Low
Love River Estuary	120.29	22.62	Low
Gaoping River Estuary	120.42	22.47	Low
Zhanjiang Bay Estuary	110.43	21.18	Low
Martinez-Baker estuary	-74.36	-47.77	Low
Badung River Estuary	115.22	-8.73	Low
Adour Estuary	-1.52	43.53	Low
Chienchen River Estuary	120.30	22.58	Low

Estuary name	Longitude	Latitude	PLI
Delaware Bay Estuary	-75.38	39.33	Medium
Canon River Estuary	120.30	22.60	Medium
Lawaan River Estuary	125.30	11.14	Medium
Dongshan Bay Estuary	117.61	23.73	Medium
Elbe Estuary	8.95	53.87	Medium
Vellar Estuary	79.77	11.50	Medium
Pearl River estuary	113.60	22.77	Medium
Tallo river Estuary	119.45	-5.10	Medium
Ebro River Delta	0.72	40.71	High
Ofanto River Estuary	16.20	41.36	High
Chao Phraya River Estuary	100.58	13.55	High
Sinne River Estuary	1.20	44.81	High
Port Phillip Bay Estuary	144.90	-37.84	High
Lis River Mouth	8.96	39.88	Extremely high
Po Delta Estuary	12.51	44.96	Extremely high
Qin River Estuary	108.58	21.83	Extremely high
Scheldt River Estuary	3.50	51.49	Extremely high
Jiulong River Estuary	118.03	24.42	Extremely high
Sebou Estuary	-6.55	34.34	Extremely high
San Francisco Bay Estuary	-122.47	37.81	Extremely high
Clyde Estuary	150.21	-35.70	Extremely high
Río de la Plata Estuary	-58.44	-34.48	Extremely high
Cochin Estuary	76.27	10.01	Extremely high
Nakdong River Estuary	128.92	35.05	Extremely high
Tampa Bay Estuary	-82.57	27.61	Extremely high
Bage Estuary	150.07	-36.42	Extremely high
Terengganu estuary	103.12	5.32	Extremely high
Yangtze River Estuary	121.84	31.68	Extremely high
Weser Estuary	8.87	53.06	Extremely high
Rio Formoso Estuary	-35.09	-8.69	Extremely high

Estuary name	Longitude	Latitude	PLI
Hunter Estuary	151.74	-32.85	Extremely high
Minjiang River Estuary	120.95	27.98	Extremely high
Jiaozhou Bay Estuary	120.14	36.18	Extremely high
Bohai Bay Estuary	117.72	38.96	Extremely high
Rayong River Estuary	101.28	12.66	Extremely high
Tweed River Estuary	153.42	-27.97	Extremely high
Klang River Estuary	101.39	3.00	Extremely high
Bahía Blanca Estuary	-62.05	-38.93	Extremely high
Xiamen Bay Estuary	118.19	24.64	Extremely high
Maowei Sea Estuary	108.56	21.84	Extremely high
Hamble and Beaulieu Estuary	-1.31	50.85	Extremely high
Charleston Harbor Estuary	-79.89	32.79	Extremely high
Maowei Sea Estuary	108.55	21.89	Extremely high
San Gabriel River Estuary	-118.11	33.74	Extremely high
Sal estuary	73.95	15.16	Extremely high
Saigon River Estuary	106.72	10.76	Extremely high
Têt River Estuary	3.04	42.71	Extremely high
Yellow River Estuary	119.24	37.79	Extremely high
Ou River Estuary	120.94	27.94	Extremely high

Table 2.4 PLI in estuarine sediment.

Estuary name	Longitude	Latitude	PLI
Dafeng River Estuary	108.55	21.59	Low
Cowichan-Koksilah Estuary	-123.63	48.74	Low
Vellar Estuary	79.77	11.50	Low
Ría de Arousa Estuary	-8.78	42.64	Low
Warnow Estuary	12.09	54.18	Low
Bay Champagne Estuary	-90.18	30.17	Low
Chao Phraya River Estuary	100.58	13.55	Low
Karnaphuli River Estuary	91.80	22.23	Low
Vitoria Bay estuarine	-40.29	-20.32	Low
Yangtze Estuary	121.84	31.68	Low
Mekong River Estuary	106.76	10.27	Low
Mississippi Gulf Coast Marshes	-88.57	30.42	Low
Ría de vigo Estuary	-8.68	42.28	Low
Sebou Estuary	-6.55	34.34	Low
Port Phillip Bay Estuary	144.90	-37.84	Low
Ría de Pontevedra Estuary	-8.70	42.42	Low
Charleston Harbor Estuary	108.55	21.89	Low
Liaohu Estuary	121.97	40.67	Low
Cecina River Estuary	10.49	43.30	Low
Tallo River Estuary	119.45	-5.10	Low
KwaZulu-Natal Estuary	31.13	-29.63	Low
Estuary in Gulf of Mexico	-95.00	18.50	Low
Cochin Estuary	76.27	10.01	Low
Jiaozhou Bay Estuary	120.32	36.26	Low
Ría de Muros Estuary	-8.93	42.79	Low
Jiulong River Estuary	118.05	24.42	Low
Fuhe River Estuary	113.67	38.17	Low
Têt River Estuary	3.04	42.72	Low
Tampa Bay Estuary	-82.39	27.86	Low

Estuary name	Longitude	Latitude	PLI
Fangchenggang Mangrove	107.95	21.47	Low
Scheldt River Estuary	3.50	51.49	Low
Xiamen Bay Estuary	118.19	24.64	Low
Qiantang River Esturay	121.19	30.38	Low
Galachipa and Andharmanik River Estuary	90.27	21.87	Low
Rayong River Estuary	101.28	12.66	Low
Estuary in Bay of Biscay	-4.61	43.40	Low
Bang Yai Canal Mouth	98.41	7.86	Low
Jagir Estuary	112.85	-7.32	Low
Atlantic Argentinean Estuaries	-62.31	-38.74	Low
Zhanjiang Mangrove	109.50	20.20	Low
Seine River Estuary	0.61	49.43	Low
Little Lake Estuary	-90.08	30.10	Low
Kayamkulam Estuary	76.48	9.13	Low
Fuzhou River Estuary	121.51	39.67	Low
Lis River Mouth	8.96	39.88	Low
Osaka Bay estuary	135.49	34.72	Low
Miri River Estuary	113.98	4.40	Low
Oder/Peene Estuary	14.22	53.87	Low
Maowei Sea Estuary	108.58	21.83	Low
Dongzhaigang Mangrove	110.53	19.85	Low
Yunxiao Mangrove	117.40	23.88	Low
Pearl River Estuary	113.60	22.77	Low
Guanabara Bay Estuary	-43.18	-22.86	Low
Baram River Estuary	113.97	4.59	Low
Dongfang Mangrove	108.60	18.72	Low
Ebro River Delta	0.76	40.70	Low
Red River Delta	106.60	20.27	Low
Dagu Estuary	117.72	38.96	Low

Estuary name	Longitude	Latitude	PLI
San Francisco Bay Estuary	-122.47	37.81	Low
Golden Horn Estuary	28.96	40.99	Medium
Jinjiang Estuary	118.63	24.79	Medium
Futian Mangrove	113.93	22.50	Medium
Derwent Estuary	147.29	-42.79	Medium
Sal Estuary	73.95	15.16	Medium
Mandovi-Zuari Estuary	73.83	15.43	Medium
Maozhou River Estuary	113.78	23.75	High
North Setiu wetland	102.86	5.67	Extremely high
Great Bay Estuary	-70.87	43.07	Extremely high

Table 2.5 ERI in estuarine water.

Estuary name	Longitude	Latitude	ERI
Jiaozhou Bay	120.32	36.26	III
Zhanjiang Bay Estuary	110.43	21.18	IV
Northern Dvina River Delta	40.43	64.63	IV
Lis River Mouth	8.96	39.88	IV
Vellar Estuary	79.77	11.50	IV
Dafeng River Estuary	108.55	21.59	IV
Chesapeake Bay Estuary	-76.37	38.35	IV
Rayong River Estuary	101.28	12.66	V
longjiao Bay Estuary	118.11	24.26	V
Minjiang River Estuary	119.71	25.98	V
Chao Phraya River Estuary	100.59	13.54	V
Portuguese Estuary	-8.89	38.52	V
Tallo River Estuary	119.45	-5.10	V
Têt River Estuary	3.04	42.71	V
Ofanto River Estuary	16.20	41.36	V
Dongshan Bay Estuary	117.61	23.73	V
Delaware Bay Estuary	-75.38	39.33	V
San Francisco Bay Estuary	-122.50	37.47	V
Río de la Plata Estuary	-58.62	-35.35	V
Ebro River Delta	0.72	40.71	V
Maowei Sea Estuary	108.55	21.89	V
Jiulong River Estuary	117.97	24.42	V
Bahía Blanca Estuary	-62.38	-38.74	V
Yangtze River Estuary	121.72	31.32	V
Pearl River Estuary	113.62	22.63	V
Tweed River Estuary	153.42	-27.97	V

Table 2.6 ERI in estuarine sediment.

Estuary name	Longitude	Latitude	ERI
Dafeng River Estuary	108.55	21.59	I
Yangtze Estuary	121.82	31.56	I
Liaohe Estuary	121.97	40.67	I
Chao Phraya River Estuary	100.58	13.56	I
Karnaphuli River Estuary	91.82	22.23	I
Rayong River Estuary	101.28	12.66	II
Qiantang River Estuary	121.17	30.38	II
Jiaozhou Bay Estuary	120.14	36.18	III
Vellar Estuary	79.77	11.50	III
Mekong River Estuary	106.76	10.27	IV
Maowei Sea Estuary	108.59	21.75	IV
Tallor River estuary	119.45	-5.10	IV
Pearl River Estuary	108.60	18.72	IV
Têt River Estuary	3.04	42.72	V
Western Port Bay Estuary	144.90	-37.84	V
Scheldt River Estuary	3.50	51.49	V
San Francisco Bay Estuary	-122.06	37.47	V
Osaka Bay Estuary	135.49	34.72	V
Estuary in Phuket Province	98.41	7.86	V
Lis River mouth	8.96	39.88	V
Jagir Estuary	112.82	-7.31	V
Kayamkulam Estuary	76.48	9.13	V

## 2.3 Discussion

### 2.3.1 The impact of environmental and anthropogenic factors on MP abundance in estuaries

MP abundance in estuaries is governed by an array of interdependent environmental factors. Climate is a pivotal aspect governing the regimes of MP abundance in estuaries, as reflected by season, climatic zone, and latitude in this study. High precipitation may result in a high river flux, transporting more MPs from land to water and from water to ocean (Mai et al., 2020). The wet tropics are distinguished by an increase in precipitation intensity, and higher temperatures and solar radiation accelerate the fragmentation of plastic debris (Wang et al., 2021). On a local scale, however, inconsistent results were observed because the presence of MPs is governed by numerous factors, such as local anthropogenic activities and land use. For example, Cheung et al. (2016) found that the MP abundance in beach sediments was significantly higher during the rainy season than the dry season. Gupta et al. (2021) observed that the MP abundance was higher in both water and sediment during wet season on the west coast of India. On the contrary, another study found that MP abundance can be higher during the dry season than during the rainy season due to the dilution of precipitation (Cheng et al., 2021). By summarizing global-scale data in the present study, the Geodetector identified a significant effect of the aridity index on MP abundance by compiling global-scale data. A significant positive correlation is also found between the aridity index and MP abundance in sediment, implying higher MP abundance could be found in humid area.

Estuaries are distinguished by high population density and intensive anthropogenic activities. A variety of pathways contribute to the discharge of plastics into the water, including runoff, atmospheric transport, littering, sewage discharge, aquaculture, fisheries, and shipping. As a

result of their topography and fertility, estuaries are ideal locations for fish farms. Fish farms in brackish water occupy a sizeable area (Hickling, 1971). Under long-term sunlight radiation and wave- and wind-induced friction, plastic gear, floating material, fishing nets, ropes, and net cages could serve as a significant source of MPs in local seawater. Zhu et al. (2019) discovered that MP abundance in the Maowei Sea displayed significant spatial variability, with high MP abundance detected in the oyster nursery. Moreover, compared to water-based sources, terrestrial sources are considered to be the primary contributors of plastics to the environment (GESAMP, 2016). Consequently, land use, industrialization, and urbanization surrounding estuaries act a significant role in determining MP input. In the present study, however, the majority of the collected articles do not indicate the land use types surrounding the estuaries. A wastewater treatment facility could effectively prevent the discharge of MPs into the environment. Sucharitakul et al. (2021) investigated whether treated wastewater alters the concentration and composition of MPs in the receiving water in two estuaries in southeast Queensland. They concluded that treated wastewater discharge had no discernible effect on the concentration or composition of MPs in water. A case study conducted in Bristol and Plymouth showed that the atmospheric deposition of microfibers was several orders of magnitude greater than the treated wastewater effluent (Napper et al., 2023).

As indicated in the present study, MP abundance in water is significantly negatively correlated with per capita plastic waste (kg/person/day) and HDI, while it is significantly positively correlated with population density as well as share of global mismanaged plastic waste. However, there is only a significant positive correlation between MP abundance in sediment and the probability of plastic being emitted to ocean. There is no significant linear relationship between MP abundance in sediment and population, HDI, or share of global mismanaged plastic waste. The difference between the sampling procedures for water and sediment can explain these results.

MPs in water are typically sampled via volume reduction or bulk sampling, whereas sediment is primarily sampled via bulk sampling. Volume reduction and bulk sampling for water samples cover a large area or several liters of water, which can reflect the real environment to a great extent. However, MPs in sediment are usually sampled several kilograms by point, and only a small amount (several to dozens of grams) is subjected to MP extraction and quantification, which is a poor representation of the real environment. Except for the impact of sampling and processing on MP abundance, anthropogenic activities reflected by population density, HDI, and the usage and management of waste plastics are critical in determining the MP abundance as suggested in the present study. Mai et al. (2020) developed a robust model by calibrating and validating riverine plastic outflow using field data, the main predictor of which is HDI combined with population density and municipal solid waste generation. Within the Tejo estuary, the concentration of microfibers in the sediment and bivalves were positively correlated to the population size of the closest township (Lourenco et al., 2017). Rochman et al. (2022) found significant positive correlation between suspected anthropogenic particles and population in different waterbodies of four regions across North America. Proper management of plastic products has great potential to reduce the MP abundance in environment. Data regarding plastic use and disposal show robust capacity to predict MP abundance in environment.

Several studies in the present dataset explored the relationship between MP abundance and related water properties such as turbidity, dissolved oxygen, salinity, electrical conductivity, and pH (Payton et al., 2020; Liu et al., 2021). Estuaries are intermediate zones of brackish water characterized by salinity gradients. The majority of debris is accumulating along the coast upstream from the frontal position probably related to the low circulation and high sedimentation rates normally found in these areas during drought periods (Acha et al., 2003). However,

regression analysis between salinity and MP abundance for all available data in the present dataset yielded insignificant results (Figure 2.7). On a local scale, results with respect to the relationship between water properties and MP abundance are inconsistent. Several studies that measured salinity found no correlation between salinity and MP abundance (Rodrigues et al., 2019; Liu et al., 2021; Roscher et al., 2021). Nevertheless, Li et al. (2021) discovered a negative correlation between large MPs (0.33–5 mm) and salinity at Jiulong estuary. Liu et al. (2021) found a strong positive correlation between turbidity and MPs in a mangrove. Payton et al. (2020) discovered that fibers per liter decreased significantly with increasing salinity at the Cooper River front, while MPs increased significantly with increasing salinity at the Ashley River front. Lourenco et al. (2017) discovered that small-sized plastics appear to have a positive correlation with fine sediment concentration. These findings suggested that water properties may not be suitable for predicting MP abundance across different regions at a large scale.

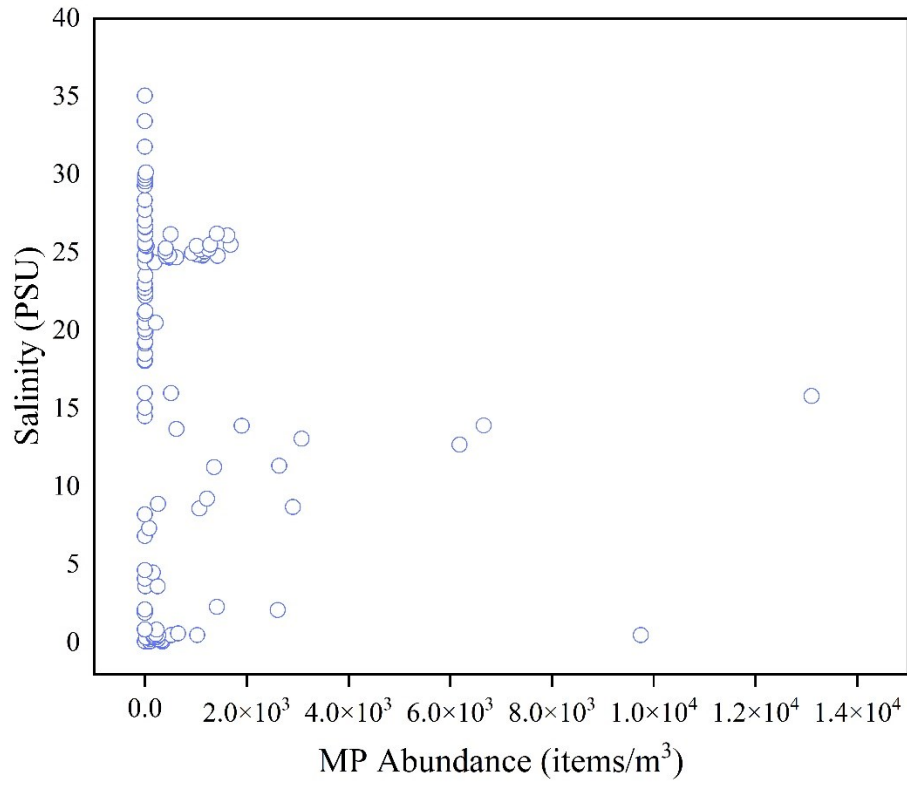


**Figure 2.7** MP abundance in water versus salinity.

### 2.3.2 The impact of MP sampling and processing on MP abundance in estuaries

In the present study, bulk sampling yielded a higher concentration of MP in water samples than volume reduction sampling. Volume reduction entails reducing the volume of the bulk sample until only specific items requiring further analysis remain. As a result, a substantial portion of the sample is discarded. Consequently, surface water samples are typically collected using this technique because it allows for large sampling areas. Nevertheless, because significant portions of the sample are discarded, volume-reduced sampling may underrepresent the MP abundance in a sample (Crawford and Quinn, 2017). When bulk sampling is performed, the entire sample is taken without being reduced in volume. It is theoretically possible to collect, store, and process all MPs regardless of their size or visibility in a sample, despite certain limitations in practice. Reducing the amount of time the sample is exposed to the environment can also aid in minimizing contamination. Both MP abundance in water and sediment are significantly negatively correlated with mesh size or filter size, as shown in Figure 2.5. Small sizes may increase the risk of clogging, whereas large sizes permit more particles to escape from the net. Dris et al. (2015) ascertained that net with mesh size of 100  $\mu\text{m}$  captured 100 times as many MPs as a net with a mesh size of 330  $\mu\text{m}$ . Lima et al. (2021) observed that the pump-collected MP abundance was at least three orders of magnitude higher than those collected with plankton net tows, which is inefficient at collecting small-sized plastics and soft fibers, which comprise 50% to 90% of all MPs in aquatic ecosystems. Ryan et al. (2020) claimed that 300–500  $\mu\text{m}$  mesh nets are too coarse to collect fibers and fiber abundance increased as mesh size decreased. Since MP abundances vary greatly between methods, it is probable that MP emissions were underestimated. Moreover, nanoplastics have not been discussed in estuarine environments due to methodological limitations.

Sampling depth is an important factor in quantifying the MPs. Not only is there an abundance of MP in the surface layer, but also the sublayers of water and sediment. In the current dataset, seven studies sampled sediments deeper than 50 cm (Willis et al., 2017; Wang et al., 2018; Fan et al., 2019; Li et al., 2020; Belivermis et al., 2021; Culligan et al., 2021; Viet Dung et al., 2021). In general, MP abundance declines in line with plastic production and consumption (Fan et al., 2019). Interestingly, Fan et al. (2019) discovered that the abundance of MPs smaller than 0.45 mm showed obviously downward increase. The depth of MP infiltration is influenced by the size and shape of MPs as well as the permeability of sediments, which varies with sediment types and depths. Smaller MP size and large porosity of substrate exhibit deep MP infiltration (Waldschlager and Schuttrumpf, 2020). Besides, various factors influence sedimentation processes, such as waves, tides, atmospheric pressure, and currents. With estuaries being very dynamic, sediment deposition is highly influenced by these forces and can vary substantially (Ward et al., 2014). Sediments deposited on the surface can be translocated to deeper layers through sediment mixing or bioturbation processes taking plastic particles with them (Martinetto et al., 2016). For a comprehensive understanding of MP inventory in estuaries, it is essential to analyze deeper sediment layers, as has been done for other contaminants.

The extraction procedures of MPs have a substantial effect on MP abundance. MPs extracted from water only through filtration and MPs extracted from sediment through density separation followed by sieve or filtration have a relatively high abundance. Besides, a higher MP abundance in sediment through digestion followed by density separation compared to density separation followed by digestion was shown in the present dataset. The digestion process can assist in removing biological material and enhancing the identification of plastics, thereby preventing organic matter or biofilm from interfering with MP extraction during density separation and

subsequent quantification. Phuong et al. (2016) proved that repeated extraction procedures could contribute to a high extraction yield. Extraction of MPs without chemical digestion and density separation may lead to the over-quantification of MPs. Geodetector's analysis demonstrates that the density of separation fluid has a substantial effect on MP abundance. A large proportion of studies use saturated NaCl solution ( $1.2 \text{ g/cm}^3$ ) to float MPs because of the low procurement cost, high availability, and environmental friendliness (Duong et al., 2022). Nevertheless, saturated NaCl solution only allows particles with a density less than the value to float, which may explain why high-density MPs are less likely to be detected.

### 2.3.3 The impact of morphological characteristics on MP behaviors

The shape of MPs can affect the movement of MPs in media. Corey Shape Factor ( $CSF = c/\sqrt{ab}$ ) can be used to quantify the shapes of MPs, where a, b, and c are the longest, intermediate, and shortest lengths of the particles. Fast settling or rising velocities are recorded at high CSF values, indicating irregular particles move more slowly than spheric particles (Waldschlager and Schuttrumpf, 2019). Additionally, irregular particles, such as fibers and tire abrasion particles, entangled with sediment more readily, inhibiting their infiltration (Keller et al., 2020; Waldschlager and Schuttrumpf, 2020). Additionally, fouling organisms are more likely to colonize flat, elongated, or irregularly shaped MPs with higher surface-to-volume ratios (Ryan, 2015). It is noteworthy that the morphological assemblages of MPs can be used to indicate their source. Fibers, for example, could represent treated wastewater effluent and agricultural runoff, whereas rubbery fragment is a symbol of stormwater (Rochman et al., 2022). Browne et al. (2011) found that fibers were the predominant form in coastal wetlands, suggesting a sewage source given that a single synthetic garment can release up to 1900 fibers per washing cycle. Although

agricultural runoff shares similarities with wastewater and urban runoff, glassy fragments are unique to agricultural runoff (Rochman et al., 2022). Fibers are the most prevalent MP type in estuaries, suggesting that intense anthropogenic disturbances, such as sewage discharge and agricultural runoff, are the primary sources of MPs in the estuarine zone. This result is consistent with the findings of other global reviews that more than 60% of MPs are fibers in the water and sediment of reservoirs and wetlands (Guo et al., 2021; Ouyang et al., 2022). Local monitoring can provide important insight into how MP loads enter waterbodies across pathways by obtaining the typical morphology of MPs. Such information is critical to guide the management and mitigation of MPs from the source. However, it should be noted that some of the detected fibers are made of cellulosic materials, which should not be considered as MPs (Stanton et al., 2019; Finnegan et al., 2022).

Most MPs detected in estuarine water are PP and PES (22.88% and 17.40%), respectively. Sediments from estuaries contain high amounts of PP, PE, and PES, which have a ratio of 25.75%, 14.79%, and 10.12%, respectively. A review of the global presence of MPs in coastal wetland sediments indicates that PE, PP, and PS are the most abundant types (Ouyang et al., 2022). According to a review of MP abundance in global reservoirs, PP and PE are the predominant types in water and sediment (Guo et al., 2021). 90% of the synthetic plastic worldwide is one of the following types: low and high density PE, PP, PVC, PS, and PET (Shah et al., 2008). MPs made from PE or PP that are derived from plastic bags, bottles, caps, straws, fishing nets, and ropes typically float on the surface of the water. Typically, PS is used in food packaging. MPs containing PA, PET, and PVC from plastic cups, bottles, plastic foil, as well as fishing nets and traps, have densities greater than seawater. The density of plastic acts a critical role in dictating the fate of MPs, which is determined by plastic composition, additives in plastics,

aggregation with other particles, and biofilm coverage. Denser plastics ( $>1.03 \text{ g/cm}^3$ ) will sink and accumulate in sediments. Ivar do Sul et al. (2014) observed that PE tubs traveled farther than PET bottles from their release point in a Brazilian estuary. MPs may experience biofouling during their residence in estuaries. For instance, microorganisms rapidly developed biofilms on PE plastic food bags soaked for three weeks in seawater (Lobelle and Cunliffe, 2011). Buoyant MPs may sink as a result of epiphytic or fouling organisms colonizing the plastic particles (Michels et al., 2018). The anticipated sinking rate of MPs was raised by an order of magnitude each day by aggregating with phytoplankton (Long et al., 2017). Nonetheless, the density of MPs covered with biofilm or agglomerated with other particles is not precisely known.

In the present study, the most abundant MPs color in water are transparent, white, black, and blue. Such summarization is consistent with previous global-scale reviews (Guo et al., 2021; Ouyang et al., 2022). The proportion of colored MPs in the environment is determined by the origin of plastic production and the fragmentation rate of MPs in various colors. Color wavelengths with longer wavelengths absorb more light, resulting in a lower UV transmittance, therefore, a slower rate of photoaging. Due to the inability of blue plastics to effectively absorb ultraviolet light, a high proportion of bluish MPs are commonly found in the environment, especially in small sizes (Zhao et al., 2022). Blue has also been suggested as a color for camouflaging on the ocean surface (Umbers, 2012). Therefore, the lower removal rate of bluish plastics from the water surface by predators could result in a higher fraction of bluish MPs (Shaw and Day, 1994). Compared to white plastics, black pigments age more rapidly in sunlight, as they have the greatest ability to absorb light, thereby inhibiting ultraviolet light from entering polymers (Zhao et al., 2022). The dissolved and released substances from MPs of different colors should be considered, as different color pigments may contain different chemical components.

#### 2.3.4 Potential risks of MPs in global estuaries

PLI and ERI are used to evaluate the risks of MPs in estuarine environment. The PLI is determined by comparing the detected MP abundance to a selected background MP abundance. Therefore, the selection of background MP abundance can significantly impact the results. Commonly, the lowest MP concentration in the study area or a safe concentration is utilized. ERI is calculated by taking into account the percentage of MPs' composition and the hazardous score assigned to each plastic type. Plastic products may contain catalysts, solvents, additives, and raw materials. Throughout the entire life cycle, plastic may release hazardous substances. Polymers contain several thousand types of additives. PVC, which accounts for 73% of the world's additive manufacturing by volume, is by far the most additive-intensive form of plastic, followed by polyolefins (10% by volume) and styrenics (5% by volume) (Murphy, 2001). The most hazardous additives include lead-based heat stabilizers, phthalate-based plasticizers, and brominated flame retardants. The majority of chemical leaching and emissions from plastic materials are frequently attributed to additives with low molecular weight since they are frequently unlinked from the polymer matrix (Lithner et al., 2011). This current risky scoring system possesses several limitations. Due to a lack of information, not all polymers are scored because of the lack of information. Persistent, toxic, and bioaccumulation endocrine disrupting properties are not considered in the current scoring system.

MPs of comparable size to plankton can be ingested unintentionally by planktivores (Cole et al., 2013). The presence of MPs in creatures has been extensively recorded (Guo et al., 2021). The interactions between MPs and contaminants are governed by electrostatic,  $\pi$ - $\pi$ , hydrophobic, H-

bond, and complexation interaction, determined by the properties of pollutants and MPs (Feng et al., 2021). The concentration of pollutants on MPs is affected by the concentration and properties of pollutants, the environmental conditions, and the MP properties. For instance, polychlorinated biphenyl concentrations on PP pellets sampled in Japan were up to two orders of magnitude higher than those in the surrounding saltwater and comparable to those in sediments (Mato et al., 2001). Approximately 14,815 µg/g of Zn was detected on MPs in sediments from Beijing, China (Wang et al., 2017). O'Connor et al. (2016) reviewed that the partitioning distribution of chemicals on MPs follow the order of PE > PP > PVC > PS. The exposure effect of MPs on organisms is an area of intense research, and various toxic effects and mechanical damages have been identified. For example, MPs may block the digestive tract, harm the intestinal tract, and alter the phagocytosis and filtering abilities of organisms (Guo and Wang, 2019). MPs pose risks to both organisms and humans due to their ability to absorb and transfer various types of contaminants through the food chain (Wang et al., 2018). However, the current hazardous scoring system does not consider the MP size and sorption capacity, pollutant concentration and types in environment, and mechanical damages to organisms.

## Chapter 3 Characterization of aged MPs<sup>†</sup>

### 3.1 Methods

Seawater-aged MPs were prepared by adding 0.5 g of MPs to 30 mL seawater in a 250 mL flask, then treating them in a shaker at 300 rpm and 25°C for 10, 20, 30, 40, 50, and 60 days. All the aged samples were rinsed several times with deionized water, filtered with a 0.22 µm membrane to remove the water phase, then dried before further characterization and batch experimentation. UV aging of the MPs was carried out in a UV chamber with a wavelength of 254 nm (CX-2000, UVP/Analytik Jena, USA). The pristine MPs were evenly spread into glass petri dishes for UV exposure. The petri dishes were shaken every 2 days to keep uniform irradiation. The MPs were taken out after 10, 20, 30, 40, 50, and 60 days. To clearly distinguish the degree of aging, MPs treated by seawater for various periods were abbreviated as SW10, SW20, SW30, SW40, SW50, and SW60. The MPs treated by UV for various periods were abbreviated as UV10, UV20, UV30, UV40, UV50, and UV60.

A scanning electron microscope (SEM, S-3400N, Hitachi, Japan) was employed to observe the effect of seawater and UV aging on the surface morphology of the MPs. The particle size distribution and mean particle size were measured using Laser In-Situ Scattering and Transmissometry (LISST-200X, Sequoia Scientific, USA). The contact angle was measured following the sessile drop method and employing an OCA 30 optical contact angle goniometer (Dataphysics Instruments GmbH, Germany). Alterations to the chemical composition of the MPs

---

<sup>†</sup> This work has been published as Feng, Q., An, C., Chen, Z., Yin, J., Zhang, B., Lee, K., Wang, Z., 2021. Investigation into the impact of aged microplastics on oil behavior in shoreline environments. *Journal of Hazardous Materials*, 421, 126711

and oiled sand, meanwhile, were measured using a Fourier transform infrared spectroscopy (FTIR, Optics Tensor 27, Bruker, USA). The surface chemical compositions of various aged MPs were identified using X-ray photoelectron spectroscopy (XPS, Thermo Scientific K-Alpha, UK). The fluorescence microscope was used to detect the presence of MPs on sand particles.

### **3.2 Results and discussion**

Surface characteristics of the pristine and aged MPs were evaluated employing SEM (Figure. 3.1). The surface of the pristine MP was flat while the edges were sharp. After 60 days of seawater aging, though, the surface became uneven and wrinkled, and the edges became obtuse. Moreover, pores and pit structures appeared on the MPs surface after seawater aging. The MPs may have been subject to abrasion due to the shearing effect attributable to hydrodynamic force in the shaking seawater environment. However, in the case of the UV60 MPs, the surface morphology had not changed significantly after aging. In a similar study, Shi et al. (2021) observed MPs becoming smooth again after 960 hr of UV radiation, a phenomenon that may be attributable to the chemical stripping.

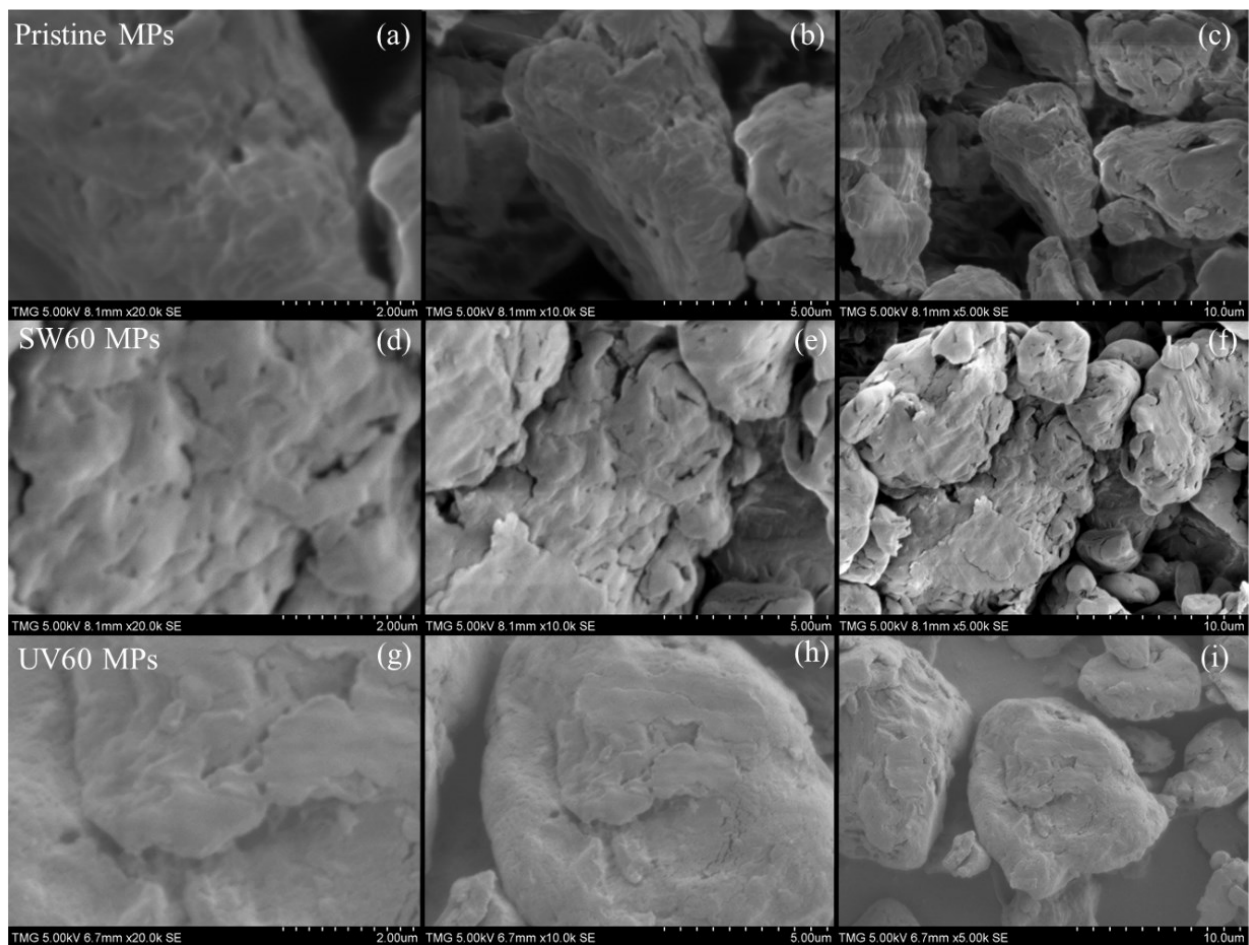


**Figure 3.1** SEM images of the pristine (a, b, c), SW60 (d, e, f), and UV60 (g, h, i) MPs.

Crystallinity degree refers to the proportion of the polymer that is crystalline, a feature that can be characterized by XRD analysis. As can be seen from Figure 3.2, after 60 days of aging in seawater, the pristine and SW60 MPs showed similar distributions of crystalline intensity, indicating that seawater aging did not alter significantly the crystallinity of MPs. UV aging, in contrast, was found to significantly increase the crystallinity of MPs. This finding aligns with a recent study by Oelschlägel et al. (2018) in which weathering low-density PE under UV radiation in artificial seawater for 28 days was found to increase the crystallinity from 32% to 36%. Hu et al. (2020), similarly, observed that PE, PS, and PVC all saw an increase in crystallinity after exposure to UV for 96 hr. Initial phase of weathering increased the crystallinity degree of the MPs. Two factors lead to this phenomenon: (1) the amorphous fraction of polymer is preferentially degraded during weathering, increasing the fractional crystallinity; and (2) the short segments of polymer created by chain scission in weathering move together and crystallize by chemi-crystallization (Sun et al., 2020).

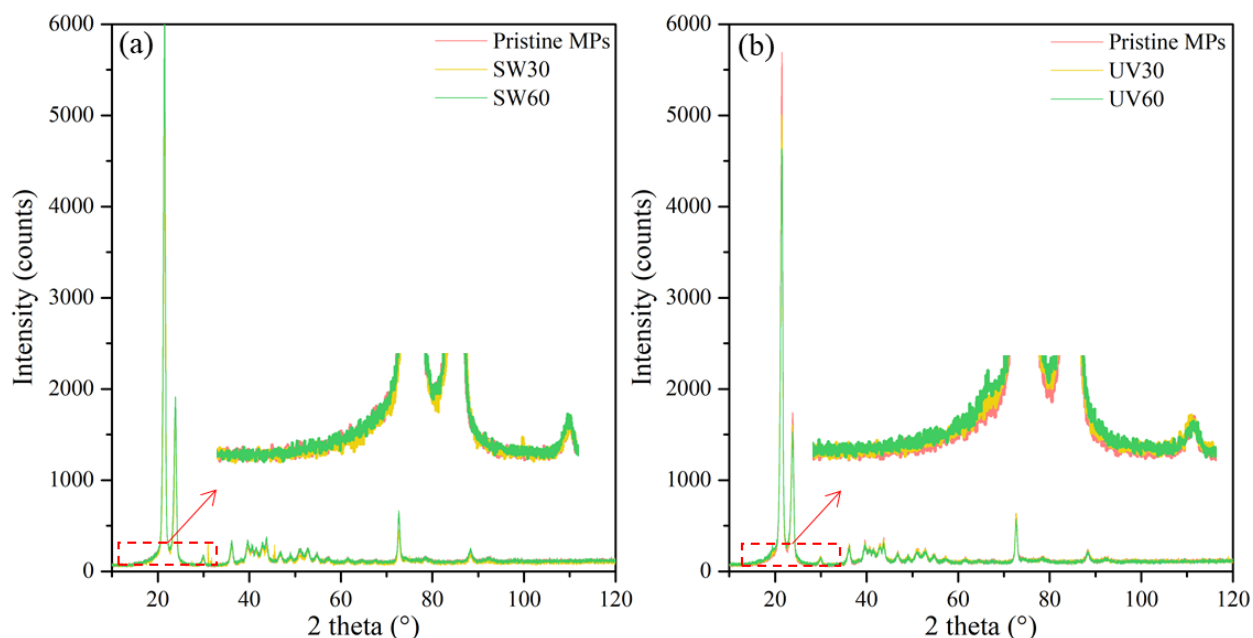


**Figure 3.2** XRD spectra of pristine and aged MPs.

The contact angles of different aged MPs were measured as a way of gauging their hydrophilicity. As shown in Figure 3.5, the pristine and aged MPs were both strongly hydrophobic. UV radiation decreased the contact angles of MPs from  $142.6^\circ$  to  $132.0^\circ$ , while the decrease due to seawater aging was less pronounced ( $142.6^\circ$  to  $137.2^\circ$ ). This difference in the rate of decrease of contact angle may be attributable to the differing degradation mechanisms between seawater and UV aging. The decreased contact angles of UV-aged MPs may be attributable to the presence of more hydrophilic groups (i.e., C–OH, C=O, –COOH) on PE (Lin et al., 2020). This hypothesis was confirmed through FTIR and XPS analysis. However, seawater aging was seen to induce increased surface roughness and pores on MPs, which may also be in favor of the wetting (Aghilinasrollahabadi et al., 2020).

Carbonyl index (CI) is generally applied in order to quantify the degree of aging, described as the ratio of the intensity of carbonyl to the methylene peak ( $1,712 / 2,915 \text{ cm}^{-1}$  for PE) (Liu et al., 2019). The breakdown and cracking that occur in aging promote the accessibility of free radicals and oxygen to the inward layer, resulting in oxidation of the sub-surface layers of MPs. Breakdown of the MP material also exposes more substances that may diminish the CI values. In this study, the CI increased linearly with UV aging time except in the initial stages of UV aging, where the pristine MPs, UV10, and UV20 had CI values of 0.080, 0.051, and 0.083, respectively (Figure 3.5). The overall increasing trend of CI from 0.081 to 0.130 observed under the UV aging implies that the oxidation process was dominant in the course of the 60-day UV radiation. The CI values of the MPs subjected to seawater aging ranged from 0.062 to 0.079 for SW10 to SW60, indicating that seawater aging triggered very little change compared to the UV aging process.

High-resolution XPS spectra of the C 1s and O 1s regions were measured in order to examine the bonding modes of various aging MPs (Figure 3.3). Since the oxidation reaction originated in the polymer surface, interior oxidation of the MPs took a longer time (Gewert et al., 2015). Natural weathering, especially UV irradiation, was mainly limited to the surface, confined by the penetrability of light and diffusion of oxygen within the MPs. Moreover, the O/C ratio would have been influenced by oxygen functional groups (e.g., O–H and C–O) that may not have been reflected in the CI values. This is evidenced by the difference between CI and O/C of MPs under UV radiation. The O/C values of MPs increased from 0.001 to 0.037 during the 60 days of UV radiation (Figure 3.5d), while the CI values over the same period first decreased, then increased before plateauing (Figure 3.5c). With respect to seawater-aged MPs, the O/C values did not change significantly during the seawater aging process (Figure 3.5d).

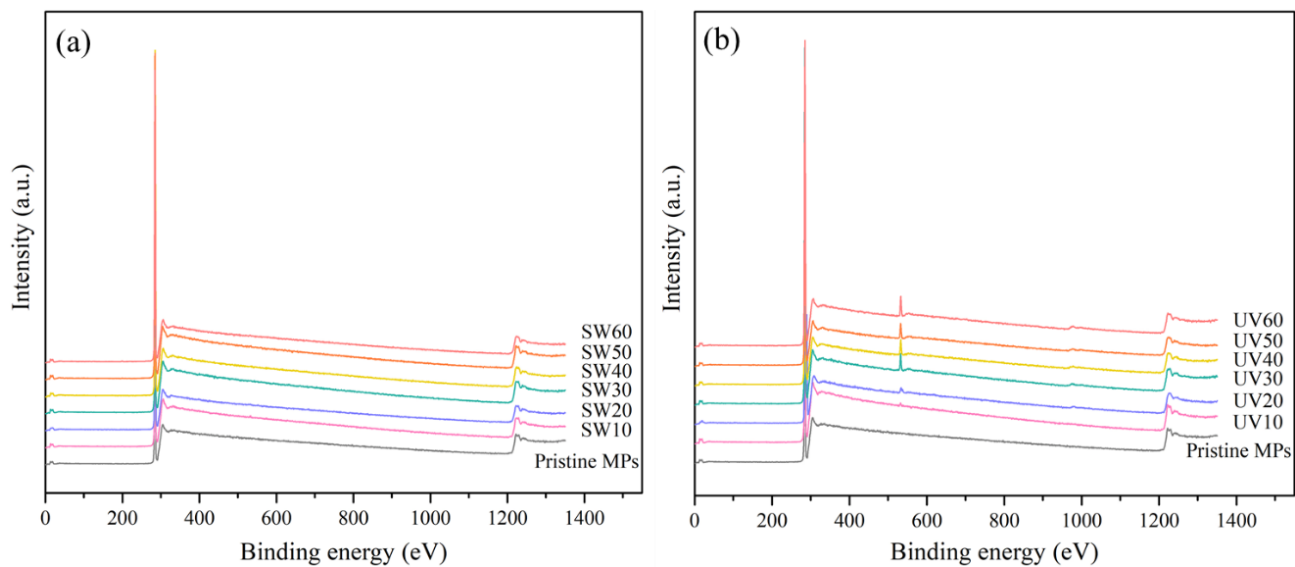


**Figure 3.3** XPS survey scan of seawater-aged MPs (a) and UV-aged MPs (b).

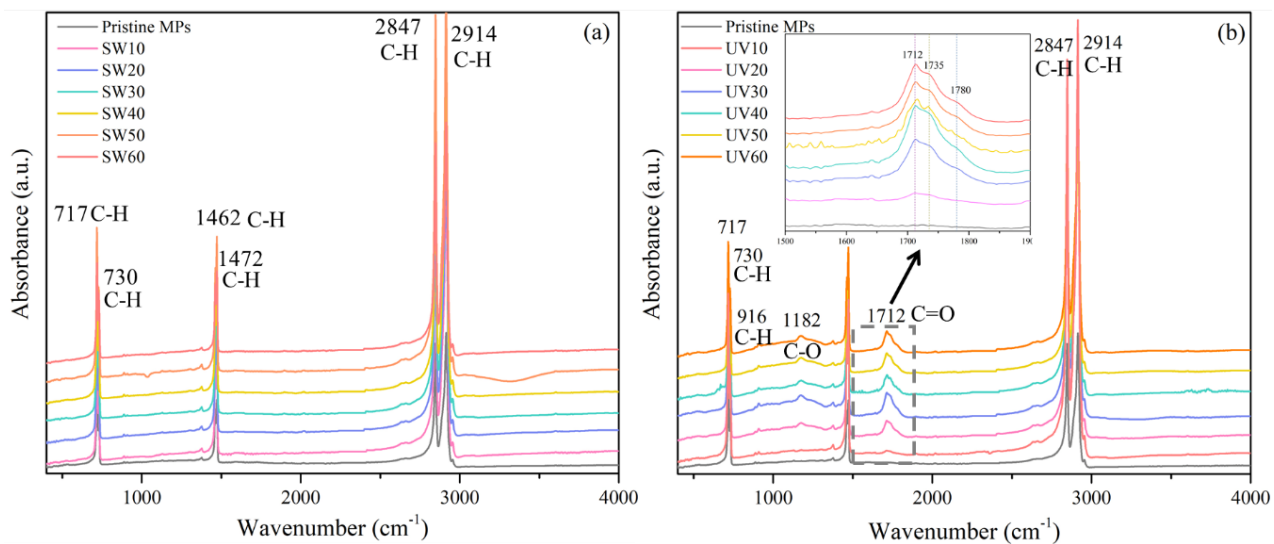


**Figure 3.4** FTIR spectra of the pristine and aged MPs under (a) seawater and (b) UV aging conditions.

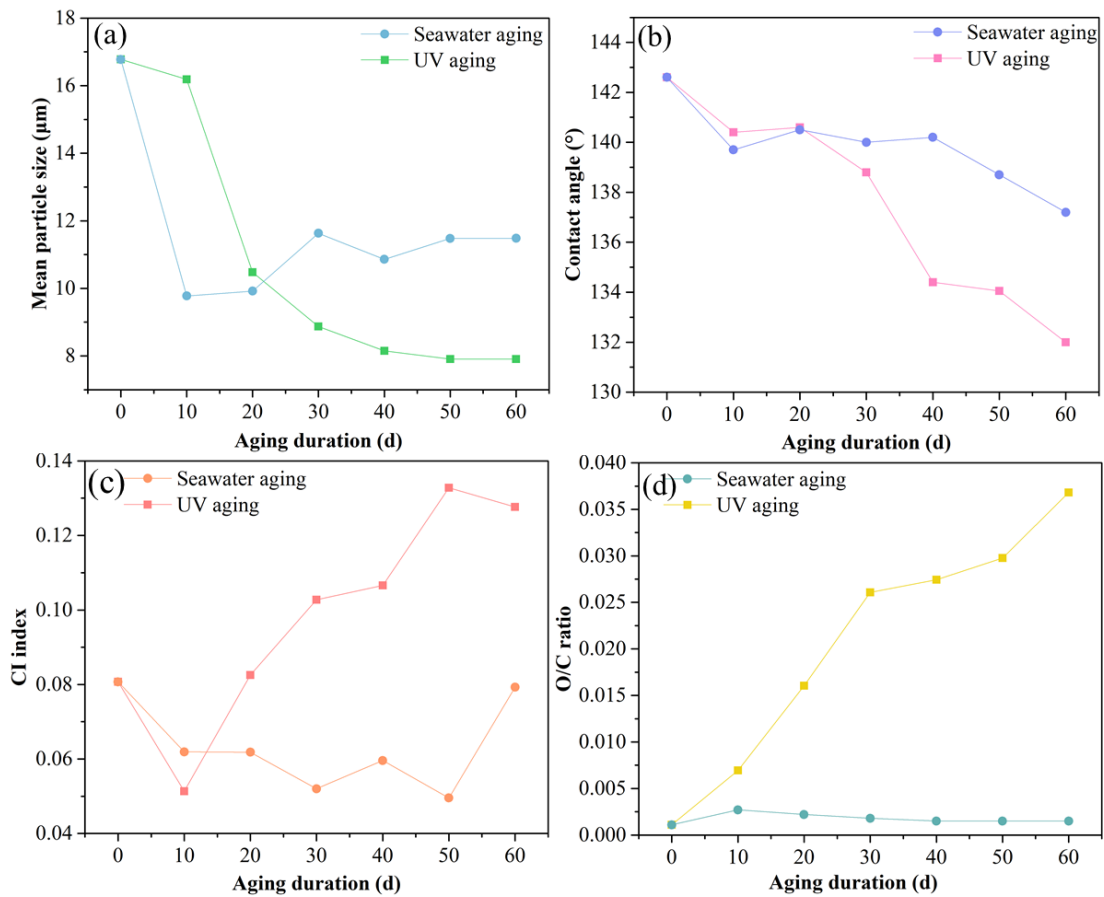


**Figure 3.5** Changes of mean particle size (a), contact angle (b), CI index (c), and O/C ratio (d) of seawater aged and UV aged MPs with different aging durations.

To uncover in sequential order the structural changes undergone by the MPs under aging, the FTIR spectra of pristine and modified MPs were investigated by two-dimensional correlation spectroscopy (2D COS). The synchronous map shows simultaneous evolution among the spectra with varying aging durations, where the intensities of the auto-peaks along the diagonal line denote the degree of spectral evolution. By contrast, the cross-peaks situated off the diagonal line in the asynchronous map give insight into the sequential order of the functional groups observed upon an external perturbation (aging time, in the case of the present study) (Noda, 2017). In the synchronous maps representing seawater aging, five auto peaks, at 2914, 2847, 1462, 1043, and 717  $\text{cm}^{-1}$ , were observed. In the synchronous maps representing UV radiation, meanwhile, eight auto peaks were observed, at 2,914, 2,847, 1,780-1,705, 1,462, 1,182, 1,043, 916, and 717  $\text{cm}^{-1}$  along the diagonal line (Figure 3.6), were observed. Positive signs were observed for both seawater and UV aging in the cross-peaks in synchronous maps, implying that all cross-peaks were synchronized with the aging process.

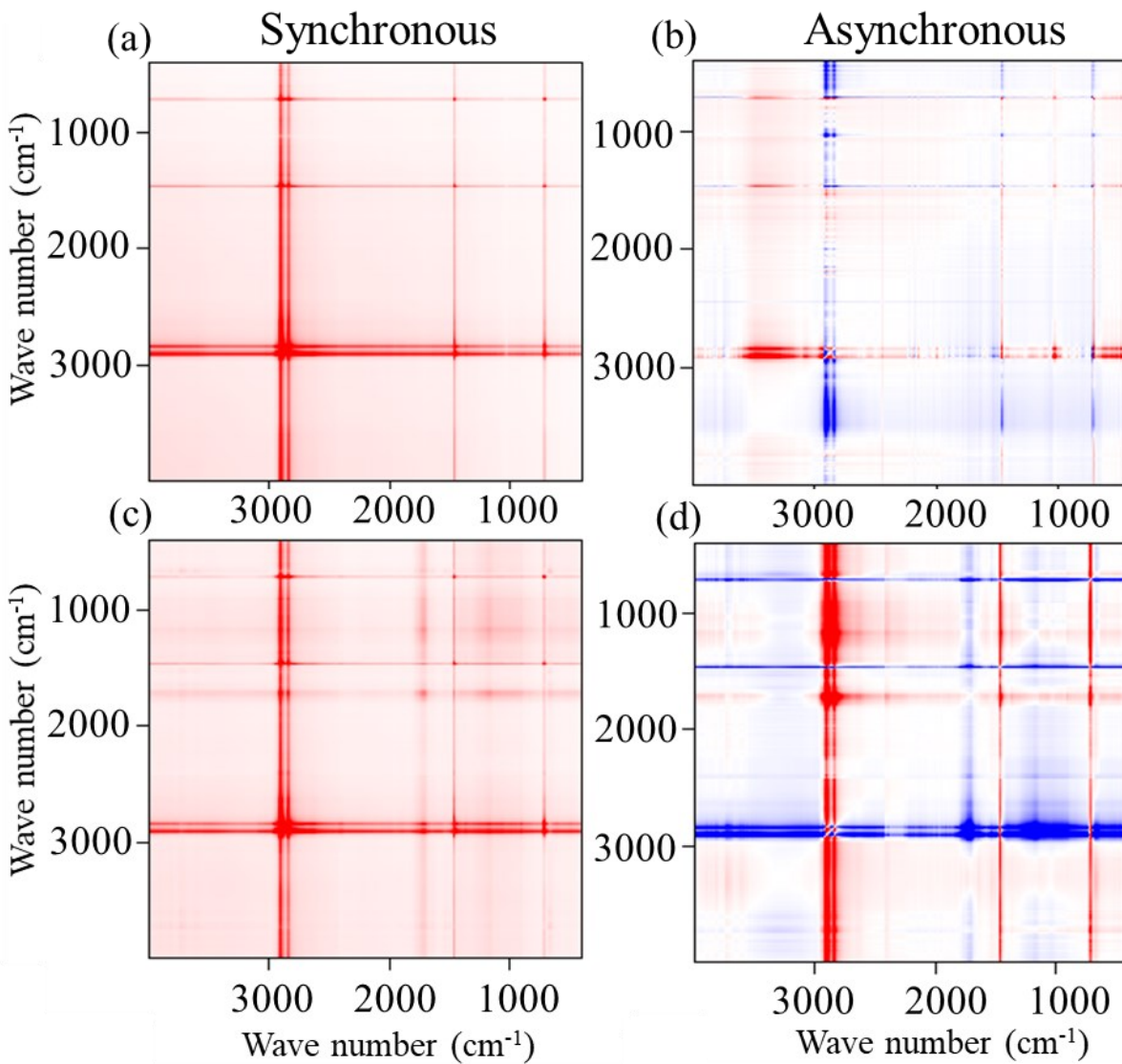


**Figure 3.6** Synchronous (a, c) and asynchronous (b, d) 2D COS maps drawn based on time-dependent FTIR spectra of MPs under seawater (a, b) and UV (c, d) aging. Red color and blue color symbolize positive and negative correlation, respectively. Darker color demotes a stronger positive or negative correlation.

As can be seen from Figure 3.6 and Table 3.1, on the basis of Noda's rules (Noda, 1990), the sequential changes under the UV aging followed the order of  $717\text{ cm}^{-1}$  ( $-(\text{CH}_2)_n-$  wagging vibration in plane)  $> 1462\text{ cm}^{-1}$  (C–H deformation)  $> 2914\text{ cm}^{-1}$  (C–H stretching)  $> 2847\text{ cm}^{-1}$  (C–H stretching)  $> 916\text{ cm}^{-1}$  ( $-\text{CH}=\text{CH}_2$  out of plane deformation)  $> 1043\text{ cm}^{-1}$  (C–O stretching)  $> 1182\text{ cm}^{-1}$  (C–O stretching)  $> 1780\text{--}1705\text{ cm}^{-1}$  (C=O stretching). UV-caused abiotic oxidation on PE was identified as the initial and rate-determining degradation phenomenon in the environment, where the degradation occurs in three steps: initiation, propagation, and termination. UV radiation initiates the fragmentation of the polymer chains, while free radicals form when the C–H bonds are broken as a result of exposure to UV light. The process continues with the MPs reacting with oxygen in the environment to form peroxy radicals. Then, the peroxy abstracts hydrogen to form hydroperoxide prone to UV photon. The weak O–O bonds, meanwhile, break to form pairs of hydroxyl and alkoxy radicals that may further react, such as hydrogen abstraction, rearrangement, and chain scission. These processes lead to the creation of oxygen-containing groups (C=O, C–O) (Gewert et al., 2015; Chang et al., 2020). In terms of the seawater aged MPs, the sequential order followed the order of  $717\text{ cm}^{-1}$  ( $-(\text{CH}_2)_n-$  wagging vibration in plane)  $> 1462\text{ cm}^{-1}$  (C–H deformation)  $> 2847\text{ cm}^{-1}$  (C–H stretching)  $> 2914\text{ cm}^{-1}$  (C–H stretching). No oxygen-containing functional group appeared in the seawater aging process.

Table 3.1 Synchronous and asynchronous (in the brackets) 2D COS results on the bond assignment and sign of each cross-peak with increasing seawater or UV aging duration (signs were obtained from the upper-left corner of the maps).

Peak (cm <sup>-1</sup> )	Bond assignments	Sign							
		2914	2847	1780–1705	1462	1182	1043	916	717
2914	C–H stretching		++(--)	+(+)	++(--)	+(+)	+(+)	+(+)	++(--)
2847	C–H stretching			+(+)	++(--)	+(+)	+(+)	+(+)	++(--)
1705-1780	C=O stretching				+(-)	+(-)	+(-)	+(-)	+(-)
1462	C–H deformation					+(+)	+(+)	+(+)	++(--)
1182	C–O stretching						+(-)	+(-)	+(-)
1043	C–O stretching							+(-)	+(-)
916	–CH=CH <sub>2</sub> out of plane deformation								+(-)
	–(CH <sub>2</sub> ) <sub>n</sub> – wagging vibration								
717	in plane								

# **Chapter 4 The effects of water content and flow patterns on MP mobilization**

## **4.1 Background**

The presence of MPs has been detected widely in terrestrial and aquatic ecosystem. The amount of plastic waste ends up in landfills or environment was estimated to be approximately 12,000 million metric tons by 2050 (Geyer et al., 2017). Around 21–42% of the global plastic waste disposed in landfills may release to the sediment (Alimi et al., 2018). MPs can enter the sediment through diverse pathways, including agricultural practices, biosolid application, irrigation, flooding, bioturbation, and atmospheric deposition. MP loadings have been estimated to be ranged from 63 to 430 thousand tons in European agricultural lands and from 44 to 300 thousand tons in North American agricultural lands (Nizzetto et al., 2016). However, the fate and behavior of MPs in sediments has been relatively understudied compared to aquatic environments.

MPs released into sediment undergo attachment to the solid-water interface, straining into pores, retention near grain-grain contacts under saturated conditions, attachment at the air-water interface, straining at the air-water-solid contact lines, and trapping in thin water films under unsaturated conditions (Torkzaban et al., 2008). Due to their poor biodegradability, MPs could remain in sediment for an extended period of time and experience a train of weathering processes that transform their physical and chemical properties, influencing their environmental behavior. For one thing, the small size and large specific area of MPs make them favorable vectors for organic and inorganic pollutants. The existence of mobile particles allows contaminants to move

quickly and farther than the buffering and filtering capacity of the sediment (Knappenberger et al., 2014). MPs and the absorbed chemicals may enter the food chain as they can be ingested by soil organisms. For another thing, MPs may alter soil physiochemical properties. For instance, Wan et al. (2019) observed that the inclusion of polyethylene film at a concentration of 1% (w/w) resulted in amplified water evaporation rates and occurrence of desiccation cracking in clay soils. de Souza Machado et al. (2019) noted that the introduction of polyester fibers enhanced water-holding capacity and evapotranspiration, while dwindled the bulk density and water-stable aggregates within loamy sandy soils. Hence, it is important to understand and predict the fate and behavior of MPs in sediment.

Considerable previous studies have been dedicated to the fate and transport of small particles in porous media. For instance, Gao et al. (2021) demonstrated that the infiltration depth of MPs decreased with increasing MP particle size and smaller sand diameter. Hou et al. (2020) observed that the vertical migration of MPs in sand was promoted by wet-dry cycles and the presence of dissolved organic matter. However, most previous studies focus on the infiltration behavior of MPs in porous media, referring to the process that MPs were introduced into the media, less is known regarding how MPs that already deposited in porous media are detached. Transport of small particles in the unsaturated zone, also known as the vadose zone, is inherently complex compared to saturated conditions, arising from the existence of air, capillary forces, and transient changes in flow and chemistry. Additionally, the heterogeneity in soil structure further complicates water flow and particle transport. Unsaturated zone serves as an initial natural layer to inhibit contaminants from entering groundwater, while the governing mechanisms of fine particle mobilization are still under question (Torkzaban et al., 2008).

One of the factors that may affect the mobilization of MPs in sediment is water content. Soil moisture influences the formation of soil aggregates, which can adsorb and retain MPs. In addition, the interaction between fine particles and air-water interface has been recognized as a prominent mechanism influencing colloid retention in vadose zone (Flury and Qiu, 2008). Water saturation at which pendular rings form plays a critical role in particle mobilization since when pendular rings are unconnected, particle transport is confined to adsorbed water films (Shang et al., 2008). Chen et al. (2005) found that decreased volumetric moisture restricted colloid and contaminant mobility, attributed to reduced colloid mobility and increased contaminant desorption from mobile colloids. As re-saturation progresses, the water film surrounding the solid phase thickens, leading to re-entrainment of retained colloids into the mobile phase (Crist et al., 2005). Soil moisture may change dramatically under the influence of precipitation, irrigation, soil properties, topography, vegetation, and land use practices. In the context of climate change, the intensification of the hydrological cycle is anticipated to worsen drought conditions in various regions worldwide. This is primarily attributed to shifts in precipitation patterns, modifications in snow accumulation and melt dynamics, and elevated evapotranspiration (Satoh et al., 2022). There has been an increase in aridity over many land areas since 1950 according to historical records of precipitation, streamflow, and drought indices (Cook et al., 2018). However, the effect of prolonged drying on the detachment of MPs from sediment is still not well documented.

Flow regime has far-reaching influence on particle transport in porous media. Unsteady flow is particularly crucial in mitigating nonpoint source pollution since it closely mimics the phenomenon of colloid transport in a real subsurface environment where flow conditions vary constantly (Russell et al., 2012). Flows with unsteady state can cause changes in chemical aspects (pH, surface charge, pore water chemistry) and physical aspects (pore size distribution, shrinkage,

and swelling) in unsaturated zones (Ryan and Elimelech, 1996). For instance, transient flow, e.g., temporal variations in moisture content and flow velocity, has been observed to have a greater potential for mobilizing fine particles. This is attributed to the dynamic changes in local water potential, pore water saturation, air-water interface, and thickness of water films caused by variations in water content (Quirk and Schofield, 1955; Zhuang et al., 2007). Zhuang et al. (2007) demonstrated that multi-pulse infiltration released 30% more colloids than single-pulse infiltration. The higher particle concentrations observed during flow transients emphasize the importance of investigating short-lived yet frequently sudden changes in water content, flow velocity, and pore water chemistry. Therefore, the objectives of the present study are to investigate (1) the effects of steady and intermittent flow on MP detachment from both wet and air-dried substrate; (2) the effects of flow transient in ionic strength on MP detachment from both wet and air-dried substrate; (3) the effects flow with temporal variation in flow rate on MP detachment from both wet and air-dried substrate. The obtained results provide insights into the influence of prolonged drying on the transport of MPs in soil under complicated unsteady flow conditions, which assists in soil management practices aimed at mitigating MP risks in a real subsurface environment.

## **4.2 Methods**

### **4.2.1 Chemicals and materials**

4–6  $\mu\text{m}$  Polyethylene (PE) and 20–25  $\mu\text{m}$  PE were purchased from Micro Powders Inc. (New York, USA). Polymethylmethacrylate (PMMA) with a mean particle size of 6.0  $\mu\text{m}$  was purchased from Goodfellow Cambridge Ltd. (Huntingdon, UK). Tween 20, Sodium chloride, and 1 mm glass beads were obtained from Sigma Chemical Company (Ontario, Canada). Aged MPs were prepared in an ultraviolet (UV) chamber with a wavelength of 254 nm (CX-2000,

UVP/Analytik Jena, USA). A glass petri dish was used to expose the pristine MPs to UV light evenly. To maintain uniform irradiation, the Petri dishes were shaken every two days. The MPs were taken out after 60 days, referred to as UV60.

#### 4.2.2 Simulated MP release with column test

##### 4.2.2.1 MP loading on the substrate

Glass beads with a diameter of 1 mm were selected as the substrate due to their precise size and the ability to wash them without particle release, which could interfere with the measurement of MP concentrations. To ensure the removal of any fine particles, the glass beads were washed with deionized water in 250 mL flask. The rinsing water was then analyzed using a turbidimeter (Oakton T-100, OAKTON Instruments, Illinois, USA) to confirm that the Nephelometric Turbidity unit (NTU) is 0.00. Subsequently, deionized water was added to flask containing glass beads, and the mixture was placed in a shaker at 150 rpm for 24 h to further clean the glass beads. After the shaking process, the glass beads were removed and rinsed multiple times with deionized water to ensure a 0.00 NTU. A polyvinyl chloride column with an inner diameter of 26 mm was sealed at the bottom with a metal screen (30-mesh) using a stainless-steel hose clamp. The column was marked with measurement lines every 1 cm to track the depth of column. A preliminary test confirmed that the mesh did not affect MP concentration after passing through it. The concentration of MPs in water was determined by turbidimeter. Turbidimeter has been employed to quantify the concentration of single-kind MPs in several previous studies (Hou et al., 2020; Bayarkhuu and Byun, 2022). Calibration curves between the concentration of MPs and NTU were established. The  $R^2$  value can reach above 0.99 (Figure 4.1).

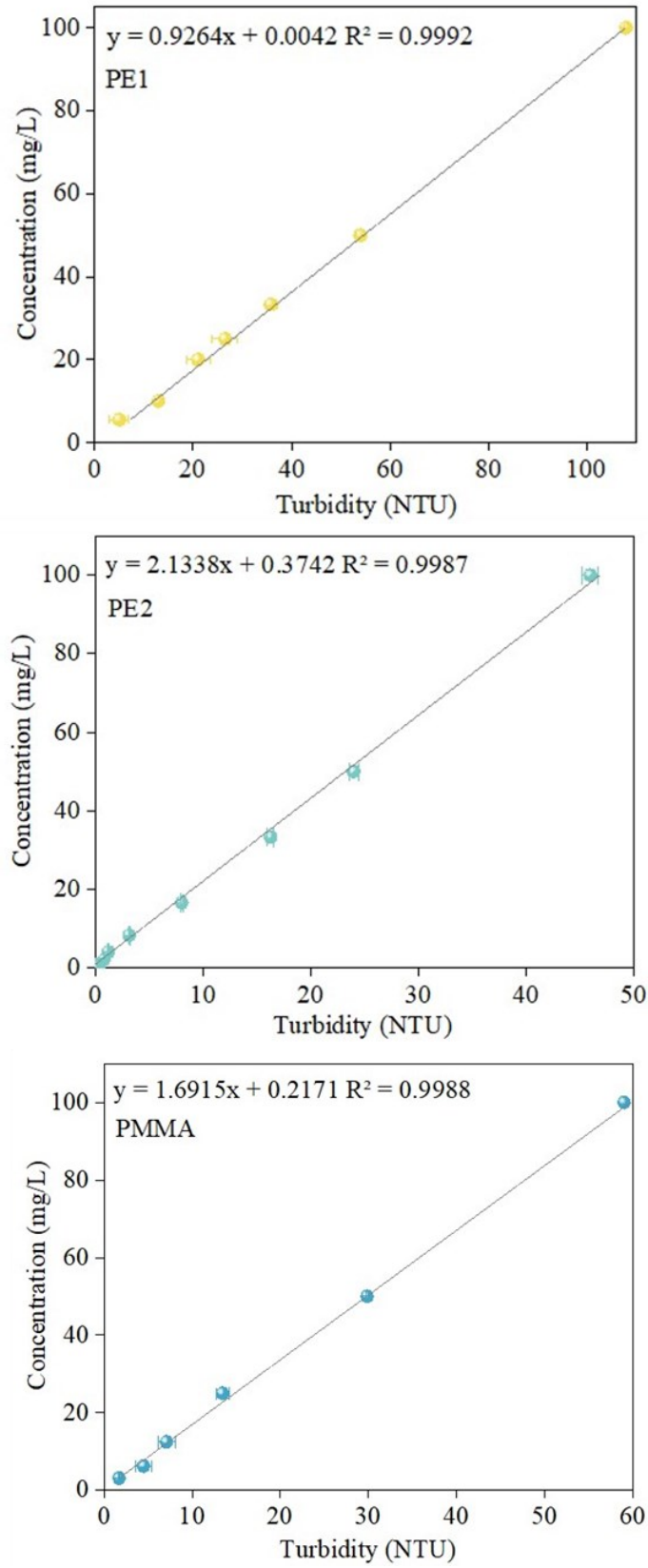


**Figure 4.1** Calibration curves of PE1, PE2, and PMMA.

The MP dispersion was prepared by adding 0.050 g of MPs to 500 mL of deionized water containing 0.01 % v/v Tween20. The mixture was dispersed using a homogenizer (Ultra-Turrax T25, IKA, Germany).at 10,000 rpm for 10 mins. Before each column test, the initial concentration of MPs in the dispersion was determined using a turbidimeter. Before introducing MPs dispersion into column, 100 mL background solution (0.01 mM NaCl, ~4.76 pore volumes (PV)) was pumped (Masterflex, Cole-Parmer Instrument Co., USA) into column at a flow rate of 10 mL/min to precondition the packed column. The effluent was collected and subjected to turbidity measurement to ensure MPs were not present in effluent. Closely followed by the background solution, the prepared MPs dispersion (500 mL) was successively introduced into column to load MPs into the substrate at the same flow rate of 20 mL/min. To prevent particle aggregation and settling, the MP dispersion in the reservoir was continuously dispersed during the experiment. During column test, an empty beaker was positioned underneath the column to collect MP dispersion effluent, which was then measured using a turbidimeter to determine the outflow MP concentration. The difference value between the inlet MP mass and outlet MP mass was the MP mass retained in each column.

#### 4.2.2.2 MPs release experiment

To test MP detachment under wet conditions, the loaded column was subjected to inflow free of MPs immediately. For MPs release under air-dried condition, the loaded column was hung in an iron stand for various durations (24 h, 48 h, and 72 h). Several flow regimes were conducted for both the wet and air-dried column. (1) MPs release under continuous flow. 500 mL ionic solution (0.01 mM NaCl) free of MPs was pumped into the column. Flow rates of 5. 10. 15 mL/min were tested. The effluent from the column was collected every 0.19 PV (4 mL) to determine the concentration of MPs to obtain the curves between PVs and MP detachment concentration. (2)

MP release under intermittent flow. The pump (5 mL/min) was stopped for 10 min after each 100 mL inflow of ionic solution (0.01 mmol/L NaCl). The total inflow volume is 500 mL which means 4 pauses during one column experiment. (3) MP detachment under flow transient decrease in ionic strength of inlet solution. In stage 1, 100 mL of MPs-free solution with ionic strength of 34.22 mmol/L NaCl at flow rate of 5 mL/min was introduced into the column. In stage 2, the ionic strength of inflow solution was switched to 8.56 mmol/L. 100 mL solution was introduced at the same flow rate of 5 mL/min. In stage 3, the ionic strength of inflow solution (100 mL, 5 mL/min) was switched to 0.17 mmol/L. In stage 4, the ionic strength of inflow solution (100 mL, 5 mL/min) was switched to 0.01 mmol/L. In stage 5, 100 mL of deionized water was introduced into the column at a flow rate of 5 mL/min. (4) MPs release under changing flow rate. The flow rate was sequentially and incrementally increased from 5, 10, 15, to 20 mL/min. In the first three stages (5, 10, 15 mL/min), 100 mL solution with ionic strength of 0.01 mmol/L was introduced into the column respectively. In the last stage of 20 mL/min flow rate, 200 mL solution with ionic strength of 0.01 mmol/L was introduced into the column. Both the wet and air-dried columns were subjected to all the flow regimes. All the detachment tests employed 500 mL solution free of MPs as inflow. Reynolds number confirmed that the flow remained within laminar regime.

#### 4.2.3 Theoretical considerations

Particles moving in substrate are understood to be subject to a number of different forces. As such, the Derjaguin-Landau-Verwey-Overbeek (DLVO) theory was applied to calculate the interaction energies ( $V_{TOT}$ )—i.e., the sum of the van der Waals ( $V_{VDW}$ ) and electrostatic double layer ( $V_{EDL}$ ) interactions—between the MPs and the GBs (sphere to plate) (Dong et al., 2018).

$$V_{TOT} = V_{VDW} + V_{EDL} \quad (4.1)$$

The total DLVO forces were calculated as follows:

$$F_{DLVO} = \frac{d(V_{TOT})}{dh} \quad (4.2)$$

where  $F_{DLVO}$  is the DLVO forces (N), and  $h$  is the separation distance (m). The associated equations and parameters are described in Feng et al. (2022). In porous media, particles tend to adhere to the GB surface by capillary forces when the water content is low because a water bridge exists between the particles and the GBs. In response to an increase in water content, the water bridge thickens and forms a free water surface covering the GBs, resulting in the capillary force pulling the particles from the GBs. Accordingly, the maximum repulsive capillary force (detachment force) was calculated using the following equation (Preuss and Butt, 1998):

$$F_{det} = 2\pi R\gamma \sin^2\left(\frac{\theta}{2}\right) \quad (4.3)$$

where  $R$  is the particle radius,  $\theta$  is the contact angle of particles, and  $\gamma$  is the surface tension of the fluid. The shear force, the fluid drag exerted on MPs, was calculated using the equation proposed by Sharma et al. (1992) as follows:

$$F_s = 1.7(6\pi)\mu \frac{H}{2} v \quad (4.4)$$

where  $\mu$  is the dynamic viscosity of water (Ns/m<sup>2</sup>), and  $v$  is the fluid velocity.  $H$  is the height of water film. If water fully covers the particle,  $H/2 = R$ . The difference between gravity and buoyancy forces is calculated as follows:

$$F_G = \frac{4}{3}\pi r R^3 (\rho_p - \rho_f) g \quad (4.5)$$

#### 4.2.4 Detachment modeling

The detachment of MPs under different air-drying durations was modeled using a two-site kinetic model within Hydrus-1D software, which competently simulates one-dimensional water flow in sediment (Šimůnek et al., 2008). Model parameters fitted were used to elucidate mechanisms controlling MP detachment. The time-dependent deposition model incorporates reversible and

irreversible attachment processes on two sites (site 1 and site 2). This model accounted for advective and dispersive transport by the following equations:

$$\frac{\partial C}{\partial t} + \frac{\rho}{\theta} \left( \frac{\partial S_1}{\partial t} + \frac{\partial S_2}{\partial t} \right) = D \frac{\partial^2 C}{\partial x^2} - V \frac{\partial C}{\partial x} \quad (4.6)$$

$$\frac{\partial S_1}{\partial t} = \frac{\theta}{\rho} K_{att1} C - K_{det1} S_1 \quad (4.7)$$

$$\frac{\partial S_2}{\partial t} = \frac{\theta}{\rho} K_{att2} C - K_{det2} S_2 \quad (4.8)$$

where C is the MP concentration (g/cm<sup>3</sup>), t is time (min), D is dispersion coefficient (cm<sup>2</sup>/min), V is the pore-water velocity, x is the column depth (cm), ρ is bulk density (g/cm<sup>3</sup>), S is the solid phase mass concentration of MPs, k<sub>att</sub> is first-order attachment rate (min<sup>-1</sup>), and k<sub>det</sub> is first-order detachment rate (min<sup>-1</sup>). Subscript 1 and 2 denote site 1 and site 2. The graphs were plotted using Origin 2021 (OriginLab Corporation, USA).

### 4.3 Results and discussion

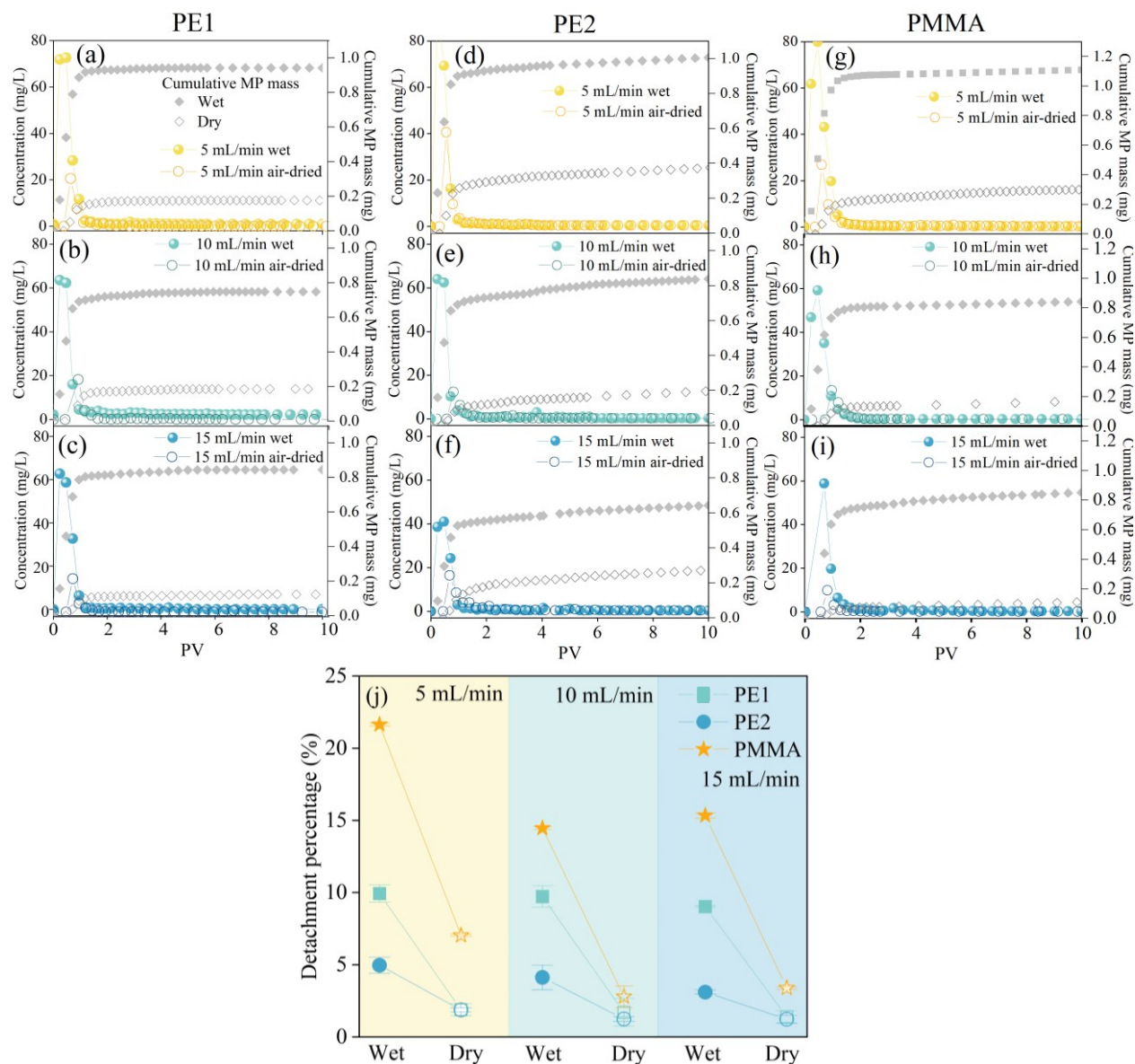
#### 4.3.1 The effect of flow rate on MP detachment under steady flow

Figure 4.2 illustrates the effects of flow velocity on MPs detachment in both wet and air-dried scenarios. As can be seen from Figure 4.2, at all flow rates, the release of MPs from air-dried porous media was significantly reduced. The increase of flow velocities from 5, 10, to 15 mL/min decreased the release of PE1 from 9.93%, 9.72%, to 9.03%, PE2 from 4.96%, 4.12%, to 3.11%, and PMMA from 21.63%, 14.46%, to 15.34% under the wet conditions, respectively. Nevertheless, the increase of flow velocities from 5, 10, to 15 mL/min decreased the release of PE1 from 1.88%, 1.70%, and 1.39%, PE2 from 1.87, 1.24, and 1.23%, PMMA from 7.03%, 2.79%, and 3.39%, respectively, for the air-dried porous media. Both the increase and decrease of fine particle release with increasing flow rate have been reported in the previous studies. For

instance, Bedrikovetsky et al. (2011) reported that colloid release is largely dependent on flow rate, while Sharma et al. (2008) suggested that colloid removal increased with declining velocity at the air–water interface. Gómez Suárez et al. (1999) also observed that the highest particle removal rate with the lowest velocity of air-water interface. Knappenberger et al. (2014) noted that more colloids released with lower pore water velocity, whereas attributed to higher initial colloid retention in column. The release of particles from a porous media is determined by the balance between detachment and adhesive torques. The attachment of fine particles to air-water interface occurs when their contact time surpasses their induction time, which refers to the duration required for a three-phase contact line to establish between air-water interface and particle. Consequently, colloids detach from solid surfaces only when the velocity of the interface is sufficiently low to exceed the colloid's induction time (Sharma et al., 2008).

Air drying of the column greatly hindered the detachment of MPs from substrate surface. Particles in unsaturated porous media preferentially associate with the water phase, the air-water interface, the solid-water interface, the triple phase contact of air, water, and solid (Flury and Aramrak, 2017). In addition, film straining is recognized as an important mechanism for particle retention in unsaturated media, especially at lower water saturation levels. This process involves the retention of colloidal particles within the thin water film surrounding the porous medium (Wan and Tokunaga, 1997). At low water content, MPs become pinned to sediment surface through the formation of a water bridge between MPs and sediment. This phenomenon is supported by capillary forces. With increasing water content, the water bridge expands and eventually forms a free water surface over the porous media. The capillary forces maintain the attachment of MPs to solid surface until the water level surpasses a specific threshold, causing a transition in the curvature of the air-water interface from concave to convex. At this stage, the

capillary forces detach MPs from sediment surface. Therefore, colloids sorbed on the air-water interface, solid water interface or retained by film straining could be mobilized with air or released into the mobile phase given to the increase in water content (Keller and Sirivithayapakorn, 2004). It is anticipated that MPs associated with secondary energy minimum, as opposed to strong primary energy minimum, will be more sensitive to hydrodynamic forces. Hydrodynamic forces can move these weakly linked colloids across grain surfaces so they can either be kept on the surface or discharged into the aqueous phase. Nevertheless, during extremely low water content, such as when water on the surface evaporates and water film becomes thinner, capillary forces between particles and the solid phase intensify, pushing particles closer to the substrate surface. Consequently, it is plausible that some colloids overcome the repulsive energy barrier and migrate into the primary energy minimum during water evaporation. The MPs become strongly attached to resist detachment during air-water interface passages in the air-dried surface, leading to significantly less MP release. The evidence that particle release restricted by drying or water content have been noticed in previous studies. For instance, Mohanty et al. (2014) noted that extending the pause duration from 0.5 hours to 21 hours resulted in a decrease in the proportion of mobilized *E. coli* bacteria in sand from 15% to 8%. Keller and Sirivithayapakorn (2004) found that decrease in initial water saturation significantly enhanced the retention of colloid in porous media.



**Figure 4.2** Detachment curves of PE1, PE2, and PMMA at different flow velocities under wet and air-dried conditions (a-i). Detachment percentages of MPs at different flow velocities under wet and air-dried conditions (j).

#### 4.3.2 The effect of MP properties on detachment

The properties, such as size, shape, density, surface charge, surface chemical composition of particles profoundly affect MP transport in porous media. In the present study, PE1 and PE2 possess the same surface properties but have different particle sizes. PE1 and PMMA possess similar particle size while distinctive surface properties. The contact angle of the pristine PE1 and PMMA are  $141.80^\circ$  and  $42.20^\circ$ , respectively. As can be seen from Figure 4.2, the release percentages of PE2 were significantly lower than that of PE1. Even though PE2 exhibits a higher detachment force, its larger particle size also contributes to enhanced retention by the glass beads. According to Bradford et al. (2002), increase in colloid size and decrease in the median grain size of sediment led to a decrease in relative peak effluent concentration and increase in colloid removal by sediment. Larger colloids are more susceptible to physical removal mechanisms, such as straining by the solid substrate and pore blockage, other than sorption on the air-water interface. Particle removal through straining becomes less significant when the particle size is smaller than the substrate pore size, and attachment becomes more important.

In terms of the hydrophobicity, the release percentages of hydrophilic PMMA were significantly higher than that of hydrophobic PE1. At unsaturated condition, hydrophobic colloids have a higher potential for retention or slower migration compared to hydrophilic colloids due to their stronger sorption onto the solid phase and air-water interface (Corapcioglu and Choi, 1996). The rate coefficients associated with colloidal deposition on solid matrix and air-water interface are one order of magnitude smaller for hydrophilic colloids when compared to hydrophobic colloids. Wan and Wilson (1994) claimed that there is an increase in colloid sorption to the air-water interface with greater colloid surface hydrophobicity. Crist et al. (2004, 2005) observed that

negatively charged hydrophilic colloids did not attach to air-water interface in three-dimensional porous media.

Once MPs enter the environment, they experience a series of aging that alter their physical and chemical properties and affect the way they behave in the environment. To further test how MP properties affect their mobilization, detachment experiment of UV aged MPs were conducted. After 60-day UV aging, the detachment percentages of PE1 decreased from 9.93% to 9.82% in wet condition, and decreased from 1.88% to 1.68% in air dried condition (Figure 4.3). However, the release percentages of PMMA enhanced from 21.63% to 28.75% in wet conditions, and increased from 7.03% to 13.11% in air dried condition. The results implied that UV aging weakened the inhibition effect of drying on hydrophilic PMMA, facilitating their detachment, while the effect of aging on PE1 detachment was not pronounced. Such changes could be explained by the property alteration after UV aging. UV aging may alter both the physical and chemical properties of MPs. The water contact angles of PE1 decreased from  $141.80^{\circ}$  to  $133.90^{\circ}$ , while it increased from  $42.2^{\circ}$  to  $61.35^{\circ}$  for PMMA. The zeta potential of PE1 decreased from  $-30.97$  to  $-33.30$ , and decreased from  $-5.49$  to  $-23.88$  for PMMA in ionic strength of  $0.001\text{mmol/L}$ .

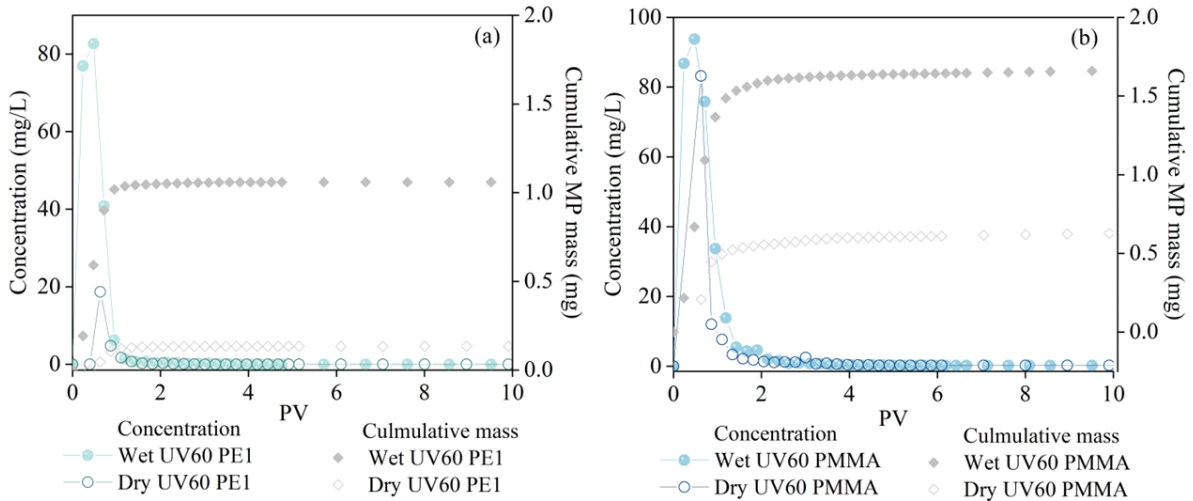


**Figure 4.3** Detachment curves for aged PE1 and PMMA under wet and air-dried conditions. For display purpose, only the first 10 PVs are presented.

#### 4.3.3 MP detachment during intermittent flow

Understanding the transport of particles in porous media under transient-flow is essential for gaining insight into contaminants transport in unsaturated substrates, particularly in the vadose zone, where flow conditions experience constant variation. The detachment curves of intermittent flow are presented in Figure 4.4, a small peak was observed after each resumption of flow with only a finite amount of released MPs. On a macropore scale, transient flow promotes particle transport by disrupting the force equilibrium that holds particles on sediment. Flow interruptions are anticipated to remove pore blockages caused by hydrodynamic bridging, allowing entrapped particles to diffuse freely in and out of pore constrictions. Torkezaban et al. (2015) observed that hydraulic conductivity increased when the flow was resumed after a cessation of flow for about 2 min, and a sharp peak of released colloids was witnessed following the resumed flow. Zhuang et al. (2007) also observed that, compared to steady-state flow, transient flow leads to increased colloid mobilization. Gao et al. (2004) noticed that under steady-flow, the mobilization of kaolinite colloids was minimal or slow, whereas transient flow led to rapid release of colloids..

El-Farhan et al. (2000) conducted infiltration experiments on a dry soil to explore the impacts of transient flow on the mobilization rate of fine particles, which identified release peaks after each infiltration event and the average concentration showed an approximate 25% decrease between the initial 10-cm event and the ensuing 10-cm event across all plots.

PE2 with a larger particle size was more sensitive to the resumption of flow, in which significantly higher peaks were observed compared to PE1, attributed to a higher detachment force of PE2 (1435.14 and 3392.93 nN for PE1 and PE2, respectively). The mass of MP particles detached from substrate was similar between continuous and intermittent flow under the same moisture condition, while for the three MPs used, MP detached from wet substrate were significantly lower than those detached from the air-dried substrate. The release of PE1, PE2, and PMMA were 9.83%, 4.85%, and 19.57% from wet substrate, while decreased to 1.98%, 1.96%, and 7.11% under air-dried condition. This result indicated that drying greatly impeded MP detachment even under intermittent flow.

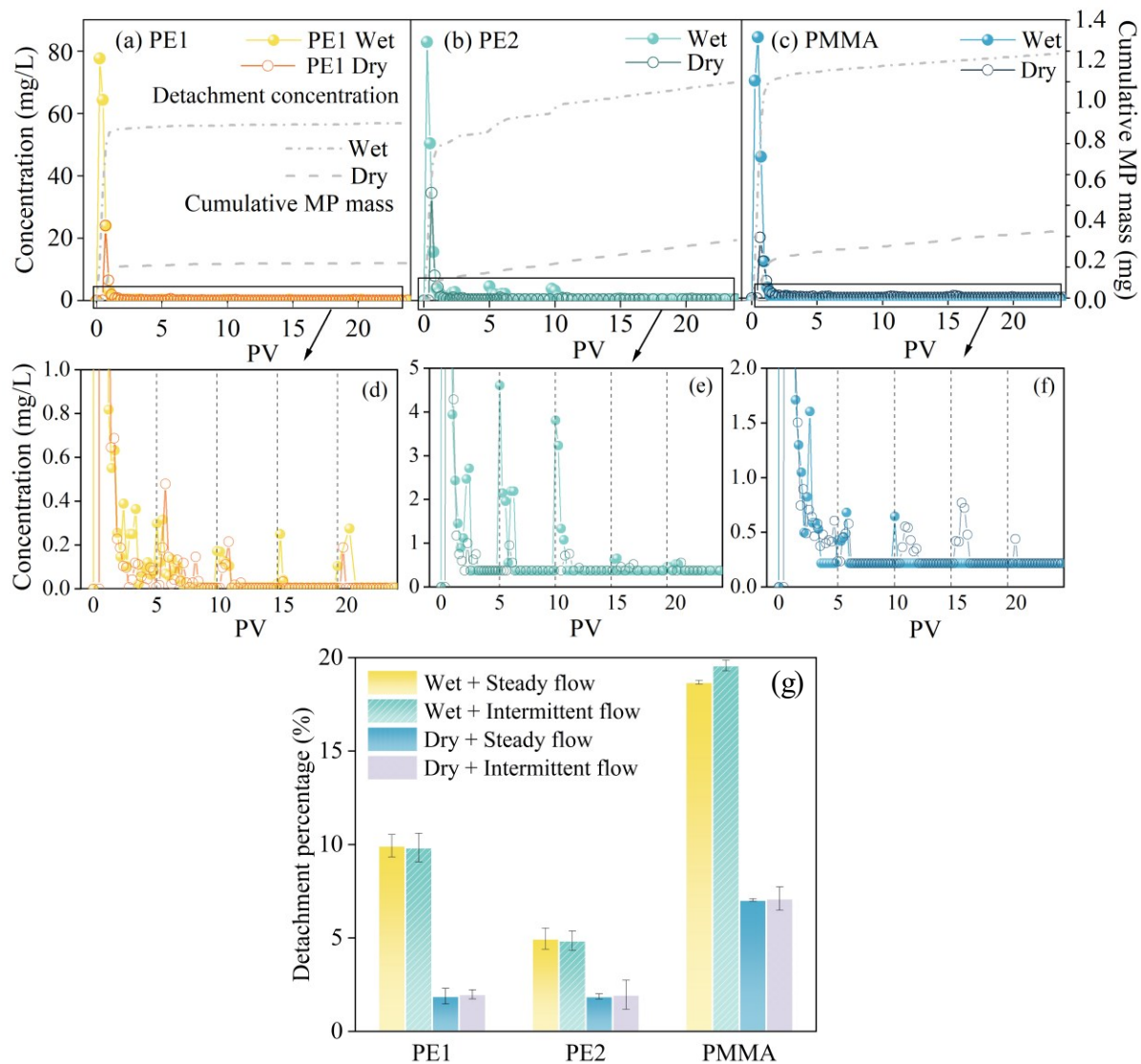


**Figure 4.4** Detachment curves for PE1, PE2, and PMMA under intermittent flow (a-f). Detachment percentages of PE1, PE2, and PMMA under intermittent flow (g).

#### 4.3.4 MP detachment during flow transient in ionic strength

Solution chemistry can affect the interactions of particles with substrate surface in bulk solution. Changes in ionic strength of inflow can be attributed to infiltration of precipitation, irrigation by fresh water, or injection of fresh water for artificial recharge. Figure 4.5 illustrates that a stepwise decrease in the ionic strength resulted in the release of MP deposited on grain surfaces. As can be seen from the breakthrough curves, the change in ionic strength led to sudden peaks followed by prolonged tails for both the wet and air-dried column, with the peak timing coinciding with the arrival of the ionic strength front. The occurrence of these peaks may be attributed to the detachment of adhered MPs from asperity tips at lower ionic strengths. Compared to MPs release under steady-state ionic strength of 0.01 mmol/L, inflow with higher ionic strength resulted in less MPs release mass (Figure 4.5). Under wet conditions, the release of PE1, PE2, and PMMA under steady-state ionic strength of 0.01 mmol/L led to 9.93%, 4.96%, and 18.68% release, while only 7.68%, 2.95%, and 14.84% were released under decreased ionic strength from 34.22 mmol/L, to deionized water. Similar results can be observed for air-dried column, 1.88%, 1.87%, and 7.03% of PE1, PE2, and PMMA were released at steady ionic strength of 0.01mmol, while only 0.41%, 1.77%, and 4.28% were released under flow of decreased ionic strength. DLVO theory suggests that with the increase of ionic strength, the double-layer repulsion between the MPs and GBs dissipates, and their attraction enhances. Most of the MPs deposited on the GBs were retained in a deep primary energy minimum and were not released even under the transient in ionic strength. Only a portion of MPs that adhere to soil grains can be remobilized by fluctuations in ionic strength. The release peaks for air-dried column are generally smaller than that for the wet column. the detachment of MPs from air-dried substrate was significantly less than that from the wet conditions.

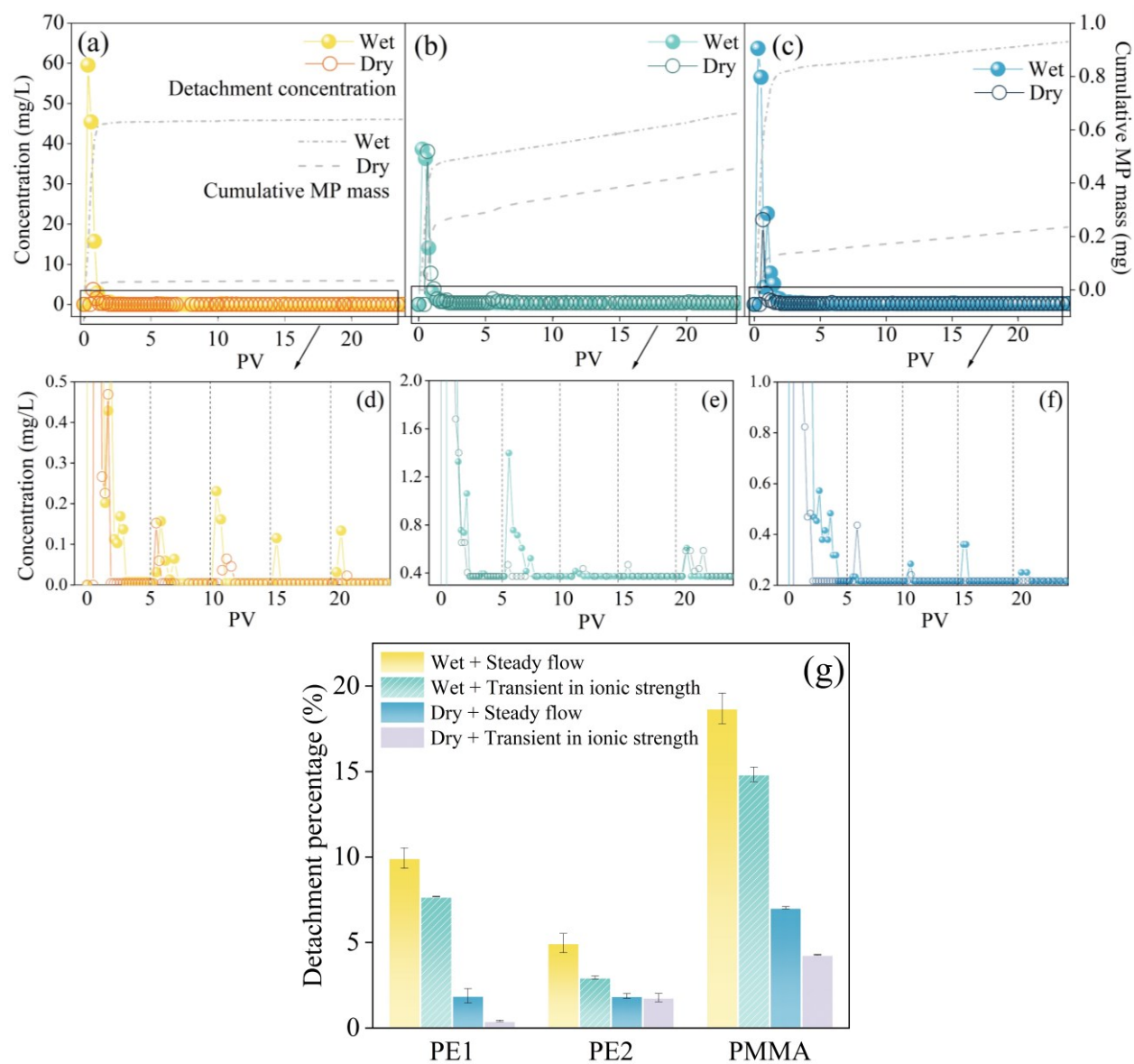


**Figure 4.5** Detachment curves for PE1, PE2, and PMMA under transients in solution ionic strength (a-f). Detachment percentages of PE1, PE2, and PMMA under transients in solution ionic strength (g).

#### 4.3.5 MP detachment during temporal variation in flow rate

In order to examine the influence of dynamic hydrodynamic forces on MP release, the average flow velocity was accelerated in stepwise fashion. For each step increase in flow velocity, the MP release presented an abrupt peak followed by slow release for both wet and air-dried conditions (Figure 4.6). Thus, a higher mass of MP detachment can be observed during stepwise increased flow compared to that under steady flow. This can be attributed to the changes in torque and force balances that occur on the MPs attached to the grain surfaces. The increase in flow rate leads to greater hydrodynamic shear force, which in turn generate a higher hydrodynamic torque that overcome the adhesive torque (Chequer et al., 2020). This fraction of released MPs was depleted as the inflow reached a specific velocity. Similar to previous sections, air drying significantly restricted the release of MPs compared to wet condition. The release of PE1, PE2, and PMMA in wet substrates was 9.52%, 5.17%, and 20.13%, with stepwise increase in flow rate, while in air-dried substrates it decreased to 1.87%, 1.95%, and 7.51%, respectively.

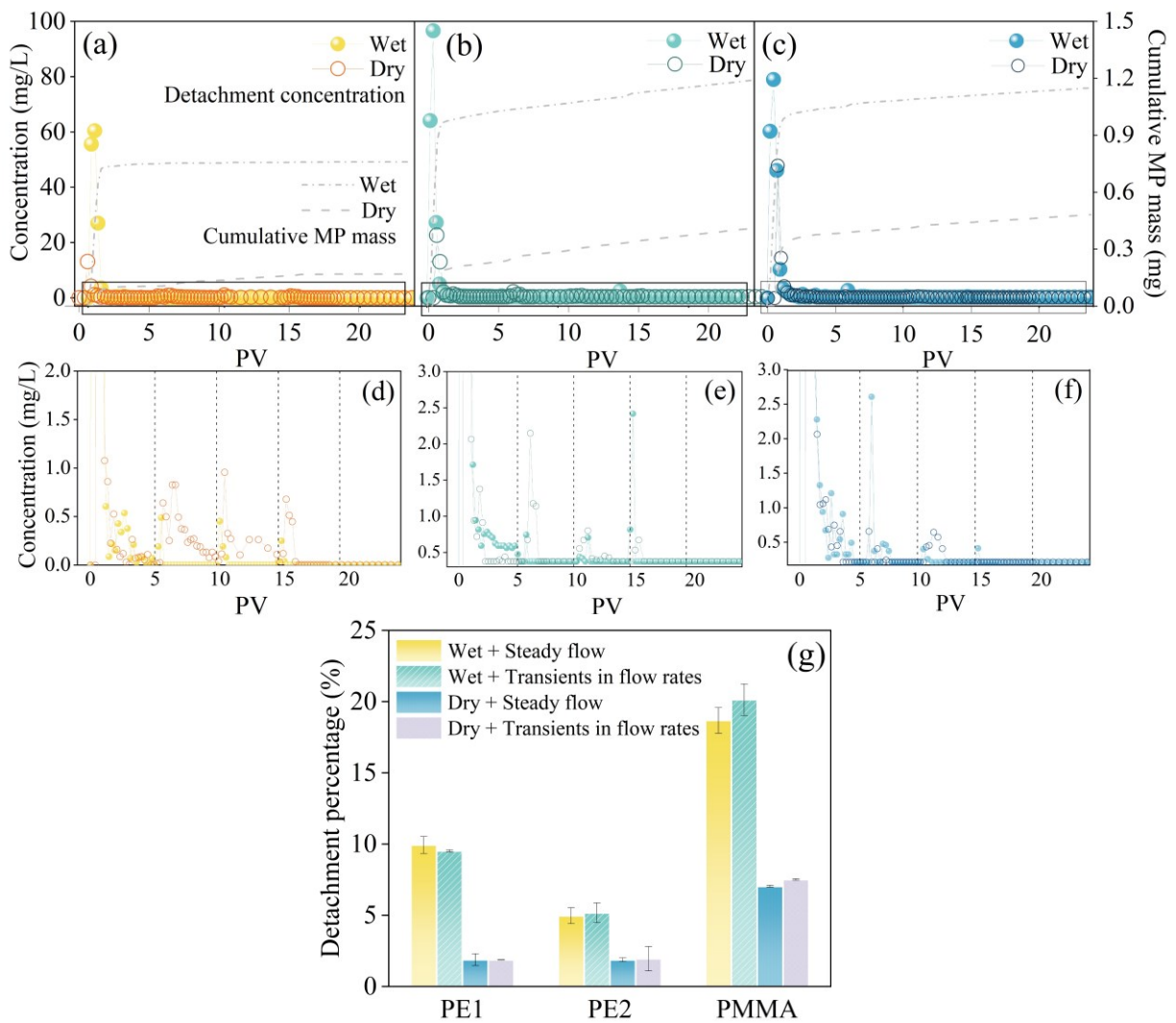


**Figure 4.6** Detachment curves for PE1, PE2, and PMMA under transients in flow rates (a-f). Detachment percentages of PE1, PE2, and PMMA under transients in flow rates (g).

#### 4.3.6 The effect of prolonged drying

To further verify the effects of drying on MPs release, prolonged drying for 48 hr and 72 hr was implemented. It is evident that the release of MPs decreased pronouncedly with the increase in air drying time (Figure 4.7). With the increase in air drying time from 0, 24, 48, to 72 hr, the release of PE1 decrease from 9.93%, 1.88%, 1.29%, to 1.62, the release of PE2 decrease from 4.96%, 1.87%, 1.46%, 1.67%, and the release of PMMA decrease from 18.68%, 7.03%, 5.78%, to 4.70%, respectively. In order to reveal the influencing mechanisms of MP properties and drying time on the detachment of MPs in column, detachment curves were fitted in the Hydrus-1D model (Figure 4.8). The fitted model incorporates both advective and dispersive transport, assuming site 1 denoting irreversible attachment and site 2 denoting reversible attachment. The fitted parameters and corresponding  $R^2$  values for column experiments are summarized in Table 4.1. The Hydrus-1D model demonstrated good fitting for the detachment curves, as demonstrated by the high  $R^2$ . After 72 h air drying, the  $k_{att1}$  significantly decreased from 1.41E-02 to 4.34E-04 for PE1, 1.97E-02 to 4.07E-04 for PMMA, and 1.04E-03 to 3.46E-04 for PE2, respectively, indicating higher energy barrier after air drying. As the height of the energy barriers increases, the rate coefficients of attachment ( $k_{att}$ ) and detachment ( $k_{det}$ ) are expected to decrease exponentially according to  $k_{att} \propto \exp(\frac{\phi_{max}}{k_B T})$  and  $k_{det} \propto \exp(-\frac{|\phi_{max} - \phi_{min1}|}{k_B T})$ , where  $k_B$  is Boltzmann's constant and  $T$  is the absolute temperature (Ryan and Elimelech, 1996). MPs attached on sediment must possess sufficient energy to overcome the energy barrier to detach. Therefore, the fitted parameters highlight the significance of drying in impeding MP detachment from substrate by heightening the energy barrier. Saiers and Lenhart (2003) proposed a model where immobile colloids were categorized into compartments based on their critical moisture content,  $q_c$ . Colloids are released from a specific compartment when the moisture content

surpasses the assigned  $q_c$  value. In the present study, MP detachment under transient flow was not simulated. The concurrent occurrence of multiple transport phenomena, such as site-blocking, ripening, aggregation, straining, and size exclusion has led to challenges in selecting and applying appropriate modeling approaches (Babakhani et al., 2017). Besides, the incomplete understanding of fine particle transport in transient flow systems poses challenges for numerical modeling. Currently, most existing colloid transport models focus on steady-state conditions and only a few attempts to simulate transient flow conditions (Russell et al., 2012; Torkzaban et al., 2015). Since steady-state systems in saturated conditions can be analytically solved based on location, whereas transient flow conditions involve both spatial and temporal variations, turning to numerical solutions. Additionally, current laboratory studies are not capable of capturing the mobilization processes at high-resolution spatial and temporal scales (Van Genuchten et al., 2004).

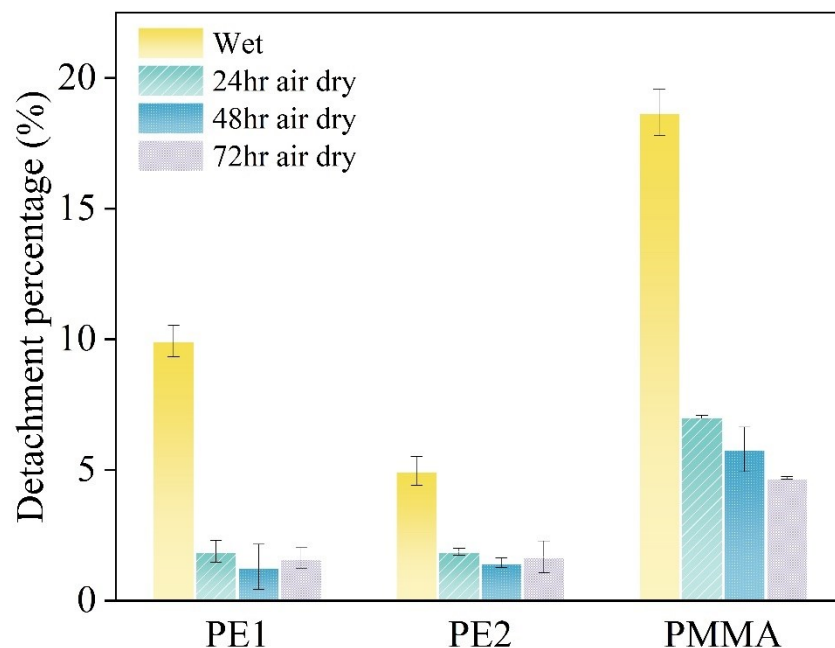


**Figure 4.7** Detachment percentages of PE1, PE2 and PMMA under wet and various air-dry durations.

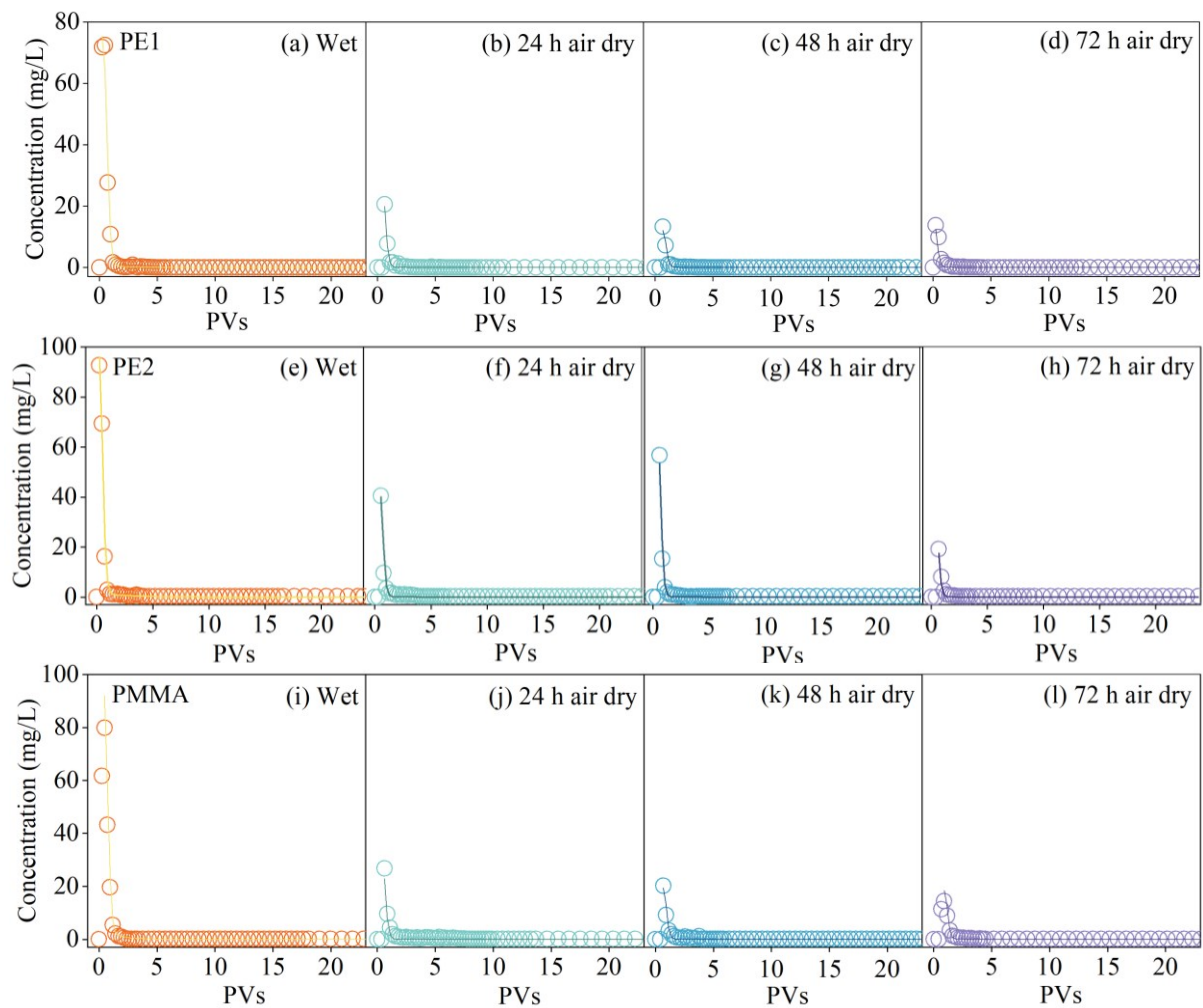


**Figure 4.8** Experimental (dot) and simulated (line) detachment curves of PE1, PE2 and PMMA under wet and various air-dry durations.

Table 4.1 Fitted parameters by Hydrus-1D.

Polymer types	Dry duration	Fitted parameters				Model statistics
		attachsolid2	DetachSolid2	attachsolid1	DetachSolid1	R2
PE1	0 hr	2.64E-03	0.2106	1.41E-02	0	0.9847
	24 hr	2.64E-03	0.2106	9.60E-04	0	0.9926
	48 hr	2.64E-03	0.2106	7.26E-04	0	0.9722
	96 hr	2.64E-03	0.2106	4.34E-04	0	0.9151
PMMA	0 hr	6.50E-03	0.1701	1.97E-02	0	0.9926
	24 hr	6.50E-03	0.1701	9.17E-04	0	0.9913
	48 hr	6.50E-03	0.1701	5.90E-04	0	0.9536
	96 hr	6.50E-03	0.1701	4.07E-04	0	0.9935
PE2	0 hr	3.68E-03	0.0915	1.04E-03	0	0.9907
	24 hr	3.68E-03	0.0915	6.18E-04	0	0.9520
	48 hr	3.68E-03	0.0915	1.91E-04	0	0.9790
	96 hr	3.68E-03	0.0915	3.46E-04	0	0.9903

#### 4.3.7 Environmental implications

This study investigated the detachment behavior of MPs from porous media taking two critical as well as practical factors, water content and flow regime, into consideration. Infiltration can remobilize attached MPs from substrate, indicating sediment could also act as sources of MPs to sublayers and groundwater, not only a sink. The results indicate that water content affects MP detachment for all the MPs studied, even for aged MPs and in the presence of transient flow. Unsteady flow, such as intermittent flow, flow transient in ionic strength and flow velocity, have been proved to give rise to the sudden release of previously balanced particles. However, low water content as prolonged drying significantly inhibit MP detachment even under suddenly changed flow conditions. The results highlight the significance of antecedent conditions in determining the mobilization of MPs in sediment. In the context of fluctuating weather condition, the intensified drought may give rise to the accumulation of MPs in sediment. The consequent impacts may require further investigation.

The present study employed the glass beads as substrate and only the surface interaction between glass beads, MPs, air, and water are considered. However, glass beads are different from natural sediment in various ways. Moisture evaporation can cause desiccation cracks and shrinkage in natural soil, which enlarge macropore size and modify soil structure and hydraulic properties by forming preferential flow paths for water and contaminants. Previous studies have shown that dry-wet cycles affected colloid mobilization by changing soil structures. For instance, Majdalani et al. (2008) noted that increased drying duration could break macropore walls under capillary stress, generating colloids, while when drying duration exceeded a critical time, colloid mobilization was impeded due to the binding with salts or minerals. Additionally, natural sediment presents heterogeneity in surface roughness, morphology, shape, and density. Shen et al.

(2011) highlighted the importance of surface roughness in colloid deposition, observing that polystyrene latex microspheres were more effectively retained in sand compared to glass beads. They claimed that the sharp asperities on sand surface reduced the energy barrier, promoting particle deposition in primary minima, and valleys on sand also enhanced attachment in secondary minima. Therefore, further research is needed to explore the interaction between MPs and natural sediment considering soil structures and the presence of minerals and salts.

# **Chapter 5 Transport of microplastics in shore substrates over tidal cycles: roles of polymer characteristics and environmental factors<sup>‡</sup>**

## **5.1 Background**

MPs are widely present in the environment. MPs can be classified as either primary or secondary, depending on their origin. Primary MPs are small plastic particles produced for commercial use. Secondary MPs, meanwhile, are the result of the fragmentation of larger pieces through processes such as mechanical abrasion, fluctuating temperatures, ultraviolet (UV) radiation, and biodegradation (Eerkes-Medrano et al., 2015; Wang et al., 2021). Due to the increasing demand and use of plastics and the ongoing breakdown of discarded plastics, the amount of MPs in the environment is projected to reach around 10 million tons by 2040 (Lau et al., 2020). The presence of MPs in oceans (Pabortsava and Lampitt, 2020), coastlines (Nor and Obbard, 2014), lagoons (Quesadas-Rojas et al., 2021), estuaries (Liu et al., 2021), sediment (Corcoran et al., 2020), vegetation, and organisms (Cole et al., 2013) has been well documented. However, compared to the literature on MPs in water, our knowledge regarding the fate of MPs in sediment is still somewhat limited.

Sediments are of critical importance due to their interaction with contaminants. With porosity and large chemically reactive surface areas, sediments adsorb and concentrate many pollutants from the water column, and, as a result, act as a major sink for pollutants (Wang et al., 2021). The

---

<sup>‡</sup> This work has been published as Feng, Q., Chen, Z., Greer, C.W., An, C., Wang, Z., 2022. Transport of microplastics in shore substrates over tidal cycles: roles of polymer characteristics and environmental factors. *Environmental Science & Technology*, 56 (12), 8187–8196.

existence of plastics in sediment has been reported in numerous field studies (Alomar et al., 2016; Bosker et al., 2019; Bridson et al., 2020). Studying the distribution of MPs and determining factors provides vital information required for managing MPs pollution and estimating their ecological risks. In this regard, MPs distribution patterns in sediment have been found to vary significantly both temporally and spatially, being subject to a number of interconnected factors, such as substrate and MPs characteristics, geographic factors, climate, and hydrodynamic forces. Hydrological processes are the most important physical processes in aquatic systems, acting an essential role in the retention and transportation of inorganic substances (Wang et al., 2018). For instance, floating plastics can be flushed onto shores by currents and waves, while plastics stranded along the shoreline can be flushed back into the open water. Moreover, turbulent mixing with sediment can accelerate the breaking down of plastics, burying them into the sediment (Turra et al., 2014). The infiltration depth, retention time, and remobilization of MPs in sediment, meanwhile, are of great ecotoxicological significance since they have a bearing on the extent of organisms' exposure to them. Many aquatic vertebrate and invertebrate communities depend on habitable substrate and groundwater–surface–water interactions (Hunt et al., 2006). Nutrient uptake is also sensitive to substrate composition and hyporheic exchange (Roche et al., 2019). Therefore, the existence of MPs in sediment may have fundamental impacts on the surrounding environment and the organisms that inhabit it.

Tidal zones, such as estuarine and coastal ecosystems, providing habitat for an array of plants, birds, and benthic species, are particularly vulnerable to MPs pollution (French, 1996; Bi et al., 2021). The majority of the existing research on the distribution of MPs in tidal zones concentrated on large spatial distributions, whereas there is a lack of validated, precise analysis of MPs transport under the influence of tidal cycles. Inconsistent results were identified in these studies

concerning the impacts of spring/neap tide and flood/ebb tide on the MPs concentration in the water or sediment phase. For instance, Sukhsangchan et al. (2020) reported neap tide to have a greater abundance of MPs compared to spring tide in surface water near a river mouth, whereas Sadri and Thompson (2014) found that more MPs were observed in the surface water during spring tides. Wu et al. (2020) found MPs to be more abundant in the surface sediment layer in the neap tide compared to in the spring tide, where the concentration of MPs exhibited a negative correlation with hydrological forces in an estuary. Zhang et al. (2020) observed linear relationships between MPs concentration growth rates and the tidal current velocity, but not between MPs concentration growth rate and tidal range. Meanwhile, studies on MPs presence in tidal zones revealed that the abundance of MPs in high tide is higher than that in low tide (Piehl et al., 2019; Sathish et al., 2019). Other studies have explored the effects of tidal cycles on MPs, with the consensus among these studies being that MPs concentration can vary greatly within or between tidal cycles, resulting in considerable uncertainty in interpreting data from field sampling (Moreira et al., 2016; Cohen et al., 2019; Balthazar-Silva et al., 2020). Indeed, no concrete trend in MPs concentration in response to changes in tidal cycles has been observed, as field experiments have not been able to uncover the complex interplay of various factors at work. Besides, density separation is generally used in sample extraction processing. According to a review by Harris (2020), the fluid density used for floating the MPs in such studies is approximately  $1.60 \text{ g/cm}^3$ , although densities as high as  $1.80 \text{ g/cm}^3$  have been employed. Polypropylene (PP), polyethylene terephthalate (PET), polyethylene (PE), polystyrene (PS), expanded polystyrene (EPS), polyamide (PA), polycarbonate (PC), and polyvinylchloride (PVC) are the most commonly detected MPs in the environment, these having densities of 0.92, 1.38, 0.97, 1.05, 0.02, 1.15, 1.20, and  $1.31 \text{ g/m}^3$ , respectively (Waldschlager et al., 2020; Guo et al., 2021). Accordingly, MPs with densities higher than  $1.80 \text{ g/cm}^3$  have received far less attention.

Some laboratory studies have been conducted to uncover the detailed mechanisms underlying MPs transport in sediment. The mobility of MPs in sediments is closely associated with porewater chemistry, such as ionic strength, organic carbon content, MPs properties (size, shape, density, surface charge, surface chemical composition), and substrate properties (size distribution, shape). Waldschlager and Schuttrumpf (2020) considered the properties of MPs and substrate, suggesting that the infiltration depth of MPs increases with decreasing MPs diameter and with a larger diameter of substrate. Additionally, it has been noted that MPs in sediment undergo a series of transformations, influencing their aggregation, transportation, and deposition. According to the Derjaguin–Landau–Verwey–Overbeek (DLVO) theory, increasing ionic strength compresses the electrical double layer and thereby reduces repulsive forces, leading to higher aggregation or deposition efficiency (Li et al., 2019; Wang et al., 2022). Alimi et al. (2021) concluded that exposure to 10 freeze–thaw cycles consistently led to significant aggregation and mobility reduction of nanoplastics compared to nanoplastics kept at 10 °C, especially at high ionic strengths in the absence of natural organic matter. Nevertheless, due to the determination restriction of MP concentration, previous transport studies have focused primarily on nanoplastics, meaning that PS has typically been selected for these studies due to the size control (Hou et al., 2020). Research on the transport of MPs with size of several or tens of microns and other types of MPs, meanwhile, are still limited. At present, knowledge on the effect of hydrodynamic forces (e.g., tidal cycles, flow velocity, submerging time) on MPs transport and related mechanisms are still insufficient.

In this context, in the present study, the transport of MPs in shore substrates over tidal cycles were comprehensive investigated. The objectives of this study were to explore (1) the effects of MP properties (e.g., size, density, and aging) in combination with tidal cycles on the transport of MPs;

and (2) the effects of environmental factors (e.g., substrate size, flow rate, and salinity) in combination with tidal cycles on the transport of MPs. The results obtained have significant implications in terms of predicting MPs behavior under the influence of tidal forces.

## **5.2 Methods**

### **5.2.1 Chemicals and materials**

PE is the most commonly utilized plastic due to its adaptability and toughness, hence its wide use as a packaging material. PTFE is chemically highly stable and is very resistant to extreme temperatures, and as such it has become the most widely employed fluororesin (Aderikha and Shapovalov, 2010). PE in sizes ranging from 4.00 to 6.00  $\mu\text{m}$  and PTFE ranging in size from 5 to 6  $\mu\text{m}$  were obtained from Micro Powders Inc. (New York, USA) for use in this study. In addition, PE of 125  $\mu\text{m}$  size, sea salt, and Tween 20 were purchased from Sigma Chemical Company (Ontario, Canada). Artificial seawater was prepared by adding sea salt (0.5, 20, and 34 g, respectively) to 1 L of deionized water, then passing it through a 0.22  $\mu\text{m}$  membrane to eliminate particles that might disturb the experiment. GB in sizes of 1, 2, 3, 4, and 5 mm were obtained, also from Sigma Chemical Company (Ontario, Canada).

### **5.2.2 Preparation of aged MPs**

Seawater-aged MPs were prepared by adding 0.5 g of MPs to 30 mL of the prepared seawater in a 250 mL flask, then agitating it in a shaker at 300 rpm and 20 °C for 30 or 60 days. The seawater-aged MP preparations are abbreviated herein as SW30 and SW60, respectively, based on the number of days of seawater aging. The aged MPs were then rinsed several times with deionized water, passed through a 0.22  $\mu\text{m}$  membrane to obtain the MPs particles, then dried in an oven at

60 °C. UV aging, meanwhile, was performed in a UV chamber with a wavelength of 254 nm (CX-2000, UVP/ Analytik Jena, USA). The pristine MPs were evenly spread onto glass petri dishes for UV radiation, and the dishes were shaken every 2 days in order to ensure uniform aging. The MPs were taken out after 30 or 60 days, which are abbreviated herein as UV30 and UV60, respectively, based on the number of days of UV aging.

### 5.2.3 MPs characterization

The pristine, seawater-aged, and UV-aged MPs were subject to particle size distribution analysis using Laser In-Situ Scattering and Transmissometry (LISST-200X, Sequoia Scientific, Bellevue, USA). The LISST-200X, it should be noted, can measure particle sizes in the range of 1  $\mu\text{m}$  to 500  $\mu\text{m}$ . For the characterization, 20 mL MPs mixtures were added to the LISST-200X chamber. For each iteration of the procedure, 20 measurements were recorded once the readings had stabilized. The contact angle was determined by means of the sessile drop method using an OCA 30 optical contact angle goniometer (Dataphysics Instruments GmbH, Germany). The MPs powder was flattened on double-sided tape affixed to a glass slide. Then, a 1.5  $\mu\text{L}$  deionized water droplet was dropped onto a pre-flattened MP particle, and a digital photo of the water droplet was taken. Following this, Fourier transform infrared spectroscopy (FTIR, INVENIO-S, Bruker, USA) was used for the analysis, while the surface morphology of the MPs was characterized using a scanning electron microscope (Regulus 8230, Hitachi, Japan). A small quantity of MPs was affixed to double-coated carbon tape on a holder. Then, the holder was coated with Au for 60 s to facilitate the conductivity of the MPs. The zeta potential of pristine and aged MPs particles (10 mg/L) was then determined using a Zetasizer Nano ZS (Malvern, UK).

### 5.2.4 Simulated tidal cycles with column test

GBs of 1, 2, 3, 4, and 5 mm were selected to represent the sediment substrate because GB can provide accurate sizes of substrate and it can be cleaned through a washing procedure without further release of particles that may disturb the measurement of MPs concentration. The GBs were initially washed in a 250 mL flask using deionized water. The rinsing water was subjected to LISST-200X until the particle concentration was less than 0.1  $\mu\text{L/L}$ . Then, the deionized water was added to the flask with the washed GB, which was agitated in a shaker at 150 rpm for 24 hr to further clean the GB. The GB was then washed several times using deionized water to make sure the particle concentration was still less than 0.1  $\mu\text{L/L}$ . The porosity of the GB packing was measured using the water displacement method.

The schematic diagram of the simulated tidal system is presented in Figure 5.1. The column was made of transparent polyvinyl chloride (5 cm inner diameter), with the bottom sealed by a 30-mesh metal screen fixed to the column using a stainless-steel hose clamp. To measure the MPs distribution in the column, lines were drawn on the cylinder at 1 cm depth intervals. In each simulated tidal cycle experiment, the cylinder was packed with GB up to 10 cm by tapping the column wall. GB sizes of 1, 2, 4 mm were used to represent uniform substrate, while 3 mm GB mixed with 5 mm GB was used to represent a bimodal substrate composition. 4 mm and 3+5 mm GBs have the same mean size. If assuming the diameters of three spheres tangenting with each other are  $d_1$ ,  $d_2$ , and  $d_3$ , respectively and  $d$  is the diameter of sphere fitting in the middle of these three spheres, the  $d$  can be calculated as:  $((d_1 + d_2 + d_3)d_1d_2d_3)^{\frac{1}{2}} = ((d_1 + d_2 + d)d_1d_2d)^{\frac{1}{2}} + ((d_1 + d + d_3)d_1dd_3)^{\frac{1}{2}} + ((d + d_2 + d)dd_2d)^{\frac{1}{2}}$  according to Zamani (2020). Therefore, 3+5 mm GBs have smaller porosity compared to uniform 4 mm GBs. The top of the column was packed with 6 mm GB to pre-equilibrate the water flow. Three types of MPs, 4–6  $\mu\text{m}$  PE

(abbreviated as PE1,  $0.97 \text{ g/cm}^3$ ),  $125 \text{ }\mu\text{m}$  PE (abbreviated as PE2,  $0.97 \text{ g/cm}^3$ ), and  $5\text{--}6 \text{ }\mu\text{m}$  polytetrafluoroethylene (PTFE,  $2.20 \text{ g/cm}^3$ ), were applied to represent MPs of different sizes and densities. A PE1 solution of  $0.1 \text{ g/L}$  was prepared by adding  $0.1 \text{ g}$  PE1 into  $1 \text{ L}$  deionized water with  $0.001\%$  v/v Tween 20 (to help disperse the MPs), then mixed using a homogenizer (Ultra-Turrax T25, IKA, Germany) at  $10,000 \text{ rpm}$  for  $10 \text{ min}$  to disperse the MPs uniformly. Similarly, a PE2 solution of  $0.1 \text{ g/L}$  and a PTFE solution of  $0.3 \text{ g/L}$  were prepared. The concentrations of MPs in the solutions were determined based on the experimental design and the measuring range of the LISST-200X. Before the start of each column test,  $20 \text{ mL}$  of the MPs solution was used to determine the initial MPs concentration. Then,  $980 \text{ mL}$  of MPs solution was introduced into the column using a peristaltic pump (Masterflex, Cole-Parmer Instrument Co., USA). When the MPs solution had passed through the column, the beaker containing the outflow solution was placed under the mixer, and the empty beaker was used to contain the column, which was mounted to an iron stand. MPs solution was added to the beaker until the water level reached the  $10 \text{ cm}$  mark on the column. The water flow direction was then changed using a pump to decrease the water level. The MPs suspension was continuously mixed to prevent aggregation of the MPs. One increment and one decrease of water level were assumed to represent one tidal cycle. The solution passing through the column with no water level increase was defined as  $0.5$  cycles for the purpose of the study. The key factors influencing MPs transport, including MPs properties, substrate size, salinity, flow rate, and aging, were considered. Detailed experiment is summarized in Table 5.1.

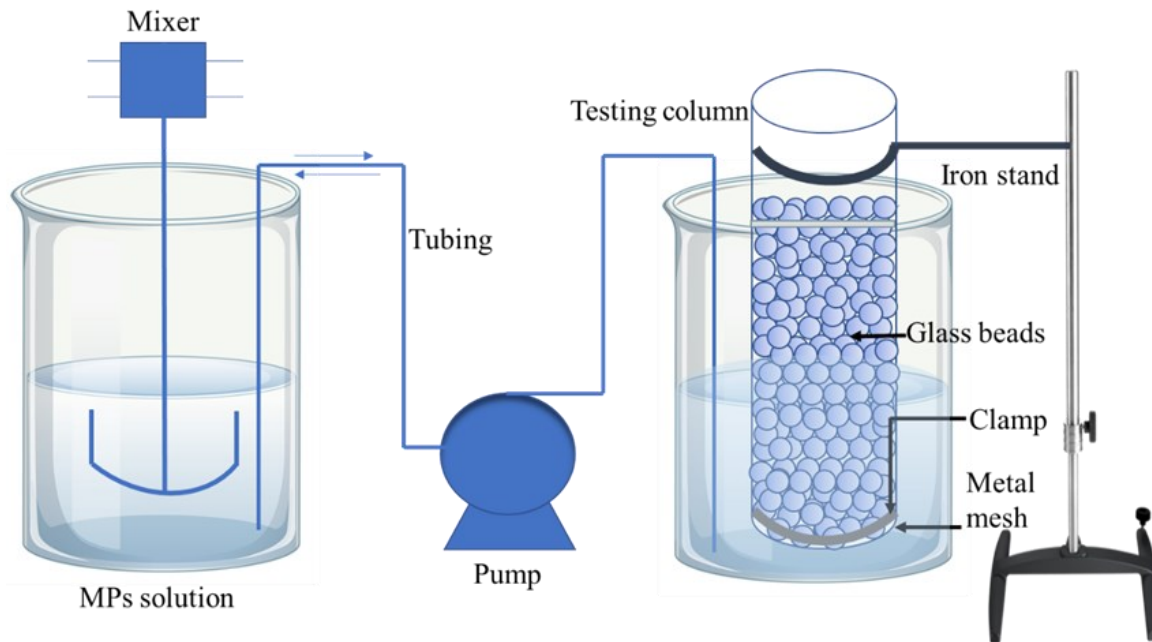


**Figure 5.1** Sketch of column test setup.

Table 5.1 Experimental design

Experiment No.	Glass beads size (mm)	MPs type	MPs aging	Tidal cycle	Flow velocity (cm/min)	Salinity (psu)
1	1	PE1	Without aging	0.5	3.34	0
2	1	PE1	Without aging	5	3.34	0
3	1	PE1	Without aging	10	3.34	0
4	1	PE1	Without aging	15	3.34	0
5	1	PE1	Without aging	20	3.34	0
6	2	PE1	Without aging	0.5	3.34	0
7	2	PE1	Without aging	5	3.34	0
8	2	PE1	Without aging	10	3.34	0
9	2	PE1	Without aging	15	3.34	0
10	2	PE1	Without aging	20	3.34	0
11	3+5	PE1	Without aging	0.5	3.34	0
12	3+5	PE1	Without aging	5	3.34	0
13	3+5	PE1	Without aging	10	3.34	0
14	3+5	PE1	Without aging	15	3.34	0
15	3+5	PE1	Without aging	20	3.34	0
16	4	PE1	Without aging	0.5	3.34	0
17	4	PE1	Without aging	5	3.34	0
18	4	PE1	Without aging	10	3.34	0
19	4	PE1	Without aging	15	3.34	0
20	4	PE1	Without aging	20	3.34	0
21	1	PE2	Without aging	0.5	3.34	0
22	1	PE2	Without aging	5	3.34	0
23	1	PE2	Without aging	10	3.34	0
24	1	PE2	Without aging	15	3.34	0
25	1	PE2	Without aging	20	3.34	0

Experiment No.	Glass beads size (mm)	MPs type	MPs aging	Tidal cycle	Flow velocity (cm/min)	Salinity (psu)
26	1	PTFE	Without aging	0.5	3.34	0
27	1	PTFE	Without aging	5	3.34	0
28	1	PTFE	Without aging	10	3.34	0
29	1	PTFE	Without aging	15	3.34	0
30	1	PTFE	Without aging	20	3.34	0
31	2	PTFE	Without aging	0.5	3.34	0
32	2	PTFE	Without aging	5	3.34	0
33	2	PTFE	Without aging	10	3.34	0
34	2	PTFE	Without aging	15	3.34	0
35	2	PTFE	Without aging	20	3.34	0
36	3+5	PTFE	Without aging	0.5	3.34	0
37	3+5	PTFE	Without aging	5	3.34	0
38	3+5	PTFE	Without aging	10	3.34	0
39	3+5	PTFE	Without aging	15	3.34	0
40	3+5	PTFE	Without aging	20	3.34	0
41	4	PTFE	Without aging	0.5	3.34	0
42	4	PTFE	Without aging	5	3.34	0
43	4	PTFE	Without aging	10	3.34	0
44	4	PTFE	Without aging	15	3.34	0
45	4	PTFE	Without aging	20	3.34	0
46	1	PE1	Without aging	10	3.34	5
47	1	PE1	Without aging	10	3.34	20
48	1	PE1	Without aging	10	3.34	34
49	1	PTFE	Without aging	10	3.34	5
50	1	PTFE	Without aging	10	3.34	20

Experiment No.	Glass beads size (mm)	MPs type	MPs aging	Tidal cycle	Flow velocity (cm/min)	Salinity (psu)
51	1	PTFE	Without aging	10	3.34	34
52	1	PE1	Without aging	5	0.67	0
53	1	PE1	Without aging	5	2.00	0
54	1	PTFE	Without aging	5	0.67	0
55	1	PTFE	Without aging	5	2.00	0
56	1	PE1	SW30	10	3.34	0
57	1	PE1	SW60	10	3.34	0
58	1	PE1	UV30	10	3.34	0
59	1	PE1	UV60	10	3.34	0
60	1	PTFE	SW30	10	3.34	0
61	1	PTFE	SW60	10	3.34	0
62	1	PTFE	UV30	10	3.34	0
63	1	PTFE	UV60	10	3.34	0

After each experiment, the GB was carefully removed in 1 cm increments of depth from the surface using a long-dipper scoop, and transferring to a 250 mL flask. Next, 100 mL deionized water was added to each flask. The flasks were agitated in a shaker at 150 rpm for 24 h to fully resuspend the MPs retained in each GB layer. Then, the supernatant of each flask was used to determine the MPs concentration employing LISST-200X. The concentrations of PE1 and PTFE were measured using the LISST-200X with a 20 mL vial. The large particle size of PE2 rendered the particles with higher floatation (which cannot be evenly distributed to obtain a steady reading without stirring). The concentration of PE2 was measured by mounting the instrument on an iron stand. The 100 mL supernatant was transferred into a 1 L beaker, and the remaining GB in the flasks was rinsed several times with 600 mL of deionized water. The rinsing water was also transferred into the 1 L beaker, which resulted in a 700 mL solution in the beaker. The beaker was then placed on a magnetic stirrer operating at 1,000 rpm, and the LISST-200X detector was submerged into the solution to obtain the data. MPs solutions before and after column tests were also measured. The MPs retention percentages were calculated using the following equation:

$$\text{MP retention percentage per 1 cm layer} = \frac{M}{M_0} \times 100\%,$$

where  $M$  is the mass of MPs obtained in each flask (MPs retained on GB layer of the column) for a given MPs concentration multiplied by 0.1 (100 mL volume), and  $M_0$  is the original MPs mass (prior to the column experiment), obtained by multiplying the MPs concentration by 0.98 (980 mL volume).

### 5.2.5 Statistic Analysis

The stratification ratio (used to denote the soil quality) was used to determine the difference in MPs retention between the bottom and surface layers.(Franzluebbers, 2002) Stratification ratios

allow for a wide range of soil indicators to be compared on the same scale due to an internal normalization step. The stratification ratio was calculated by dividing the MPs retention percentages at the surface layer (0–1 cm) by those at the bottom layer (9–10 cm). Moreover, the DLVO interaction energy, incorporating the Lifshitz-van der Waals and electrostatic double-layer interactions, were quantified for particle–media interactions under various ionic strengths. The Carbonyl index (CI), it should be noted, is defined as the ratio of absorption intensity obtained from FTIR at carbonyl groups around  $1,870\text{ cm}^{-1}$  to  $1,650\text{ cm}^{-1}$  to an internal constant band (Song et al., 2017), which is carbonyl to the methylene peak ( $1,712\text{ cm}^{-1} / 2,915\text{ cm}^{-1}$ ) in the case of PE, and carbonyl to the carbon–fluorine bond ( $1,712\text{ cm}^{-1} / 1,143\text{ cm}^{-1}$ ) in the case of PTFE. Spearman correlations following linear regression were conducted to identify potential correlations between MPs retention and various factors. The graphs were plotted using Origin 2021 (OriginLab Corporation, USA).

### **5.3. Results and discussion**

#### **5.3.1 Characterization of pristine and aged MPs**

The surface of the pristine and aged MPs was characterized using SEM (Figure 5.2). The pristine PE1 was observed to have a relatively flat surface and sharp edges. The surface of the SW60-PE1, though, was uneven and the edges were obtuse. The MP particles showed signs of abrasion resulting from the shearing effect in the shaking seawater. The surface morphology of the UV60-PE1 showed more cracks as a result of aging and can be easily fractured by the electrons from FESEM. Different aging methods have different energy inputs, leading to different morphology features of aged MPs. UV aging altered both physical and chemical properties of PE1. UV radiation triggered the generation of more hydrophilic groups (i.e., C–OH, –COOH, C=O) on PE

(Figure 5.4), which was confirmed by the increased CI index from 0.08 to 0.13 (Figure 5.3). The oxygen-containing functional groups on the surface also contributed to decreased contact angles from 141.8 to 134.1° and decreased zeta potential from -15.5 to -33.3 mV under 60-day UV radiation (Feng et al., 2021; Yang et al., 2021). UV radiation has high-enough energy to cause the breaking of polymer chains, generating free radicals reacting with oxygen in environment to form peroxy, hydroperoxide, or pairs of hydroxyl and alkoxy radicals. This process leads to the generation of functional-containing functional groups (Gewert et al., 2015). Shi et al. (2021) noticed that the surface of MPs turned out to be smooth after 960 hr UV aging, which could be attributed to chemical stripping. Shaking seawater in the present study mainly caused physical changes resulting from the shearing effect and it may not provide enough energy to cause chain scission to generate new surface functional groups. As shown in Figure 5.3, the CI indexes of PE1-SW30 and PE1-SW 60 were 0.05 and 0.10, respectively, which were similar to that of pristine PE1. The contact angles of PE1 decreased from 141.8° to 137.2° under 60-day seawater aging and zeta potential of PE1-SW30 and PE1-SW 60 were -12.4 and -31.7 mV, respectively, attributed to surface change, and the decreases were less pronounced than those under UV aging. The mean particle size of PE1 under both UV and seawater aging did not show great alteration. Compared to PE1, the CI index and mean particle size of PTFE were not significantly altered after 60 days of UV and seawater aging. No new surface functional group was detected by FTIR for both aging methods (Figure 5.4b). Interestingly, the contact angles increased after aging while zeta potential decreased after 60 days seawater and UV aging (Figure 5.3b). Besides, UV radiation triggered more pronounced alteration, which could be attributed to higher energy provided by UV radiation. Koh et al. (1997) observed that increasing ion dose of Ar<sup>+</sup> irradiation increased the surface roughness of PTFE and the wettability was inversely proportional to the surface roughness.

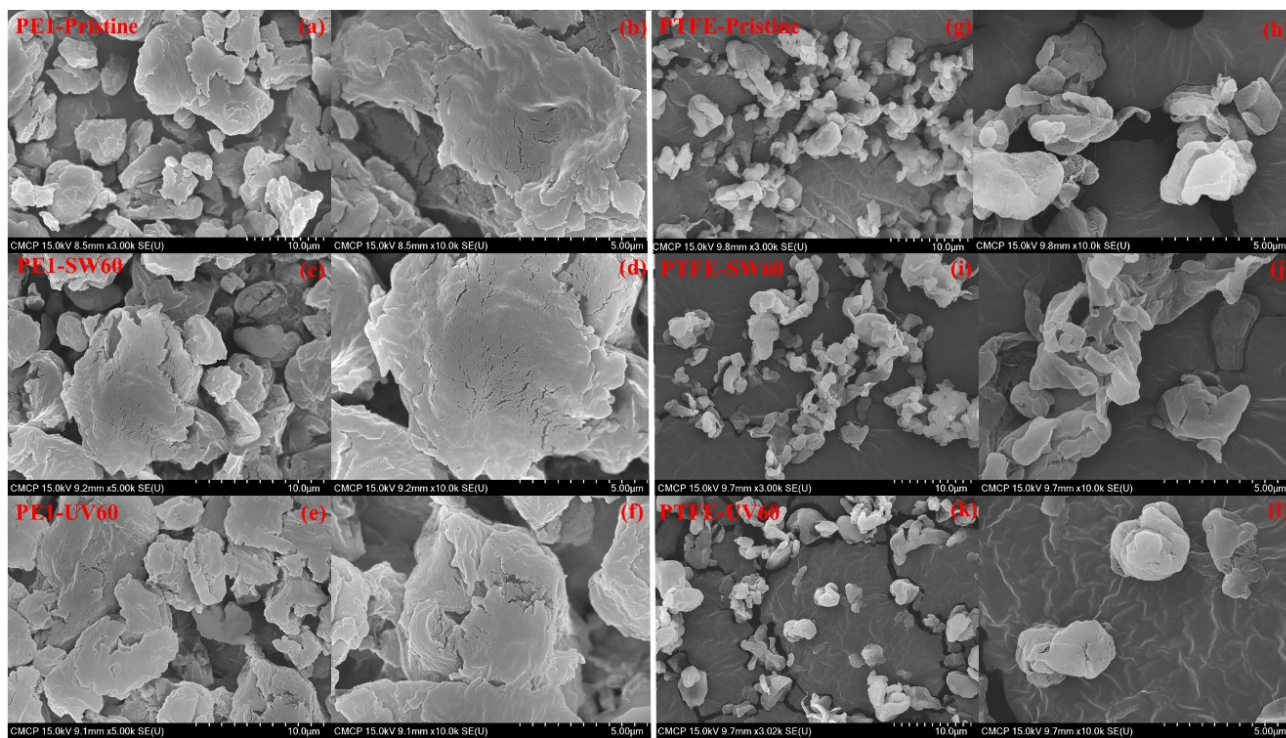


**Figure 5.2** SEM images of the pristine and aged PE1 (a–f) and PTFE (g–l) particles.

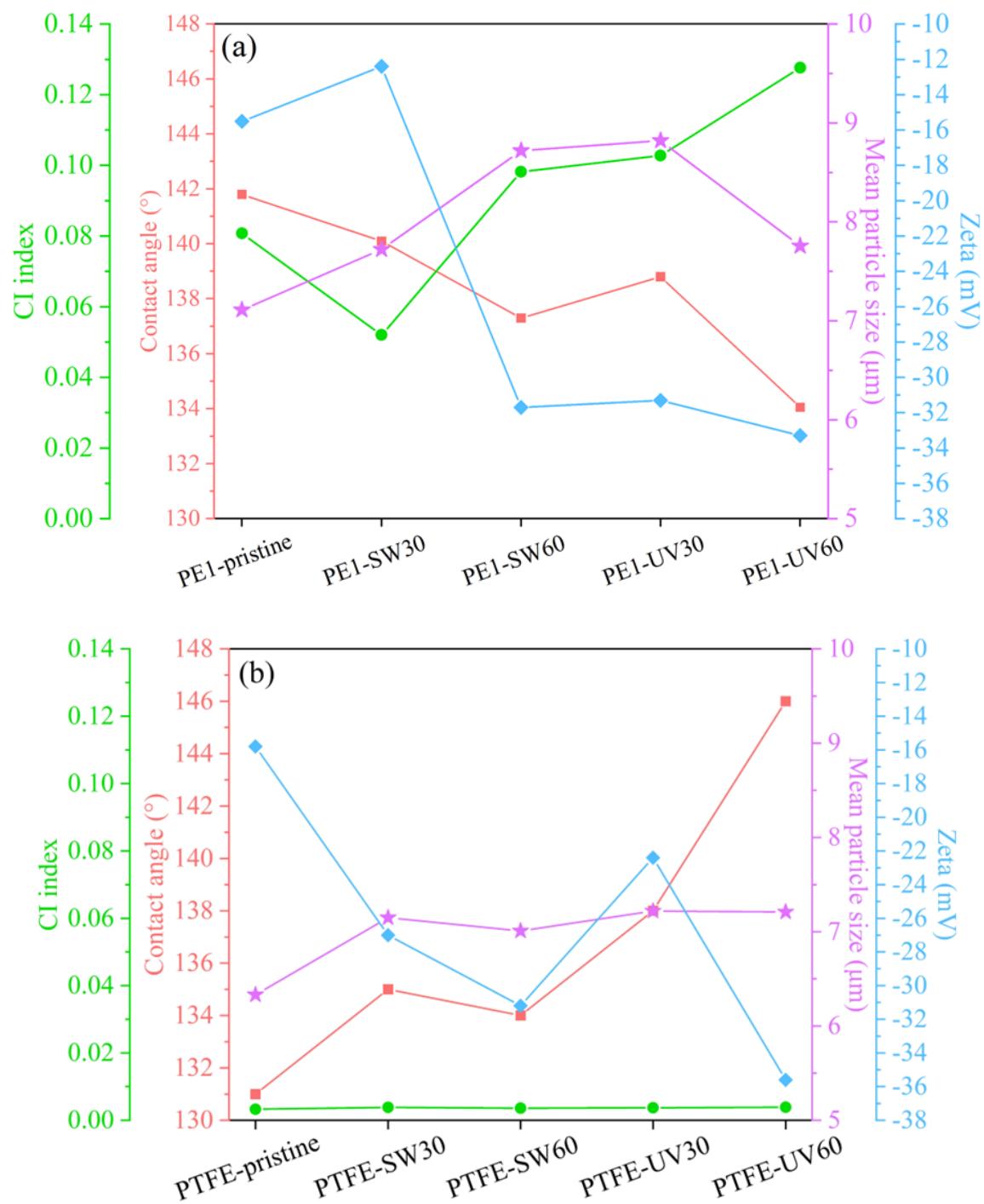


**Figure 5.3** CI index, contact angle, mean particle size, and zeta potential of various aged PE1 and PTFE.

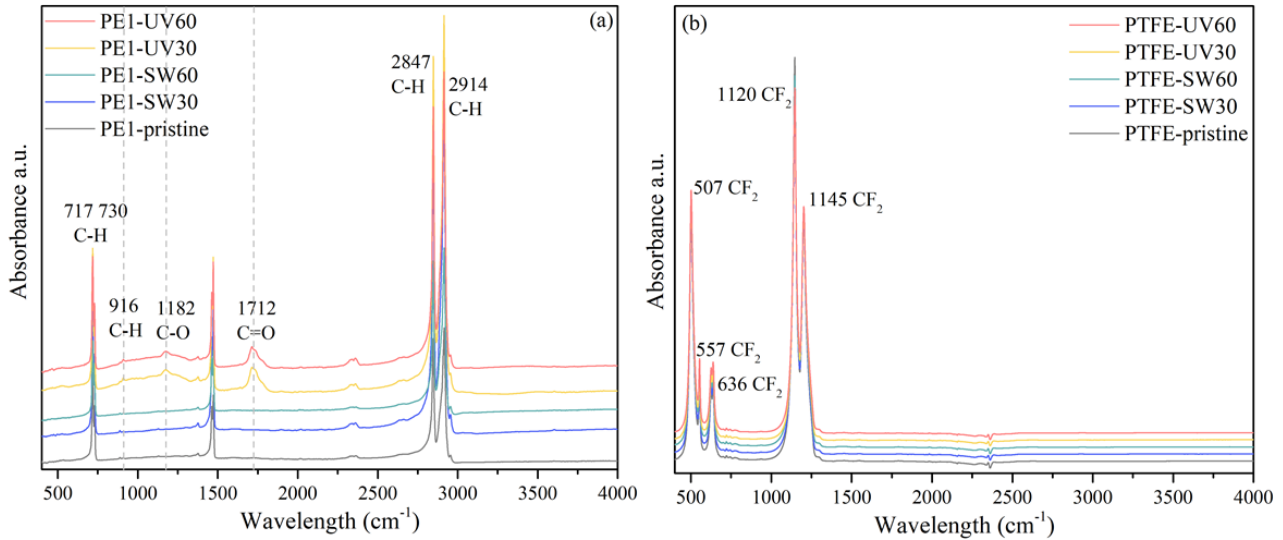


**Figure 5.4** The FTIR spectra of pristine and various aged MPs.

### 5.3.2 Effects of substrate size on MPs transport

Substrate size plays a significant role in determining the transport of particles in porous media. Particles have different types of interactions with the substrate: (1) by straining, depending on the texture (grain size distribution) and structure (macropores and micropores distribution), and (2) by physical and chemical interaction forces between particles and the substrate. (McDowell-Boyer et al., 1986) In this study, three uniform GB of 1, 2, and 4 mm and one bimodal GB of 3+5 mm were selected. When considering the one-direction infiltration (0.5 cycles), more MPs were retained in the upper layer of smaller substrates (sizes of 1 mm and 2 mm) compared to that of larger substrates (3+5 mm and 4 mm), as shown in Figure 5.5. This phenomenon could be attributable to the bridging process. In substrate with a porosity significantly larger than the infiltrating particles, particles move through the porous medium in unimpeded static percolation (Gibson et al., 2009). The bridging process may also occur if particles embed into the substrate to form a clogging layer, thereby preventing the particles from further transport. Subsequently, with the water moving up and down, the clogged particles could be remobilized into the pore water, leading to transport in

the pore water once again. The PTFE retention percentages, meanwhile, also decreased with an increase in GB size (Figure 5.5j). A larger substrate size entails larger pore sizes, higher pore connectivity, and weaker straining, making the substrate more conducive to MPs transport (Bradford et al., 2007). With the increase of cycles, the vertical distribution of MPs in the column became more uniform, confirming a downward movement of MPs along the profile. The PE1 retention percentages of 1 mm, 2 mm, 3+5 mm, and 4 mm GB decreased from 31.83% to 4.77%, 19.89% to 4.05%, 15.83% to 3.07%, and 13.93% to 2.13%, respectively, with the increase of tidal cycles (Figure 5.5i). In addition, with an increase in number of cycles, the PTFE retention percentages in 1, 2, 3+5, and 4 mm substrate decreased from 33.76% to 21.62%, 33.48% to 11.31%, 28.45% to 11.78%, and 27.70% to 9.58%, respectively (Figure 5.5j). It should be noted that, although 3+5 and 4 mm GBs have the same mean particle size, bimodal substrate contributed to higher retention percentages compared to that of uniform substrate due to smaller porosity. This result is consistent with the findings of Waldschlager and Schuttrumpf (2020) who suggested that bimodal GB had lower infiltration depths for MPs debris than the uniform GB.

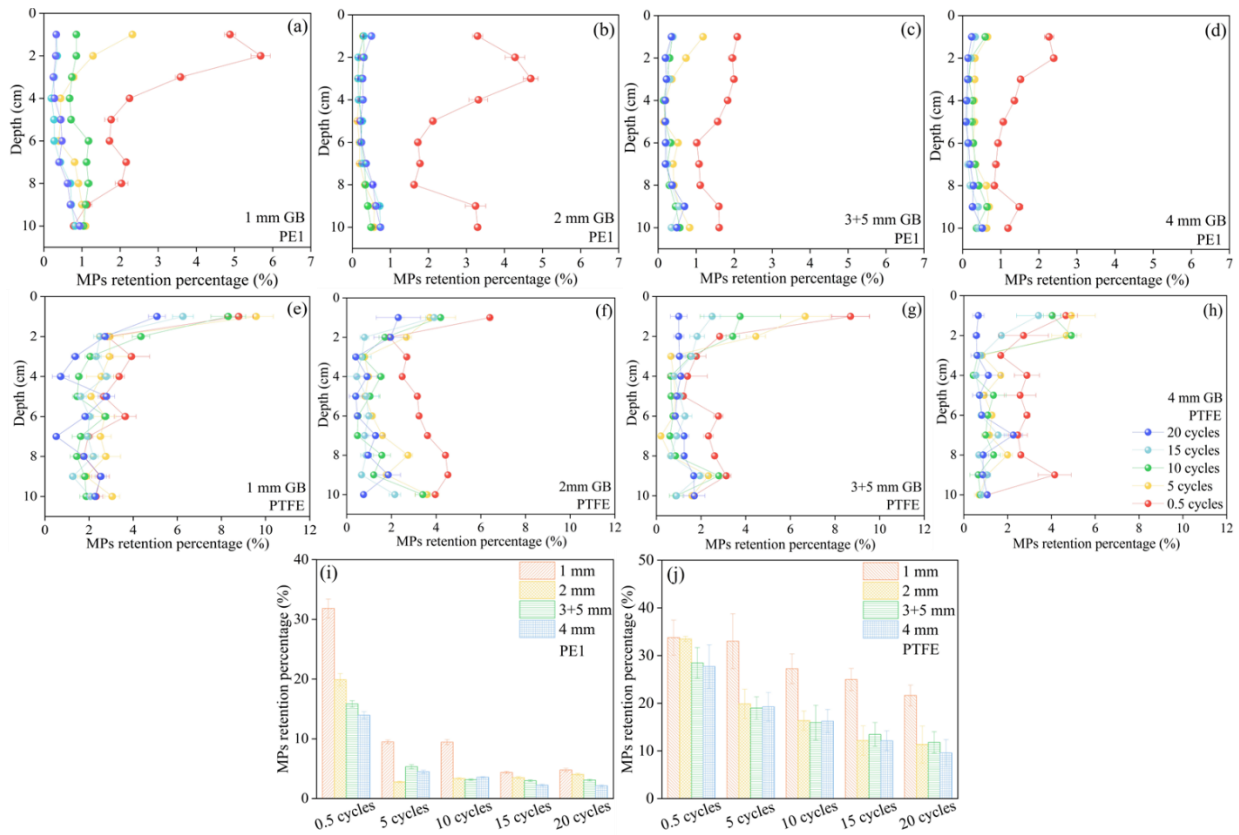


**Figure 5.5** Effects of substrate size on MPs distribution and retention. (a–d) PE1 distribution in columns with 1, 2, 3+5, and 4 mm GB under different tidal cycles; (e–h) PTFE distribution in columns with 1, 2, 3+5, and 4 mm GB under different tidal cycles. (i–j) PE1 and PTFE retention in the whole columns with 1, 2, 3+5, and 4 mm GB under different tidal cycles.

### 5.3.3 Effects of size and density of MPs on transport in tide-influenced substrates

MPs behave distinctively in the environment depending on their properties. For instance, if a MP is buoyant in water, it can be transferred shoreward and beached by wind and currents. If a MP is non-buoyant, it may sink to the bottom, or be transported off-shore by the return flow, or jump upward from the bottom by means of the Stokes drift (Chubarenko et al., 2018), or be washed onto the beach during an upwelling event (Chubarenko and Stepanova, 2017). In the present study, PE1 and PTFE with similar particle sizes but different densities showed different retention behavior under the influence of tidal cycles. Although the increase in cycle number enhanced the transport of both PE1 and PTFE, PE1 was washed out more with water level changes (Figure 5.6). For instance, in 1 mm substrate, 85% of the PE1 retained by 0.5 cycles was washed out by 20 cycles, while only 36% of the PTFE retained by 0.5 cycles was washed out by 20 cycles. This phenomenon can be attributed to the difference in their densities and sizes, as depicted in the Graphic Abstract. Taking one layer of substrate as an example, a specific number of MPs was retained on the surface of the substrate when the water level dropped. When the water level rose, meanwhile, a certain amount of MPs was trapped under the substrate, and some of the pre-retained MPs became re-suspended into the mobile water phase. Due to its low density and slightly larger mean particle size, PE1 showed a higher likelihood of being resuspended compared to PTFE that has a higher density than water and slightly smaller mean particle size. Nevertheless, PTFE exhibited a lower likelihood of becoming resuspended as the water level rose, resulting in a slower removal of PTFE particles on the top surface of the substrate as the number of cycles increased. Chen et al. (2010) mentioned that gravitational forces can have a substantial impact on the deposition of colloids of micrometer size. Chrysikopoulos and Syngouna (2014) suggested that, in a saturated porous medium, gravity is a significant force for colloid transport under unfavorable deposition conditions. Regarding the particle size, PE2 with a larger size demonstrated higher

retention percentages compared to PE1. After 20 cycles, only 27% of the PE2 particles retained in 1 mm substrate by 0.5 cycles were washed out from the substrate, which was much lower than that of PE1. Larger particles were observed to be more easily trapped in the pores of the substrate before traversing the length of the filter.

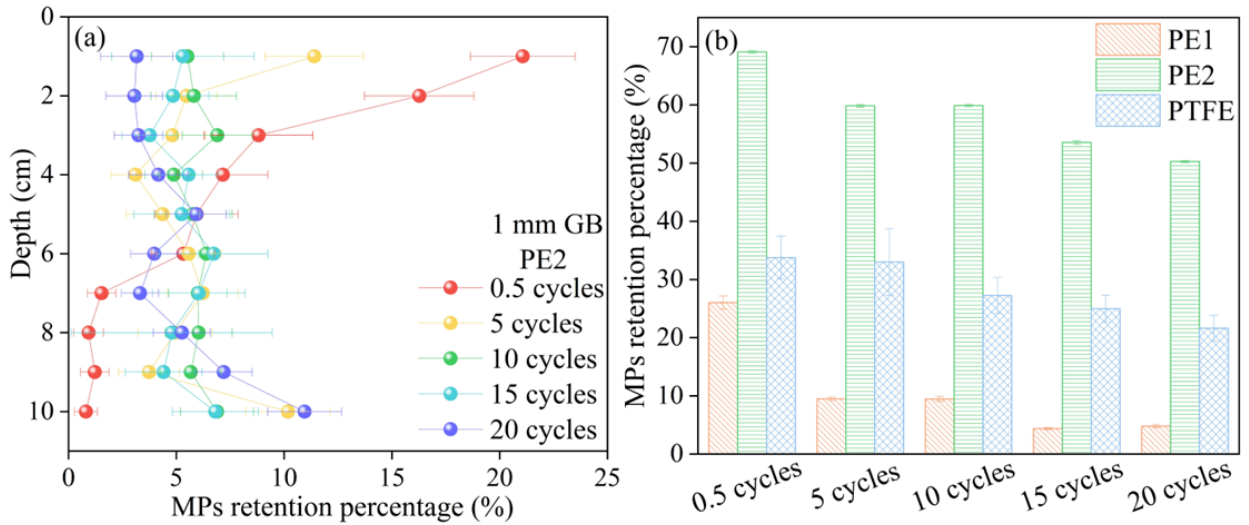


**Figure 5.6** Effects of MPs properties on their distribution and retention. (a) PE2 distribution in column with 1 mm GB under different tidal cycles. (b) Retention of PE1, PE2, and PTFE in the whole column with 1, 2, 3+5, 4 mm GB under different tidal cycles.

#### 5.3.4. Effects of aging on MPs transport in tide-influenced substrates

MPs in aquatic environments undergo a series of physical and chemical alterations that in turn influence their environmental behavior. Figure 5.7 shows the distribution of pristine MPs and aged MPs in the column after 10 cycles. As can be seen, the distribution of different aged MPs is reflective of similar patterns, though with different retention percentages. The retention percentages of PE1-pristine, PE1-SW30, and PE1-SW60 were 9.44%, 8.28%, and 6.40%, respectively, which were significantly different between each other ( $p < 0.05$ ). The retention percentages of PE1-UV30, and PE1-UV60, meanwhile, were 5.09% and 3.63%, respectively, which were significantly lower than PE1-pristine and significantly different between each other. Aged PE1 became more negatively charged compared to pristine MPs, thereby increasing the repulsion between aged MPs and negatively charged GB, in turn facilitating MPs transport in porous media. In this regard, Li et al. (2020) suggested that the transport of the heteroaggregates of negatively-charged MPs and kaolinite was significantly higher than that of the heteroaggregates of positively charged MPs and kaolinite, proving that the transport of MPs is highly correlated with its surface charge. The retention percentages of PTFE-SW30, PTFE-SW60, PTFE-UV30, PTFE-UV60 were 32.77%, 30.93%, 39.56%, and 39.40%, respectively, which were not significantly different between each other but significantly higher than that of PTFE-pristine (27.23%). After seawater and UV aging, the water contact angles of PTFE increased while the zeta potential decreased, indicating an increased surface roughness (Koh et al., 1997). These coupled changes may contribute to the enhanced retention of PTFE particles.

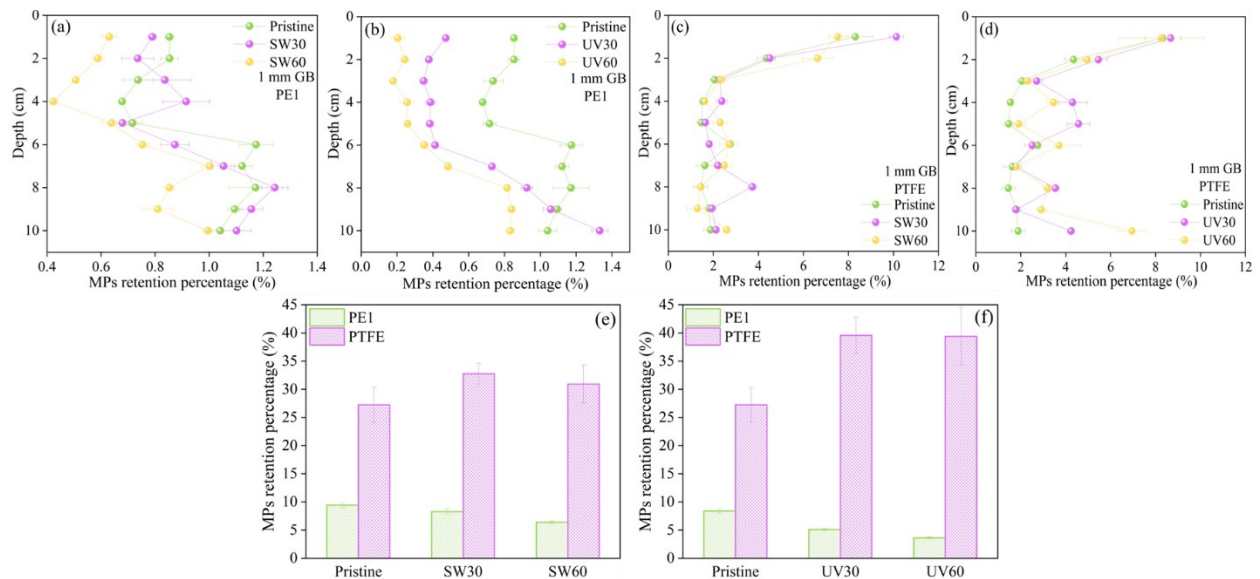


**Figure 5.7** Effects of aging on MPs distribution and retention. (a) PE1-pristine, PE1-SW30, PE1-SW60 distributions in the columns with 10 tidal cycles. (b) PE1-pristine, PE1-UV30, PE1-UV60 distributions in the columns with 10 tidal cycles. (c) PTFE-pristine, PTFE-SW30, PTFE-SW60 distributions in the columns with 10 tidal cycles. (d) PTFE-pristine, PTFE-UV30, PTFE-UV60 distributions in the columns with 10 tidal cycles. (e–f) Retention of PE1 and PTFE with various aging conditions in the whole column with 10 tidal cycles.

### 5.3.5 Effects of salinity on MPs transport in tide-influenced substrates

The salinity can vary considerably in aquatic environments. For instance, salinity in estuaries varies depending on the season. During the dry season, upstream and coastal waters have a greater impact on the channel, thereby increasing the salinity in the estuary. In the rainy season, on the other hand, the salt wedge retreats towards the lower estuary, causing a decrease in salinity in the estuary. The average salinity of sea water is 35 practical salinity unit (psu) and even reaches 42 psu during the dry season in estuary (Benfer et al., 2007). In this regard, previous porous media tests have proven that salinity/ionic strength affects MPs infiltration significantly (Chu et al., 2019; Li et al., 2019). In keeping with this finding in the literature, as can be seen in Figure 5.8, in the present study a higher salinity resulted in higher PE1 retention in the column, with the retention

percentage increasing from 9.44% (at 0 psu) to 9.68%, 11.17%, and 11.67% with salinities of 5, 20, and 34 psu, respectively. The retention percentages of PTFE, meanwhile, increased from 27.23% (at 0 psu), to 36.56%, 38.67%, and 36.22% with salinities of 5, 20, and 34 psu, respectively. Increasing ionic strength contributed to higher fluid density and ionic strength. As ionic strength elevated, the zeta potential of PE1 and PTFE changed from  $-15.50$ ,  $-3.50$ ,  $2.38$ , to  $4.52$  mV and from  $-15.8$ ,  $-4.78$ ,  $4.54$ , to  $6.13$  mV, respectively. In accordance with DLVO theory, as the ionic strength increased, the double layer repulsion between MPs and GB gradually disappeared and the attraction between the two gradually increased accordingly (Figure 5.8d–e). Moreover, the MPs became unstable in the system, thus restraining the mobility of MPs and making it easier for them to be intercepted by GB. Organic matter is an important component of biogeochemical cycles, which varies due to different input and output flux (Goñi et al., 2003). Contrary to ionic strength, the existence of organic matter leads to higher DLVO energy barriers between MPs and substrate, showing unfavorable condition attachment, enhanced transport of MPs, and fewer MPs retention (Alimi et al., 2021; Wang et al., 2022).

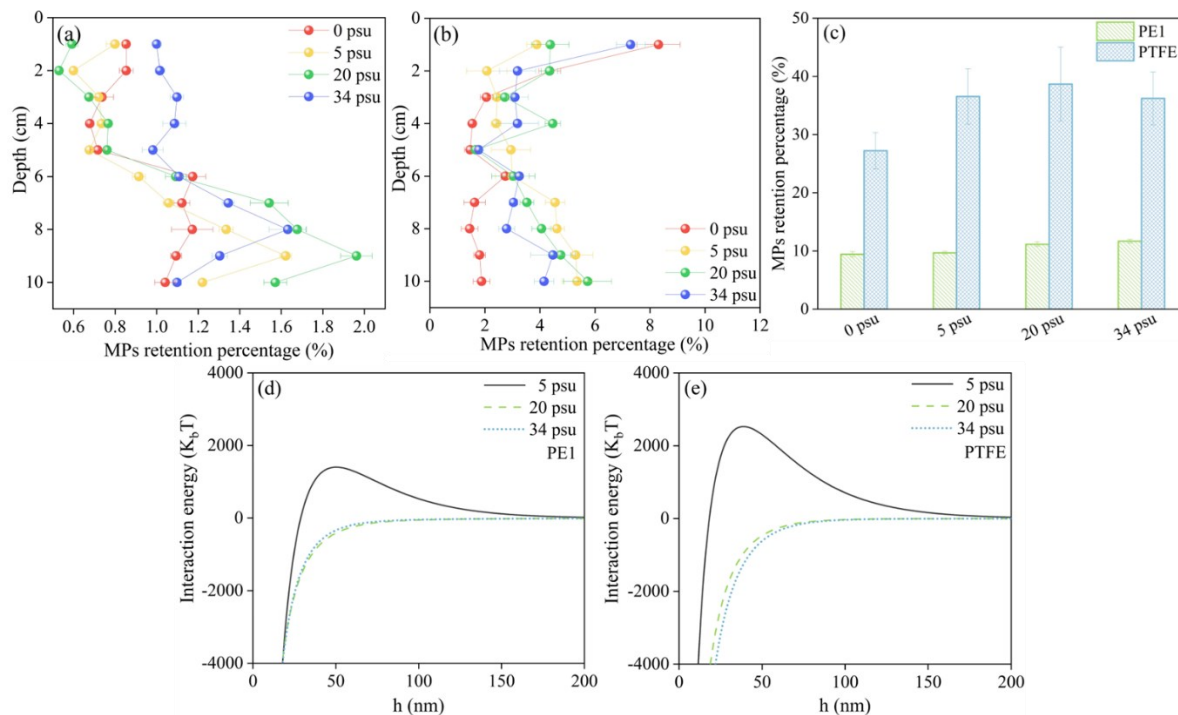


**Figure 5.8** Effects of salinity on MPs transport and the calculated interaction energy. (a–b) PE1 and PTFE distribution in columns at various ionic strengths with 10 tidal cycles. (c) Retention of PE1 and PTFE in the whole columns at various ionic strengths with 10 tidal cycles. (d–e) Interaction energy versus surface-to-surface separation distance for PE1/PTFE and GB at various ionic strengths.

### 5.3.6 Effects of tidal velocity on MPs transport in tide-influenced substrates

Tides can be classified as either spring tide or neap tide. Neap tides typically have a lower high tide and a higher low tide compared to spring tides. Hence, the current velocity of neap tides is slower than that of spring tides (Artal et al., 2019). In the present study, for under 5 cycles, an increase in flow rate from 0.67, 2.00, to 3.34 cm/min decreased PE1 retention percentages from 16.38%, 14.40%, to 9.48%, respectively, and decreased the PTFE retention percentages from 37.70%, 35.27%, to 33.00%, respectively (Figure 5.9). Lower hydrodynamic forces contributed to a higher retention of MPs in the surface layer. This result is consistent with a field sampling by Wu et al. (2020), who found that MPs are more abundant in surface sediments during neap tide

compared to during spring tide. Moreover, it has also been observed that low flow rates enhance the horizontal diffusing of MPs (Braun et al., 2015). When the flow rate increased, MPs were discharged into the mobile phase not only from the inlet fluid, but also from the substrate where they had been deposited. High flow rates, it should be noted, entail large thrust and shear force, leading to high mobility through the column (Chowdhury et al., 2011). In this regard, Lima et al. (2015) observed that all types of MPs in estuary water showed a strong positive correlation with high rainfall rates. In a more energetic aquatic environment, such as a tide-dominated estuary or a wave-dominated coastline, fine-grained particles can escape from the nearshore and be transported offshore (Harris, 2020).

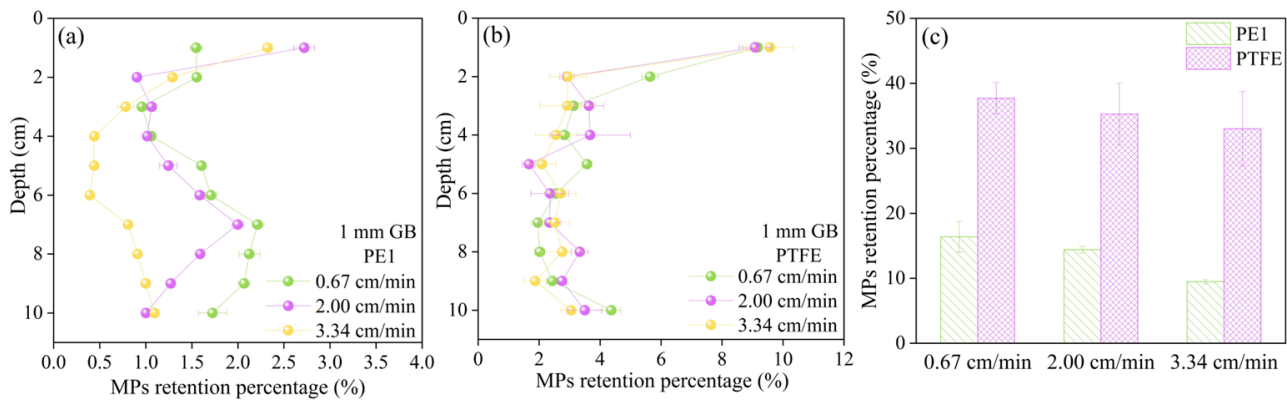


**Figure 5.9** Effects of flow velocities on MPs distribution and retention. PE1 (a) and PTFE (b) distribution in column under various flow velocities with 5 tidal cycles. (c) Retention of PE1 and PTFE in the whole column under various flow velocities with 5 tidal cycles.

### 5.3.7 Insights from correlation analysis and environmental implications

The MPs retention percentages throughout the 10 cm column were found to be significantly positively correlated with stratification ratio, MPs size, and MPs density, with  $r$ -values of 0.48, 0.81, and 0.51 ( $p < 0.05$ ), respectively. GB size, GB porosity, tidal cycles, and zeta potential, meanwhile, were found to be negatively related to retention percentage throughout the column, with  $r$ -values of  $-0.45$ ,  $-0.45$ ,  $-0.35$ , and  $-0.58$  ( $p < 0.05$ ), respectively (Figure 5.10). The stratification ratios in each iteration of the column experiment showed significant positive correlations with MPs size and MPs density ( $r = 0.39, 0.53$ , respectively,  $p < 0.05$ ), but a negative correlation with tidal cycles and zeta potential ( $r = -0.47, -0.34$ ,  $p < 0.05$ ). Furthermore, the factors influencing MPs retention also varied depending on the density of the MPs. If considering all the MPs used in this study, tidal cycles affected MPs retention and stratification, accounting for 21.5% of the variation (Figure 5.10b). The MPs with a density of  $0.97 \text{ g/cm}^3$  were mainly influenced by the number of cycles (accounting for 75.7% of the variation) (Figure 5.10c), while the variation in the retention and stratification of MPs with a density of  $2.2 \text{ g/cm}^3$  were explained by the tidal cycle as 35% (Figure 5.10d). These results imply that MPs less dense than water are prone to be transported, then escape from sediment and remobilize into water, whereas MPs denser than water have a lower likelihood to be affected by tidal cycles once stranded in a substrate compared to buoyant MPs.

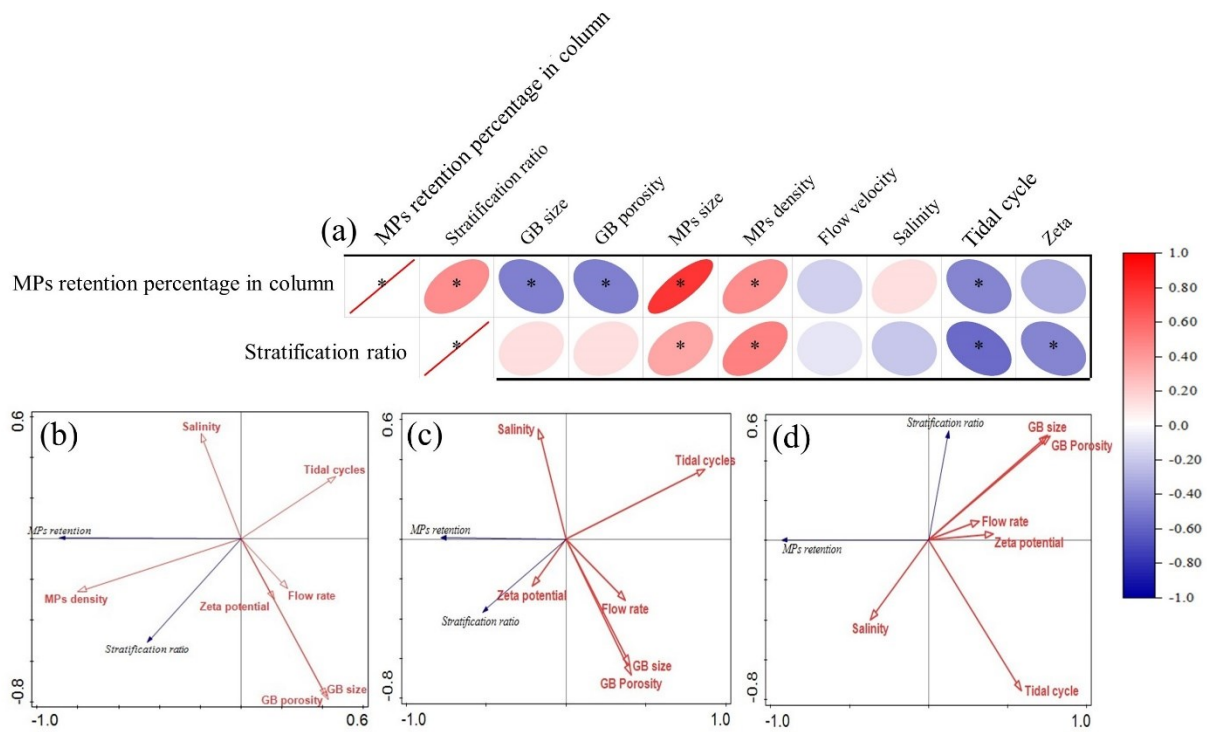


**Figure 5.10** Relationship between MPs retention and stratification in the column with various MPs and environmental properties. (a) Correlation of MPs (PE1, PE2, PTFE) retention and stratification with various MPs and environmental properties. (b, c, d) RDA plot for MPs (PE1, PE2, PTFE), PE1, PTFE retention and stratification with various MPs and environmental properties.

This study highlights the significance of MPs size and density in determining MPs behavior in a tidal environment. Hydraulic equivalence refers to the situation in which MPs possess a particle size, shape, and density similar to those of natural sediment, and, accordingly, may behave comparably to natural sediments (Harris, 2020). In fact, most natural particles are denser than plastic, ranging between 1.7 to 3.0 g/cm<sup>3</sup>. Compared to those trapped in the water phase, MPs trapped in sediment are more difficult to separate (Razeghi et al., 2021). The cleanup of stranded MPs in sediment involves the application of floating pool skimmers with fine mesh screens (Zhang et al., 2021). Even then, it is difficult to distinguish based on density between dense MPs and natural sediment.

There is still no clear consensus among the field studies available in the literature concerning the relationship between sediment characteristics and MPs. Enders et al. (2019) found that MPs concentration in estuarine sediments ranging from 1,000 to 5,000 µm and having a density > 1 g/cm<sup>3</sup> correlated with 125 to 250 µm fine sand, and those ranging from 500 to 1,000 µm correlated with sand grain sizes ranging from 16 to 125 µm. However, low-density particulate polymers and fibers showed no clear correlation with either of these fractions. Constant et al. (2021) found no relationship between the sediment features and MPs concentration in dredging disposal sites along the Aa River. Willis et al. (2017) found that MPs abundance decreases with depth down-core in an urban estuary. They also observed that the variations in MPs concentration were in line with the rate of global plastic production (Willis et al., 2017). As observed in the present study, various factors, including the number of cycles, substrate and MPs properties, and pore water chemistry, can influence the MPs concentration in a given layer of sediment. Indeed, the distribution of MPs in the natural environment is governed by a complex host of drivers. However, MPs sampling is expensive and laborious, often focusing on a limited depth or failing to account for the complex

hydrodynamic processes that control particle distribution, thereby overlooking the association between MPs distribution and these variables in the external environment. Therefore, long-term monitoring or pre-cleanup of the studied area are recommended.

The aquatic environment is facing intensifying threats from the release of plastic waste and commercial plastic pellet products. For instance, a cargo at Sri Lanka's Colombo Harbor caught fire and discharged billions of commercial plastic pellets to the shoreline in May, 2021 (Mongabay, 2021). In light of this, to ensure efficient response to spill incidents in a given area, the spill trajectory must be predicted, and the cleanup planned accordingly, in advance. A crucial part of the planning is to identify the environmental features that would be severely compromised by the pollution. The sediments that are least likely to trap MPs are high-energy, non-depositional sedimentary sections such as rocky shores, coarse sand and gravel shores, and high-energy and tide-dominated sections. On the other hand, muddy, low-energy estuaries, lagoons, and fjords that have relatively high efficiency for trapping fine sediment could also be effective in trapping MPs (Harris, 2020). As such, hydrodynamic and geomorphic information, such as shore type, wave height, tidal range, and wave fetch, gathered through aerial photographs and satellite images, can be used to discern the relative sensitivity among substrate sections (Rodrigues et al., 2021). In the present study, the horizontal movement of tides, the biofilm on MPs, the aggregation of MPs with phytoplankton, and the surface roughness of substrate were not considered, which deserve further exploration. Besides, more MP types with different structures, morphologies, and surfaces can be further considered in the future study.

## Chapter 6 A new perspective on the mobilization of MPs through capillary fringe fluctuation in a tidal aquifer environment<sup>§</sup>

### 6.1. Background

Due to the ubiquity of MPs in our environment, their behavior, fate, and biological toxicity have received considerable attention. Approximately 10 million tons of MPs are expected to be in the environment by 2040 (Lau et al., 2020). The presence of MPs in the ecosystem, including in sediment, organisms, and water—i.e., oceans (Pabortsava and Lampitt, 2020; Yang et al., 2022), coastlines (Nor and Obbard, 2014), lakes (Grbic et al., 2020), lagoons (Quesadas-Rojas et al., 2021), and estuaries (Liu et al., 2021)—has been well reported. For instance, a systematic global meta-analysis summarized that, in coastal wetlands, the average MPs concentrations in sediment, water, and biota are 156.7, 0.43, and 98.3 pieces/kg, respectively (Ouyang et al., 2022). Another review reported that the global average MPs concentrations in reservoir water, sediment, and biota are 10,129.19 pieces/m<sup>3</sup>, 1,289.39 pieces/kg, and 7.6 pieces/sample, respectively (Guo et al., 2021). Kosuth et al. (2018) found MPs in 158 of 159 drinking water samples (considering 3 samples of bottled water from the United States and 156 tap water samples from 14 countries). Mintenig et al. (2019) indicated that groundwater and drinking water in Germany contained only few polymer particles (mean 0.7 particles/m<sup>3</sup>). Panno et al. (2019) found the maximum concentration of MPs to be 15.2 pieces/L in wells from two karst aquifers in Illinois, USA. In spite of this and a few other studies, research on the presence of MPs in aquifers is still relatively

---

<sup>§</sup> This work has been published as Feng, Q., An, C., Chen, Z., Wang, Z., 2023. New perspective on the mobilization of microplastics through capillary fringe fluctuation in a tidal aquifer environment. *Environmental Science & Technology*, 57 (2), 929-938.

limited in comparison with the information on MPs in freshwater and ocean environments, this being largely attributable to the fact that aquifers are difficult to access.

Aquifers are a primary drinking water source for billions of people worldwide (Ferguson and Gleeson, 2012). The capillary fringe is a phenomenon occurring in aquifers that results from the adhesion of water molecules to subsurface solids. The capillary fringe serves as a transition zone between horizontal saturated groundwater flow and vadose zone with vertical unsaturated flow. Active mixing can occur between the capillary fringe and the zone below the water table, governed by local groundwater gradients (Dunn et al., 2005). Sharma et al. (2008) have noted in this regard that fluid can actively migrate from the area below the water table into the capillary fringe, or that the inverse phenomenon can also occur.

Water levels in the aquifer are a crucial parameter in groundwater hydrology and in examining the aquifer system more broadly. The groundwater table can fluctuate in response to tidal pumping, rainfall infiltration, groundwater withdrawals, evapotranspiration, and interaction with surface water bodies (Singaraja et al., 2018). Capillary fringe fluctuation is especially noticeable for water tables near the substrate and near the zones where periodic changes drive the groundwater table to oscillate. Previous studies concerning groundwater have suggested that cyclic alterations in water table level lead to a higher average depth of water saturation over the water table (Cartwright et al., 2005; Wu and Zhuang, 2010). In this regard, Singaraja et al. (2018) studied the groundwater levels along the Devanampatnam coast, and observed an increase of 6 cm in groundwater level during full moon and an 8 cm increase during new moon. Nepper (2001) showed that aquifers subject to oscillations caused by tidal cycles exhibit enhanced vertical diffusivity compared to environments

in which the porewater is static. However, the manner in which, and the extent to which, the capillary fringe affects MP movement in the substrate remains an open question.

In groundwater evaluation, the capillary fringe can have a significant effect on (1) particles and solutes approaching the water table from the vadose zone, (2) geochemical and biodegradation transformation of pollution bordering the water table, (3) the horizontal transport of pollution near the water table, and (4) the geochemical signature of mixed water infiltrating the groundwater (Silliman et al., 2002; Dunn et al., 2005). For instance, Kurt et al. (2016) conducted a column test and found that most of the biodegradation occurred within the lower part of the capillary fringe, indicating that the capillary fringe can create a sink for non-volatile contaminants. Haberer et al. (2012), meanwhile, experimented with a periodically changing boundary and found that, compared with steady-state conditions, highly dynamic variation of the water table enhances the mass transfer of oxygen from the atmosphere into the groundwater. Zhang et al. (2021) found that the concentration of trichloroethylene at cracks increased one order of magnitude compared with that at a static groundwater table when the groundwater table fluctuated by 0.2 m and a duration of one day.

The unique mechanisms in play in the capillary fringe will also affect particles existing in or moving into this region. Aramrak et al. (2014) used confocal microscopy to visualize the transport of the aqueous phase under the effects of capillary fringe fluctuation. Their study demonstrated that colloid mobilization occurs mainly during imbibition, and that colloids can be relocated into the deeper saturated zone as a result of fluctuations of the capillary fringe. Sharma et al. (2008) found that the colloids deposited on glass slide were most pronouncedly removed through the first two passings of air–water interface, while succeeding passings of the air–water interface did not

show significant extra colloid removal. Dunn et al. (2005) confirmed that microbes can be advected from the zone below the water table into the capillary fringe driven by steady flow. Nevertheless, the capillary fringe fluctuation influences MPs transport and deposition in porous media has yet to be investigated.

Sediment/soil not only functions as a sink for MPs, but it may also represent a potential source of MPs transport from solid phase to groundwater induced by agricultural activities, surface runoff, and flooding (Ren et al., 2021). In this regard, knowledge is still lacking with respect to the key processes and pathways underlying MPs behavior, transport, and fate in the soil/sediment–groundwater system. In this context, we investigated the impact of capillary fringe fluctuation on the transport and deposition of MPs in substrate. The main objective was to investigate the effects of (1) MP properties in association with water table fluctuation, and (2) environmental factors in association with water table fluctuation on MPs mobilization. The obtained results shed light on the potential risk of MPs being stranded in the substrate to coastal aquifer as well as on the pathway of MPs to the aquifer.

## **6.2 Methods**

### 6.2.1 Chemicals and materials

Polyethylene (PE) samples of 4 to 6  $\mu\text{m}$  and 20 to 25  $\mu\text{m}$  and polytetrafluoroethylene (PTFE) samples of 5 to 6  $\mu\text{m}$  were purchased from Micro Powders Inc. (New York, USA). PE is the most widely used plastic, as it can be molded easily and is strong and durable, making it an ideal packaging material. PTFE, meanwhile, is the most widely used fluororesin due to its chemical stability and resistance to extreme temperatures (Aderikha and Shapovalov, 2010). Also for use in

the study, sea salt, sodium chloride, Rhodamine B, Tween 20, and GBs in sizes of 0.5, 1, and 2 mm were purchased from Sigma Chemical Company (Ontario, Canada). UV60 refers to MPs aged under ultraviolet (UV) for 60 days and SW60 refers to MPs aged in shaking seawater for 60 days.

### 6.2.2 Simulated capillary fringe fluctuation with column test

GBs of 0.5, 1, and 2 mm were chosen as substrate because they are accurate in size and they can be washed without particles being released (given that particle release may interfere with the measurement of MPs concentration). Figure 6.1 depicts the set-up diagram of the capillary fringe fluctuation system. A metal screen (30-mesh) was used to seal the bottom of a polyvinyl chloride column (5 cm diameter) with a stainless-steel hose clamp. The cylinder was marked with lines every 1 cm to measure the depth in the column. The bottom of the column was filled with 4 cm of GBs to represent the aquifer. Above the aquifer, a 120  $\mu\text{m}$  metal screen of 5 cm diameter was placed to separate the aquifer from the GBs above. A pretest was conducted, showing that this mesh did not affect the MPs concentration after passing the mesh. Then, the next 10 cm of the cylinder was filled with GBs (i.e., to the 14 cm mark measuring from the bottom of the column) packing the GBs in this layer by tapping the column wall. Finally, GBs were packed at the top of the column in a depth of 3 cm to pre-equilibrate the inflow. GB sizes of 0.5, 1, and 2 mm were used (other than in the top layer, in which 6 mm GBs were used in all of the preparations) to represent different substrate sizes. Moreover, three types of MPs of various sizes and densities were used: 4–6  $\mu\text{m}$  PE (PE1, 0.97  $\text{g}/\text{cm}^3$ ), 20–25  $\mu\text{m}$  PE (PE2, 0.97  $\text{g}/\text{cm}^3$ ), and 5–6  $\mu\text{m}$  polytetrafluoroethylene (PTFE, 2.20  $\text{g}/\text{cm}^3$ ). On the basis of the measurement range of the Laser In-Situ Scattering and Transmissometry (LISST-200X, Sequoia Scientific, Bellevue, USA) and experimental design, the concentrations of the MPs solutions were calculated accordingly. 0.1 g of PE1 was added in 1 L deionized water with 0.01 percent v/v Tween20, then dispersed at 10,000

rpm for 10 min with a homogenizer (Ultra-Turrax T25, IKA, Germany). A 0.13 g/L PE2 dispersion and a 0.3 g/L PTFE dispersion were prepared in a similar manner. The original concentration of both the PE1 and PE2 dispersions was approximately 100  $\mu\text{L/L}$ . The original concentration of the PTFE solution was approximately 20  $\mu\text{L/L}$  (because it could not be dispersed evenly to reach 100  $\mu\text{L/L}$ ). The initial MPs concentration was identified by measuring the concentration of a 20 mL sample of the MPs dispersion before each column test. To load the MPs to the substrate, a peristaltic pump (Masterflex, Cole-Parmer Instrument Co., USA) was used to introduce the rest of MPs dispersion (980 mL) into the column. An empty beaker was placed under the column to contain the outflow MPs dispersion. Once the MPs dispersion had flowed through the column, another beaker containing 500 mL of deionized water or NaCl solution was placed on the left side as a reservoir. A magnetic stirrer at 100 rpm was placed in a beaker that placed on the right side to simulate groundwater flow, and a peristaltic pump was used to introduce the fluid from the left beaker to the right beaker until the water level arrived at the 4 cm mark on the column. The flow direction was then reversed with a pump, allowing the water level to be brought back to the 0 cm mark on the column. One iteration of increasing and then decreasing the water level in this manner was assumed to represent one cycle of water table fluctuation. MPs dispersion flowing through the column with no water table fluctuation was regarded as 0 cycles. This study considered MPs size and density, aging, substrate size, salinity, and flow rate as factors influencing MPs transport. Detailed experiment is summarized in Table 6.1.

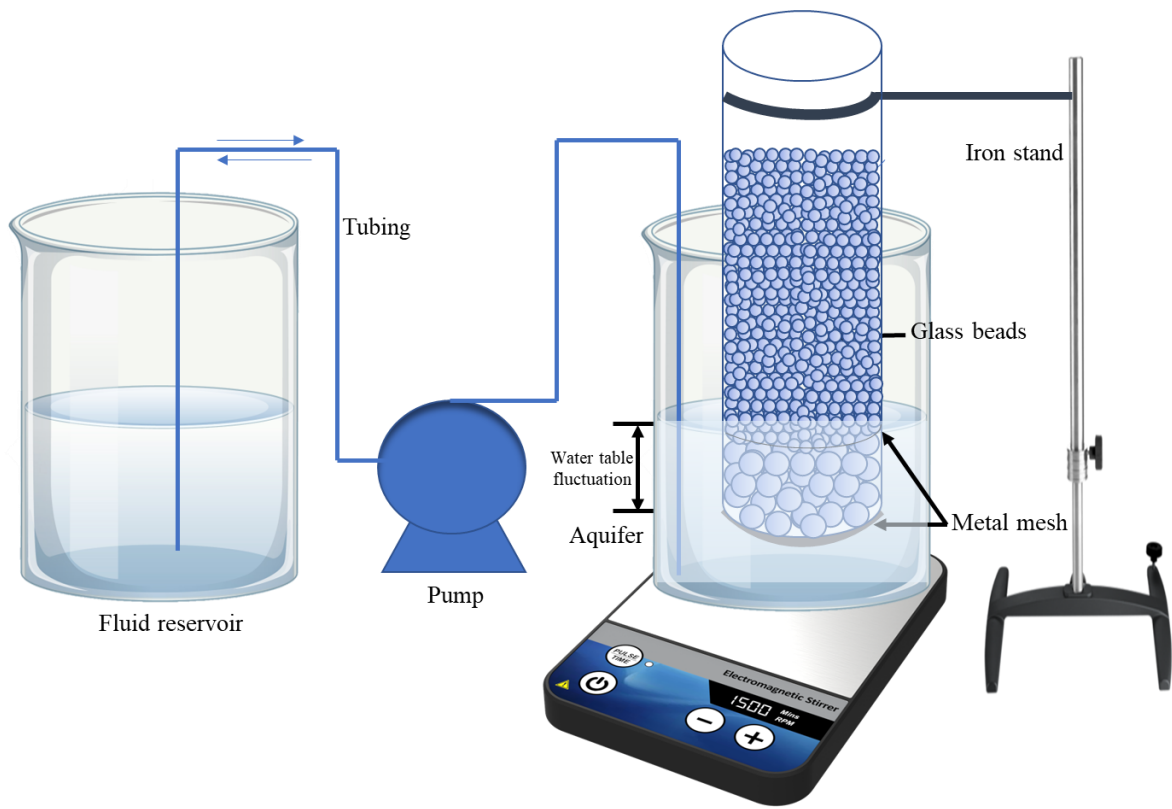


**Figure 6.1** Sketch of the column test setup.

Table 6.1 Experiment design.

Experiment No.	Glass beads size (mm)	MPs type	MPs aging	Cycle	Water table fluctuation rate (cm/min)	Salinity (psu)
1	0.5	PE1	Without aging	0.5	0.67	0
2	0.5	PE1	Without aging	5	0.67	0
3	0.5	PE1	Without aging	10	0.67	0
4	0.5	PE1	Without aging	15	0.67	0
5	1	PE1	Without aging	0.5	0.67	0
6	1	PE1	Without aging	5	0.67	0
7	1	PE1	Without aging	10	0.67	0
8	1	PE1	Without aging	15	0.67	0
9	2	PE1	Without aging	0.5	0.67	0
10	2	PE1	Without aging	5	0.67	0
11	2	PE1	Without aging	10	0.67	0
12	2	PE1	Without aging	15	0.67	0
13	0.5	PTFE	Without aging	0.5	0.67	0
14	0.5	PTFE	Without aging	5	0.67	0
15	0.5	PTFE	Without aging	10	0.67	0
16	0.5	PTFE	Without aging	15	0.67	0
17	1	PTFE	Without aging	0.5	0.67	0
18	1	PTFE	Without aging	5	0.67	0
19	1	PTFE	Without aging	10	0.67	0
20	1	PTFE	Without aging	15	0.67	0
21	2	PTFE	Without aging	0.5	0.67	0
22	2	PTFE	Without aging	5	0.67	0
23	2	PTFE	Without aging	10	0.67	0
24	2	PTFE	Without aging	15	0.67	0
25	1	PE2	Without aging	0.5	0.67	0
26	1	PE2	Without aging	5	0.67	0
27	1	PE2	Without aging	10	0.67	0

Experiment No.	Glass beads size (mm)	MPs type	MPs aging	Cycle	Water table fluctuation rate (cm/min)	Salinity (psu)
28	1	PE2	Without aging	15	0.67	0
29	1	PE1	Without aging	10	0.67	5
30	1	PE1	Without aging	10	0.67	20
31	1	PE1	Without aging	10	0.67	34
32	1	PTFE	Without aging	10	0.67	5
33	1	PTFE	Without aging	10	0.67	20
34	1	PTFE	Without aging	10	0.67	34
35	1	PE1	Without aging	5	0.22	0
36	1	PE1	Without aging	5	1.30	0
37	1	PTFE	Without aging	5	0.22	0
38	1	PTFE	Without aging	5	1.30	0
39	1	PE1	SW60	10	0.67	0
40	1	PE1	UV60	10	0.67	0
41	1	PTFE	SW60	10	0.67	0
42	1	PTFE	UV60	10	0.67	0

To transfer the GBs to the flask after each experiment, they were carefully scooped out using a long-dipper scoop in increments of 1 cm. Each flask was then filled with 100 mL of deionized water and shaken at 150 rpm for 24 h to fully resuspend the MPs. LISST-200X was used to determine the MPs concentration in the supernatants of each flask. The following equation was used to calculate the MP retention percentages: MP retention percentage per 1 cm layer =  $(V/V_0) \times 100\%$ , where  $V$  is the volume of MPs retained in each GB layer calculated by multiplying the MP concentration in each flask by 0.1 (100 mL volume), and  $V_0$  is the original MPs volume, which is determined by multiplying the MPs concentration prior to each column experiment by 0.98 (980 mL volume).

### 6.2.3 Characterization of capillary fringe fluctuation

To characterize the fluctuation of the capillary fringe, the column was packed with GBs in the same manner as in the MPs transport experiment. A volume of 500 mL of 500 mg/L Rhodamine B solution was used to simulate groundwater (for visualization of flow). Rhodamine B is a dye that is frequently employed as a tracer dye in water to visualize the flow rate and direction (Seyfried and Rao, 1987; Xia and Dutta, 2013). The color at this tracer concentration was sufficient to allow flow visualization without inducing density effects. Fluctuation of the groundwater table was simulated in the same manner as in the previous section, with a velocity of 0.67 cm/min. Fifteen cycles of water table fluctuation were conducted, and photos were taken when the groundwater table reached both the 0 cm (bottom) and 4 cm marks on the column. To gain confidence of the experiment results, Hydrus-2D was used to numerically reproduce the experiment results.

## 6.3 Results and discussion

### 6.3.1 Rise of capillary in substrate under the influence of water table fluctuations

A column test with dyed water was used to demonstrate the capillary action under the influence of fluctuations in water table. As shown in Figure 6.2a–b, increasing the number of cycles of water table fluctuations led to gradual capillary rise in the column. Figure 6.2c, meanwhile, shows a typical simulation of the motion of the capillary with the same number of cycles applied as in the experiment. The agreement between the experiment and simulation served to increase confidence in the experiment results in confirming the influence of water table fluctuations in a rising capillary fringe. Previous studies have demonstrated in this regard that periodic fluctuations of the water table may lead to higher than anticipated average water saturation depth over the water table

(Cartwright et al., 2005; Wu and Zhuang, 2010). Webb and Theodor (1968) reported that dye injected 5 cm into a sandy substrate under waves took a much shorter time to reach the sediment surface compared to that under molecular diffusion. With respect to the substrate size, the capillary rise in a 1 mm substrate was found to be higher than that in a 2 mm substrate in the present study. This finding is aligned with the empirical formula proposed by Peck et al. (1994) for calculating the maximum capillary rise height:  $hc = \frac{C}{eD_{10}}$ , where  $d_{10}$  is 10% particle size,  $e$  is the void ratio, and  $C$  is the coefficient, according to which capillary rise will be higher in a smaller substrate than in a larger substrate.

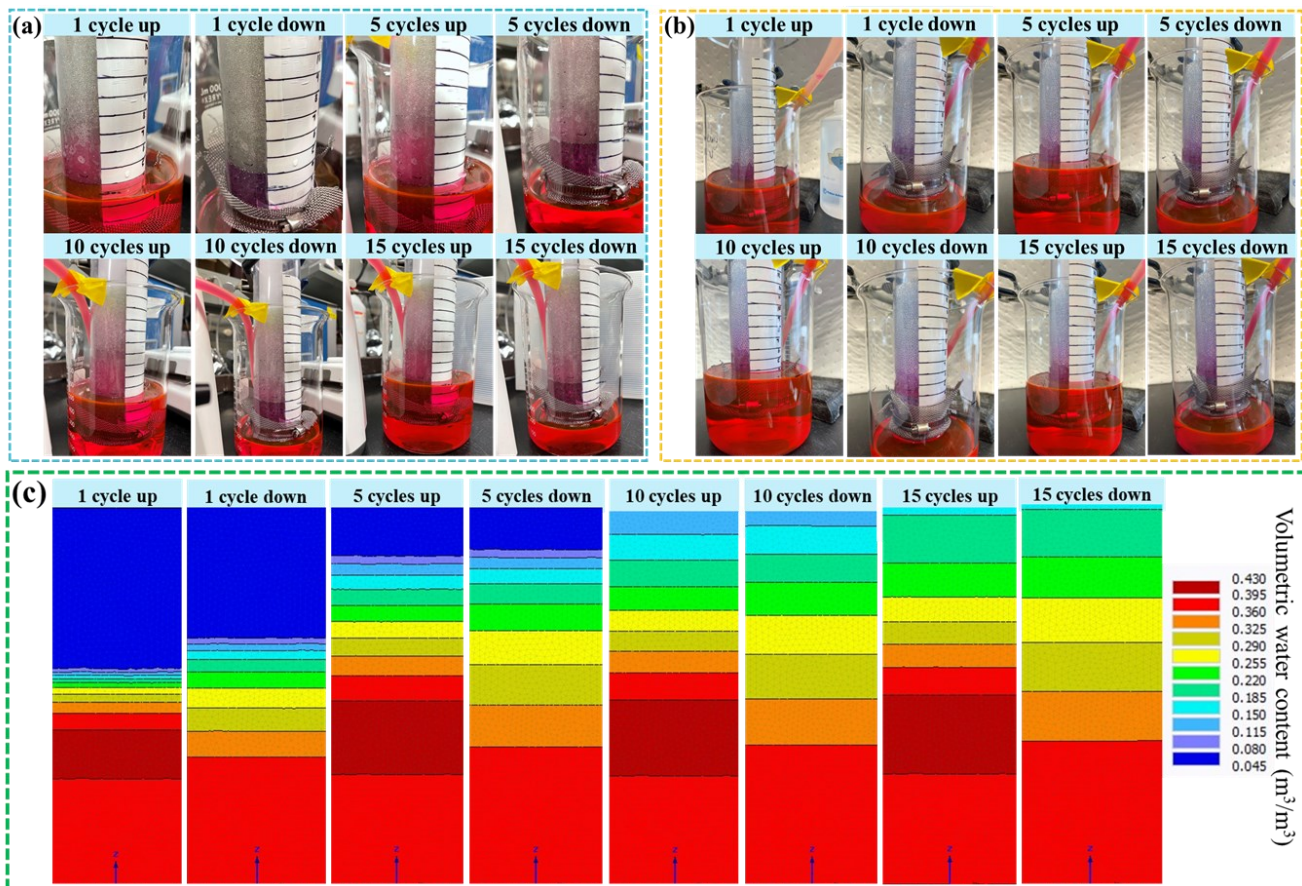


**Figure 6.2** Capillary rise in experiment and simulation by Hydrus-2D under the influence of water table fluctuation. (a) Capillary rise in 1 mm GBs. (b) Capillary rise in 2 mm GBs. (c) Hydrus-2D simulation results.

### 6.3.2 Effects of substrate size on MPs transport in substrate under fluctuating capillary fringe

Figure 6.3 exhibits the distributions of MPs in substrates with different sizes. As can be seen, the PE1 distribution in the 2 mm GBs without tidal influence was more uniform along the column compared to that in the 0.5 and 1 mm substrates. The PTFE distribution in the 2 mm substrate tended to be more concentrated in the lower section of the column compared to that in the 0.5 and 1 mm substrates. Increased number of cycles of water table fluctuations did not significantly change the MPs retention percentages in 0.5 mm GBs (26.58%, 24.27%, 25.03%, and 25.52% for PE1 and 34.00%, 32.20%, 32.27%, and 33.06% for PTFE under 0, 5, 10, 15 cycles, respectively) (Figure 6.3g–h), but it did alter the MPs distribution along the column (Figure 6.3a–b). More PE1 was retained in the top section of the column relative to the other sections of the column as the cycles increased, whereas the distribution of PTFE was largely unaffected by the increased number of cycles. In the 1 and 2 mm GBs, increasing the number of cycles from 0 to 15 resulted in a decrease in the PE1 retention percentage from 26.73% to 19.99% and from 25.52% to 21.91%, respectively. The PE1 distribution in the upper section of the column did not change significantly as a result, while the PE1 retention in the lower part of the substrate decreased with increased number of cycles. For the PTFE, increased number of cycles from 0 to 15 resulted in a decrease in the retention percentage from 34.39% to 25.92% in 1 mm GBs and from 28.46% to 23.21% in 2 mm GBs. Additionally, a downward movement of the PTFE in the column was observed as the cycles increased from 0 to 15.

Particles transport through porous media in unimpeded static percolation if the porosity of the substrate is significantly larger than that of the particles (Gibson et al., 2009). Accordingly, a bridging process can be observed if clogging layers form by particles embedded into the substrate, thereby restricting further movement. However, the blocked particles can be remobilized into the

porewater through the movement of water up and down. Particles are removed from solid surfaces through moving air–water interfaces in three steps: particle interception, attachment or thinning of the aqueous film between the air–water interface and the colloid, and particle stabilization on the air–water interface (Sharma et al., 2008). Aramrak et al. (2014) visualized colloids under the influence of moving air–water interfaces in GBs during capillary fringe fluctuation using confocal microscopy. In a scenario in which colloids attached to initially wet GBs, they observed that colloids were easily removed from the solid–water interface and pinned to a moving air–water interface. These colloids became trapped in, and transported together with the air–water interface, and exit the column by extracting the air–water interface (Aramrak et al., 2014). Our results implied that, although a larger substrate exhibits less capillary rise, nevertheless more MPs were transferred from the substrate to the aquifer in the case of the larger substrate compared to the smaller substrate. Flowrate passing a porous medium is proportional to the pressure gradient and to the substrate permeability (Darcy, 1856). Therefore, coarse sand is more permeable, allowing porewater to exchange more readily there than in fine sand. Indeed, a larger substrate size comes with larger pores, greater pore connectivity, and less strain, rendering the substrate more conducive to particle transport (Bradford et al., 2007). Moreover, interstitial water motions could be an effective transport mechanism in relatively large size sandy sediments. The repetitive action of waves running up a beach, infiltrating the sand, and then draining, leads to vigorous exchange between sediment and the water column. For the transport of solutes through cohesive sediments of small particle size, the main mechanisms are diffusion and possibly the activities of fauna. However, interstitial water transport can exceed molecular diffusion by several orders of magnitude in terms of its influence on particle transport, and as such it may act a major role in determining the fluxes of solutes and particles across the sediment–water interface (Huettel and Webster, 2001).

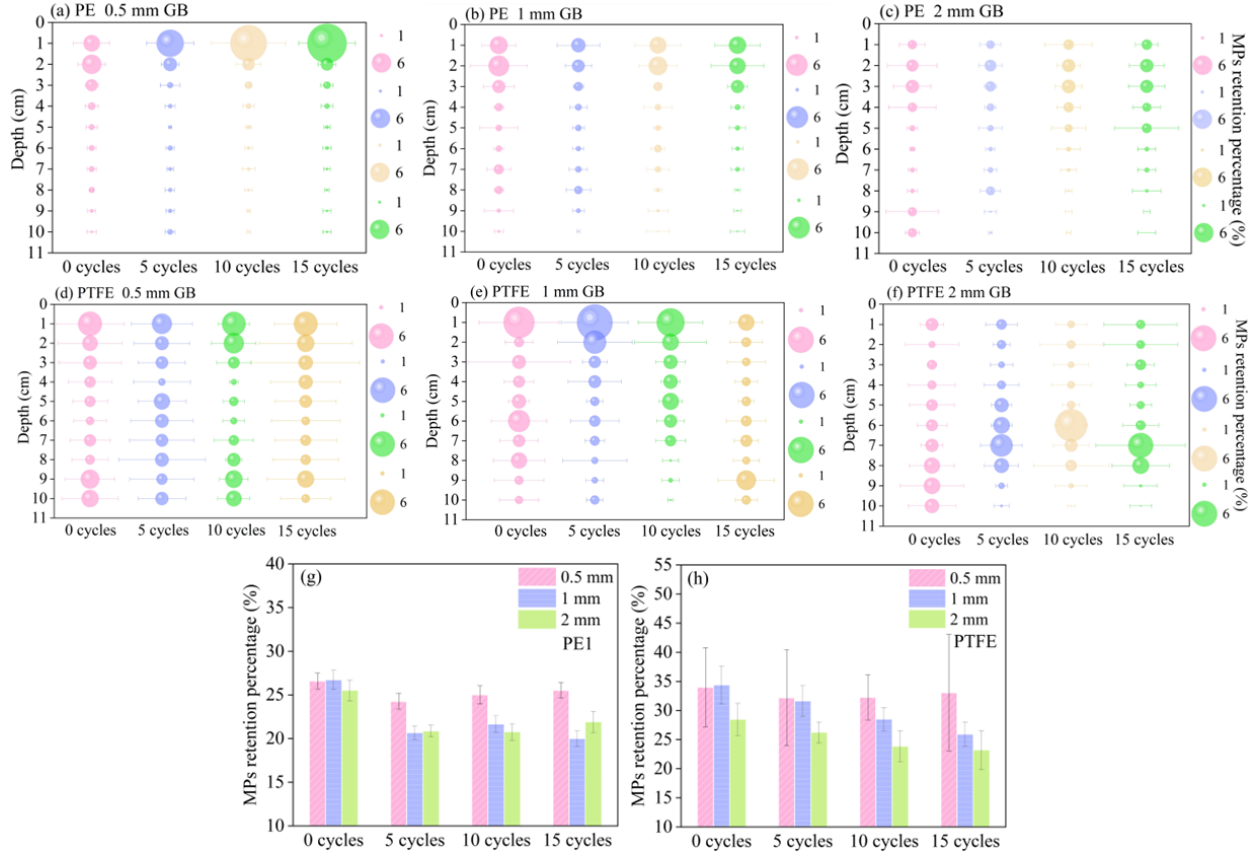


**Figure 6.3** Effects of substrate size on MPs mobilization under the influence of water table fluctuation. (a–c) PE1 distribution in 0.5, 1, and 2 mm GBs packed column under different fluctuation cycles; (d–f) PTFE distribution in 0.5, 1, and 2 mm GBs packed column under different fluctuation cycles. (g–h) Retention percentages of PE1 and PTFE in the 0.5, 1, and 2 mm GBs packed columns under different fluctuation cycles. The size of the bubble denotes the MP retention percentages.

### 6.3.3 Effects of MPs properties on transport in substrates under fluctuating capillary fringe

In terms of MPs size, the larger-size PE2 was retained in the substrate at a higher percentage compared to the smaller-size PE1 (Figure 6.4). It was found that 18.64% of the PE2 retained in GBs (0 cycles) was removed after 15 cycles, while 25.22% of the PE1 was removed after 15 cycles. 24.63% of the PTFE was removed after 15 cycles—less than that of the PE1. Moreover, the retained PTFE was removed slower (34.39%, 31.64%, 28.52%, 25.92%) compared to PE1 (26.73%, 20.67%, 21.66%, 19.99%) with the increase in cycles. As per Eq. (3), the calculated detachment forces by water film pulling the particles from the solid phase for PE1, PE2, and PTFE were found to be  $1.29 \times 10^3$ ,  $3.39 \times 10^3$ , and  $1.01 \times 10^3$  nN, respectively. The shear forces by fluid flow, meanwhile, were  $1.15 \times 10^{-2}$ ,  $3.59 \times 10^{-2}$ , and  $9.68 \times 10^{-3}$  nN for PE1, PE2, and PTFE, respectively (Eq. 4). The force differences between gravity and buoyancy, finally, were  $-3.71 \times 10^{-5}$ ,  $-1.13 \times 10^{-3}$ , and  $9.92 \times 10^{-4}$  nN for PE1, PE2, and PTFE, respectively (Eq. 5). One notable inference based on these findings is that although PE2 has a higher detachment force, its larger particle size causes it to be retained more effectively by the GBs. The slightly higher detachment force exhibited by PE1 compared to PTFE, meanwhile, may be attributable to its slighter larger mean particle size (7.11  $\mu\text{m}$  and 6.33  $\mu\text{m}$ ). Moreover, the high density of PTFE rendered it less likely to be resuspended in water, resulting in a lower removal rate than PE1. In this regard, Chen et al. (2010) stated that gravitational forces can substantially influence the deposition of micron colloids. Chrysikopoulos and Syngouna (2014), meanwhile, suggested that gravity is an important force for colloid transport in a saturated porous medium under unfavorable deposition conditions. James and Chrysikopoulos (2004), moreover, simulated colloid transport in a bifurcating fracture and demonstrated that dense particles preferentially leave from the downward fractures. In other words, gravity acts a considerable role in determining MPs' transport, and overlooking the role of gravity may lead to inaccurate predictions of MPs' trajectory.

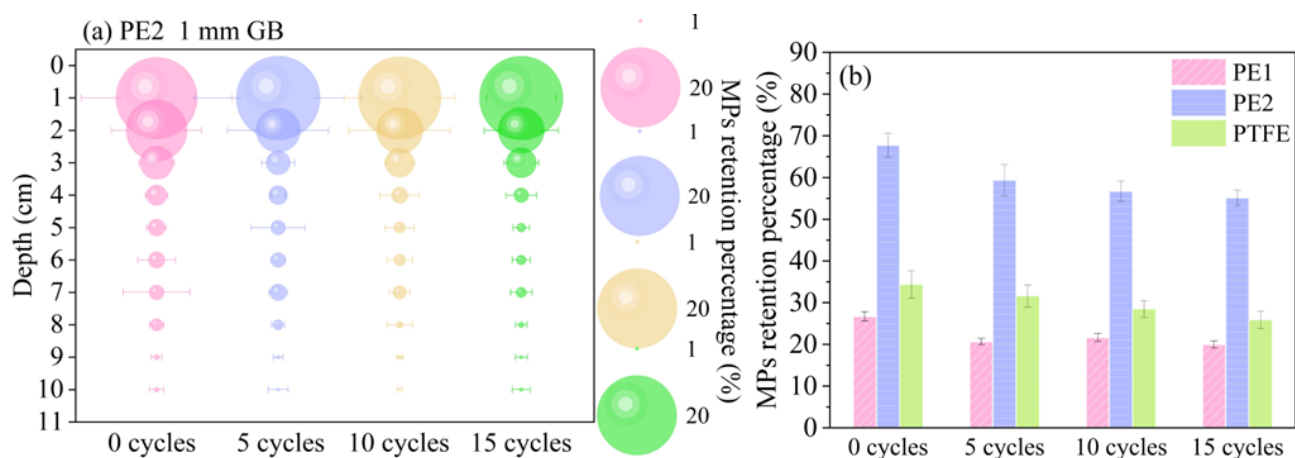


**Figure 6.4** Effects of MPs properties on their mobilization under the influence of water table fluctuation. (a) PE2 distribution in 1 mm GBs packed column under the influence of water table fluctuation. (b) Retention percentages of PE1, PE2, and PTFE in 0.5, 1, and 2 mm GBs packed columns under the influence of water table fluctuation. The size of the bubble denotes the MP retention percentages.

#### 6.3.4 Effects of aging on MPs transport in substrates under fluctuating capillary fringe

MPs undergo a series of aging processes after entering the environment, altering their physical and chemical properties and leading to changes in their environmental behavior (Wang et al., 2022). In our study, after UV aging for 60 days, the retention percentages of PE1 decreased from 20.67% to 18.99%, while, after seawater aging for 60 days, the retention percentages did not change significantly (20.22%) (Figure 6.5c). Aged PE1 was more negatively charged compared with pristine PE1 ( $-15.5$ ,  $-31.7$ , and  $-33.3$  for pristine, SW60, and UV60 PE1, respectively), enhancing the repulsion between negatively charged GBs and aged MPs, in turn facilitating MPs transport. Although SW60 PE1 was more negatively charged, seawater aging increased its surface roughness, thereby enhancing its deposition. Both UV60 PE1 and SW60 PE1 exhibited lower contact angles compared to pristine PE1; this decrease in the case of the UV60 PE1 was due to the

generation of oxygen-containing functional groups, while in the case of SW60 PE1, it can be attributed to the increase of surface roughness (Feng et al., 2021). In this respect, Li et al. (2020) reported that the negatively charged MPs-kaolinite aggregates showed higher transportation compared to positively charged MPs-kaolinite aggregates. The retention percentages of the pristine, UV60, and SW60 PTFE were found to be 31.64%, 44.93, to 57.39%, respectively. The zeta potential of the PTFE decreased after seawater and UV aging, while the water contact angles increased, suggesting an aggrandized surface roughness (Koh et al., 1997).

#### 6.3.5 Effects of fluctuating velocity on MPs transport in substrates under fluctuating capillary fringe

The fluctuation of the groundwater table is affected by various factors, including rainfall infiltration, pumping, and tides, leading to different fluctuation velocities and capillary fluctuation velocities. Tidal current velocity was found to vary greatly for different sites and changes between neap and spring tides. For instance, some previous studies reported that tidal velocities ranged between 0.01 to approximately 1 m/s (Panchenko et al., 2019; Sukhsangchan et al., 2020; Wu et al., 2020). This can be expected to lead to different rates of change to the water table. Figure 6.5d–f demonstrates the effects of water table fluctuation velocity on MPs movement in the substrate. The PE1 retention percentages were found to decrease from 28.60% to 19.91% and PTFE retention percentages from 33.47% to 29.61% when the velocity increased from 0.22 and 0.67 to 1.30 cm/min. The reduction in MPs retention percentage was more pronounced in the lower section of the column than in the upper section. Sharma et al. (2008) found, in this regard, that higher interface velocity reduced colloid removal if the solid phase was dried after particle deposition. However, in the present study, MPs were deposited on wet solid surface under unfavorable conditions, representing a lower-energy interaction compared to that under favorable

condition. Accompanied by the passage of the air–water interface, MPs were released from the media where they had been deposited into the mobile phase. In this regard, high flow rates imply high shear and thrust force, resulting in high mobility of particles (Chowdhury et al., 2011).

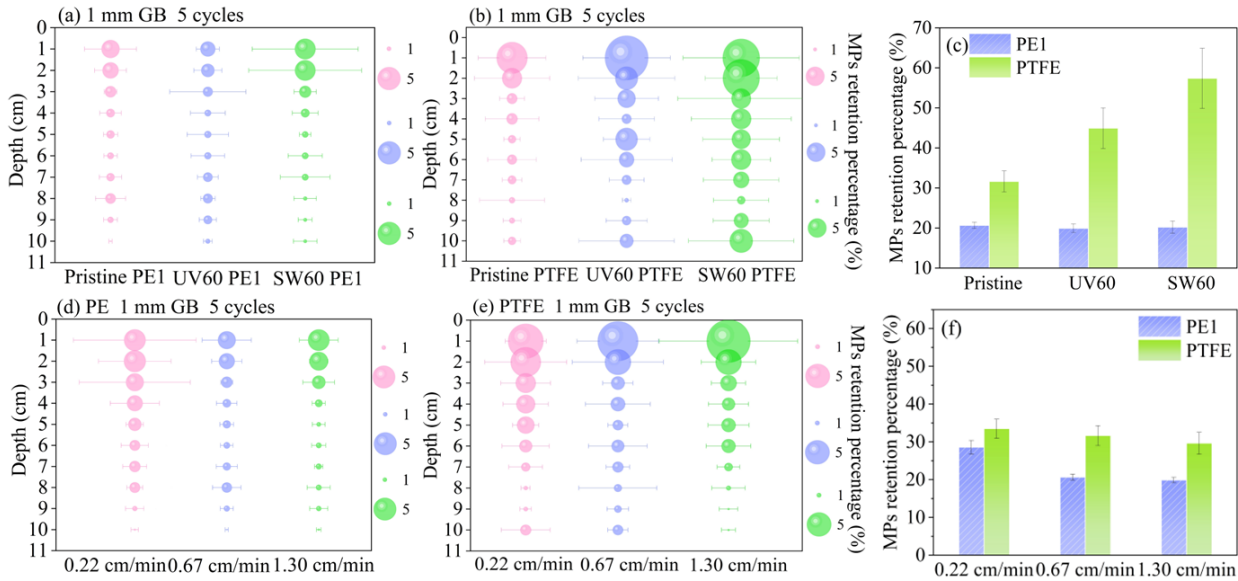


**Figure 6.5** Effects of aging and water table fluctuation velocity on MPs mobilization. (a) Pristine PE1, UV60 PE1, and SW60 PE1 distributions in substrate under 5 cycles of water table fluctuation. (b) Pristine PTFE, UV60 PTFE, and SW30 PTFE distributions in substrate under 5 cycles of water table fluctuation. (c) Retention percentages of aged PE1 and PTFE in substrate under 5 cycles of water table fluctuation. PE1 (d) and PTFE (e) distribution in substrate under 5 cycles of water table fluctuation at various velocities. (f) Retention percentages of PE1 and PTFE in substrate under 5 cycles of water table fluctuation at various velocities. The size of the bubble denotes the MP retention percentages.

### 6.3.6 Effects of groundwater salinity on MPs transport in substrates under fluctuating capillary fringe

During flood tides, seawater levels are higher than the beach groundwater, and this allows seawater to infiltrate unconfined aquifers. During the ebb tide, then, groundwater will eject from the coastal unconfined aquifer, and this process may alter the salinity of the aquifer. As shown in Figure 6.6, under the same number of cycles of water table fluctuations, fewer MPs were released from the substrate with increasing aquifer salinity. The PEI retention percentage increased from 20.57%, 23.94%, 22.52%, to 27.05%, and the PTFE retention percentage increased from 31.64%, 33.36%, 34.31%, to 36.85% with NaCl concentration increasing from 0 psu, 5 psu, 20 psu, to 34 psu, respectively. Moreover, as ionic strength increased, the zeta potential changed from  $-15.50$  mV,  $-3.50$  mV,  $2.38$  mV, to  $4.52$  mV for PEI and from  $-15.8$  mV,  $-4.78$  mV,  $4.54$  mV, to  $6.13$  mV for PTFE, respectively. Particles interact with solid phase either by straining or physical/chemical interaction (McDowell-Boyer et al., 1986). DLVO theory suggests that, with the increase of ionic strength, the double-layer repulsion between the MPs and GBs dissipates and their attraction increases (Figure 6.7). Our results showed that positively charged particles that were settled in the primary energy minimum adhered to the solid-water interface more strongly than negatively charged colloids did, as per Sharma et al. (2008). Moreover, the MPs became unstable, limiting their mobility and allowing them to be more easily intercepted by the GBs, as per Hou et al. (2020). During the passing of the air–water interface, as demonstrated in Figure 6.6d–e, the detachment forces were found to be orders of magnitude greater than the attachment force (DLVO force), shear force, and the force difference between gravity and buoyancy force, implying that detachment forces are dominant in the detachment of MPs from GBs. As a result, the detachment from the solid-water interface and attachment to the air-water interface are strong and can be assumed to be irreversible.

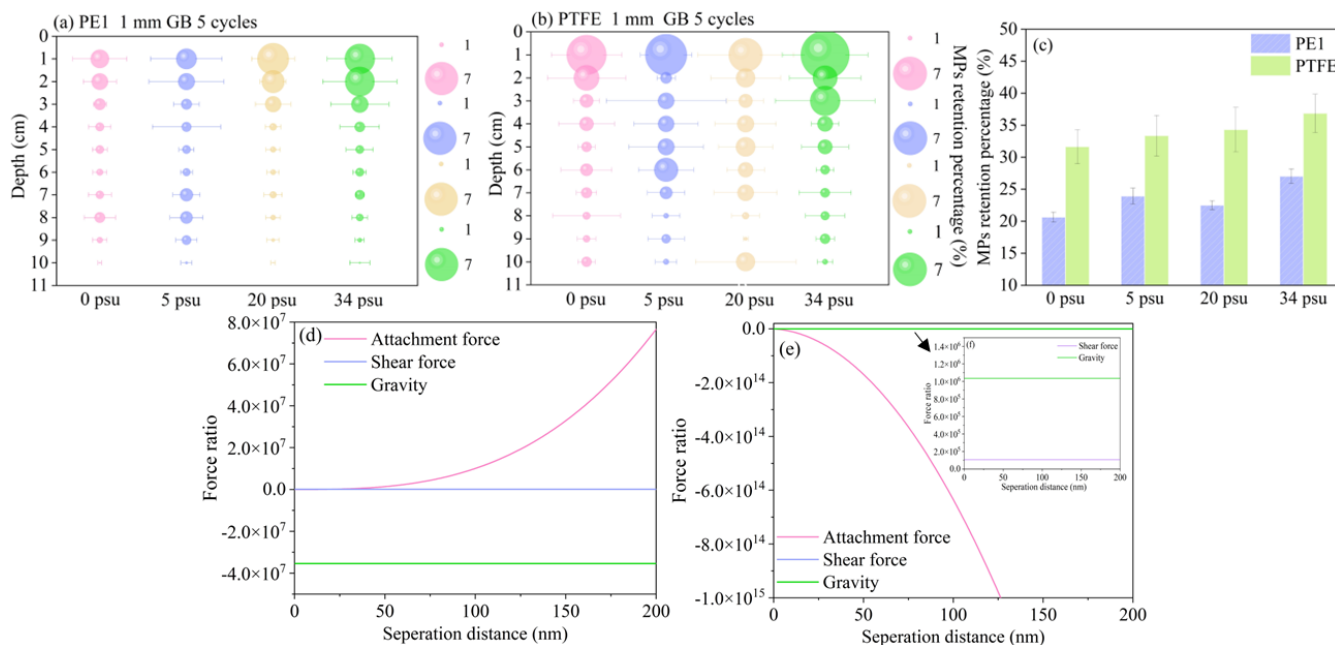


**Figure 6.6** Effects of salinity on MPs mobilization under the influence of water table fluctuation. (a–b) PE1 and PTFE distribution in substrate at various ionic strengths under 5 cycles of water table fluctuation. (c) Retention percentages of PE1 and PTFE in substrate at various ionic strengths under 5 cycles of water table fluctuation. (d–e) Ratios of detachment force to attachment force (DLVO force), shear force, and force difference between gravity and buoyancy force for PE1 and PTFE. The size of the bubble denotes the MP retention percentages.

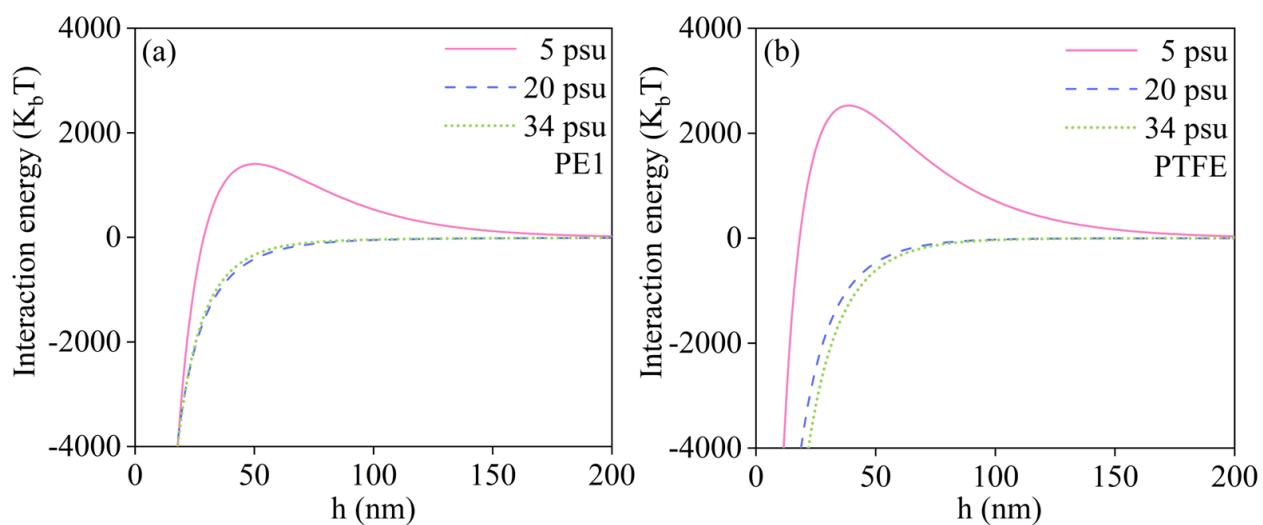


**Figure 6.7** Interaction energy versus surface-to-surface separation distance for PE1/PTFE and GB at various ionic strengths.

### 6.3.7 Environmental implications of MPs being influenced by the capillary fringe

The retention percentages of MPs in column were significantly positively correlated with MPs density and with gravity ( $r = 0.39$  and  $0.59$ ,  $p < 0.05$ ), respectively. The MPs retention percentages in the upper section of the substrate (which is less affected by capillary rise) were mainly dependent on GB size ( $r = -0.36$ ,  $p < 0.05$ ). MPs retention percentages in the lower 5 cm of the column, meanwhile, were found to be negatively correlated with MPs size, zeta potential, but positively correlated with MPs density ( $p < 0.05$ ). These results imply that capillary fringe fluctuation mainly affects MPs' transport from the bottom of the substrate, and that MPs size, density, and aging status are the predominant factors affecting MPs' transport from the substrate to the aquifer.

Capillary fringe may affect the aquifer far more significantly than is normally assumed (Silliman et al., 2002). Capillary fringe is active in the transport of solutes and the mixing of water from the

vadose zone with that below the water table. Porewater flowing through high-permeability beds enhances the solute and particle exchange between sediment and water. For instance, porewater advection transports dissolved substances, fine particles, seawater, bacteria, and phytoplankton into sediments while also releasing them from sediments (Santos et al., 2012; Xin et al., 2019). In the present study, we demonstrated that capillary fringe fluctuation can also influence the release and uptake of MPs from substrate to below aquifer. Identifying areas where MPs release may severely compromise aquifers is a crucial aspect of MPs risk assessment. As demonstrated in the present study, large sediment grain size, high salinity, and fluctuating velocity may contribute more to MPs release to the aquifer under the influence of capillary fringe fluctuation. Through aerial photography and satellite imagery, hydrodynamic and geomorphic data, such as shore substrate type, wave height and fetch, and tidal range and velocity, can be collected to determine the relative vulnerability of a coastal aquifer (Rodrigues et al., 2021; Zhou et al., 2021).

Water treatment plant acts a crucial role in preventing MPs from moving into the drinking water (Kosuth et al., 2018). Traditional water treatment processes that may assist in MPs removal mainly include coagulation, sedimentation, filtration, and clarification, while the use of some new techniques such as electrocoagulation, magnetic extraction, and membrane separation was also studied recently. Pivokonsky et al. (2018) sampled the MPs in raw water and drinking water after being treated by 3 water treatment plants. They found that the removal efficiency of MPs reached 70% for plant 1 (coagulation/flocculation and sand filtration), 81% for plant 2 (coagulation/flocculation, sedimentation, sand filtration, and activated carbon filtration), and 83% for plant 3 (coagulation/ flocculation, flotation, sand filtration, and activated carbon filtration), respectively. The results showed that traditional treatment techniques are promising practices for removing MPs. However, currently, there have not been specific legislative standards for the

presence of MPs in drinking water.

In the present study, GBs were used as a model to study the effect of substrate size on infiltration, owing to their transparency and easily measurable size. However, sediment in the natural environment is more complex, given its variability in terms of surface morphology, shape, and density. Besides, groundwater flow simplified in this study can be vertical, horizontal, or both, which deserve to be considered in future investigations.

# **Chapter 7 Tide-induced infiltration and resuspension of MPs in shorelines: insights from tidal tank experiments\*\***

## **7.1 Background**

Environmental pollution with plastic is a growing problem. Global plastic production has soared since the 1940s, reaching approximately 400 million tonnes per year (PlasticsEurope, 2022). Plastics enter the environment via a variety of pathways, including runoff, atmospheric transport, littering, sewage discharge, aquaculture, fisheries, and shipping. Ocean and ocean sediment can serve as an ultimate sink for plastics (Martin et al., 2022). Based on the Human Development Index (HDI), a study predicted that 57,000–265,000 MT of plastic would flow into the ocean from rivers in 2018 (Mai et al., 2020). Large plastic in the ocean can be fragmented into small pieces by waves and currents, abrasion by solid particles, photodegradation, or biochemical degradation in marine environments (Wang et al., 2022). These MPs feature a small size, high specific area, high adsorption capacity, high mobility, and resistance, posing long-term potential threats to vegetation, animals, and human beings (Akhbarizadeh et al., 2017).

Coastal areas offer a collection of services and goods, such as water supply, disturbance regulation, waste processing, carbon sequestration, biodiversity maintenance, and provisioning services. The coastal tidal zones are home to a wide variety of plants and birds, as well as benthic species, which play significant ecological and socioeconomic roles (French, 1996). Nevertheless, the coastal zone is often characterized by a high population density and intense anthropogenic activities, such as

---

\*\* This work has been published as Feng, Q., Chen, Z., An, C., Yang, X., Wang, Z., 2023. Tide-induced infiltration and resuspension of microplastics in shorelines: insights from tidal tank experiments. *Water Research*, 236, 119970.

shipping, industry, fishery, and commerce, making it a hotspot for plastic pollution (Feng et al., 2021). Land-based plastic debris is transported through the coastal zone to reach the open ocean. A high abundance of MPs has been recorded in tidal water, sediment, and biota. A global-scale meta-analysis revealed that, in coastal wetland sediments and marine animals, the abundance of plastics reached 156.7 and 98.3 items/kg, respectively, 200 times higher than in water (0.43 items/kg) (Ouyang et al., 2022). Li et al. (2021) found that the abundance of MPs during the rainy season reached 545.5 particles/m<sup>3</sup> in the Pearl River Estuary in the South China Sea. Pazos et al. (2018) observed that the mean density of MPs reached 139 items/m<sup>3</sup> in the inner zone of the Río de la Plata estuary. Leads and Weinstein (2019) reported that intertidal sediment, subtidal sediment, and sea surface microlayer MP concentrations ranged from 0 to 652 items/m<sup>2</sup>, 3–4,375 items/kg, and 3–36 items/L, respectively, within the Charleston Harbor Estuary tributaries. Previous field studies mainly focused on water and the surface sediment layer, while less attention has been paid to the subsurface layer.

The large chemically reactive area and porosity of sediments render them a considerable sink for pollutants (Wang et al., 2021). Sediments can also serve as a source of contaminants when they are disturbed, thereby remobilizing contaminants into water columns. The substrate is a habitat for many aquatic biotic communities (Hunt et al., 2006). The presence of MPs in sediment may fundamentally affect the surrounding ecosystem and the creatures that live there (Roche et al., 2019). The infiltration, retention periods, and migration of MPs in substrates are of great toxicological significance to organisms. The occurrence of MPs in sediments has been recorded in many field studies (Alomar et al., 2016; Bosker et al., 2019; Bridson et al., 2020). In this regard, the patterns of MP distribution in sediments differ tremendously in both temporal and spatial scales due to a variety of factors, such as substrate and MP properties (size, shape, aging stage,

color), geographic factors, climate, and hydrodynamic forces. However, previous studies of MP distributions in tidal zones have primarily focused on a large spatial scale, whereas an accurate and validated analysis of MP behavior under hydrodynamic forces has yet to be completed.

Hydrodynamic forces play a major role in transporting inorganic substances in aquatic ecosystem (Wang et al., 2018; Khadanga et al., 2022). For instance, the tide in the Severn Estuary leads to highly mobile sediments and suspended sediment concentrations up to 5000 mg/L (Duquesne et al., 2006). Tidally driven resuspension can remobilize heavy metals from sediments (Jonas and Millward, 2010). Currents and waves can flush plastics onto shores, while plastic stranded in the shoreline substrate can be washed back into the sea. However, these studies are inconsistent concerning the impact of tidal forces on MP concentrations in water and sediments. For instance, Rowley et al. (2020) found more MPs in water during ebb tide when compared to flood tide, whereas Stead et al. (2020) and Li et al. (2023) claimed that MP abundance in water decreased from flood tide to ebb tide. Wu et al. (2022) reported the abundance of fine MPs (45–300  $\mu\text{m}$ ) increased while the large MPs (>300  $\mu\text{m}$ ) increased during the flood tide, implying flood tide carried more fine MPs into the estuary than large ones. Yin et al. (2022) observed that tides had opposite effects on the inner and outer harbors as spring tides enriched MPs in the outer harbor area. Additionally, the effects of tidal cycles on MPs have been examined by multiple studies, with the consensus that concentrations of MPs can vary significantly within or between tidal cycles, leading to considerable uncertainties when interpreting field data (Moreira et al., 2016; Cohen et al., 2019; Balthazar-Silva et al., 2020). In fact, due to the complex interplay of various factors, no concrete trend in MP concentration has been observed in response to tidal forces.

To date, a limited number of studies have empirically investigated the transport of MPs in coastal

zones under dynamic boundaries. Only the influence of waves on MP transport has been investigated using a wave tank (Alsina et al., 2020; Kerpen et al., 2020; Guler et al., 2022; Schuster-Wallace et al., 2022). It is still unclear how tides transport plastic. Furthermore, most global numerical models that predict plastic fluxes do not explicitly account for plastic motion in coastal regions, including plastic beaching (Neumann et al., 2014) (Neumann et al., 2014). Due to the lack of related information, current coastal models are not suited for capturing small-scale variability, which is vital for monitoring and predicting MP distributions (Rodrigues et al., 2021). Therefore, the objectives of this study are to investigate (1) the infiltration of MPs under the influence of tidal cycles combined with the rates of tidal level change and MP characteristics, and (2) the upward movement of MPs under the influence of tidal cycles combined with the rates of tidal level change and MP characteristics. The obtained results can provide significant information for MP fate and guidance for cleanup in tidal zones.

## **7.2 Methods**

### **7.2.1 Particle characteristics**

Throughout the experiments, 13 MP groups of various shapes, densities, and sizes were used, including polypropylene (PP), polyethylene (PE), nylon, polylactic acid (PLA), and polyvinyl chloride (PVC). The plastic materials were purchased from Amazon. 90% of the synthetic plastic worldwide is one of the following types: low and high density PE, PP, PVC, PS, and PET (Shah et al., 2008). According to reviews conducted by Ouyang et al. (2022) and Guo et al. (2021) regarding global presence of MPs in coastal wetland and global reservoirs, PE and PP are the most abundant types. The properties of all the particles are given in Table 7.1 and Figure 7.1. The particle dimension was based on the measurement of 10 particles each. The selected MPs varied

in shape, representing most of the typical particle shape in Sphericity-form diagram. The equivalent particle diameter  $d_{MP}$  was determined using the formula:

$$d_{MP} = \sqrt[3]{abc} \quad (7.1)$$

The Corey shape factor (CSF), used as a parameter for particle shape, was determined by:

$$CSF = \frac{c}{\sqrt{ab}} \quad (7.2)$$

where  $a$ ,  $b$ , and  $c$  are the longest, medium, and shortest particle side lengths, respectively. For a cube or sphere, CFS equals 1 and decreases with grain flatness. Capillary force withstanding gravity was calculated as follows:

$$F_{cap} \cong \gamma \xi \sin \theta \quad (7.3)$$

where  $\gamma$  is the surface tension of the fluid and  $\xi_{max}$  is the maximal perimeter of the cross-section area parallel to the water surface.  $\theta$  is the indentation angle between the horizontal water surface and the object. When only vertical forces are present, the capillary force is maximal.

All the MP particles were rinsed with deionized water and soaked in water for 24 h before the tank experiment. The 15.82-mm diameter GBs were used as an alternative to natural sediments to provide the exact grain size. The GBs were transparent, which helped identify MP particles clearly. The GBs were placed in the tank at a 26.6° slope.

Table 7.1 MP types and properties used in tank experiment.

Polymer type	Abbr.	Color	Longest length (mm)	Medium length (mm)	Shortest length (mm)	Density (g/cm <sup>3</sup> )	d <sub>MP</sub> (mm)	Corey shape factor (CSF)
Polypropylene (PP)	PP2	Blue	5.06	5.18	0.05	0.91	1.09	0.010
Polypropylene	PP1	Blue	5.25	2.29	0.05	0.91	0.84	0.014
Polyethylene (PE)	PE3	White	5.40	5.40	2.30	0.97	4.06	0.426
Polyethylene	PE2	White	5.38	2.70	2.30	0.97	3.22	0.603
Polyethylene	PE1	White	2.70	2.70	2.30	0.97	2.56	0.852
Nylon	NY2	Yellow	10.03	0.30	0.30	1.14	0.97	0.173
Nylon	NY1	Yellow	5.37	0.30	0.30	1.14	0.77	0.236
Polylactic acid (PLA)	PLA2	Pink	5.08	1.70	1.70	1.25	2.44	0.578
Polylactic acid	PLA1	Blue	2.00	1.70	1.70	1.25	1.79	0.922
Polyvinyl chloride (PVC)	PVC2	Green	5.05	5.00	0.24	1.35	1.82	0.048
Polyvinyl chloride	PVC1	Yellow	5.18	2.00	0.24	1.35	1.35	0.075
Clear vinyl	V2	Clear	3.89	1.84	1.59	1.35	2.25	0.593
Clear vinyl	V1	Clear	2.00	1.84	1.59	1.35	1.80	0.828

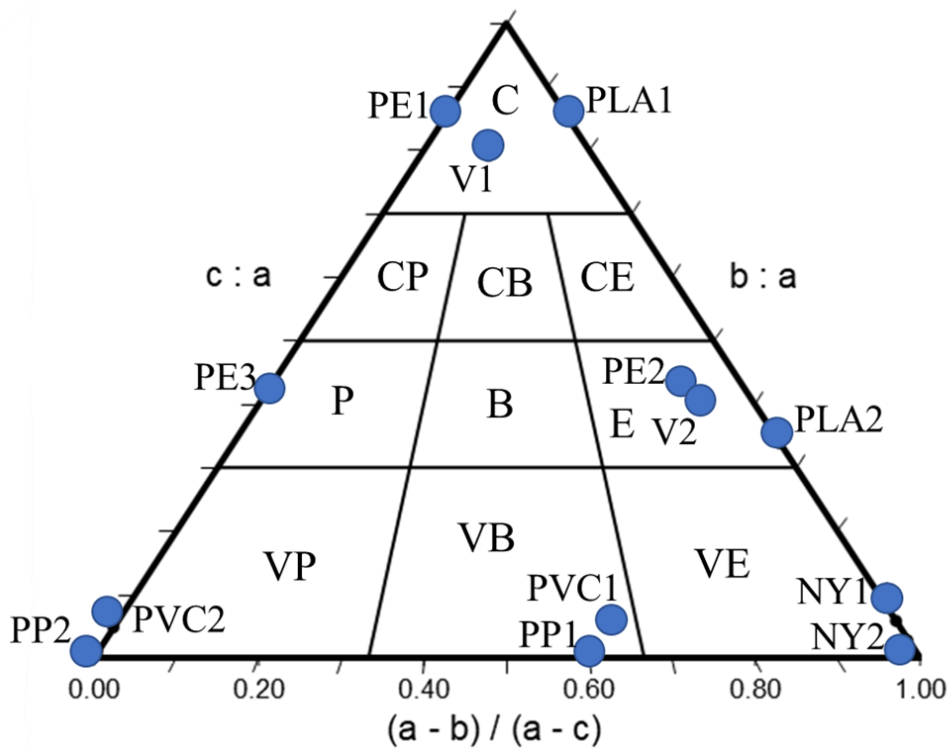
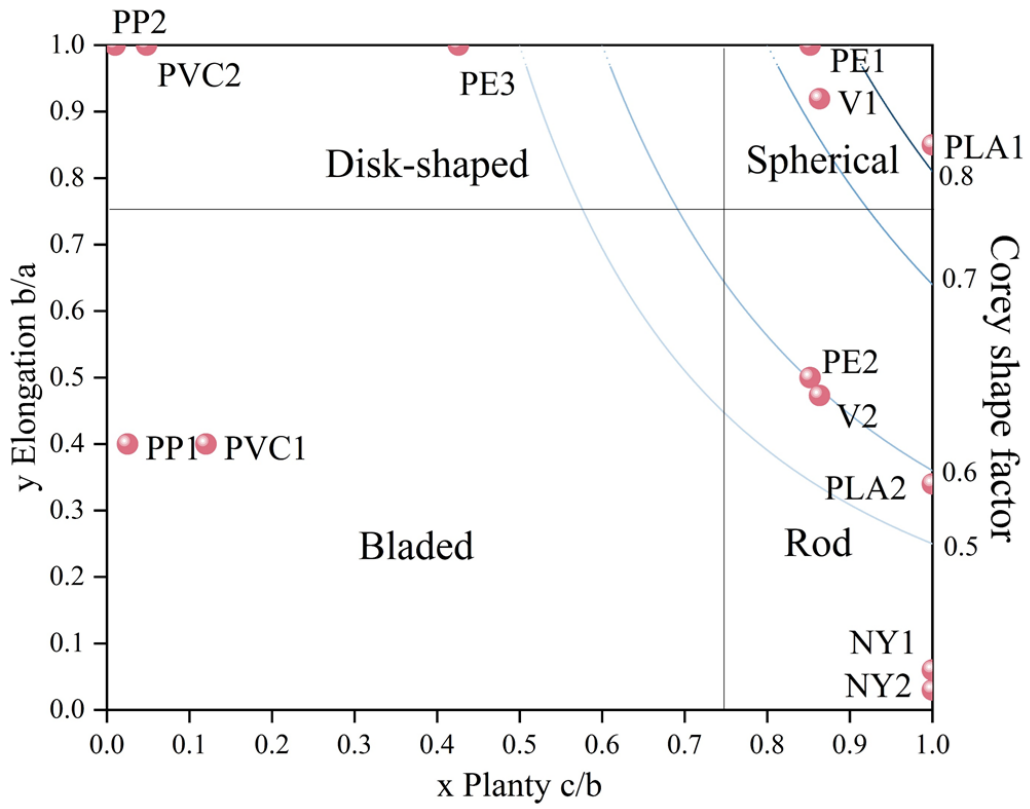


**Figure 7.1** Shape of the selected MPs. (a) Relation between axis ratio and particle shape/sphericity classification (Krumbein, 1941; Corey, 1949). (B) Sphericity-form diagram

(Sneed and Folk, 1958). C= Compact, CP = Compact platy, CB = Compact bladed, CE = Compact elongated, P = Platy, B = Bladed, E = Elongated, VP = Very platy, VB = Very bladed, VE = Very elongated.

### 7.2.2 Experiment setup

The physical model experiments were carried out in a tidal simulator. As shown in Figure 7.2, the simulator consists of a tidal tank (40 cm in length and 30 cm in width), a control cabinet, a feed tank, and an effluent container. Metal mesh was placed at each side of the substrate to avoid the escape of particles. In each run, 30 particles per particle type were placed in the tank, resulting in 360 MP particles. Cross-shore coordinate  $x$  is defined as positive toward the lower tide zone, and vertical coordinate  $z$  is defined as positive in the downward direction. Ten particles of each MP type were placed at the 5 cm, 20 cm, and 35 cm horizontal positions, respectively. During each cycle, the tap water flooded the substrate and reached a high level of 20 cm, then drained to 0 cm. Ten tidal cycles were implemented for each run. Three rates of tidal level change of 0.25, 0.50, and 0.75 cm/min were used for both scenarios. The actual fluctuating velocity of tide in environment varied greatly. For instance, Panchenko et al. (2019) found the tidal current amplitude varied from about 0.16 to 1.2 m/s in spring tide and 0.01 to 0.57 m/s in neap tide. Zhang et al. (2020) found that the tidal velocity ranged from 0.5 to 1 m/s. Wu et al. (2020) revealed that the tidal velocity ranged from 0.05 to 0.3 m/s. Therefore, the rates of tidal level change selected in the experiment mainly aimed to reveal the transport of MPs along with the rate change. Two scenarios were conducted. In the first scenario, MPs were placed on the top of the substrate slope at the 5, 20, and 35 cm horizontal positions. In the second scenario, MPs were placed at the bottom of the substrate at the 5, 20, and 35 cm horizontal positions. To avoid MPs being pinned under the GBs, the bottom of the tank was first packed with one layer of GBs, and then the MPs

were placed in the void space among the GBs. The remaining GBs were then packed following the bottom layer.

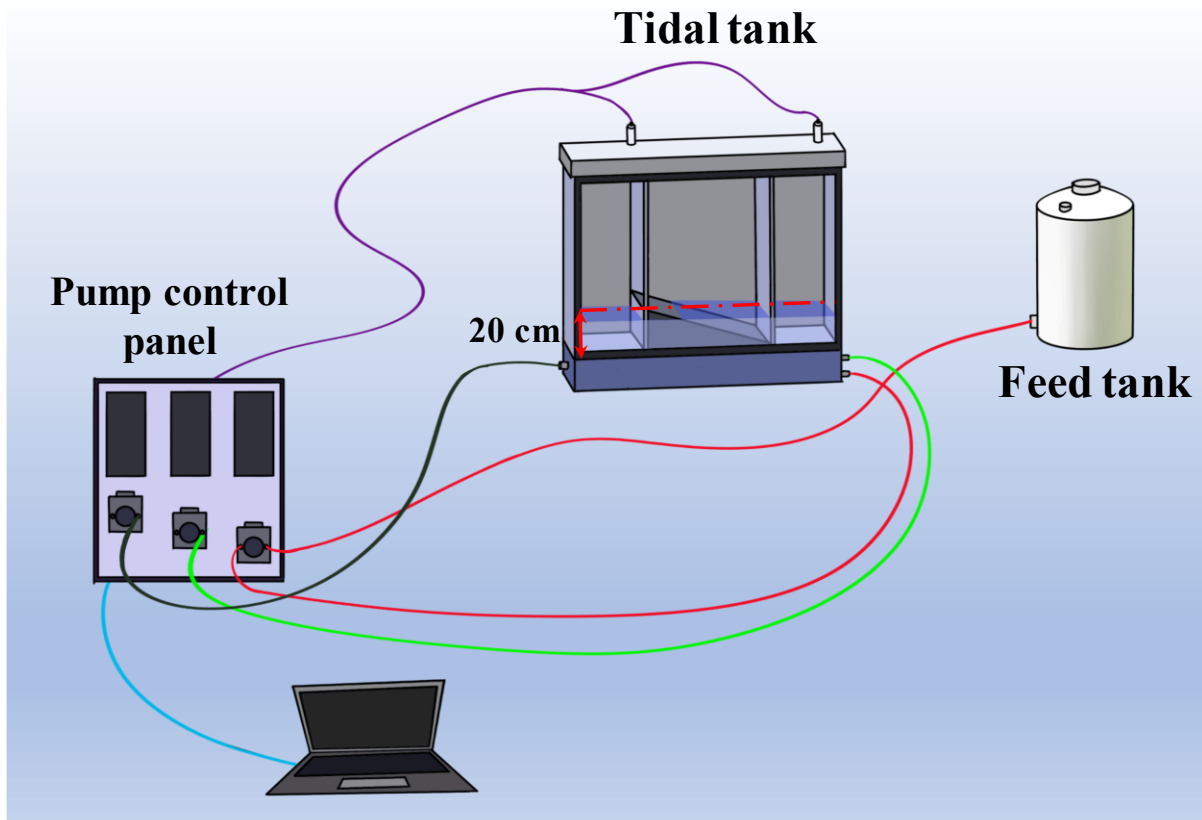


**Figure 7.2** The schematic diagram of the tidal tank simulator.

### 7.2.3 MP quantification and distribution analysis

During the tidal experiment, when the water level increased to 20 cm height, the number of each MP type floating on the water surface was counted. The floating percentage was calculated as the ratio of the floating MP number to the initial added MP number in tank. After 10 tidal cycles, GBs were carefully taken out in a 1-cm depth and 5-cm width interval for the whole substrate, resulting in a total of 89 sampling fractions for determining the overall MP distribution. In each sampling, the GBs taken from the tank were placed in a beaker. The GBs were then rinsed with water to adequately separate the MPs for the quantification of each type of MP in each substrate fraction. All tank experiments were conducted as duplicates, and the batch with higher MP recovery rate was selected for analysis. After counting all the MPs in substrate, the recovery rates of PP1 and PP2 ranged from 83.33% to 100% and 93.33% to 100%. The recovery rates of PE1, PE2, PE3 ranged from 86.67% to 100, 90% to 100%, and 90% to 100%, respectively. The recovery rates of NY1 and NY2 ranged from 83.33% to 100 and 90% to 100%. The recovery rates of PLA1, PLA2, PVC1, PVC2, V1, and V2 ranged from 93.33% to 100%, and 90.00% to 100%, respectively.

## 7.3 Results and discussion

### 7.3.1 The infiltration of MPs under the influence of tidal cycles

Schruff (2018) defined several infiltration behaviors according to the ratio of particle diameter to substrate diameter. Unimpeded static percolation could be observed when the ratio is smaller than 0.11. The ratios between 0.11 to 0.32 and  $> 0.32$  correspond to finite depth infiltration and fine surface sealing. In the present study, the ratio of  $d_{MP}$  to substrate diameter ranged between 0.05 to 0.26. Figure 7.3 shows the floating percentages of MPs after each increase in tidal water levels.

More particles with smaller  $d_{MP}$  floated on the water surface as the water level increased. Further, 90–100% of the PP1 floated on the surface after 10 tidal cycles, while the floating percentage was 77–90% for PP2 at different rates of tidal level change. For PE particles, more PE1 and PE2 floated on the surface after 10 tidal cycles compared to PE3. With regard to high-density particles, their presence on the surface water surprisingly increased with tidal cycles. For instance, the floated NY1 changed from 47% to 70% after 10 cycles under a rate of tidal level change of 0.25 cm/min, whereas the floated NY2 changed from 37% to 43%. The floated PLA1 increased from 17% to 47%, and the PLA2 increased from 33% to 40% after 10 cycles. The PVC1 observed on the surface increased from 43% to 73%, and the PVC2 increased from 40% to 67% after 10 cycles. The V1 on the surface increased from 30% to 53%, and the V2 increased from 40% to 43% after 10 cycles. We observed that larger particles floated to the surface at the first water level increase since large particles had more difficulty infiltrating the substrate. However, as the tidal cycles increased, smaller particles floated on the water surface due to buoyance force or surface tension force.

With respect to particle density, more particles with a density lower than water floated on the surface compared to the high-density particles. As suggested by the results, it was hard for low-density particles to infiltrate the sublayer of substrate under the influence of repeated water level changes. The change in rates of tidal level did not change the particle floating greatly (Figure 7.3). The number of floated particles was similar among the tests with different rates of tidal level change. An analysis was conducted to correlate the floating percentages of MPs and indicators, including the rate of tidal level change, longest (*a*), medium (*b*), and shortest particle side lengths (*c*) of MPs, MP density, MP weight,  $d_{MP}$ , the largest cross-section area, perimeter, and CFS. Considering all the MP particles, the floating percentages increased significantly with the increase

of  $b$  and the largest cross-section area, whereas decreased significantly with the increase of MP density and CSF (Figure 7.4a). Accounting for only the low-density particles, the floating percentages showed a significantly negative correlation with rates of tidal level change,  $c$ , MP density, weight,  $d_{MP}$  (Figure 7.4b). The floating percentages of high-density particles demonstrated a significant positive correlation with  $b$ , whereas they showed a significant negative correlation with  $c$  and CSF (Figure 7.4c). The results imply that particles with a large cross-section area, low density, and flat particles had difficulty infiltrating the substrate and tended to float on the water surface with tidal movement. Lower rate of tidal level change contributed to higher floating percentage for low-density MPs. The floating of low-density particles results from buoyance force (MP density smaller than aqueous phase density) and surface tension, whereas the floating of high-density particles results mainly from surface tension. As a result, lower rates of tidal level change have longer inundation times, allowing more time for low-density particles to float.

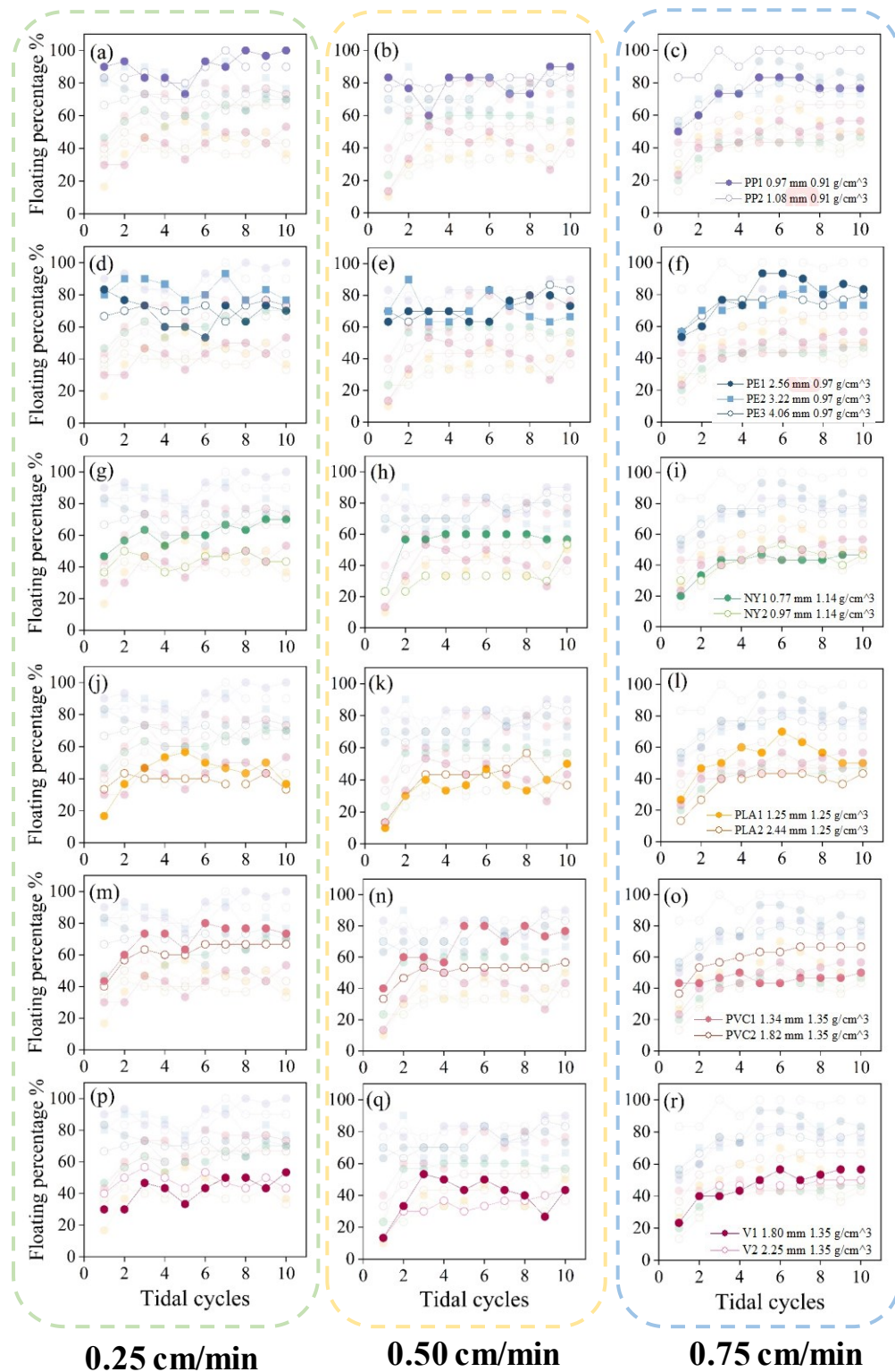


**Figure 7.3** The floating percentages of MPs after each water level increase at the rates of tidal level change of 0.25, 0.50, and 0.75 cm/min.

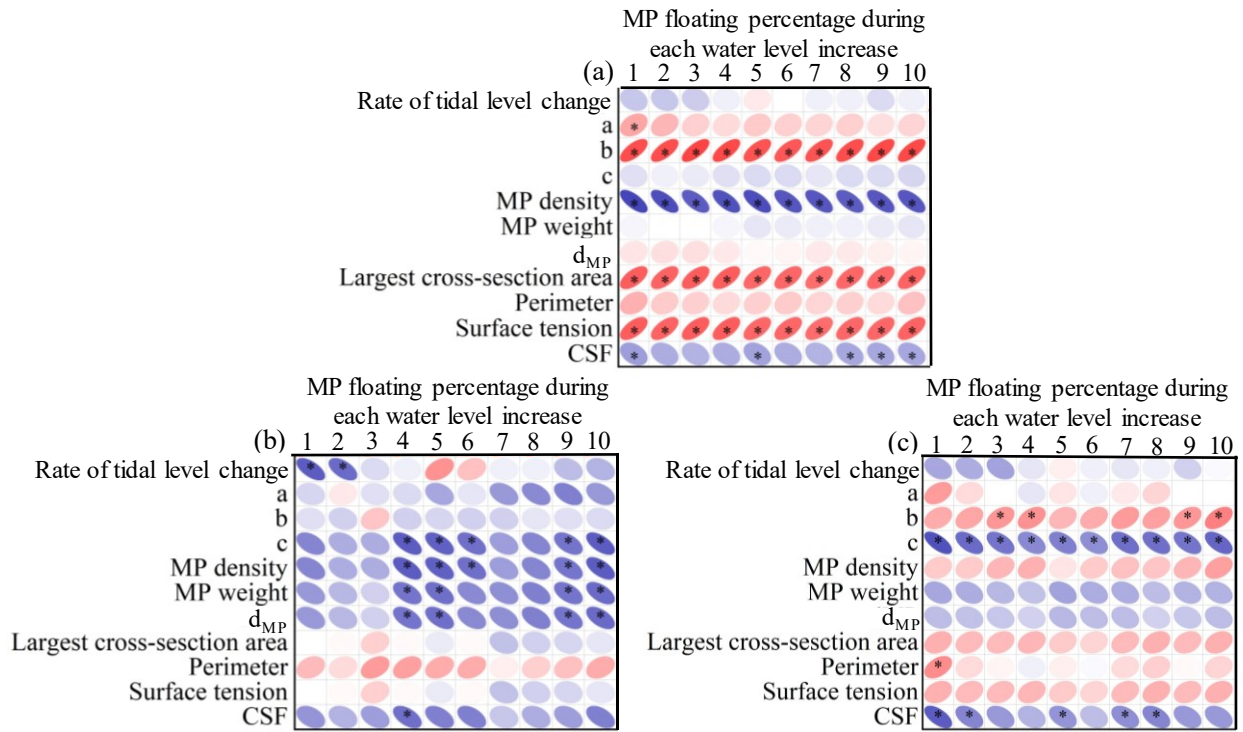


**Figure 7.4** Spearman correlation analysis between floating percentages of MPs and various indicators considering all the MP types (a), only the low-density MPs (b), and only the high-density MPs (c). ( $p < 0.05$ ).

The distribution of MP particles in the substrate after 10 tidal cycles is shown in Figure 7.5. More small  $d_{MP}$  particles, such as PP1, PP2, NY1, and NY2, were distributed on the top of the substrate profile, while large  $d_{MP}$  particles were concentrated in the lower part of the profile. Figure 7.5j, k, l presents the distribution of MPs in the top 1 cm surface substrate. Only a small portion of the MPs was retained on the surface layer. More MPs with small  $d_{MP}$ , such as PP1, PP2, NY1, and NY2, were retained on the surface layer compared to other MPs with large  $d_{MP}$ . As shown in Figure 5j, more MPs with small  $d_{MP}$  remained in the high tidal zone, whereas MPs with large  $d_{MP}$  in the surface layer tended to be distributed in the lower tidal zone (Figure 5l). It should be noted that the tank experiment was assumed to be a closed system since the two sides of the substrate were

intercepted by the meshes. Therefore, if the mesh were not present, MPs retained in the lower substrate might have been transported further downward.

To further explore the underlying relationship between MP transport and its properties, a correlation analysis was conducted between the positions of each MP and the MP properties (Figure 7.6a). In the scenario in which MPs were placed on top of the GBs, the horizontal location of MPs,  $x$ , showed significant positive correlation with the shortest length  $c$ , MP density, MP weight,  $d_{MP}$ , and CSF, while it had significant negative correlation with the rate of tidal level change and the longest length  $a$ . The vertical distribution of MPs showed significant positive correlation with the shortest length  $c$ , MP density, MP weight,  $d_{MP}$ , and CSF, while demonstrating significant negative correlation with the medium length  $b$ , largest cross-section area, perimeter, and surface tension of MPs. The results imply that the large, high-density, and less flat particles tended to move downward along the beach slope and infiltrate the deep substrate layer under the influence of repeated tidal forces. The one-direction infiltration of MPs has been investigated in previous studies, suggesting that the depth of MP infiltration is influenced by the size and shape of MPs, as well as the permeability of sediments. A smaller MP size and large substrate porosity support deep MP infiltration (Waldschlager and Schuttrumpf, 2020). Nevertheless, in the present study, the particles with small  $d_{MP}$  tended to retain in the surface layer and upper tidal zone under repeated water level changes, indicating that the hydrodynamic forces in the natural environment greatly complicate MP transport. Only a few studies have used water tanks to study the transport of MPs and have focused mainly on the effects of waves. For instance, Kerpen et al. (2020) found that, during the formation of the bed profile, particles with a density greater than that of water ( $>1.25 \text{ g/cm}^3$ ) were partly confined to deeper layers of the sloping beach, whereas particles with a density lower than that of water floated continuously in the surf zone or were deposited on the

beach during wave action. Alsina et al. (2020) found that floating particles stay near the water surface, whereas nonfloating particles migrate close to the bed at slower velocities than floating particles. These results are similar to the present study in that the high-density particles tended to distribute in the deep substrate layer and low tidal zone. The transport of particles in the substrate is distinctive from that of other substances. For instance, Vandermeulen et al. (1988) found that the depth of oil penetration increases with tidal cycles, as the repeated downward movement of water carries viscous oil into deeper substrates and adheres to the substrate surface.

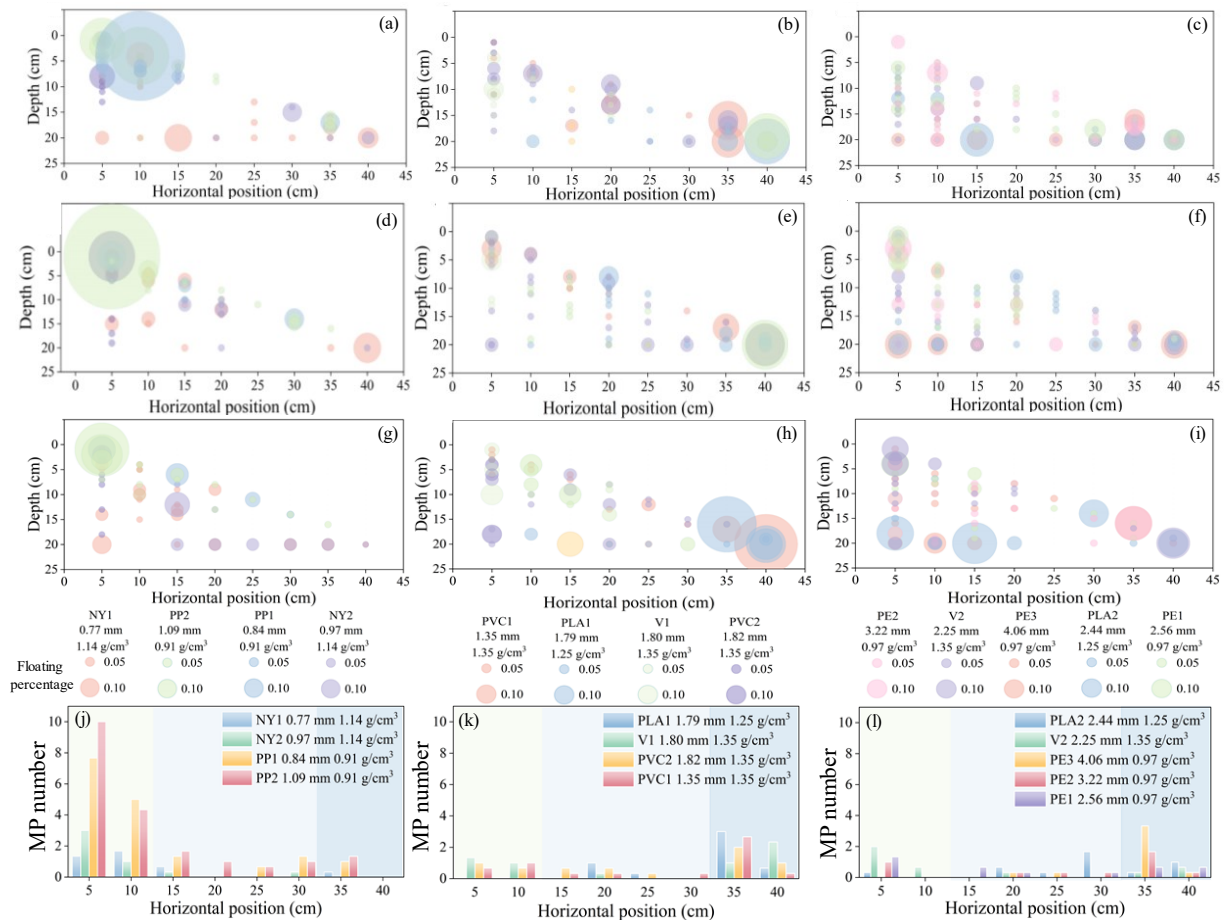


**Figure 7.5** The distribution of various MPs in substrate under the rates of tidal level change of 0.25 cm/min (a–c), 0.50 cm/min (d–f), and 0.75 cm/min (g–i). The distribution of various MPs in

the top 1 cm layer under the rates of tidal level change of 0.25 cm/min (j), 0.50 cm/min. (k), and 0.75 cm/min (l).

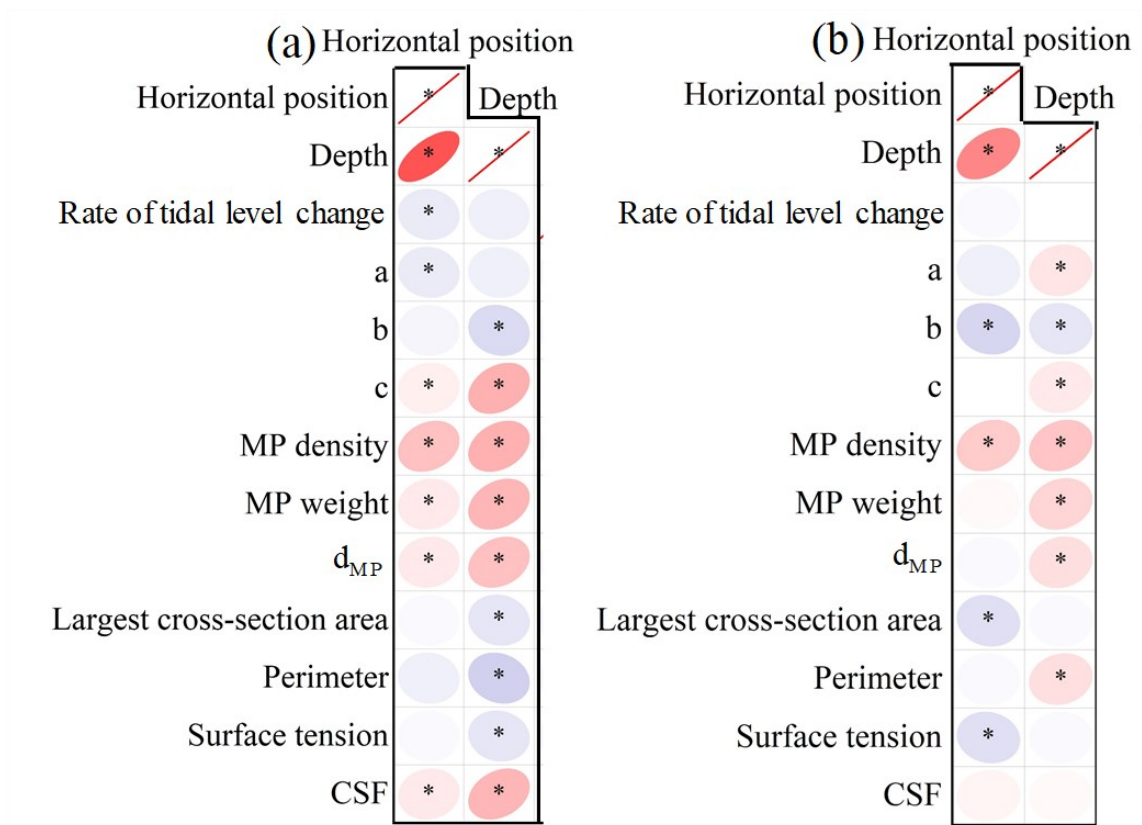


**Figure 7.6** Spearman correlation analysis between MP horizontal/vertical position and various indicators for the scenario that MP placed on the substrate surface (n=1139) (a) and MPs placed in the bottom of substrate (n=1128) (b). (p < 0.05)

### 7.3.2 The resuspension of MPs under the influence of tidal cycles

Through sediment mixing or bioturbation, surface sediments can be translocated into deeper layers, taking plastic particles with them (Martinetto et al., 2016). Hence, the transport of MPs beneath the substrate under tidal influence was also studied. In terms of particle size, smaller particles floated on the water surface. For instance, in a rate of tidal level change of 0.25 cm/min, 57% and 17% of PP1 and PP2, respectively, floated to the surface after 10 tidal cycles (Figure 7.7a). The floating percentages of PE1, PE2, and PE3 were 70%, 53%, and 10%, respectively (Figure 7.7b). Surprisingly, high-density particles at the bottom of the substrate were increasingly transported to the water surface under the influence of water level changes. Similarly, high-density particles with smaller particle size showed a higher probability of floating on the water surface. Taking the results of 0.25 cm/min as an example, 27% and 10% of NY1 and NY2, respectively, floated to the surface after 10 tidal cycles. PLA2 did not float to the water surface, whereas 33% of PLA1 floated to the surface after 10 tidal cycles. Similarly, 33% of PVC1 was moved to the surface, although no PVC2 was seen on the water surface, and 27% and 7% of V1 and V2, respectively, were moved to the surface after 10 cycles. With respect to particle density, more low-density particles were transported to surface water compared to high-density particles. NY1 and PP1 had similar  $d_{MP}$  of 0.77 and 0.84 mm, respectively. However, 57% and 27% of PP1 and NY1, respectively, moved to the surface after 10 tidal cycles under a rate of tidal level change of 0.25 cm/min. The  $d_{MP}$  of PP2 and NY2 were 1.09 and 0.97 mm, respectively, but their floating percentages were 17% and 10% after 10 tidal cycles under a rate of tidal level change of 0.25 cm/min. PLA2 and PE1 had  $d_{MP}$  of 2.44 and 2.56 mm, respectively, whereas their floating percentages were 0% and 70%.

The rate of tidal level change also affected the upward migration of the particles. A decrease in the

change rate resulted in increased floating of particles, especially small particles. With increasing rates of tidal level change of 0.25, 0.50, and 0.75 cm/min, 57%, 50%, and 33% of the PP1 were moved to the water surface after 10 tidal cycles, whereas 70%, 73%, and 63% of PE1, respectively, were observed on the water surface (Figure 7.7a–f). For high-density particles, the increase in the rate of tidal level change decreased the floating percentage from 27% to 17% for NY1, from 33% to 20% for PLA1, and from 27% to 20% for V1 (Figure 7.7g–r). However, the floating percentages of larger particles did not vary greatly with the changed rate. The floating of high-density particles on the water surface is attributed to the balance between surface tension and gravity. A small disturbance to such balance may lead to the settling of particles. A higher flow rate may lead to an unsteady water surface and more disturbance to the particles. However, such disturbances do not interrupt the floating of low-density particles. The greater floating of low-density particles is attributed to a longer submerge time for floating. The correlation analysis considering all MP particles revealed floating percentages significantly decreased with the increase of MP density and perimeter (Figure 7.8a). When only low-density particles were considered, the floating percentages decreased significantly with the increase of the longest length  $a$ , the medium length  $b$ , the largest cross-section area, perimeter, and surface tension of MPs, while they showed a positive correlation with CSF (Figure 7.8b). The floating percentages of high-density particles demonstrated a significant decrease with the increase of the rate of tidal level change, the longest length  $a$ , weight,  $d_{MP}$ , and perimeter (Figure 7.8c). The results suggest that the smaller, low-density, and less flat particles had a higher possibility of moving upward to the water surface under repeated tidal forces.

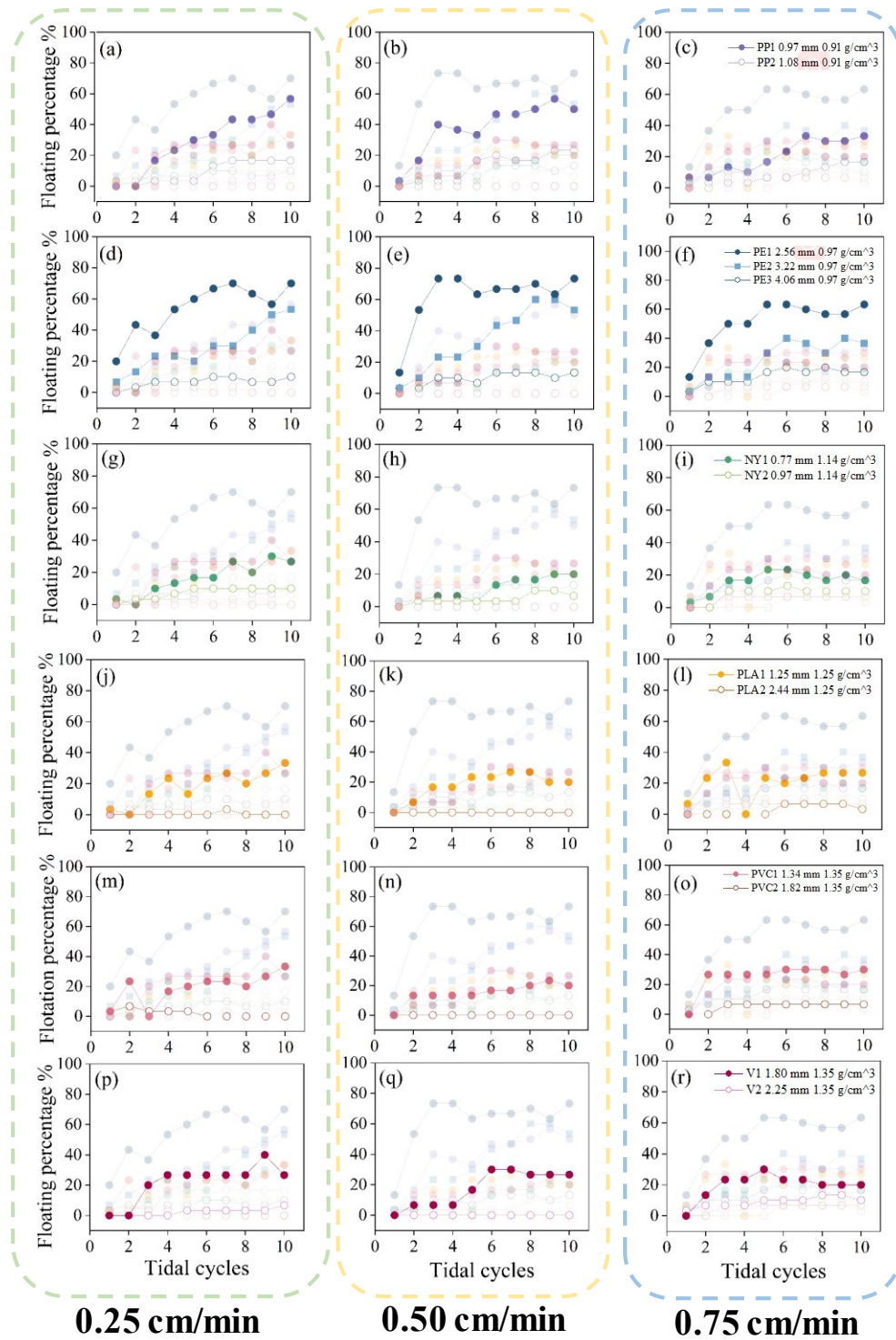


**Figure 7.7** The floating percentages of MP at the rates of tidal level change of 0.25, 0.50, and 0.75 cm/min.

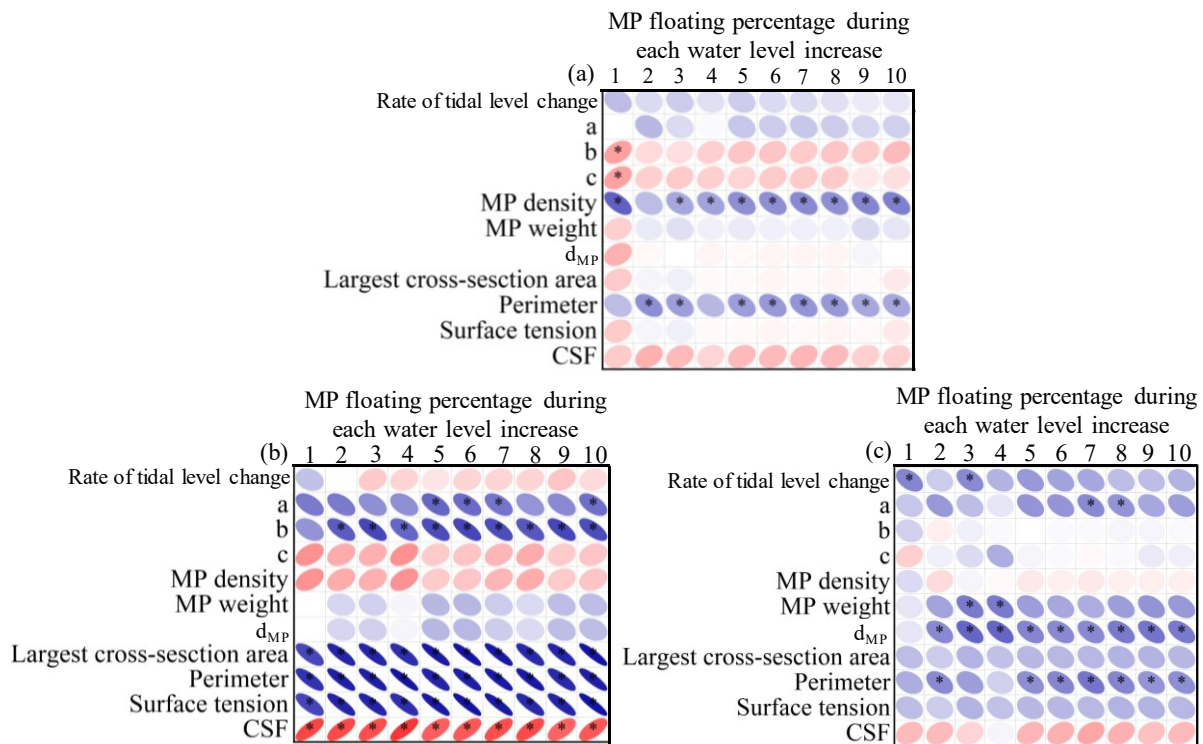


**Figure 7.8** Spearman correlation analysis between floating percentages of MPs and various indicators considering all the MP types (a), only the low-density MPs (b), and only the high-density MPs (c). ( $p < 0.05$ )

The distribution of various MP particles in the substrate profile is shown in Figure 7.9, clearly demonstrating that both the low- and high-density MPs moved upward. Similar to the results from the previous section, smaller  $d_{MP}$  particles were retained in the surface substrate layer compared to large  $d_{MP}$  particles. With a focus on the surface layer (top 1 cm), more MPs were detected in the upper tidal zone (Figure 7.9j, k, l). In the scenario in which MPs were buried at the bottom of the substrate, the horizontal positions,  $x$ , of various MPs showed significant positive correlation with MP density, whereas they demonstrated significant negative correlation with the medium length  $b$ , the largest cross-section area and surface tension of MPs (Fig. 7.6b). The vertical positions,  $z$ , of MPs showed significant positive correlation with the longest length  $a$  of MPs, MP density, MP

weight, and  $d_{MP}$ . This result implies that high-density and large particles tended to distribute in the lower tidal zone and deeper substrate layer.

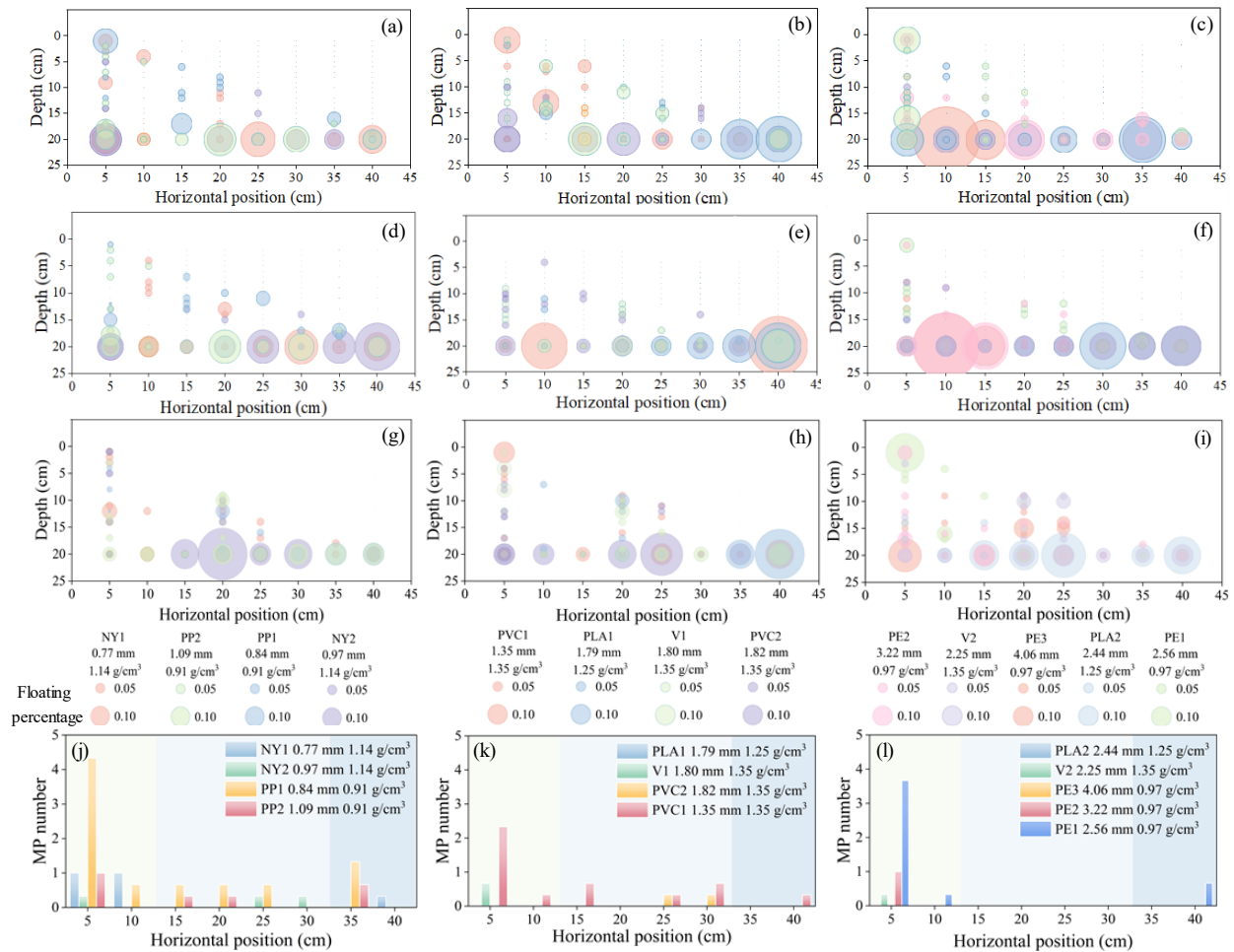


**Figure 7.9** The distribution of various MPs in substrate under the rates of tidal level change of 0.25 cm/min (a–c), 0.50 cm/min (d–f), and 0.75 cm/min (g–i). The distribution of various MPs in the top 1 cm layer under the rates of tidal level change of 0.25 cm/min (j), 0.50 cm/min (k), and 0.75 cm/min (l).

### 7.3.3 The significance of surface tension in determining the transport of MPs

Most of the shore is free of hydrodynamic forces at low tide. The water arrives at intermediate tidal levels and can crash directly onto particles where particles were previously present, imposing impinging forces. As the tide rises and the particles are fully submerged in water, drag and lift forces take over, and the impinging disappears. During this repeated process in the tidal zone, the impact of surface tension on MP behavior is evident but has not been noted extensively. Stolte et al. (2015) discussed grain floating by surface tension during the density separation process for extracting MPs from sediment samples. After extraction by density separation, hundreds of particles float on top of the deionized water. These particles are stirred from the bottom and kept afloat by surface tension, which counterbalances the gravity that causes nonfloating particles to sink. Stolte et al. (2015) also proved that more particles are extracted from finer-grained sediments, indicating that finer particles are easier to support by surface tension; thus, more particles are extracted.

Hydrostatic pressure and surface tension make up the force that counteracts gravity (Vella, 2015). Floating bodies with lateral dimensions much smaller than capillary length have negligible buoyancy, and their floating is due to surface tension. It is crucial to understand floating for a variety of biological and engineering problems (Vella, 2015). Assuming the indentation angle between the water surface and a sphere surface is  $30^\circ$ , the surface tension can support a 3-mm diameter sphere particle with a density of  $2,500 \text{ kg/m}^3$  and around 5-mm sphere particles with a density of  $1,000 \text{ kg/m}^3$  (Figure 7.10). As a result, most of the MPs can float on the water surface with the support of surface tension force. This is confirmed by the present study, which found that not only the low-density particles migrated upward under tidal influence but also the high-density particles. Therefore, it is necessary to reconsider the presumption that MP particles remain on the

surface because their density is lower than that of water.

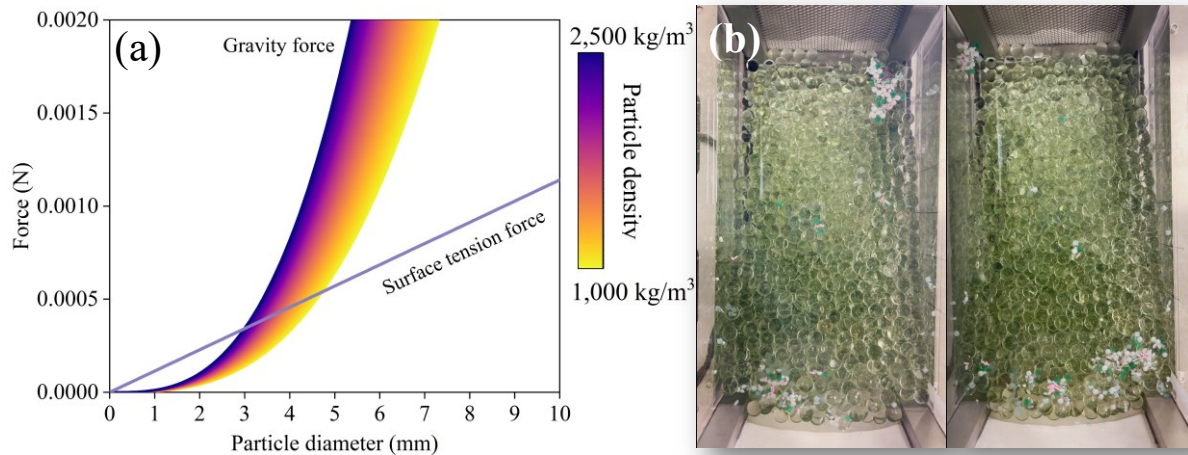


**Figure 7.10** Gravity force and surface tension force for sphere particles, adapted from (Stolte et al., 2015) (a). The aggregates of MPs on water surface (b).

The aggregation of plastic particles was another commonly observed phenomenon on the water surface during the experiment (Fig. 7.10b). Aggregates can form through attractive interactions, depending on the forces and positions among the particles. Different floating particles with different wetting properties can repel each other, while particles of the same properties always attract each other. When particles come into contact with a liquid, the slope of the liquid interface at the contact line decreases because the liquid rises between particles. As a result, the horizontal projection of tension force is greater between particles than on the outside, resulting in an attractive force (Dalbe et al., 2011).

In a natural environment, the aggregation of floating litter is named windrow, irrespective of the force, such as convergence, wind, tides, or density-driven currents (Cózar et al., 2021). Marine life interacts frequently with windrows. However, since litter windrows are dispersed, small, and

ephemeral, they are generally overlooked in research. Marine litter pollution can be prevented primarily by restricting litter from entering the sea, followed by its collection. High loads of patchy floating litter raise expectations for marine litter cleanup. Only a large quantity of litter can form litter windrows, making it possible to mark zones and periods of heavy pollution by employing aerial surveys. There has also been evidence that active fishing for windrows can effectively capture large amounts of litter. For instance, Ruiz et al. (2020) conducted 196 tows and collected 16.2 tons of floating marine litter. Most of the litter windrows were around 1 km in length and, on average, accumulated 77.75 kg of floating marine litter, with plastic being the most common type of material, accounting for 96%. It may be worthwhile to conduct ocean cleanups when sensitive zones of high ecological and economic value, such as tourist beaches, marine protected areas, aquaculture facilities, or shipping routes, are at risk of contamination. Prior to implementing these recommended actions, it is imperative to conduct a proper environmental impact assessment. Although large mesh openings and slow tow speeds can help reduce fish, turtles, and mammals being caught, mechanical cleanups on ocean surfaces may also remove drifting seaweed, fish eggs, or planktons (Cózar et al., 2021; Wang et al., 2022).

#### 7.3.4 Implications for field sampling and data interpretation

Previous field sampling mainly focused on the top beach surface (0–5 cm) as an indicator of plastic pollution in a specific area (Bissen and Chawchai, 2020; Corcoran et al., 2020; Egessa et al., 2020; Exposito et al., 2021; Jaubet et al., 2021; Fred-Ahmadu et al., 2022). As suggested in the present study, only a small proportion of the added MPs were retained on the surface layer. The vertical distribution of MPs was uneven among the various MP types. Smaller particles were retained in the top 1 cm substrate and upper tidal zone compared to the large particles in the  $d_{MP}/\text{substrate}$  diameter range of the present study. Sampling depth is an important aspect in

quantifying MP abundance. However, only a few studies sampled sediments deeper than 50 cm (Willis et al., 2017; Wang et al., 2018; Fan et al., 2019; Li et al., 2020; Belivermis et al., 2021; Culligan et al., 2021; Viet Dung et al., 2021). In general, MP abundance declines from the surface to the deep layer, which is in line with plastic production and consumption (Fan et al., 2019). For a comprehensive understanding of MP inventory on shorelines, it is essential to analyze deeper sediment layers, as has been done for other contaminants.

In previous field studies exploring the litter or MP distribution along the beach, the high tideline is generally selected as the sampling location, since more litter or plastics were detected on the surface layer (Silva-Cavalcanti et al., 2009; Costa et al., 2010; Jayasiri et al., 2013; Prarat and Hongsawat, 2022). For instance, Bancin et al. (2019) found that the concentration of plastic particles above the high tideline was higher than the intertidal zone, and PE, PP, and PS were the primarily detected particle types. Heo et al. (2013) recorded the mean abundance of small plastics to be  $473 \pm 866$  particles/m<sup>2</sup> at the cross-section perpendicular to the shoreline and  $976 \pm 405$  particles/m<sup>2</sup> at the high strandline in the upper tidal zone. Specifically, low-density Styrofoam spherules accounted for 96.3% in the cross-section and 90.7% of the total plastic abundance in the high strandline. The cross-section distribution of Styrofoam, fragment, and pellet was distinctive. Constant et al. (2019) found that the high deposition line had the highest MP concentration, with a mean concentration of 115 items/kg, compared to the overall mean of 30 items/kg. As indicated by the present study, the low-weight and low-density MPs have a higher possibility of being retained in the upper tidal zone, while the high-density, high-weight, less flat MPs have a tendency to move along the beach slope with the receding water and are hard to move upward by water level increase. Previous tank studies proved that high-density MPs were confined to the deeper layer of the beach and moved close to the bed (Alsina et al., 2020). Therefore, a large quantity of MPs with

high density may be retained in the deep substrate or at the bottom of the sea, leading to an underestimation of MP loads in coastal zones. In addition, the density of MPs can be increased through aggregation with natural suspended particles, or through being covered by a biofilm of microorganisms (Yang et al., 2021; Yang et al., 2022). Biofilms facilitate the aggregation of MPs by producing sticky substances on MPs, and therefore play a crucial role in the vertical migration of MPs.

Currently, the response and cleanup techniques of MPs in the environment are still under development. The M/V X-Press Pearl caught fire in May 2021, spilling 1680 tons of spherical plastic (5 mm; white) 18 km off the west coast of Sri Lanka (Mongabay, 2021). The response techniques utilized were similar to oiled shoreline responses, including manual removal, handheld sieving, floating, trommel, and large-scale sieving. However, the separation of high-density particles with sizes similar to those of sediments is still difficult.

In the present study, GBs were used as a model substrate owing to their transparency and easily measurable size. However, sediment in the natural environment is more complex, given its variability in terms of surface morphology, shape, and density. In this regard, Shen et al. (2011) suggested that surface roughness plays a key role in colloid deposition, finding that polystyrene latex microspheres were retained at higher concentrations in sand than in GBs. They also found that the sharp asperities on the surface of sand particles enhance particle deposition in primary minima by decreasing the energy barrier, and that the presence of valleys on the surface of the sand particles increases attachment in secondary minima. Sand, gravel, or pebble, notably, could be much smaller or have an uneven grain distribution than the GBs used in the present study. As such, a higher trapping efficiency can be expected for these materials in the natural environment.

The present study did not consider the groundwater and related process, for instance, the intertidal circulation cell (Geng and Boufadel, 2015; Geng et al., 2020), which require further investigation.

#### **7.4 Summary**

This is the first study to investigate the transport of MPs under dynamic boundary conditions using a tidal tank. The effects of tidal level changes on the infiltration and resuspension of MPs featured with various sizes, densities, and shapes were revealed ( $d_{MP}/$ substrate diameter ranged from 0.05 to 0.26). Our results confirmed that as tidal cycle increases, the number of particles on the water surface also increased. More particles of small  $d_{MP}$  and low density floated to the water surface. High-density particles also migrated to water surface due to surface tension force. Further, a lower rate of tidal level change contributed to more floating of particles. The distribution of MPs in substrate proved that large, high-density, and less flat particles tend to be distributed in the lower tidal zone and deeper substrate layers. These findings can help understand the redistribution of MPs and assess their risk in the shoreline environment.

# **Chapter 8 Contributions and significance of thesis research, and suggestions for future work**

## **8.1 Contributions and significance of thesis research**

1. A comprehensive global meta-analysis of MP presence in estuaries is presented to systematically assess the global load of MPs. The relationships between environmental and anthropogenic factors and MP abundance were uncovered.
2. Water content plays critical role in determining MP mobilization. Decreased water content significantly impeded the remobilization of MPs even during transient flow, which provides valuable evidence in understanding the fate of MPs in porous media under a context of prolonged drought event.
3. The transport of MPs was facilitated with increased numbers of air-water interface oscillations. Small substrate size, large MP size, hydrophobic MPs, high salinity, low flow velocity led to enhanced MP retention in substrate. A majority of the micro-sized MPs are suggested to end up in the open ocean under the influence of tidal movements.
4. The fluctuation of capillary fringe facilitates the remobilization of MPs from substrate, which can serve as a pathway to relocate MPs to the tidal aquifer.
5. During repeated water level changes, surface tension is vital for MP transport. High-density particles could migrate to water surface due to surface tension. Increasing number of particles were observed on water surface as tidal cycles increased. Large, high-density, less flat MP particles tend to distribute in low-tide zone.

## 8.2 Suggestions for future work

- The density of MPs could be increased through aggregation with natural suspended particles, or through being covered by a biofilm. Biofilms facilitate the aggregation of MPs by producing sticky substances on MPs and therefore play a crucial role in the vertical transportation of MPs. For a better understanding of MPs transport, the generation of biofilm and aggregation needs further investigation.
- To link the experiment and field results, it is important to implement standardized sampling and extraction procedures. Non-uniform sampling methods and locations can lead to misinterpretation of MP patterns in estuaries. However, standardized procedure is not easy to achieve as various trade-offs and research needs. Hence, studies aim to determine the fraction of total MP load captured by each method are needed.
- It is crucial to take weather conditions into consideration when conducting field sampling. Increased rainfall, heavy storms, and typhoon prior to sampling may increase the abundance of plastic debris in water. It is important to identify the remobilization thresholds of MPs in a real environment under the influence of interplayed hydrodynamic forces.
- Modeling is an effective tool to predict the potential fate of MPs in sediment. Lagrangian and Eulerian techniques for particle tracking, for example, are effective tools to forecast particle tracking and have been routinely utilized to estimate the paths of polymers based on their physical parameters. Modeling tools have not been widely applied to explore MP distribution and transport in estuaries based on spatial and temporal parameters. The complexity of the link between abundance and physicochemical properties, the wide variety of types and sources, and the fragmentation routes make tracking the distribution of MPs much more

challenging.

- Almost all the studies used net or filter to capture MPs in the current dataset. The pore size restricted the collection of nanoplastics or small-sized MPs in the environment. Additionally, the identification and quantification of nanoplastics or small-sized MPs are still challenging. The amount of nanoplastics in natural environment is still a mysterious number, requiring advanced quantitative method.

## Journal publications

- [1] **Feng, Q.**, An, C., Chen, Z., Lee, K., Wang, Z., 2023. Identification of the Driving Factors of Microplastic Load and Morphology in Estuaries for Improving Monitoring and Management Strategies: A Global Meta-analysis. *Environmental Pollution*, 333, 122014. DOI: <https://doi.org/10.1016/j.envpol.2023.122014>
- [2] **Feng, Q.**, Chen, Z., An, C., Yang, X., Wang, Z., 2023. Tide-induced infiltration and resuspension of microplastics in shorelines: insights from tidal tank experiments. *Water Research*, 236, 119970. DOI: <https://doi.org/10.1016/j.watres.2023.119970>
- [3] **Feng, Q.**, An, C., Chen, Z., Wang, Z., 2023. New perspective on the mobilization of microplastics through capillary fringe fluctuation in a tidal aquifer environment. *Environmental Science & Technology*, 57 (2), 929-938. DOI: <https://doi.org/10.1021/acs.est.2c04686>
- [4] **Feng, Q.**, An, C., Chen, Z., Zhang, Y., Owens, E., Lee, K., Li, B., Taylor, E., Wang, Z., 2022. Exploring the effects of substrate mineral fines on oil translocation in the shoreline environment: Experimental analysis, numerical simulation, and implications for spill response. *Journal of Hazardous Materials*, 437, 129341. DOI: <https://doi.org/10.1016/j.jhazmat.2022.129341>
- [5] **Feng, Q.**, Chen, Z., Greer, C.W., An, C., Wang, Z., 2022. Transport of microplastics in shore substrates over tidal cycles: roles of polymer characteristics and environmental factors. *Environmental Science & Technology*, 56 (12), 8187–8196. DOI: <https://doi.org/10.1021/acs.est.2c01599>
- [6] **Feng, Q.**, An, C., Chen, Z., Owens, E., Niu, H., Wang, Z., 2021. Assessing the coastal sensitivity to oil spills from the perspective of ecosystem services: a case study for Canada's pacific coast. *Journal of Environmental Management*, 296, 113240. DOI: <https://doi.org/10.1016/j.jenvman.2021.113240>
- [7] **Feng, Q.**, An, C., Chen, Z., Yin, J., Zhang, B., Lee, K., Wang, Z., 2021. Investigation into the impact of aged microplastics on oil behavior in shoreline environments. *Journal of Hazardous Materials*, 421, 126711. DOI: <https://doi.org/10.1016/j.jhazmat.2021.126711>.
- [8] **Feng, Q.**, An, C., Chen, Z., Wang, Z., 2020. Can deep tillage enhance carbon sequestration in soils? A meta-analysis towards GHG mitigation and sustainable agricultural management. *Renewable and Sustainable Energy Reviews*, 133, 110293. DOI: <https://doi.org/10.1016/j.rser.2020.110293>
- [9] **Feng, Q.**, An, C., Cao, Y., Chen, Z., Owens, E., Taylor, E., Wang, Z., Saad, E.A., 2021. An

analysis of selected oil spill case studies on the shorelines of Canada. *Journal of environmental informatics letters*, 5 (1), 39-47. DOI: [10.3808/jeil.202100052](https://doi.org/10.3808/jeil.202100052).

- [10] Wang, Z., An, C., Lee, K., Feng, Q., 2023. Overlooked role of bulk nanobubbles in the alteration and motion of microplastics in the ocean environment. *Environmental Science & Technology*. DOI: <https://doi.org/10.1021/acs.est.3c03270>
- [11] Wang, Z., An, C., Lee, K., Feng, Q., Zhang, B., 2023. Exploring the role of nanobubbles in the fate and transport of spilled oil on shorelines. *ACS ES&T Water*, 3 (1), 30-40. DOI: <https://pubs.acs.org/doi/10.1021/acsestwater.2c00344>.
- [12] Yang, X., An, C., Feng, Q., Boufadel, M., Ji, W., 2022. Aggregation of microplastics and clay particles in the nearshore environment: Characteristics, influencing factors, and implications. *Water Research*, 224, 119077. DOI: <https://doi.org/10.1016/j.watres.2022.119077>.
- [13] Cai, M., Qi, Z., Guy, C., An, C., Chen, X., Wang, Z., Feng, Q., 2023. Insights into the abiotic fragmentation of biodegradable mulches under accelerated weathering conditions. *Journal of Hazardous Materials*, 454, 131477. DOI: <https://doi.org/10.1016/j.jhazmat.2023.131477>
- [14] Qu, Z., An, C., Mei, Z., Yue, R., Zhao, S., Feng, Q., Cai, M., Wen, J., 2022. An experimental and modeling study on the penetration of spilled oil into thawing frozen soil. *Environ Sci Process Impacts*, 24 (12), 2398-2408. DOI: <https://doi.org/10.1039/D2EM00368F>
- [15] Chen, Z., Feng, Q., Yue, R., Chen, Z., Moselhi, O., Soliman, A., Hammad, A., An, C., 2022. Construction, renovation, and demolition waste in landfill: a review of waste characteristics, environmental impacts, and mitigation measures. *Environmental Science and Pollution Research*, 29, 46509–46526. DOI: <https://doi.org/10.1007/s11356-022-20479-5>.
- [16] Bi, H., Mulligan, C.N., An, C., Owens, E., Taylor, E., McCourt, J., Yin, J., Feng, Q., Chen, X., Yue, R., 2022. Development of a calcium alginate-cellulose nanocrystal-based coating to reduce the impact of oil spills on shorelines. *Journal of Hazardous Materials*, 436, 129228. DOI: <https://doi.org/10.1016/j.jhazmat.2022.129228>
- [17] Wang, Z., An, C., Lee, K., Chen, X., Zhang, B., Yin, J., Feng, Q., 2022. Physicochemical change and microparticle release from disposable gloves in the aqueous environment impacted by accelerated weathering. *Science of the Total Environment*. 832, 154986. *Science of the Total Environment* (2022). DOI: <https://doi.org/10.1016/j.scitotenv.2022.154986>

- [18] Wang, Z., An, C., Lee, K., Owens, E., Boufadel, M., **Feng, Q.**, 2022. Dispersion modeling of particulate matter from the in-situ burning of spilled oil in the northwest Arctic area of Canada. *Journal of Environmental Management*, 301, 113913. DOI: <https://doi.org/10.1016/j.jenvman.2021.113913>
- [19] Wang, Z., An, C., Chen, X., Lee, K., Zhang, B., **Feng, Q.**, 2021. Disposable masks release microplastics to the aqueous environment with exacerbation by natural weathering. *Journal of Hazardous Materials*, 417, 126036. DOI: [10.1016/j.jhazmat.2021.126036](https://doi.org/10.1016/j.jhazmat.2021.126036)
- [20] Wang, Z., An, C., Lee, K., Owens, E., Chen, Z., Boufadel, M., Taylor, E., **Feng, Q.**, 2020. Factors influencing the fate of oil spilled on shorelines: a review. *Environmental Chemistry Letters*, 19, 1611-1628. DOI: <https://doi.org/10.1007/s10311-020-01097-4>

## References

- Acha, E.M., Mianzan, H.W., Iribarne, O., Gagliardini, D.A., Lasta, C., Daleo, P., 2003. The role of the Río de la Plata bottom salinity front in accumulating debris. *Mar. Pollut. Bull.* 46 (2), 197-202.
- Aderikha, V.N., Shapovalov, V.A., 2010. Effect of filler surface properties on structure, mechanical and tribological behavior of PTFE-carbon black composites. *Wear.* 268 (11), 1455-1464.
- Aghilinasrollahabadi, K., Salehi, M., Fujiwara, T., 2020. Investigate the influence of microplastics weathering on their heavy metals uptake in stormwater. *J. Hazard. Mater.* 480, 124439.
- Akhbarizadeh, R., Moore, F., Keshavarzi, B., Moeinpour, A., 2017. Microplastics and potentially toxic elements in coastal sediments of Iran's main oil terminal (Khark Island). *Environ. Pollut.* 220 (Pt A), 720-731.
- Alimi, O.S., Farner Budariz, J., Hernandez, L.M., Tufenkji, N., 2018. Microplastics and nanoplastics in aquatic environments: aggregation, deposition, and enhanced contaminant transport. *Environ. Sci. Technol.* 52 (4), 1704-1724.
- Alimi, O.S., Farner, J.M., Tufenkji, N., 2021. Exposure of nanoplastics to freeze-thaw leads to aggregation and reduced transport in model groundwater environments. *Water Res.* 189, 116533.
- Alomar, C., Estarellas, F., Deudero, S., 2016. Microplastics in the mediterranean sea: deposition in coastal shallow sediments, spatial variation and preferential grain size. *Mar. Environ. Res.* 115, 1-10.
- Alsina, J.M., Jongedijk, C.E., van Sebille, E., 2020. Laboratory Measurements of the Wave-Induced Motion of Plastic Particles: Influence of Wave Period, Plastic Size and Plastic Density. *J Geophys Res Oceans.* 125 (12), e2020JC016294.
- Aramrak, S., Flury, M., Harsh, J.B., Zollars, R.L., 2014. Colloid mobilization and transport during capillary fringe fluctuations. *Environ. Sci. Technol.* 48 (13), 7272-7279.
- Artal, O., Pizarro, O., Sepúlveda, H.H., 2019. The impact of spring-neap tidal-stream cycles in tidal energy assessments in the Chilean Inland Sea. *Renew. Energ.* 139, 496-506.

- Babakhani, P., Bridge, J., Doong, R.A., Phenrat, T., 2017. Continuum-based models and concepts for the transport of nanoparticles in saturated porous media: A state-of-the-science review. *Adv. Colloid Interface Sci.* 246, 75-104.
- Balthazar-Silva, D., Turra, A., Moreira, F.T., Camargo, R.M., Oliveira, A.L., Barbosa, L., Gorman, D., 2020. Rainfall and tidal cycle regulate seasonal inputs of microplastic pellets to sandy beaches. *Front. Environ. Sci.* 8, 123.
- Bancin, L.J., Walther, B.A., Lee, Y.C., Kunz, A., 2019. Two-dimensional distribution and abundance of micro- and mesoplastic pollution in the surface sediment of Xialiao Beach, New Taipei City, Taiwan. *Mar. Pollut. Bull.* 140, 75-85.
- Bayarkhuu, B., Byun, J., 2022. Optimization of coagulation and sedimentation conditions by turbidity measurement for nano- and microplastic removal. *Chemosphere.* 306, 135572.
- Bedrikovetsky, P., Zeinijahromi, A., Siqueira, F.D., Furtado, C.A., de Souza, A.L.S., 2011. Particle detachment under velocity alternation during suspension transport in porous media. *Transport in Porous Media.* 91 (1), 173-197.
- Belivermis, M., Kilic, O., Sezer, N., Sikdokur, E., Gungor, N.D., Altug, G., 2021. Microplastic inventory in sediment profile: A case study of Golden Horn Estuary, Sea of Marmara. *Mar. Pollut. Bull.* 173, 113117.
- Benfer, N.P., King, B.A., Lemckert, C.J., 2007. Salinity observations in a subtropical estuarine system on the Gold Coast, Australia. *J. Coast. Res.*, 646-651.
- Bermudez, M., Vilas, C., Quintana, R., Gonzalez-Fernandez, D., Cozar, A., Diez-Minguito, M., 2021. Unravelling spatio-temporal patterns of suspended microplastic concentration in the Natura 2000 Guadalquivir estuary (SW Spain): Observations and model simulations. *Mar. Pollut. Bull.* 170, 112622.
- Bi, H., An, C., Mulligan, C.N., Wang, Z., Zhang, B., Lee, K., 2021. Exploring the use of alginate hydrogel coating as a new initiative for emergent shoreline oiling prevention. *Sci. Total Environ.* 797, 149234.
- Bissen, R., Chawchai, S., 2020. Microplastics on beaches along the eastern Gulf of Thailand - A preliminary study. *Mar. Pollut. Bull.* 157, 111345.
- Bosker, T., Bouwman, L.J., Brun, N.R., Behrens, P., Vijver, M.G., 2019. Microplastics accumulate on pores in seed capsule and delay germination and root growth of the terrestrial vascular plant *Lepidium sativum*. *Chemosphere.* 226, 774-781.

- Bradford, S.A., Torkzaban, S., Walker, S.L., 2007. Coupling of physical and chemical mechanisms of colloid straining in saturated porous media. *Water Res.* 41 (13), 3012-3024.
- Bradford, S.A., Yates, S.R., Bettahar, M., Simunek, J., 2002. Physical factors affecting the transport and fate of colloids in saturated porous media. *Water Resour. Res.* 38 (12), 63-61-63-12.
- Braun, A., Klumpp, E., Azzam, R., Neukum, C., 2015. Transport and deposition of stabilized engineered silver nanoparticles in water saturated loamy sand and silty loam. *Sci. Total Environ.* 535, 102-112.
- Bridson, J.H., Patel, M., Lewis, A., Gaw, S., Parker, K., 2020. Microplastic contamination in Auckland (New Zealand) beach sediments. *Mar. Pollut. Bull.* 151, 110867.
- Browne, M.A., Crump, P., Niven, S.J., Teuten, E., Tonkin, A., Galloway, T., Thompson, R., 2011. Accumulation of microplastic on shorelines worldwide: sources and sinks. *Environ. Sci. Technol.* 45 (21), 9175-9179.
- Cartwright, N., Nielsen, P., Perrochet, P., 2005. Influence of capillarity on a simple harmonic oscillating water table: Sand column experiments and modeling. *Water Resour. Res.* 41 (8), W08416.
- Chang, B.P., Mohanty, A.K., Misra, M., 2020. Studies on durability of sustainable biobased composites: a review. *RSC Adv.* 10 (31), 17955-17999.
- Chen, G., Flury, M., Harsh, J.B., Lichtner, P.C., 2005. Colloid-facilitated transport of cesium in variably saturated hanford sediments. *Environ. Sci. Technol.* 39 (10), 3435-3442.
- Chen, G., Hong, Y., Walker, S.L., 2010. Colloidal and bacterial deposition: role of gravity. *Langmuir.* 26 (1), 314-319.
- Chen, Z., An, C., Elektorowicz, M., Tian, X., 2022. Sources, behaviors, transformations, and environmental risks of organophosphate esters in the coastal environment: A review. *Mar. Pollut. Bull.* 180, 113779.
- Cheng, Y., Mai, L., Lu, X., Li, Z., Guo, Y., Chen, D., Wang, F., 2021. Occurrence and abundance of poly- and perfluoroalkyl substances (PFASs) on microplastics (MPs) in Pearl River Estuary (PRE) region: Spatial and temporal variations. *Environ. Pollut.* 281, 117025.

- Chequer, L., Bedrikovetsky, P., Badalyan, A., Gitis, V., 2020. Water level and mobilisation of colloids in porous media. *Adv. Water Resour.* 143.
- Cheung, P.K., Cheung, L.T.O., Fok, L., 2016. Seasonal variation in the abundance of marine plastic debris in the estuary of a subtropical macro-scale drainage basin in South China. *Sci. Total Environ.* 562, 658-665.
- Chinfak, N., Sompongchaiyakul, P., Charoenpong, C., Shi, H., Yeemin, T., Zhang, J., 2021. Abundance, composition, and fate of microplastics in water, sediment, and shellfish in the Tapi-Phumduang River system and Bandon Bay, Thailand. *Sci. Total Environ.* 781, 146700.
- Chowdhury, I., Hong, Y., Honda, R.J., Walker, S.L., 2011. Mechanisms of TiO<sub>2</sub> nanoparticle transport in porous media: Role of solution chemistry, nanoparticle concentration, and flowrate. *J. Colloid Interface Sci.* 360 (2), 548-555.
- Chrysikopoulos, C.V., Syngouna, V.I., 2014. Effect of gravity on colloid transport through water-saturated columns packed with glass beads: modeling and experiments. *Environ. Sci. Technol.* 48 (12), 6805-6813.
- Chu, X., Li, T., Li, Z., Yan, A., Shen, C., 2019. Transport of microplastic particles in saturated porous media. *Water.* 11 (12), 2474.
- Chubarenko, I., Stepanova, N., 2017. Microplastics in sea coastal zone: Lessons learned from the Baltic amber. *Environ. Pollut.* 224, 243-254.
- Chubarenko, I.P., Esiukova, E.E., Bagaev, A.V., Bagaeva, M.A., Grave, A.N., 2018. Three-dimensional distribution of anthropogenic microparticles in the body of sandy beaches. *Sci. Total Environ.* 628-629, 1340-1351.
- CIESIN, 2018. Center for International Earth Science Information Network - CIESIN - Columbia University. 2018. Gridded population of the world, Version 4.11 (GPWv4): Population count, Revision 11. Palisades, NY: NASA Socioeconomic Data and Applications Center (SEDAC). <https://doi.org/10.7927/H4JW8BX5>. Accessed 1 June 2022.
- Cohen, J.H., Internicola, A.M., Mason, R.A., Kukulka, T., 2019. Observations and simulations of microplastic debris in a tide, wind, and freshwater-driven estuarine environment: the Delaware Bay. *Environ. Sci. Technol.* 53 (24), 14204-14211.
- Cole, M., Lindeque, P., Fileman, E., Halsband, C., Goodhead, R., Moger, J., Galloway, T.S., 2013. Microplastic ingestion by zooplankton. *Environ. Sci. Technol.* 47 (12), 6646-6655.

- Constant, M., Alary, C., De Waele, I., Dumoulin, D., Breton, N., Billon, G., 2021. To what extent can micro- and macroplastics be trapped in sedimentary particles? a case study investigating dredged sediments. *Environ. Sci. Technol.* 55 (9), 5898-5905.
- Constant, M., Kerherve, P., Mino-Vercellio-Verollet, M., Dumontier, M., Sanchez Vidal, A., Canals, M., Heussner, S., 2019. Beached microplastics in the Northwestern Mediterranean Sea. *Mar. Pollut. Bull.* 142, 263-273.
- Cook, B.I., Mankin, J.S., Anchukaitis, K.J., 2018. Climate change and drought: from past to future. *Current Climate Change Reports.* 4 (2), 164-179.
- Corapcioglu, M.Y., Choi, H., 1996. Modeling colloid transport in unsaturated porous media and validation with laboratory column data. *Water Resour. Res.* 32 (12), 3437-3449.
- Corcoran, P.L., Belontz, S.L., Ryan, K., Walzak, M.J., 2020. Factors controlling the distribution of microplastic particles in benthic sediment of the Thames River, Canada. *Environ. Sci. Technol.* 54 (2), 818-825.
- Corcoran, P.L., de Haan Ward, J., Arturo, I.A., Belontz, S.L., Moore, T., Hill-Svehla, C.M., Robertson, K., Wood, K., Jazvac, K., 2020. A comprehensive investigation of industrial plastic pellets on beaches across the Laurentian Great Lakes and the factors governing their distribution. *Sci. Total Environ.* 747, 141227.
- Corey, A.T., 1949. Influence of Shape on the Fall Velocity of Sand Grains, Colorado Agricultural and Mechanical College.
- Costa, M.F., Ivar do Sul, J.A., Silva-Cavalcanti, J.S., Araujo, M.C., Spengler, A., Tourinho, P.S., 2010. On the importance of size of plastic fragments and pellets on the strandline: a snapshot of a Brazilian beach. *Environ. Monit. Assess.* 168 (1-4), 299-304.
- Costanza, R., Arge, Groot, R.D., Farberk, S., Belt, M.V.D., 1997. The value of the world's ecosystem services and natural capital. *Nature.* 387 (15), 253-260.
- Cózar, A., Aliani, S., Basurko, O.C., Arias, M., Isobe, A., Topouzelis, K., Rubio, A., Morales-Caselles, C., 2021. Marine litter windrows: A strategic target to understand and manage the ocean plastic pollution. *Front. Mar. Sci.* 8.
- Cozzolino, L., Nicastro, K.R., Zardi, G.I., de Los Santos, C.B., 2020. Species-specific plastic accumulation in the sediment and canopy of coastal vegetated habitats. *Sci. Total Environ.* 723, 138018.

- Crawford, C.B., Quinn, B. (2017). Microplastic collection techniques. *Microplastic Pollutants*. Crawford C.B., Quinn B., Elsevier: 179-202.
- Crist, J.T., Zevi, Y., McCarthy, J.F., Throop, J.A., Steenhuis, T.S., 2005. Transport and retention mechanisms of colloids in partially saturated porous media. *Vadose Zone J.* 4 (1), 184-195.
- Culligan, N., Liu, K.-b., Ribble, K., Ryu, J., Dietz, M., 2021. Sedimentary records of microplastic pollution from coastal Louisiana and their environmental implications. *J. Coast. Conserv.* 26 (1), 1-14.
- Dalbe, M.J., Cosic, D., Berhanu, M., Kudrolli, A., 2011. Aggregation of frictional particles due to capillary attraction. *Phys Rev E Stat Nonlin Soft Matter Phys.* 83 (5 Pt 1), 051403.
- Darcy, H., 1856. *Les fontaines publiques de la ville de Dijon: exposition et application*, Victor Dalmont.
- de Souza Machado, A.A., Lau, C.W., Kloas, W., Bergmann, J., Bachelier, J.B., Faltin, E., Becker, R., Gorlich, A.S., Rillig, M.C., 2019. Microplastics can change soil properties and affect plant performance. *Environ. Sci. Technol.* 53 (10), 6044-6052.
- Defontaine, S., Sous, D., Tesan, J., Monperrus, M., Lenoble, V., Lanceleur, L., 2020. Microplastics in a salt-wedge estuary: Vertical structure and tidal dynamics. *Mar. Pollut. Bull.* 160, 111688.
- Dong, Z.Q., Qiu, Y.P., Zhang, W., Yang, Z.L., Wei, L., 2018. Size-dependent transport and retention of micron-sized plastic spheres in natural sand saturated with seawater. *Water Res.* 143, 518-526.
- Dris, R., Gasperi, J., Rocher, V., Saad, M., Renault, N., Tassin, B., 2015. Microplastic contamination in an urban area: a case study in Greater Paris. *Environmental Chemistry.* 12 (5), 592.
- Dunn, A.M., Silliman, S.E., Dhamwichukorn, S., Kulpa, C.F., 2005. Demonstration of microbial transport into the capillary fringe via advection from below the water table. *J. Hydrol.* 306 (1-4), 50-58.
- Duong, T.T., Le, P.T., Nguyen, T.N.H., Hoang, T.Q., Ngo, H.M., Doan, T.O., Le, T.P.Q., Bui, H.T., Bui, M.H., Trinh, V.T., Nguyen, T.L., Da Le, N., Vu, T.M., Tran, T.K.C., Ho, T.C., Phuong, N.N., Strady, E., 2022. Selection of a density separation solution to study microplastics in tropical riverine sediment. *Environ. Monit. Assess.* 194 (2), 65.

- Duquesne, S., Newton, L.C., Giusti, L., Marriott, S.B., Stark, H.J., Bird, D.J., 2006. Evidence for declining levels of heavy-metals in the Severn Estuary and Bristol Channel, U.K. and their spatial distribution in sediments. *Environ. Pollut.* 143 (2), 187-196.
- Eerkes-Medrano, D., Thompson, R.C., Aldridge, D.C., 2015. Microplastics in freshwater systems: A review of the emerging threats, identification of knowledge gaps and prioritisation of research needs. *Water Res.* 75, 63-82.
- Egessa, R., Nankabirwa, A., Basooma, R., Nabwire, R., 2020. Occurrence, distribution and size relationships of plastic debris along shores and sediment of northern Lake Victoria. *Environ. Pollut.* 257, 113442.
- El-Farhan, Y.H., DeNovio, N.M., Herman, J.S., Hornberger, G.M., 2000. Mobilization and transport of soil particles during infiltration experiments in an agricultural field, Shenandoah Valley, Virginia. *Environ. Sci. Technol.* 34 (17), 3555-3559.
- Enders, K., Kappler, A., Biniash, O., Feldens, P., Stollberg, N., Lange, X., Fischer, D., Eichhorn, K.J., Pollehne, F., Oberbeckmann, S., Labrenz, M., 2019. Tracing microplastics in aquatic environments based on sediment analogies. *Sci. Rep.* 9 (1), 15207.
- Eriksen, M., Cowger, W., Erdle, L.M., Coffin, S., Villarrubia-Gomez, P., Moore, C.J., Carpenter, E.J., Day, R.H., Thiel, M., Wilcox, C., 2023. A growing plastic smog, now estimated to be over 170 trillion plastic particles afloat in the world's oceans-Urgent solutions required. *PLoS One.* 18 (3), e0281596.
- Everaert, G., Van Cauwenberghe, L., De Rijcke, M., Koelmans, A.A., Mees, J., Vandegehuchte, M., Janssen, C.R., 2018. Risk assessment of microplastics in the ocean: Modelling approach and first conclusions. *Environ. Pollut.* 242 (Pt B), 1930-1938.
- Exposito, N., Rovira, J., Sierra, J., Folch, J., Schuhmacher, M., 2021. Microplastics levels, size, morphology and composition in marine water, sediments and sand beaches. Case study of Tarragona coast (western Mediterranean). *Sci. Total Environ.* 786, 147453.
- Fan, Y., Zheng, K., Zhu, Z., Chen, G., Peng, X., 2019. Distribution, sedimentary record, and persistence of microplastics in the Pearl River catchment, China. *Environ. Pollut.* 251, 862-870.
- Feng, Q., An, C., Chen, Z., Owens, E., Niu, H., Wang, Z., 2021. Assessing the coastal sensitivity to oil spills from the perspective of ecosystem services: a case study for Canada's pacific coast. *J. Environ. Manage.* 296, 113240.

- Feng, Q., An, C., Chen, Z., Yin, J., Zhang, B., Lee, K., Wang, Z., 2021. Investigation into the impact of aged microplastics on oil behavior in shoreline environments. *J. Hazard. Mater.* 421, 126711.
- Feng, Q., Chen, Z., Greer, C.W., An, C., Wang, Z., 2022. Transport of microplastics in shore substrates over tidal cycles: roles of polymer characteristics and environmental factors. *Environ. Sci. Technol.* 56 (12), 8187–8196.
- Ferguson, G., Gleeson, T., 2012. Vulnerability of coastal aquifers to groundwater use and climate change. *Nat Clim Chang.* 2 (5), 342-345.
- Finnegan, A.M.D., Susserott, R., Gabbott, S.E., Gouramanis, C., 2022. Man-made natural and regenerated cellulosic fibres greatly outnumber microplastic fibres in the atmosphere. *Environ. Pollut.* 310, 119808.
- Flury, M., Aramrak, S., 2017. Role of air-water interfaces in colloid transport in porous media: A review. *Water Resour. Res.* 53 (7), 5247-5275.
- Flury, M., Qiu, H., 2008. Modeling colloid-facilitated contaminant transport in the vadose zone. *Vadose Zone J.* 7 (2), 682-697.
- Franzluebbers, A.J., 2002. Soil organic matter stratification ratio as an indicator of soil quality. *Soil Tillage Res.* 66 (2), 95-106.
- Fred-Ahmadu, O.H., Ayejuyo, O.O., Tenebe, I.T., Benson, N.U., 2022. Occurrence and distribution of micro(meso)plastic-sorbed heavy metals and metalloids in sediments, Gulf of Guinea coast (SE Atlantic). *Sci. Total Environ.* 813, 152650.
- French, D.R., M.; Jayko, K.; Feng, S.; Rines, H.; Pavignano, S.; Isaji, T.; Puckett, S.; Keller, A.; French, F. W.; Gifford, D.; McCue, J.; Brown, G.; MacDonald, E.; Quirk, J.; Natzke, S.; Bishop, R.; Welsh, M.; Phillips, M.; Ingram, B.S., 1996. The CERCLA type a natural resource damage assessment model for coastal and marine environments (NRDAM/CME), technical documentation. Vol. I - Model Description, Final Report, Contract No. 14-0001-91-C-11, Office of Environmental Policy and Compliance, U.S. Dept. of the Interior, Washington, DC.
- Gao, B., Saiers, J.E., Ryan, J.N., 2004. Deposition and mobilization of clay colloids in unsaturated porous media. *Water Resour. Res.* 40 (8).

- Gao, J., Pan, S., Li, P., Wang, L., Hou, R., Wu, W.M., Luo, J., Hou, D., 2021. Vertical migration of microplastics in porous media: Multiple controlling factors under wet-dry cycling. *J. Hazard. Mater.* 419, 126413.
- Geng, X., Boufadel, M.C., 2015. Numerical study of solute transport in shallow beach aquifers subjected to waves and tides. *Journal of Geophysical Research: Oceans.* 120 (2), 1409-1428.
- Geng, X., Michael, H.A., Boufadel, M.C., Molz, F.J., Gerges, F., Lee, K., 2020. Heterogeneity affects intertidal flow topology in coastal beach aquifers. *Geophys. Res. Lett.* 47 (17).
- GESAMP, 2016. Sources, fate and effects of microplastics in the marine environment: part two of a global assessment.
- Gewert, B., Plassmann, M.M., MacLeod, M., 2015. Pathways for degradation of plastic polymers floating in the marine environment. *Environ. Sci.: Process. Impacts.* 17 (9), 1513-1521.
- Geyer, R., Jambeck, J.R., Law, K.L., 2017. Production, use, and fate of all plastics ever made. *Sci. Adv.* 3 (7), e1700782.
- Gibson, S., Abraham, D., Heath, R., Schoellhamer, D., 2009. Vertical gradational variability of fines deposited in a gravel framework. *Sedimentology.* 56 (3), 661-676.
- Gómez Suárez, C., Noordmans, J., van der Mei, H.C., Busscher, H.J., 1999. Removal of colloidal particles from quartz collector surfaces as stimulated by the passage of liquid-air interfaces. *Langmuir.* 15 (15), 5123-5127.
- Goñi, M.A., Teixeira, M.J., Perkey, D.W., 2003. Sources and distribution of organic matter in a river-dominated estuary (Winyah Bay, SC, USA). *Estuar. Coast. Shelf Sci.* 57 (5-6), 1023-1048.
- Grbic, J., Helm, P., Athey, S., Rochman, C.M., 2020. Microplastics entering northwestern Lake Ontario are diverse and linked to urban sources. *Water Res.* 174, 115623.
- Guler, H.G., Larsen, B.E., Quintana, O., Goral, K.D., Carstensen, S., Christensen, E.D., Kerpen, N.B., Schlurmann, T., Fuhrman, D.R., 2022. Experimental study of non-buoyant microplastic transport beneath breaking irregular waves on a live sediment bed. *Mar. Pollut. Bull.* 181, 113902.
- Guo, X., Wang, J., 2019. The chemical behaviors of microplastics in marine environment: A review. *Mar. Pollut. Bull.* 142, 1-14.

- Guo, Z., Boeing, W.J., Xu, Y., Borgomeo, E., Mason, S.A., Zhu, Y.G., 2021. Global meta-analysis of microplastic contamination in reservoirs with a novel framework. *Water Res.* 207, 117828.
- Gupta, P., Saha, M., Rathore, C., Suneel, V., Ray, D., Naik, A., K, U., M, D., Daga, K., 2021. Spatial and seasonal variation of microplastics and possible sources in the estuarine system from central west coast of India. *Environ. Pollut.* 288, 117665.
- Haberer, C.M., Rolle, M., Cirpka, O.A., Grathwohl, P., 2012. Oxygen transfer in a fluctuating capillary fringe. *Vadose Zone J.* 11 (3), vzt2011.0056.
- Harris, P.T., 2020. The fate of microplastic in marine sedimentary environments: A review and synthesis. *Mar. Pollut. Bull.* 158, 111398.
- Heo, N.W., Hong, S.H., Han, G.M., Hong, S., Lee, J., Song, Y.K., Jang, M., Shim, W.J., 2013. Distribution of small plastic debris in cross-section and high strandline on Heungnam beach, South Korea. *Ocean Science Journal.* 48 (2), 225-233.
- Hickling, C.F. (1971). Estuarine fish farming. *Adv. Mar. Biol.* Russell F.S., Yonge M., Academic Press. 8: 119-213.
- Hou, J., Xu, X., Lan, L., Miao, L., Xu, Y., You, G., Liu, Z., 2020. Transport behavior of micro polyethylene particles in saturated quartz sand: Impacts of input concentration and physicochemical factors. *Environ. Pollut.* 263, 114499.
- Hu, B., Li, Y., Jiang, L., Chen, X., Wang, L., An, S., Zhang, F., 2020. Influence of microplastics occurrence on the adsorption of 17beta-estradiol in soil. *J. Hazard. Mater.* 400, 123325.
- Huettel, M., Webster, I., 2001. Porewater flow in permeable sediments. The benthic boundary layer: Transport processes and biogeochemistry. 144, 177.
- Hunt, R.J., Strand, M., Walker, J.F., 2006. Measuring groundwater–surface water interaction and its effect on wetland stream benthic productivity, Trout Lake watershed, northern Wisconsin, USA. *J. Hydrol.* 320 (3), 370-384.
- Ivar do Sul, J.A., Costa, M.F., Silva-Cavalcanti, J.S., Araujo, M.C., 2014. Plastic debris retention and exportation by a mangrove forest patch. *Mar. Pollut. Bull.* 78 (1-2), 252-257.
- James, S.C., Chrysikopoulos, C.V., 2004. Dense colloid transport in a bifurcating fracture. *J. Colloid Interface Sci.* 270 (1), 250-254.

- Jaubet, M.L., Hines, E., Elias, R., Garaffo, G.V., 2021. Factors driving the abundance and distribution of microplastics on sandy beaches in a Southwest Atlantic seaside resort. *Mar. Environ. Res.* 171, 105472.
- Jayasiri, H.B., Purushothaman, C.S., Vennila, A., 2013. Plastic litter accumulation on high-water strandline of urban beaches in Mumbai, India. *Environ. Monit. Assess.* 185 (9), 7709-7719.
- Jonas, P.J., Millward, G.E., 2010. Metals and nutrients in the Severn Estuary and Bristol Channel: contemporary inputs and distributions. *Mar. Pollut. Bull.* 61 (1-3), 52-67.
- Keller, A.A., Sirivithayapakorn, S., 2004. Transport of colloids in unsaturated porous media: Explaining large-scale behavior based on pore-scale mechanisms. *Water Resour. Res.* 40 (12).
- Keller, A.S., Jimenez-Martinez, J., Mitrano, D.M., 2020. Transport of nano- and microplastic through unsaturated porous media from sewage sludge application. *Environ. Sci. Technol.* 54 (2), 911-920.
- Kerpen, N.B., Schlurmann, T., Schendel, A., Gundlach, J., Marquard, D., Hüpgen, M., 2020. Wave-Induced Distribution of Microplastic in the Surf Zone. *Front. Mar. Sci.* 7.
- Khadanga, M.K., Mishra, R.K., Sahu, B.K., 2022. Assessment of pollution and ecological risk index of heavy metals in the surface sediment of estuary and the coastal environment of Bay of Bengal. *J. Environ. Inform.* 39 (1), 35-48.
- Knappenberger, T., Flury, M., Mattson, E.D., Harsh, J.B., 2014. Does water content or flow rate control colloid transport in unsaturated porous media? *Environ. Sci. Technol.* 48 (7), 3791-3799.
- Koh, S.K., Park, S.C., Kim, S.R., Choi, W.K., Jung, H.J., Pae, K.D., 1997. Surface modification of polytetrafluoroethylene by Ar<sup>+</sup> irradiation for improved adhesion to other materials. *J. Appl. Polym. Sci.* 64 (10), 1913-1921.
- Kosuth, M., Mason, S.A., Wattenberg, E.V., 2018. Anthropogenic contamination of tap water, beer, and sea salt. *PLoS One.* 13 (4), e0194970.
- Krumbein, W.C., 1941. Measurement and geological significance of shape and roundness of sedimentary particles. *Journal of Sedimentary Research.* 11 (2), 64-72.
- Kurt, Z., Mack, E.E., Spain, J.C., 2016. Natural attenuation of nonvolatile contaminants in the capillary fringe. *Environ. Sci. Technol.* 50 (18), 10172-10178.

- Lau, W.W.Y., Shiran, Y., Bailey, R.M., Cook, E., Stuchtey, M.R., Koskella, J., Velis, C.A., Godfrey, L., Boucher, J., Murphy, M.B., Thompson, R.C., Jankowska, E., Castillo, A.C., Pilditch, T.D., Dixon, B., Koerselman, L., Kosior, E., Favoino, E., Gutberlet, J., Baulch, S., Atreya, M.E., Fischer, D., He, K.K., Petit, M.M., Sumaila, U.R., Neil, E., Bernhofen, M.V., Lawrence, K., Palardy, J.E., 2020. Evaluating scenarios toward zero plastic pollution. *Science*. 369 (6510), 1455-1461.
- Leads, R.R., Weinstein, J.E., 2019. Occurrence of tire wear particles and other microplastics within the tributaries of the Charleston Harbor Estuary, South Carolina, USA. *Mar. Pollut. Bull.* 145, 569-582.
- Lefebvre, C., Rojas, I.J., Lasserre, J., Villette, S., Lecomte, S., Cachot, J., Morin, B., 2021. Stranded in the high tide line: Spatial and temporal variability of beached microplastics in a semi-enclosed embayment (Arcachon, France). *Sci. Total Environ.* 797, 149144.
- Lepš, J., Šmilauer, P., 2003. *Multivariate analysis of ecological data using CANOCO*, Cambridge university press.
- Li, B., Li, B., Jia, Q., Cai, Y., Xie, Y., Yuan, X., Yang, Z., 2023. Dynamic characteristics of microplastics under tidal influence and potential indirect monitoring methods. *Sci. Total Environ.* 869, 161869.
- Li, J., Huang, W., Xu, Y., Jin, A., Zhang, D., Zhang, C., 2020. Microplastics in sediment cores as indicators of temporal trends in microplastic pollution in Andong salt marsh, Hangzhou Bay, China. *Reg. Stud. Mar. Sci.* 35, 101149.
- Li, M., He, L., Zhang, M., Liu, X., Tong, M., Kim, H., 2019. Cotransport and deposition of iron oxides with different-sized plastic particles in saturated quartz sand. *Environ. Sci. Technol.* 53 (7), 3547-3557.
- Li, M., He, L., Zhang, X., Rong, H., Tong, M., 2020. Different surface charged plastic particles have different cotransport behaviors with kaolinite particles in porous media. *Environ. Pollut.* 267, 115534.
- Li, M., Zhang, M., Rong, H., Zhang, X., He, L., Han, P., Tong, M., 2021. Transport and deposition of plastic particles in porous media during seawater intrusion and groundwater-seawater displacement processes. *Sci. Total Environ.* 781, 146752.

- Li, S., Wang, Y., Liu, L., Lai, H., Zeng, X., Chen, J., Liu, C., Luo, Q., 2021. Temporal and spatial distribution of microplastics in a coastal region of the Pearl River Estuary, China. *Water*. 13 (12), 1618.
- Li, Y., Liu, S., Liu, M., Huang, W., Chen, K., Ding, Y., Wu, F., Ke, H., Lou, L., Lin, Y., Zhang, M., Liu, F., Wang, C., Cai, M., 2021. Mid-Level riverine outflow matters: A case of microplastic transport in the Jiulong River, China. *Front. Mar. Sci.* 8.
- Li, Y., Wang, X., Fu, W., Xia, X., Liu, C., Min, J., Zhang, W., Crittenden, J.C., 2019. Interactions between nano/micro plastics and suspended sediment in water: Implications on aggregation and settling. *Water Res.* 161, 486-495.
- Lima, A.R., Barletta, M., Costa, M.F., Ramos, J.A., Dantas, D.V., Melo, P.A., Justino, A.K., Ferreira, G.V., 2016. Changes in the composition of ichthyoplankton assemblage and plastic debris in mangrove creeks relative to moon phases. *J. Fish Biol.* 89 (1), 619-640.
- Lima, A.R.A., Barletta, M., Costa, M.F., 2015. Seasonal distribution and interactions between plankton and microplastics in a tropical estuary. *Estuar. Coast. Shelf Sci.* 165, 213-225.
- Lima, A.R.A., Ferreira, G.V.B., Barrows, A.P.W., Christiansen, K.S., Treinish, G., Toshack, M.C., 2021. Global patterns for the spatial distribution of floating microfibers: Arctic Ocean as a potential accumulation zone. *J. Hazard. Mater.* 403, 123796.
- Lin, J., Yan, D., Fu, J., Chen, Y., Ou, H., 2020. Ultraviolet-C and vacuum ultraviolet inducing surface degradation of microplastics. *Water Res.* 186, 116360.
- Lithner, D., Larsson, A., Dave, G., 2011. Environmental and health hazard ranking and assessment of plastic polymers based on chemical composition. *Sci. Total Environ.* 409 (18), 3309-3324.
- Liu, P., Qian, L., Wang, H., Zhan, X., Lu, K., Gu, C., Gao, S., 2019. New insights into the aging behavior of microplastics accelerated by advanced oxidation processes. *Environ. Sci. Technol.* 53 (7), 3579-3588.
- Liu, X., Liu, H., Chen, L., Wang, X., 2021. Ecological interception effect of mangroves on microplastics. *J. Hazard. Mater.* 423, 127231.
- Liu, Y., Huang, Q., Hu, W., Qin, J., Zheng, Y., Wang, J., Wang, Q., Xu, Y., Guo, G., Hu, S., Xu, L., 2021. Effects of plastic mulch film residues on soil-microbe-plant systems under different soil pH conditions. *Chemosphere.* 267, 128901.

- Lobelle, D., Cunliffe, M., 2011. Early microbial biofilm formation on marine plastic debris. *Mar. Pollut. Bull.* 62 (1), 197-200.
- Long, M., Paul-Pont, I., Hegaret, H., Moriceau, B., Lambert, C., Huvet, A., Soudant, P., 2017. Interactions between polystyrene microplastics and marine phytoplankton lead to species-specific hetero-aggregation. *Environ. Pollut.* 228, 454-463.
- Lourenco, P.M., Serra-Goncalves, C., Ferreira, J.L., Catry, T., Granadeiro, J.P., 2017. Plastic and other microfibers in sediments, macroinvertebrates and shorebirds from three intertidal wetlands of southern Europe and west Africa. *Environ. Pollut.* 231 (Pt 1), 123-133.
- Luisetti, T., Turner, R.K., Jickells, T., Andrews, J., Elliott, M., Schaafsma, M., Beaumont, N., Malcolm, S., Burdon, D., Adams, C., Watts, W., 2014. Coastal zone ecosystem services: from science to values and decision making; a case study. *Sci. Total Environ.* 493, 682-693.
- Mai, L., Sun, X.F., Xia, L.L., Bao, L.J., Liu, L.Y., Zeng, E.Y., 2020. Global riverine plastic outflows. *Environ. Sci. Technol.* 54 (16), 10049-10056.
- Majdalani, S., Michel, E., Di-Pietro, L., Angulo-Jaramillo, R., 2008. Effects of wetting and drying cycles on in situ soil particle mobilization. *Eur. J. Soil Sci.* 59 (2), 147-155.
- Mallow, O., Spacek, S., Schwarzböck, T., Fellner, J., Rechberger, H., 2020. A new thermoanalytical method for the quantification of microplastics in industrial wastewater. *Environ. Pollut.* 259, 113862.
- Manickavasagam, S., Kumar, S., Kumar, K., Rathi Bhuvaneshwari, G., Paul, T., Shukla, S.P., 2020. Quantitative assessment of influx and efflux of marine debris in a water channel of South Juhu creek, Mumbai, India. *Reg. Stud. Mar. Sci.* 34, 101095.
- Martin, C., Young, C.A., Valluzzi, L., Duarte, C.M., 2022. Ocean sediments as the global sink for marine micro- and mesoplastics. *Limnology and Oceanography Letters.* 7 (3), 235-243.
- Martinetto, P., Montemayor, D.I., Alberti, J., Costa, C.S.B., Iribarne, O., 2016. Crab bioturbation and herbivory may account for variability in carbon sequestration and stocks in south west atlantic salt marshes. *Front. Mar. Sci.* 3.
- Mato, Y., Isobe, T., Takada, H., Kanehiro, H., Ohtake, C., Kaminuma, T., 2001. Plastic resin pellets as a transport medium for toxic chemicals in the marine environment. *Environ. Sci. Technol.* 35 (2), 318-324.

- McDowell-Boyer, L.M., Hunt, J.R., Sitar, N., 1986. Particle transport through porous media. *Water Resour. Res.* 22 (13), 1901-1921.
- Meijer, L.J.J., van Emmerik, T., van der Ent, R., Schmidt, C., Lebreton, L., 2021. More than 1000 rivers account for 80% of global riverine plastic emissions into the ocean. *Sci. Adv.* 7 (18), eaaz5803.
- Michels, J., Stippkugel, A., Lenz, M., Wirtz, K., Engel, A., 2018. Rapid aggregation of biofilm-covered microplastics with marine biogenic particles. *Proc Biol Sci.* 285 (1885).
- Mintenig, S.M., Loder, M.G.J., Primpke, S., Gerdts, G., 2019. Low numbers of microplastics detected in drinking water from ground water sources. *Sci. Total Environ.* 648, 631-635.
- Mohanty, S.K., Cantrell, K.B., Nelson, K.L., Boehm, A.B., 2014. Efficacy of biochar to remove *Escherichia coli* from stormwater under steady and intermittent flow. *Water Res.* 61, 288-296.
- Mongabay, 2021. With fire contained, Sri Lanka faces plastic pellet problem from stricken ship. Available at: <https://news.mongabay.com/2021/05/with-fire-contained-sri-lanka-faces-plastic-pellet-problem-from-stricken-ship/> (Accessed 4 March 2022).
- Moreira, F.T., Prantoni, A.L., Martini, B., de Abreu, M.A., Stoiev, S.B., Turra, A., 2016. Small-scale temporal and spatial variability in the abundance of plastic pellets on sandy beaches: Methodological considerations for estimating the input of microplastics. *Mar. Pollut. Bull.* 102 (1), 114-121.
- Murphy, F., Ewins, C., Carbonnier, F., Quinn, B., 2016. Wastewater treatment works (WwTW) as a source of microplastics in the aquatic environment. *Environ. Sci. Technol.* 50 (11), 5800-5808.
- Murphy, J., 2001. *Additives for plastics handbook*, Elsevier.
- Naji, A., Esmaili, Z., Mason, S.A., Dick Vethaak, A., 2017. The occurrence of microplastic contamination in littoral sediments of the Persian Gulf, Iran. *Environ Sci Pollut Res Int.* 24 (25), 20459-20468.
- Napper, I.E., Parker-Jurd, F.N.F., Wright, S.L., Thompson, R.C., 2023. Examining the release of synthetic microfibres to the environment via two major pathways: Atmospheric deposition and treated wastewater effluent. *Sci. Total Environ.* 857 (Pt 1), 159317.
- Neeper, D.A., 2001. A model of oscillatory transport in granular soils, with application to barometric pumping and earth tides. *J. Contam. Hydrol.* 48 (3), 237-252.

- Neumann, D., Callies, U., Matthies, M., 2014. Marine litter ensemble transport simulations in the southern North Sea. *Mar. Pollut. Bull.* 86 (1-2), 219-228.
- Nizzetto, L., Langaas, S., Futter, M., 2016. Pollution: Do microplastics spill on to farm soils? *Nature.* 537 (7621), 488-488.
- Noda, I., 1990. Two-dimensional infrared (2D IR) spectroscopy: theory and applications. *Appl. Spectrosc.* 44 (4), 550-561.
- Noda, I., 2017. Vibrational two-dimensional correlation spectroscopy (2DCOS) study of proteins. *Spectrochim Acta A Mol Biomol Spectrosc.* 187, 119-129.
- Nor, N.H., Obbard, J.P., 2014. Microplastics in Singapore's coastal mangrove ecosystems. *Mar. Pollut. Bull.* 79 (1-2), 278-283.
- O'Connor, I.A., Golsteijn, L., Hendriks, A.J., 2016. Review of the partitioning of chemicals into different plastics: Consequences for the risk assessment of marine plastic debris. *Mar. Pollut. Bull.* 113 (1-2), 17-24.
- Oelschlägel, K., Pfeiffer, J., Potthoff, A. (2018). Imitating the weathering of microplastics in the marine environment. *Proceedings of the International Conference on Microplastic Pollution in the Mediterranean Sea*, Cham, Springer International Publishing.
- Oo, P.Z., Boontanon, S.K., Boontanon, N., Tanaka, S., Fujii, S., 2021. Horizontal variation of microplastics with tidal fluctuation in the Chao Phraya River Estuary, Thailand. *Mar. Pollut. Bull.* 173, 112933.
- Ouyang, X., Duarte, C.M., Cheung, S.G., Tam, N.F., Cannicci, S., Martin, C., Lo, H.S., Lee, S.Y., 2022. Fate and effects of macro- and microplastics in coastal wetlands. *Environ. Sci. Technol.* 56 (4), 2386-2397.
- Pabortsava, K., Lampitt, R.S., 2020. High concentrations of plastic hidden beneath the surface of the Atlantic Ocean. *Nat. Commun.* 11 (1), 4073.
- Panchenko, E., Lebedeva, S., Terskii, P., Leummens, M., 2019. Hydrodynamics of the Onega River tidal estuary as a basis for ecosystem monitoring. *IOP Conference Series: Earth and Environmental Science.* 263, 012014.
- Panno, S.V., Kelly, W.R., Scott, J., Zheng, W., McNeish, R.E., Holm, N., Hoellein, T.J., Baranski, E.L., 2019. Microplastic contamination in Karst groundwater systems. *Ground Water.* 57 (2), 189-196.

- Payton, T.G., Beckingham, B.A., Dustan, P., 2020. Microplastic exposure to zooplankton at tidal fronts in Charleston Harbor, SC USA. *Estuar. Coast. Shelf Sci.* 232, 106510.
- Pazos, R.S., Bauer, D.E., Gomez, N., 2018. Microplastics integrating the coastal planktonic community in the inner zone of the Rio de la Plata estuary (South America). *Environ. Pollut.* 243, 134-142.
- Peck, R.B., Hanson, W.E., Thornburn, T.H., 1994. *Foundation Engineering*, Wiley, New York, NY, USA, 2nd edition. . pp. 48.
- Peng, G., Xu, P., Zhu, B., Bai, M., Li, D., 2018. Microplastics in freshwater river sediments in Shanghai, China: A case study of risk assessment in mega-cities. *Environ. Pollut.* 234, 448-456.
- Phuong, N.N., Zalouk-Vergnoux, A., Poirier, L., Kamari, A., Chatel, A., Mouneyrac, C., Lagarde, F., 2016. Is there any consistency between the microplastics found in the field and those used in laboratory experiments? *Environ. Pollut.* 211, 111-123.
- Piehl, S., Mitterwallner, V., Atwood, E.C., Bochow, M., Laforsch, C., 2019. Abundance and distribution of large microplastics (1-5mm) within beach sediments at the Po River Delta, northeast Italy. *Mar. Pollut. Bull.* 149, 110515.
- Piehl, S., Mitterwallner, V., Atwood, E.C., Bochow, M., Laforsch, C., 2019. Abundance and distribution of large microplastics (1–5 mm) within beach sediments at the Po River Delta, northeast Italy. *Mar. Pollut. Bull.* 149, 110515.
- Pihl, L., Cattrijsse, A., Codling, I., Mathieson, S., McLusky, D., Roberts, C., 2002. Habitat use by fishes in estuaries and other brackish areas. *Fishes in estuaries.* 10-53.
- Pivokonsky, M., Cermakova, L., Novotna, K., Peer, P., Cajthaml, T., Janda, V., 2018. Occurrence of microplastics in raw and treated drinking water. *Sci. Total Environ.* 643, 1644-1651.
- PlasticsEurope, 2022. *Plastics - the Facts 2022*. Available at: <https://plasticseurope.org/knowledge-hub/plastics-the-facts-2022/>
- Polanco, H., Hayes, S., Roble, C., Krupitsky, M., Branco, B., 2020. The presence and significance of microplastics in surface water in the Lower Hudson River Estuary 2016-2019: A research note. *Mar. Pollut. Bull.* 161, 111702.

- Prarat, P., Hongsawat, P., 2022. Microplastic pollution in surface seawater and beach sand from the shore of Rayong province, Thailand: Distribution, characterization, and ecological risk assessment. *Mar. Pollut. Bull.* 174, 113200.
- Preuss, M., Butt, H.-J., 1998. Direct measurement of particle–bubble interactions in aqueous electrolyte: dependence on surfactant. *Langmuir*. 14 (12), 3164-3174.
- Pye, K., Blott, S.J., 2014. The geomorphology of UK estuaries: the role of geological controls, antecedent conditions and human activities. *Estuar. Coast. Shelf Sci.* 150, 196-214.
- Quesadas-Rojas, M., Enriquez, C., Valle-Levinson, A., 2021. Natural and anthropogenic effects on microplastic distribution in a hypersaline lagoon. *Sci. Total Environ.* 776, 145803.
- Quirk, J.P., Schofield, R.K., 1955. The effect of electrolyte concentration on soil permeability. *J. Soil Sci.* 6 (2), 163-178.
- Razeghi, N., Hamidian, A.H., Mirzajani, A., Abbasi, S., Wu, C., Zhang, Y., Yang, M., 2021. Sample preparation methods for the analysis of microplastics in freshwater ecosystems: a review. *Environ. Chem. Lett.*
- Reinold, S., Herrera, A., Stile, N., Saliu, F., Hernandez-Gonzalez, C., Martinez, I., Ortega, Z., Marrero, M.D., Lasagni, M., Gomez, M., 2021. An annual study on plastic accumulation in surface water and sediment cores from the coastline of Tenerife (Canary Island, Spain). *Mar. Pollut. Bull.* 173, 113072.
- Ren, Z., Gui, X., Xu, X., Zhao, L., Qiu, H., Cao, X., 2021. Microplastics in the soil-groundwater environment: Aging, migration, and co-transport of contaminants - A critical review. *J. Hazard. Mater.* 419, 126455.
- Ritchie, H., Roser, M., 2018. Plastic pollution. Published online at OurWorldInData.org. Retrieved from: '<https://ourworldindata.org/plastic-pollution>' [Online Resource]
- Roche, K.R., Shogren, A.J., Aubeneau, A., Tank, J.L., Bolster, D., 2019. Modeling benthic versus hyporheic nutrient uptake in unshaded streams with varying substrates. *J. Geophys. Res. Biogeosci.* 124 (2), 367-383.
- Rochman, C.M., Grbic, J., Earn, A., Helm, P.A., Hasenmueller, E.A., Trice, M., Munno, K., De Frond, H., Djuric, N., Santoro, S., Kaura, A., Denton, D., Teh, S., 2022. Local monitoring should inform local solutions: morphological assemblages of microplastics are similar within a pathway, but relative total concentrations vary regionally. *Environ. Sci. Technol.* 56 (13), 9367-9378.

- Rodrigues, M., Martins, R., Rogeiro, J., Fortunato, A.B., Oliveira, A., Cravo, A., Jacob, J., Rosa, A., Azevedo, A., Freire, P., 2021. A web-based observatory for biogeochemical assessment in coastal regions. *J. Environ. Inform.* 38 (1), 1-15.
- Rodrigues, S.M., Almeida, C.M.R., Silva, D., Cunha, J., Antunes, C., Freitas, V., Ramos, S., 2019. Microplastic contamination in an urban estuary: Abundance and distribution of microplastics and fish larvae in the Douro estuary. *Sci. Total Environ.* 659, 1071-1081.
- Roscher, L., Fehres, A., Reisel, L., Halbach, M., Scholz-Bottcher, B., Gerriets, M., Badewien, T.H., Shiravani, G., Wurpts, A., Primpke, S., Gerdts, G., 2021. Microplastic pollution in the Weser estuary and the German North Sea. *Environ. Pollut.* 288, 117681.
- Rowley, K.H., Cucknell, A.C., Smith, B.D., Clark, P.F., Morrirt, D., 2020. London's river of plastic: High levels of microplastics in the Thames water column. *Sci. Total Environ.* 740, 140018.
- Ruiz, I., Basurko, O.C., Rubio, A., Delpy, M., Granado, I., Declerck, A., Mader, J., Cózar, A., 2020. Litter Windrows in the South-East Coast of the Bay of Biscay: An Ocean Process Enabling Effective Active Fishing for Litter. *Front. Mar. Sci.* 7.
- Russell, T.L., Yamahara, K.M., Boehm, A.B., 2012. Mobilization and transport of naturally occurring enterococci in beach sands subject to transient infiltration of seawater. *Environ. Sci. Technol.* 46 (11), 5988-5996.
- Ryan, J.N., Elimelech, M., 1996. Colloid mobilization and transport in groundwater. *Colloids Surf. Physicochem. Eng. Aspects.* 107, 1-56.
- Ryan, P.G., 2015. Does size and buoyancy affect the long-distance transport of floating debris? *Environmental Research Letters.* 10 (8), 084019.
- Ryan, P.G., Suaria, G., Perold, V., Pierucci, A., Bornman, T.G., Aliani, S., 2020. Sampling microfibres at the sea surface: The effects of mesh size, sample volume and water depth. *Environ. Pollut.* 258, 113413.
- Sadri, S.S., Thompson, R.C., 2014. On the quantity and composition of floating plastic debris entering and leaving the Tamar Estuary, Southwest England. *Mar. Pollut. Bull.* 81 (1), 55-60.
- Saiers, J.E., Lenhart, J.J., 2003. Colloid mobilization and transport within unsaturated porous media under transient-flow conditions. *Water Resour. Res.* 39 (1).

- Sanford, L.P., Chen, S.-N., 2009. Axial wind effects on stratification and longitudinal salt transport in an idealized, partially mixed estuary. *J. Phys. Oceanogr.* 39 (8), 1905-1920.
- Santos, I.R., Eyre, B.D., Huettel, M., 2012. The driving forces of porewater and groundwater flow in permeable coastal sediments: A review. *Estuar. Coast. Shelf Sci.* 98, 1-15.
- Sathish, N., Jeyasanta, K.I., Patterson, J., 2019. Abundance, characteristics and surface degradation features of microplastics in beach sediments of five coastal areas in Tamil Nadu, India. *Mar. Pollut. Bull.* 142, 112-118.
- Satoh, Y., Yoshimura, K., Pokhrel, Y., Kim, H., Shiogama, H., Yokohata, T., Hanasaki, N., Wada, Y., Burek, P., Byers, E., Schmied, H.M., Gerten, D., Ostberg, S., Gosling, S.N., Boulange, J.E.S., Oki, T., 2022. The timing of unprecedented hydrological drought under climate change. *Nat Commun.* 13 (1), 3287.
- Schruff, T., 2018. Taking a closer Look at the causes and impacts of fine sediment infiltration into gravel beds: development and application of an extended theory of fine sediment infiltration based on grain scale numerical simulations. dissertation, RWTH Aachen University: Aachen,.
- Schuster-Wallace, C.J., Dickson-Anderson, S.E., Papalexiou, S.M., El Ganzouri, A., 2022. Design and Application of the Tank Simulation Model (TSM): Assessing the Ability of Rainwater Harvesting to Meet Domestic Water Demand. *J. Environ. Inform.* 40 (1), 16-29.
- Seyfried, M.S., Rao, P.S.C., 1987. Solute transport in undisturbed columns of an aggregated tropical soil: preferential flow effects. *Soil Sci. Soc. Am. J.* 51 (6), 1434-1444.
- Shah, A.A., Hasan, F., Hameed, A., Ahmed, S., 2008. Biological degradation of plastics: a comprehensive review. *Biotechnol. Adv.* 26 (3), 246-265.
- Shang, J., Flury, M., Chen, G., Zhuang, J., 2008. Impact of flow rate, water content, and capillary forces on in situ colloid mobilization during infiltration in unsaturated sediments. *Water Resour. Res.* 44 (6).
- Sharma, M.M., Chamoun, H., Sarma, D.S.H.S.R., Schechter, R.S., 1992. Factors controlling the hydrodynamic detachment of particles from surfaces. *J. Colloid Interface Sci.* 149 (1), 121-134.
- Sharma, P., Flury, M., Zhou, J., 2008. Detachment of colloids from a solid surface by a moving air-water interface. *J. Colloid Interface Sci.* 326 (1), 143-150.

- Shaw, D.G., Day, R.H., 1994. Colour- and form-dependent loss of plastic micro-debris from the North Pacific Ocean. *Mar. Pollut. Bull.* 28 (1), 39-43.
- Shen, C., Li, B., Wang, C., Huang, Y., Jin, Y., 2011. Surface roughness effect on deposition of nano- and micro-sized colloids in saturated columns at different solution ionic strengths. *Vadose Zone J.* 10 (3), 1071-1081.
- Shi, Y., Liu, P., Wu, X., Shi, H., Huang, H., Wang, H., Gao, S., 2021. Insight into chain scission and release profiles from photodegradation of polycarbonate microplastics. *Water Res.*, 116980.
- Silliman, S.E., Berkowitz, B., Simunek, J., van Genuchten, M.T., 2002. Fluid flow and solute migration within the capillary fringe. *Ground Water.* 40 (1), 76-84.
- Silva-Cavalcanti, J.S., de Araujo, M.C., da Costa, M.F., 2009. Plastic litter on an urban beach---a case study in Brazil. *Waste Manag Res.* 27 (1), 93-97.
- Šimunek, J., van Genuchten, M.T., Šejna, M., 2008. Development and applications of the HYDRUS and STANMOD software packages and related codes *Vadose Zone J.* 7 (2), 587-600.
- Singaraja, C., Chidambaram, S., Jacob, N., 2018. A study on the influence of tides on the water table conditions of the shallow coastal aquifers. *Applied Water Science.* 8 (11), 1-13.
- Sneed, E.D., Folk, R.L., 1958. Pebbles in the Lower Colorado River, Texas a Study in Particle Morphogenesis. *The Journal of Geology.* 66 (2), 114-150.
- Song, Y.K., Hong, S.H., Jang, M., Han, G.M., Jung, S.W., Shim, W.J., 2017. Combined effects of UV exposure duration and mechanical abrasion on microplastic fragmentation by polymer type. *Environ. Sci. Technol.* 51 (8), 4368-4376.
- Sousa, M.C., deCastro, M., Gago, J., Ribeiro, A.S., Des, M., Gomez-Gesteira, J.L., Dias, J.M., Gomez-Gesteira, M., 2021. Modelling the distribution of microplastics released by wastewater treatment plants in Ria de Vigo (NW Iberian Peninsula). *Mar. Pollut. Bull.* 166, 112227.
- Stanton, T., Johnson, M., Nathanail, P., MacNaughtan, W., Gomes, R.L., 2019. Freshwater and airborne textile fibre populations are dominated by 'natural', not microplastic, fibres. *Sci. Total Environ.* 666, 377-389.

- Stead, J.L., Cundy, A.B., Hudson, M.D., Thompson, C.E.L., Williams, I.D., Russell, A.E., Pabortsava, K., 2020. Identification of tidal trapping of microplastics in a temperate salt marsh system using sea surface microlayer sampling. *Sci. Rep.* 10 (1), 14147.
- Stolte, A., Forster, S., Gerdts, G., Schubert, H., 2015. Microplastic concentrations in beach sediments along the German Baltic coast. *Mar. Pollut. Bull.* 99 (1-2), 216-229.
- Sucharitakul, P., Pitt, K.A., Welsh, D.T., 2021. Assessment of microplastics in discharged treated wastewater and the utility of *Chrysaora pentastoma medusae* as bioindicators of microplastics. *Sci. Total Environ.* 790, 148076.
- Suksangchan, R., Keawsang, R., Worachananant, S., Thamrongnawasawat, T., Phaksopa, J., 2020. Suspended microplastics during a tidal cycle in sea-surface waters around Chao Phraya River mouth, Thailand. *Sci. Asia.* 46 (6), 724.
- Sun, Y., Yuan, J., Zhou, T., Zhao, Y., Yu, F., Ma, J., 2020. Laboratory simulation of microplastics weathering and its adsorption behaviors in an aqueous environment: A systematic review. *Environ. Pollut.* 265 (Pt B), 114864.
- Telesh, I.V., 2004. Plankton of the baltic estuarine ecosystems with emphasis on Neva Estuary: a review of present knowledge and research perspectives. *Mar. Pollut. Bull.* 49 (3), 206-219.
- Tien, C.J., Wang, Z.X., Chen, C.S., 2020. Microplastics in water, sediment and fish from the Fengshan River system: Relationship to aquatic factors and accumulation of polycyclic aromatic hydrocarbons by fish. *Environ. Pollut.* 265, 114962.
- Torkzaban, S., Bradford, S.A., van Genuchten, M.T., Walker, S.L., 2008. Colloid transport in unsaturated porous media: the role of water content and ionic strength on particle straining. *J. Contam. Hydrol.* 96 (1-4), 113-127.
- Torkzaban, S., Bradford, S.A., Vanderzalm, J.L., Patterson, B.M., Harris, B., Prommer, H., 2015. Colloid release and clogging in porous media: Effects of solution ionic strength and flow velocity. *J. Contam. Hydrol.* 181, 161-171.
- Trabucco, A., Zomer, R., 2019. Global aridity index and potential evapotranspiration (ET0) climate database v2.
- Tramoy, R., Gasperi, J., Colasse, L., Tassin, B., 2020. Transfer dynamic of macroplastics in estuaries - New insights from the Seine estuary: Part 1. Long term dynamic based on date-prints on stranded debris. *Mar. Pollut. Bull.* 152, 110894.

- Turra, A., Manzano, A.B., Dias, R.J., Mahiques, M.M., Barbosa, L., Balthazar-Silva, D., Moreira, F.T., 2014. Three-dimensional distribution of plastic pellets in sandy beaches: shifting paradigms. *Sci. Rep.* 4, 4435.
- Umbers, K.D.L., 2012. On the perception, production and function of blue colouration in animals. *J. Zool.* 289 (4), 229-242.
- United Nations Development Programme, 2019. Human development index (HDI). <http://hdr.undp.org/en/data> (accessed on July 1, 2022).
- Van Genuchten, M.T., Šimůnek, J., Feddes, R., 2004. Integrated modeling of vadose zone flow and transport processes. *Unsaturated-zone modelling: Progress, challenges and applications*. Frontis, Wageningen, the Netherlands. 37-69.
- Vandermeulen, J.H., Harper, J., Humphrey, B., 1988. Environmental factors influencing oil penetration and persistence in fine sediment tidal flats. *Oil Chem. Pollut.* 4, 155-177.
- Vella, D., 2015. Floating Versus Sinking. *Annual Review of Fluid Mechanics.* 47 (1), 115-135.
- Vermeiren, P., Munoz, C.C., Ikejima, K., 2016. Sources and sinks of plastic debris in estuaries: A conceptual model integrating biological, physical and chemical distribution mechanisms. *Mar. Pollut. Bull.* 113 (1-2), 7-16.
- Viet Dung, L., Huu Duc, T., Thi Khanh Linh, L., Thi Dieu Ly, T., Anh Duong, H., Thi My Hao, N., 2021. Depth profiles of microplastics in sediment cores from two mangrove forests in northern Vietnam. *J. Mar. Sci. Eng.* 9 (12), 1381.
- Waldschlager, K., Born, M., Cowger, W., Gray, A., Schuttrumpf, H., 2020. Settling and rising velocities of environmentally weathered micro- and macroplastic particles. *Environ. Res.* 191, 110192.
- Waldschlager, K., Schuttrumpf, H., 2019. Effects of particle properties on the settling and rise velocities of microplastics in freshwater under laboratory conditions. *Environ. Sci. Technol.* 53 (4), 1958-1966.
- Waldschlager, K., Schuttrumpf, H., 2020. Infiltration behavior of microplastic particles with different densities, sizes, and shapes—from glass spheres to natural sediments. *Environ. Sci. Technol.* 54 (15), 9366-9373.
- Wan, J., Tokunaga, T.K., 1997. Film straining of colloids in unsaturated porous media: conceptual model and experimental testing. *Environ. Sci. Technol.* 31 (8), 2413-2420.

- Wan, J., Wilson, J.L., 1994. Colloid transport in unsaturated porous media. *Water Resour. Res.* 30 (4), 857-864.
- Wan, Y., Wu, C., Xue, Q., Hui, X., 2019. Effects of plastic contamination on water evaporation and desiccation cracking in soil. *Sci. Total Environ.* 654, 576-582.
- Wang, F., Nian, X., Wang, J., Zhang, W., Peng, G., Ge, C., Dong, C., Qu, J., Li, D., 2018. Multiple dating approaches applied to the recent sediments in the Yangtze River (Changjiang) subaqueous delta. *The Holocene.* 28 (6), 858-866.
- Wang, F., Wong, C.S., Chen, D., Lu, X., Wang, F., Zeng, E.Y., 2018. Interaction of toxic chemicals with microplastics: A critical review. *Water Res.* 139, 208-219.
- Wang, J., Peng, J., Tan, Z., Gao, Y., Zhan, Z., Chen, Q., Cai, L., 2017. Microplastics in the surface sediments from the Beijiang River littoral zone: Composition, abundance, surface textures and interaction with heavy metals. *Chemosphere.* 171, 248-258.
- Wang, J.F., Li, X.H., Christakos, G., Liao, Y.L., Zhang, T., Gu, X., Zheng, X.Y., 2010. Geographical detectors-based health risk assessment and its application in the neural tube defects study of the Heshun Region, China. *International Journal of Geographical Information Science.* 24 (1), 107-127.
- Wang, P. (2012). Principles of sediment transport applicable in tidal environments: 19-34.
- Wang, T., Zhao, S., Zhu, L., McWilliams, J.C., Galgani, L., Amin, R.M., Nakajima, R., Jiang, W., Chen, M., 2022. Accumulation, transformation and transport of microplastics in estuarine fronts. *Nature Reviews Earth & Environment.* 3 (11), 795-805.
- Wang, Y., Ouyang, W., Lin, C., Zhu, W., Critto, A., Tysklind, M., Wang, X., He, M., Wang, B., Wu, H., 2021. Higher fine particle fraction in sediment increased phosphorus flux to estuary in restored Yellow River Basin. *Environ. Sci. Technol.* 55 (10), 6783-6790.
- Wang, Y., Xu, L., Chen, H., Zhang, M., 2022. Retention and transport behavior of microplastic particles in water-saturated porous media. *Sci. Total Environ.* 808, 152154.
- Wang, Z., An, C., Chen, X., Lee, K., Zhang, B., Feng, Q., 2021. Disposable masks release microplastics to the aqueous environment with exacerbation by natural weathering. *J. Hazard. Mater.* 417, 126036.
- Wang, Z., An, C., Lee, K., Chen, X., Zhang, B., Yin, J., Feng, Q., 2022. Physicochemical change and microparticle release from disposable gloves in the aqueous environment impacted by accelerated weathering. *Sci. Total Environ.* 832, 154986.

- Wang, Z.Y., Wang, P.F., Wang, C., Zhang, S.H., Hou, J., Ao, Y.H., 2022. Statistical optimization of microcystis growth and microcystin production in natural phytoplankton community using microcosm bioassays. *J. Environ. Inform.* 40 (1), 1-15.
- Ward, R.D., Teasdale, P.A., Burnside, N.G., Joyce, C.B., Sepp, K., 2014. Recent rates of sedimentation on irregularly flooded Boreal Baltic coastal wetlands: Responses to recent changes in sea level. *Geomorphology.* 217, 61-72.
- Webb, J.E., Theodor, J., 1968. Irrigation of submerged marine sands through wave action. *Nature.* 220 (5168), 682-683.
- Wessel, C.C., Lockridge, G.R., Battiste, D., Cebrian, J., 2016. Abundance and characteristics of microplastics in beach sediments: Insights into microplastic accumulation in northern Gulf of Mexico estuaries. *Mar. Pollut. Bull.* 109 (1), 178-183.
- Willis, K.A., Eriksen, R., Wilcox, C., Hardesty, B.D., 2017. Microplastic distribution at different sediment depths in an urban estuary. *Front. Mar. Sci.* 4, 419.
- Wu, F., Pennings, S.C., Tong, C., Xu, Y., 2020. Variation in microplastics composition at small spatial and temporal scales in a tidal flat of the Yangtze Estuary, China. *Sci. Total Environ.* 699, 134252.
- Wu, L.-h., Zhuang, S.-y., 2010. Experimental Investigation of Effect of Tide on Coastal Groundwater Table. *Journal of Hydrodynamics.* 22 (1), 66-72.
- Wu, Y., Wang, S., Wu, L., Yang, Y., Yu, X., Liu, Q., Liu, X., Li, Y., Wang, X., 2022. Vertical distribution and river-sea transport of microplastics with tidal fluctuation in a subtropical estuary, China. *Sci. Total Environ.* 822, 153603.
- Xia, L., Dutta, D., 2013. Microfluidic flow counterbalanced capillary electrophoresis. *Analyst.* 138 (7), 2126-2133.
- Xin, X., Huang, G., An, C., Feng, R., 2019. Interactive toxicity of triclosan and nano-TiO<sub>2</sub> to green alga *eremosphaera viridis* in lake Erie: A new perspective based on fourier transform infrared spectromicroscopy and synchrotron-based X-ray fluorescence imaging. *Environ. Sci. Technol.* 53 (16), 9884-9894.
- Yang, M., Zhang, B., Xin, X., Lee, K., Chen, B., 2022. Microplastic and oil pollution in oceans: Interactions and environmental impacts. *Sci. Total Environ.* 838 (Pt 2), 156142.

- Yang, M., Zhang, B., Xin, X., Liu, B., Zhu, Z., Dong, G., Zhao, Y., Lee, K., Chen, B., 2021. Microplastic-oil-dispersant agglomerates in the marine environment: Formation mechanism and impact on oil dispersion. *J. Hazard. Mater.*, 127825.
- Yin, M., Cao, H., Zhao, W., Wang, T., Huang, W., Cai, M., 2022. Tide-driven microplastics transport in an elongated semi-closed bay: A case study in Xiangshan Bay, China. *Sci. Total Environ.* 846, 157374.
- Yonkos, L.T., Friedel, E.A., Perez-Reyes, A.C., Ghosal, S., Arthur, C.D., 2014. Microplastics in four estuarine rivers in the Chesapeake Bay, U.S.A. *Environ. Sci. Technol.* 48 (24), 14195-14202.
- Zamani, K., 2020. Multi-phase 1D model for particles and constituents transport in tidal systems (Doctoral research proposal). University of California, Davis.
- Zhang, H., Ye, Y., Yang, X., Liu, R., 2021. How does the periodic groundwater table fluctuation impact on chlorinated vapor intrusion? *Geofluids*. 2021, 1-12.
- Zhang, L., Liu, J., Xie, Y., Zhong, S., Yang, B., Lu, D., Zhong, Q., 2020. Distribution of microplastics in surface water and sediments of Qin river in Beibu Gulf, China. *Sci. Total Environ.* 708, 135176.
- Zhang, L., Zhang, S., Guo, J., Yu, K., Wang, Y., Li, R., 2020. Dynamic distribution of microplastics in mangrove sediments in Beibu Gulf, South China: Implications of tidal current velocity and tidal range. *J. Hazard. Mater.* 399, 122849.
- Zhang, Y., Jiang, H., Bian, K., Wang, H., Wang, C., 2021. A critical review of control and removal strategies for microplastics from aquatic environments. *Journal of Environmental Chemical Engineering*. 9 (4), 105463.
- Zhao, X., Wang, J., Yee Leung, K.M., Wu, F., 2022. Color: an important but overlooked factor for plastic photoaging and microplastic formation. *Environ. Sci. Technol.*
- Zhou, Y.Y., Wang, J.H., Xiao, W.H., Huang, Y.H., Yang, H., Hou, B.D., Chen, Y., Zhang, H.T., 2021. A hierarchical approach for inland lake pollutant load allocation: a case study in Tangxun Lake Basin, Wuhan, China. *J. Environ. Inform.* 37 (1), 16-25.
- Zhu, J., Zhang, Q., Li, Y., Tan, S., Kang, Z., Yu, X., Lan, W., Cai, L., Wang, J., Shi, H., 2019. Microplastic pollution in the Maowei Sea, a typical mariculture bay of China. *Sci. Total Environ.* 658, 62-68.

Zhuang, J., McCarthy, J.F., Tyner, J.S., Perfect, E., Flury, M., 2007. In situ colloid mobilization in Hanford sediments under unsaturated transient flow conditions: effect of irrigation pattern. *Environ. Sci. Technol.* 41 (9), 3199-3204.

## Appendices

Text S1 Articles included in the dataset.

- (1) Naidoo T., Glassom D., Smit A. J. Plastic pollution in five urban estuaries of KwaZulu-Natal, South Africa. *Mar. Pollut. Bull.* 2015, 101 (1), 473-480.
- (2) Zaki M. R. M., Zaid S. H. M., Zainuddin A. H., Aris A. Z. Microplastic pollution in tropical estuary gastropods: Abundance, distribution and potential sources of Klang River estuary, Malaysia. *Mar. Pollut. Bull.* 2021, 162, 111866.
- (3) Gray A. D., Wertz H., Leads R. R., Weinstein J. E. Microplastic in two South Carolina Estuaries: Occurrence, distribution, and composition. *Mar. Pollut. Bull.* 2018, 128, 223-233.
- (4) Bridson J. H., Patel M., Lewis A., Gaw S., Parker K. Microplastic contamination in Auckland (New Zealand) beach sediments. *Mar. Pollut. Bull.* 2020, 151, 110867.
- (5) Defontaine S., Sous D., Tesan J., Monperrus M., Lenoble V., Lancelleur L. Microplastics in a salt-wedge estuary: Vertical structure and tidal dynamics. *Mar. Pollut. Bull.* 2020, 160, 111688.
- (6) Alava J. J., Kazmiruk T. N., Douglas T., Schuerholz G., Heath B., Flemming S. A., Bendell L., Drever M. C. Occurrence and size distribution of microplastics in mudflat sediments of the Cowichan-Koksilah Estuary, Canada: A baseline for plastic particles contamination in an anthropogenic-influenced estuary. *Mar. Pollut. Bull.* 2021, 173 (Pt A), 113033.
- (7) Cheung P. K., Cheung L. T. O., Fok L. Seasonal variation in the abundance of marine plastic debris in the estuary of a subtropical macro-scale drainage basin in South China. *Sci. Total Environ.* 2016, 562, 658-665.
- (8) Xu Q., Xing R., Sun M., Gao Y., An L. Microplastics in sediments from an interconnected river-estuary region. *Sci. Total Environ.* 2020, 729, 139025.
- (9) Taha Z. D., Md Amin R., Anuar S. T., Nasser A. A. A., Sohaimi E. S. Microplastics in seawater and zooplankton: A case study from Terengganu estuary and offshore waters, Malaysia. *Sci. Total Environ.* 2021, 786, 147466.
- (10) Zhao S., Zhu L., Li D. Microplastic in three urban estuaries, China. *Environ. Pollut.* 2015, 206, 597-604.
- (11) Silva J. D. B., Barletta M., Lima A. R. A., Ferreira G. V. B. Use of resources and microplastic contamination throughout the life cycle of grunts (Haemulidae) in a tropical estuary. *Environ. Pollut.* 2018, 242 (Pt A), 1010-1021.

- (12) Lima A. R. A., Barletta M., Costa M. F. Seasonal distribution and interactions between plankton and microplastics in a tropical estuary. *Estuar. Coast. Shelf Sci.* 2015, 165, 213-225.
- (13) Xu L., Han L., Li J., Zhang H., Jones K., Xu E. G. Missing relationship between meso- and microplastics in adjacent soils and sediments. *J. Hazard. Mater.* 2022, 424 (Pt A), 127234.
- (14) Wang F., Nian X., Wang J., Zhang W., Peng G., Ge C., Dong C., Qu J., Li D. Multiple dating approaches applied to the recent sediments in the Yangtze River (Changjiang) subaqueous delta. *The Holocene.* 2018, 28 (6), 858-866.
- (15) Cheng M. L. H., Lippmann T. C., Dijkstra J. A., Bradt G., Cook S., Choi J. G., Brown B. L. A baseline for microplastic particle occurrence and distribution in Great Bay Estuary. *Mar. Pollut. Bull.* 2021, 170, 112653.
- (16) Liu X., Liu H., Chen L., Wang X. Ecological interception effect of mangroves on microplastics. *J. Hazard. Mater.* 2021, 423, 127231.
- (17) Culligan N., Liu K.-b., Ribble K., Ryu J., Dietz M. Sedimentary records of microplastic pollution from coastal Louisiana and their environmental implications. *J. Coast. Conserv.* 2021, 26 (1), 1-14.
- (18) Li C., Zhu L., Wang X., Liu K., Li D. Cross-oceanic distribution and origin of microplastics in the subsurface water of the South China Sea and Eastern Indian Ocean. *Sci. Total Environ.* 2022, 805, 150243.
- (19) Belivermis M., Kilic O., Sezer N., Sikdokur E., Gungor N. D., Altug G. Microplastic inventory in sediment profile: A case study of Golden Horn Estuary, Sea of Marmara. *Mar. Pollut. Bull.* 2021, 173, 113117.
- (20) Oo P. Z., Boontanon S. K., Boontanon N., Tanaka S., Fujii S. Horizontal variation of microplastics with tidal fluctuation in the Chao Phraya River Estuary, Thailand. *Mar. Pollut. Bull.* 2021, 173, 112933.
- (21) Choong W. S., Hadibarata T., Yuniarto A., Tang K. H. D., Abdullah F., Syafrudin M., Al Farraj D. A., Al-Mohaimed A. M. Characterization of microplastics in the water and sediment of Baram River estuary, Borneo Island. *Mar. Pollut. Bull.* 2021, 172, 112880.
- (22) Gupta P., Saha M., Rathore C., Suneel V., Ray D., Naik A., K U., M D., Daga K. Spatial and seasonal variation of microplastics and possible sources in the estuarine system from central west coast of India. *Environ. Pollut.* 2021, 288, 117665.

- (23) Roscher L., Fehres A., Reisel L., Halbach M., Scholz-Bottcher B., Gerriets M., Badewien T. H., Shiravani G., Wurpts A., Primpke S., Gerdts G. Microplastic pollution in the Weser estuary and the German North Sea. *Environ. Pollut.* 2021, 288, 117681.
- (24) Sucharitakul P., Pitt K. A., Welsh D. T. Assessment of microplastics in discharged treated wastewater and the utility of *Chrysaora pentastoma medusae* as bioindicators of microplastics. *Sci. Total Environ.* 2021, 790, 148076.
- (25) Chen L., Li J., Tang Y., Wang S., Lu X., Cheng Z., Zhang X., Wu P., Chang X., Xia Y. Typhoon-induced turbulence redistributed microplastics in coastal areas and reformed plastisphere community. *Water Res.* 2021, 204, 117580.
- (26) Lu I. C., Chao H. R., Mansor W. N., Peng C. W., Hsu Y. C., Yu T. Y., Chang W. H., Fu L. M. Levels of Phthalates, Bisphenol-A, Nonylphenol, and Microplastics in Fish in the Estuaries of Northern Taiwan and the Impact on Human Health. *Toxics.* 2021, 9 (10).
- (27) Ibrahim Y. S., Hamzah S. R., Khalik W., Ku Yusof K. M. K., Anuar S. T. Spatiotemporal microplastic occurrence study of Setiu Wetland, South China Sea. *Sci. Total Environ.* 2021, 788, 147809.
- (28) Bermudez M., Vilas C., Quintana R., Gonzalez-Fernandez D., Cozar A., Diez-Minguito M. Unravelling spatio-temporal patterns of suspended microplastic concentration in the Natura 2000 Guadalquivir estuary (SW Spain): Observations and model simulations. *Mar. Pollut. Bull.* 2021, 170, 112622.
- (29) Forero-Lopez A. D., Rimondino G. N., Truchet D. M., Colombo C. V., Buzzi N. S., Malanca F. E., Spetter C. V., Fernandez-Severini M. D. Occurrence, distribution, and characterization of suspended microplastics in a highly impacted estuarine wetland in Argentina. *Sci. Total Environ.* 2021, 785, 147141.
- (30) Liong R. M. Y., Hadibarata T., Yuniarto A., Tang K. H. D., Khamidun M. H. Microplastic Occurrence in the Water and Sediment of Miri River Estuary, Borneo Island. *Water, Air, Soil Pollut.* 2021, 232 (8).
- (31) Li Y., Liu S., Liu M., Huang W., Chen K., Ding Y., Wu F., Ke H., Lou L., Lin Y., Zhang M., Liu F., Wang C., Cai M. Mid-Level riverine outflow matters: A case of microplastic transport in the Jiulong River, China. *Front. Mar. Sci.* 2021, 8.

- (32) Cheng Y., Mai L., Lu X., Li Z., Guo Y., Chen D., Wang F. Occurrence and abundance of poly- and perfluoroalkyl substances (PFASs) on microplastics (MPs) in Pearl River Estuary (PRE) region: Spatial and temporal variations. *Environ. Pollut.* 2021, 281, 117025.
- (33) Jiwarungrueangkul T., Phaksopa J., Sompongchaiyakul P., Tipmanee D. Seasonal microplastic variations in estuarine sediments from urban canal on the west coast of Thailand: A case study in Phuket province. *Mar. Pollut. Bull.* 2021, 168, 112452.
- (34) Lins-Silva N., Marcolin C. R., Kessler F., Schwamborn R. A fresh look at microplastics and other particles in the tropical coastal ecosystems of Tamandare, Brazil. *Mar. Environ. Res.* 2021, 169, 105327.
- (35) Pazos R. S., Amalvy J., Cochero J., Pecile A., Gomez N. Temporal patterns in the abundance, type and composition of microplastics on the coast of the Rio de la Plata estuary. *Mar. Pollut. Bull.* 2021, 168, 112382.
- (36) Radhakrishnan K., Sivapriya V., Rajkumar A., Akramkhan N., Prakasheswar P., Krishnakumar S., Hussain S. M. Characterization and distribution of microplastics in estuarine surface sediments, Kayamkulam estuary, southwest coast of India. *Mar. Pollut. Bull.* 2021, 168, 112389.
- (37) Zheng S., Zhao Y., Liu T., Liang J., Zhu M., Sun X. Seasonal characteristics of microplastics ingested by copepods in Jiaozhou Bay, the Yellow Sea. *Sci. Total Environ.* 2021, 776, 145936.
- (38) Cabansag J. B. P., Olimberio R. B., Villanobos Z. M. T. Microplastics in some fish species and their environs in Eastern Visayas, Philippines. *Mar. Pollut. Bull.* 2021, 167, 112312.
- (39) Li S., Wang Y., Liu L., Lai H., Zeng X., Chen J., Liu C., Luo Q. Temporal and Spatial Distribution of Microplastics in a Coastal Region of the Pearl River Estuary, China. *Water.* 2021, 13 (12), 1618.
- (40) Wicaksono E. A., Werorilangi S., Galloway T. S., Tahir A. Distribution and Seasonal Variation of Microplastics in Tallo River, Makassar, Eastern Indonesia. *Toxics.* 2021, 9 (6).
- (41) Mai Y., Peng S., Lai Z., Wang X. Measurement, quantification, and potential risk of microplastics in the mainstream of the Pearl River (Xijiang River) and its estuary, Southern China. *Environ Sci Pollut Res Int.* 2021, 28 (38), 53127-53140.
- (42) Haddout S., Gimiliani G. T., Priya K. L., Hogueane A. M., Casila J. C. C., Ljubenkova I. Microplastics in Surface Waters and Sediments in the Sebou Estuary and Atlantic Coast, Morocco. *Anal. Lett.* 2021, 55 (2), 256-268.

- (43) Saha M., Naik A., Desai A., Nanajkar M., Rathore C., Kumar M., Gupta P. Microplastics in seafood as an emerging threat to marine environment: A case study in Goa, west coast of India. *Chemosphere*. 2021, 270, 129359.
- (44) Weitzel S. L., Feura J. M., Rush S. A., Iglay R. B., Woodrey M. S. Availability and assessment of microplastic ingestion by marsh birds in Mississippi Gulf Coast tidal marshes. *Mar. Pollut. Bull.* 2021, 166, 112187.
- (45) Diaz-Jaramillo M., Islas M. S., Gonzalez M. Spatial distribution patterns and identification of microplastics on intertidal sediments from urban and semi-natural SW Atlantic estuaries. *Environ. Pollut.* 2021, 273, 116398.
- (46) Li Y., Chen G., Xu K., Huang K., Wang J. Microplastics Environmental Effect and Risk Assessment on the Aquaculture Systems from South China. *Int J Environ Res Public Health*. 2021, 18 (4).
- (47) Carretero O., Gago J., Vinas L. From the coast to the shelf: Microplastics in Rias Baixas and Mino River shelf sediments (NW Spain). *Mar. Pollut. Bull.* 2021, 162, 111814.
- (48) Pan Z., Liu Q., Jiang R., Li W., Sun X., Lin H., Jiang S., Huang H. Microplastic pollution and ecological risk assessment in an estuarine environment: The Dongshan Bay of China. *Chemosphere*. 2021, 262, 127876.
- (49) Zhu J., Zhang Q., Huang Y., Jiang Y., Li J., Michal J. J., Jiang Z., Xu Y., Lan W. Long-term trends of microplastics in seawater and farmed oysters in the Maowei Sea, China. *Environ. Pollut.* 2021, 273, 116450.
- (50) Zaki M. R. M., Ying P. X., Zainuddin A. H., Razak M. R., Aris A. Z. Occurrence, abundance, and distribution of microplastics pollution: an evidence in surface tropical water of Klang River estuary, Malaysia. *Environ. Geochem. Health*. 2021, 43 (9), 3733-3748.
- (51) Forero Lopez A. D., Truchet D. M., Rimondino G. N., Maisano L., Spetter C. V., Buzzi N. S., Nazzarro M. S., Malanca F. E., Furlong O., Fernandez Severini M. D. Microplastics and suspended particles in a strongly impacted coastal environment: Composition, abundance, surface texture, and interaction with metal ions. *Sci. Total Environ.* 2021, 754, 142413.
- (52) Suteja Y., Atmadipoera A. S., Riani E., Nurjaya I. W., Nugroho D., Cordova M. R. Spatial and temporal distribution of microplastic in surface water of tropical estuary: Case study in Benoa Bay, Bali, Indonesia. *Mar. Pollut. Bull.* 2021, 163, 111979.

- (53) Rodrigues D., Antunes J., Otero V., Sobral P., Costa M. H. Distribution Patterns of Microplastics in Seawater Surface at a Portuguese Estuary and Marine Park. *Front. Environ. Sci.* 2020, 8.
- (54) Ta A. T., Babel S. Microplastics pollution with heavy metals in the aquaculture zone of the Chao Phraya River Estuary, Thailand. *Mar. Pollut. Bull.* 2020, 161 (Pt A), 111747.
- (55) Castillo C., Fernandez C., Gutierrez M. H., Aranda M., Urbina M. A., Yanez J., Alvarez A., Pantoja-Gutierrez S. Water column circulation drives microplastic distribution in the Martinez-Baker channels; A large fjord ecosystem in Chilean Patagonia. *Mar. Pollut. Bull.* 2020, 160, 111591.
- (56) Deng J., Guo P., Zhang X., Su H., Zhang Y., Wu Y., Li Y. Microplastics and accumulated heavy metals in restored mangrove wetland surface sediments at Jinjiang Estuary (Fujian, China). *Mar. Pollut. Bull.* 2020, 159, 111482.
- (57) Chen C. F., Ju Y. R., Lim Y. C., Hsu N. H., Lu K. T., Hsieh S. L., Dong C. D., Chen C. W. Microplastics and their affiliated PAHs in the sea surface connected to the southwest coast of Taiwan. *Chemosphere.* 2020, 254, 126818.
- (58) Ouyang W., Zhang Y., Wang L., Barcelo D., Wang Y., Lin C. Seasonal relevance of agricultural diffuse pollutant with microplastic in the bay. *J. Hazard. Mater.* 2020, 396, 122602.
- (59) Govender J., Naidoo T., Rajkaran A., Cebekhulu S., Bhugeloo A., Sershen S. Towards Characterising Microplastic Abundance, Typology and Retention in Mangrove-Dominated Estuaries. *Water.* 2020, 12 (10), 2802.
- (60) Zobkov M., Belkina N., Kovalevski V., Zobkova M., Efremova T., Galakhina N. Microplastic abundance and accumulation behavior in Lake Onego sediments: a journey from the river mouth to pelagic waters of the large boreal lake. *Journal of Environmental Chemical Engineering.* 2020, 8 (5), 104367.
- (61) Zuo L., Sun Y., Li H., Hu Y., Lin L., Peng J., Xu X. Microplastics in mangrove sediments of the Pearl River Estuary, South China: Correlation with halogenated flame retardants' levels. *Sci. Total Environ.* 2020, 725, 138344.
- (62) Chen B., Fan Y., Huang W., Rayhan A., Chen K., Cai M. Observation of microplastics in mariculture water of Longjiao Bay, southeast China: Influence by human activities. *Mar. Pollut. Bull.* 2020, 160, 111655.

- (63) Lam T. W. L., Fok L., Lin L., Xie Q., Li H. X., Xu X. R., Yeung L. C. Spatial variation of floatable plastic debris and microplastics in the Pearl River Estuary, South China. *Mar. Pollut. Bull.* 2020, 158, 111383.
- (64) Li R., Yu L., Chai M., Wu H., Zhu X. The distribution, characteristics and ecological risks of microplastics in the mangroves of Southern China. *Sci. Total Environ.* 2020, 708, 135025.
- (65) Bikker J., Lawson J., Wilson S., Rochman C. M. Microplastics and other anthropogenic particles in the surface waters of the Chesapeake Bay. *Mar. Pollut. Bull.* 2020, 156, 111257.
- (66) Fraser M. A., Chen L., Ashar M., Huang W., Zeng J., Zhang C., Zhang D. Occurrence and distribution of microplastics and polychlorinated biphenyls in sediments from the Qiantang River and Hangzhou Bay, China. *Ecotoxicol. Environ. Saf.* 2020, 196, 110536.
- (67) Díez-Minguito M., Bermúdez M., Gago J., Carretero O., Viñas L. Observations and idealized modelling of microplastic transport in estuaries: The exemplary case of an upwelling system (Ría de Vigo, NW Spain). *Mar. Chem.* 2020, 222, 103780.
- (68) Wang S., Zhang C., Pan Z., Sun D., Zhou A., Xie S., Wang J., Zou J. Microplastics in wild freshwater fish of different feeding habits from Beijiang and Pearl River Delta regions, south China. *Chemosphere.* 2020, 258, 127345.
- (69) Piehl S., Atwood E. C., Bochow M., Imhof H. K., Franke J., Siegert F., Laforsch C. Can Water Constituents Be Used as Proxy to Map Microplastic Dispersal Within Transitional and Coastal Waters? *Front. Environ. Sci.* 2020, 8.
- (70) Huang Y., Tian M., Jin F., Chen M., Liu Z., He S., Li F., Yang L., Fang C., Mu J. Coupled effects of urbanization level and dam on microplastics in surface waters in a coastal watershed of Southeast China. *Mar. Pollut. Bull.* 2020, 154, 111089.
- (71) Wu Y., Wang S., Wu L., Yang Y., Yu X., Liu Q., Liu X., Li Y., Wang X. Vertical distribution and river-sea transport of microplastics with tidal fluctuation in a subtropical estuary, China. *Sci. Total Environ.* 2022, 822, 153603.
- (72) Zhang L., Liu J., Xie Y., Zhong S., Yang B., Lu D., Zhong Q. Distribution of microplastics in surface water and sediments of Qin river in Beibu Gulf, China. *Sci. Total Environ.* 2020, 708, 135176.
- (73) Wu F., Pennings S. C., Tong C., Xu Y. Variation in microplastics composition at small spatial and temporal scales in a tidal flat of the Yangtze Estuary, China. *Sci. Total Environ.* 2020, 699, 134252.

- (74) Pariatamby A., Hamid F. S., Bhatti M. S., Anuar N., Anuar N. Status of Microplastic Pollution in Aquatic Ecosystem with a Case Study on Cherating River, Malaysia. *Journal of Engineering and Technological Sciences*. 2020, 52 (2), 222-241.
- (75) Suresh A., Vijayaraghavan G., K.S S., K.V N., B A., S B. N. Microplastics distribution and contamination from the Cochin coastal zone, India. *Reg. Stud. Mar. Sci.* 2020, 40, 101533.
- (76) Nakao S., Ozaki A., Yamazaki K., Masumoto K., Nakatani T., Sakiyama T. Microplastics contamination in tidelands of the Osaka Bay area in western Japan. *Water and Environment Journal*. 2019, 34 (3), 474-488.
- (77) Lorenzi L., Reginato B. C., Mayer D. G., Dantas D. V. Plastic floating debris along a summer-winter estuarine environmental gradient in a coastal lagoon: how does plastic debris arrive in a conservation unit? *Environ Sci Pollut Res Int.* 2020, 27 (8), 8797-8806.
- (78) Firdaus M., Trihadiningrum Y., Lestari P. Microplastic pollution in the sediment of Jagir Estuary, Surabaya City, Indonesia. *Mar. Pollut. Bull.* 2020, 150, 110790.
- (79) Li J., Huang W., Xu Y., Jin A., Zhang D., Zhang C. Microplastics in sediment cores as indicators of temporal trends in microplastic pollution in Andong salt marsh, Hangzhou Bay, China. *Reg. Stud. Mar. Sci.* 2020, 35, 101149.
- (80) Yao W., Di D., Wang Z., Liao Z., Huang H., Mei K., Dahlgren R. A., Zhang M., Shang X. Micro- and macroplastic accumulation in a newly formed *Spartina alterniflora* colonized estuarine saltmarsh in southeast China. *Mar. Pollut. Bull.* 2019, 149, 110636.
- (81) Payton T. G., Beckingham B. A., Dustan P. Microplastic exposure to zooplankton at tidal fronts in Charleston Harbor, SC USA. *Estuar. Coast. Shelf Sci.* 2020, 232, 106510.
- (82) Li Y., Lu Z., Zheng H., Wang J., Chen C. Microplastics in surface water and sediments of Chongming Island in the Yangtze Estuary, China. *Environmental Sciences Europe*. 2020, 32 (1).
- (83) Hien T. T., Nhon N. T. T., Thu V. T. M., Quyen D. T. T., Nguyen N. T. The Distribution of Microplastics in Beach Sand in Tien Giang Province and Vung Tau City, Vietnam. *Journal of Engineering and Technological Sciences*. 2020, 52 (2), 208-221.
- (84) Su L., Sharp S. M., Pettigrove V. J., Craig N. J., Nan B., Du F., Shi H. Superimposed microplastic pollution in a coastal metropolis. *Water Res.* 2020, 168, 115140.
- (85) Fernández Severini M. D., Villagran D. M., Buzzi N. S., Sartor G. C. Microplastics in oysters (*Crassostrea gigas*) and water at the Bahía Blanca Estuary (Southwestern Atlantic): An emerging issue of global concern. *Reg. Stud. Mar. Sci.* 2019, 32, 100829.

- (86) Enders K., Kappler A., Biniash O., Feldens P., Stollberg N., Lange X., Fischer D., Eichhorn K. J., Pollehne F., Oberbeckmann S., Labrenz M. Tracing microplastics in aquatic environments based on sediment analogies. *Sci. Rep.* 2019, 9 (1), 15207.
- (87) Simon-Sanchez L., Grelaud M., Garcia-Orellana J., Ziveri P. River Deltas as hotspots of microplastic accumulation: The case study of the Ebro River (NW Mediterranean). *Sci. Total Environ.* 2019, 687, 1186-1196.
- (88) McEachern K., Alegria H., Kalagher A. L., Hansen C., Morrison S., Hastings D. Microplastics in Tampa Bay, Florida: Abundance and variability in estuarine waters and sediments. *Mar. Pollut. Bull.* 2019, 148, 97-106.
- (89) Hitchcock J. N., Mitrovic S. M. Microplastic pollution in estuaries across a gradient of human impact. *Environ. Pollut.* 2019, 247, 457-466.
- (90) Zhao S., Wang T., Zhu L., Xu P., Wang X., Gao L., Li D. Analysis of suspended microplastics in the Changjiang Estuary: Implications for riverine plastic load to the ocean. *Water Res.* 2019, 161, 560-569.
- (91) Masia P., Ardura A., Garcia-Vazquez E. Microplastics in special protected areas for migratory birds in the Bay of Biscay. *Mar. Pollut. Bull.* 2019, 146, 993-1001.
- (92) Alves V. E. N., Figueiredo G. M. Microplastic in the sediments of a highly eutrophic tropical estuary. *Mar. Pollut. Bull.* 2019, 146, 326-335.
- (93) Zhang J., Zhang C., Deng Y., Wang R., Ma E., Wang J., Bai J., Wu J., Zhou Y. Microplastics in the surface water of small-scale estuaries in Shanghai. *Mar. Pollut. Bull.* 2019, 149, 110569.
- (94) Wu N., Zhang Y., Zhang X., Zhao Z., He J., Li W., Ma Y., Niu Z. Occurrence and distribution of microplastics in the surface water and sediment of two typical estuaries in Bohai Bay, China. *Environ Sci Process Impacts.* 2019, 21 (7), 1143-1152.
- (95) Rodrigues S. M., Almeida C. M. R., Silva D., Cunha J., Antunes C., Freitas V., Ramos S. Microplastic contamination in an urban estuary: Abundance and distribution of microplastics and fish larvae in the Douro estuary. *Sci. Total Environ.* 2019, 659, 1071-1081.
- (96) Zhu J., Zhang Q., Li Y., Tan S., Kang Z., Yu X., Lan W., Cai L., Wang J., Shi H. Microplastic pollution in the Maowei Sea, a typical mariculture bay of China. *Sci. Total Environ.* 2019, 658, 62-68.

- (97) Leads R. R., Weinstein J. E. Occurrence of tire wear particles and other microplastics within the tributaries of the Charleston Harbor Estuary, South Carolina, USA. *Mar. Pollut. Bull.* 2019, 145, 569-582.
- (98) Baptista Neto J. A., Gaylarde C., Beech I., Bastos A. C., da Silva Quaresma V., de Carvalho D. G. Microplastics and attached microorganisms in sediments of the Vitória bay estuarine system in SE Brazil. *Ocean Coast. Manage.* 2019, 169, 247-253.
- (99) Wiggin K. J., Holland E. B. Validation and application of cost and time effective methods for the detection of 3-500µm sized microplastics in the urban marine and estuarine environments surrounding Long Beach, California. *Mar. Pollut. Bull.* 2019, 143, 152-162.
- (100) Blaskovic A., Guerranti C., Fastelli P., Anselmi S., Renzi M. Plastic levels in sediments closed to Cecina river estuary (Tuscany, Italy). *Mar. Pollut. Bull.* 2018, 135, 105-109.
- (101) Li R., Zhang L., Xue B., Wang Y. Abundance and characteristics of microplastics in the mangrove sediment of the semi-enclosed Maowei Sea of the south China sea: New implications for location, rhizosphere, and sediment compositions. *Environ. Pollut.* 2019, 244, 685-692.
- (102) Luo W., Su L., Craig N. J., Du F., Wu C., Shi H. Comparison of microplastic pollution in different water bodies from urban creeks to coastal waters. *Environ. Pollut.* 2019, 246, 174-182.
- (103) Tang G., Liu M., Zhou Q., He H., Chen K., Zhang H., Hu J., Huang Q., Luo Y., Ke H., Chen B., Xu X., Cai M. Microplastics and polycyclic aromatic hydrocarbons (PAHs) in Xiamen coastal areas: Implications for anthropogenic impacts. *Sci. Total Environ.* 2018, 634, 811-820.
- (104) Yan M., Nie H., Xu K., He Y., Hu Y., Huang Y., Wang J. Microplastic abundance, distribution and composition in the Pearl River along Guangzhou city and Pearl River estuary, China. *Chemosphere.* 2019, 217, 879-886.
- (105) Lahens L., Strady E., Kieu-Le T. C., Dris R., Boukerma K., Rinnert E., Gasperi J., Tassin B. Macroplastic and microplastic contamination assessment of a tropical river (Saigon River, Vietnam) transversed by a developing megacity. *Environ. Pollut.* 2018, 236, 661-671.
- (106) Alligant S., Gasperi J., Gangnery A., Maheux F., Simon B., Halm-Lemille M.-P., El Rakwe M., Dreanno C., Cachot J., Tassin B. Microplastic Contamination of Sediment and Water Column in the Seine River Estuary. 2020, 4-9.
- (107) Willis K. A., Eriksen R., Wilcox C., Hardesty B. D. Microplastic distribution at different sediment depths in an urban estuary. *Front. Mar. Sci.* 2017, 4, 419.

- (108) Cheung P. K., Fok L., Hung P. L., Cheung L. T. O. Spatio-temporal comparison of neustonic microplastic density in Hong Kong waters under the influence of the Pearl River Estuary. *Sci. Total Environ.* 2018, 628-629, 731-739.
- (109) Liu Z., Huang Q., Wang H., Zhang S. An enhanced risk assessment framework for microplastics occurring in the Westerscheldt estuary. *Sci. Total Environ.* 2022, 817, 153006.
- (110) Pazos R. S., Bauer D. E., Gomez N. Microplastics integrating the coastal planktonic community in the inner zone of the Rio de la Plata estuary (South America). *Environ. Pollut.* 2018, 243, 134-142.
- (111) Garcia T. M., Campos C. C., Mota E. M. T., Santos N. M. O., Campelo R. P. S., Prado L. C. G., Melo Junior M., Soares M. O. Microplastics in subsurface waters of the western equatorial Atlantic (Brazil). *Mar. Pollut. Bull.* 2020, 150, 110705.
- (112) Zheng Y., Li J., Cao W., Liu X., Jiang F., Ding J., Yin X., Sun C. Distribution characteristics of microplastics in the seawater and sediment: A case study in Jiaozhou Bay, China. *Sci. Total Environ.* 2019, 674, 27-35.
- (113) Zhdanov I., Lokhov A., Belesov A., Kozhevnikov A., Pakhomova S., Berezina A., Frolova N., Kotova E., Leshchev A., Wang X., Zavialov P., Yakushev E. Assessment of seasonal variability of input of microplastics from the Northern Dvina River to the Arctic Ocean. *Mar. Pollut. Bull.* 2022, 175, 113370.
- (114) Han M., Niu X., Tang M., Zhang B. T., Wang G., Yue W., Kong X., Zhu J. Distribution of microplastics in surface water of the lower Yellow River near estuary. *Sci. Total Environ.* 2020, 707, 135601.
- (115) Fan Y., Zheng K., Zhu Z., Chen G., Peng X. Distribution, sedimentary record, and persistence of microplastics in the Pearl River catchment, China. *Environ. Pollut.* 2019, 251, 862-870.
- (116) Stolte A., Forster S., Gerdts G., Schubert H. Microplastic concentrations in beach sediments along the German Baltic coast. *Mar. Pollut. Bull.* 2015, 99 (1-2), 216-29.
- (117) Cohen J. H., Internicola A. M., Mason R. A., Kukulka T. Observations and simulations of microplastic debris in a tide, wind, and freshwater-driven estuarine environment: the Delaware Bay. *Environ. Sci. Technol.* 2019, 53 (24), 14204-14211.

- (118) Zhao S., Zhu L., Wang T., Li D. Suspended microplastics in the surface water of the Yangtze Estuary System, China: First observations on occurrence, distribution. *Mar. Pollut. Bull.* 2014, 86 (1), 562-568.
- (119) Anderson Z. T., Cundy A. B., Croudace I. W., Warwick P. E., Celis-Hernandez O., Stead J. L. A rapid method for assessing the accumulation of microplastics in the sea surface microlayer (SML) of estuarine systems. *Sci. Rep.* 2018, 8 (1), 9428.
- (120) He D., Chen X., Zhao W., Zhu Z., Qi X., Zhou L., Chen W., Wan C., Li D., Zou X., Wu N. Microplastics contamination in the surface water of the Yangtze River from upstream to estuary based on different sampling methods. *Environ. Res.* 2021, 196, 110908.
- (121) Kang J. H., Kwon O. Y., Lee K. W., Song Y. K., Shim W. J. Marine neustonic microplastics around the southeastern coast of Korea. *Mar. Pollut. Bull.* 2015, 96 (1-2), 304-12.
- (122) Constant M., Kerherve P., Mino-Vercellio-Verollet M., Dumontier M., Sanchez Vidal A., Canals M., Heussner S. Beached microplastics in the Northwestern Mediterranean Sea. *Mar. Pollut. Bull.* 2019, 142, 263-273.
- (123) Campanale C., Stock F., Massarelli C., Kochleus C., Bagnuolo G., Reifferscheid G., Uricchio V. F. Microplastics and their possible sources: The example of Ofanto river in southeast Italy. *Environ. Pollut.* 2020, 258, 113284.
- (124) Constant M., Ludwig W., Kerherve P., Sola J., Charriere B., Sanchez-Vidal A., Canals M., Heussner S. Microplastic fluxes in a large and a small Mediterranean river catchments: The Tet and the Rhone, Northwestern Mediterranean Sea. *Sci. Total Environ.* 2020, 716, 136984.
- (125) Sukhsangchan R., Keawsang R., Worachananant S., Thamrongnawasawat T., Phaksopa J. Suspended microplastics during a tidal cycle in sea-surface waters around Chao Phraya River mouth, Thailand. *Sci. Asia.* 2020, 46 (6), 724.
- (126) Viet Dung L., Huu Duc T., Thi Khanh Linh L., Thi Dieu Ly T., Anh Duong H., Thi My Hao N. Depth profiles of microplastics in sediment cores from two mangrove forests in northern Vietnam. *J. Mar. Sci. Eng.* 2021, 9 (12), 1381.
- (127) Zhu X., Munno K., Grbic J., Werbowski L. M., Bikker J., Ho A., Guo E., Sedlak M., Sutton R., Box C., Lin D., Gilbreath A., Holleman R. C., Fortin M.-J., Rochman C. Holistic assessment of microplastics and other anthropogenic microdebris in an urban bay sheds light on their sources and fate. *ACS ES&T Water.* 2021, 1 (6), 1401-1410.

- (128) Prarat P., Hongswat P. Microplastic pollution in surface seawater and beach sand from the shore of Rayong province, Thailand: Distribution, characterization, and ecological risk assessment. *Mar. Pollut. Bull.* 2022, 174, 113200.
- (129) Nithin A., Sundaramanickam A., Sathish M. Seasonal distribution of microplastics in the surface water and sediments of the Vellar estuary, Parangipettai, southeast coast of India. *Mar. Pollut. Bull.* 2022, 174, 113248.
- (130) Liu S., Chen H., Wang J., Su L., Wang X., Zhu J., Lan W. The distribution of microplastics in water, sediment, and fish of the Dafeng River, a remote river in China. *Ecotoxicol. Environ. Saf.* 2021, 228, 113009.
- (131) Sá B., Pais J., Antunes J., Pequeno J., Pires A., Sobral P. Seasonal Abundance and Distribution Patterns of Microplastics in the Lis River, Portugal. *Sustainability.* 2022, 14 (4), 2255.
- (132) Chen F., Lao Q., Liu M., Huang P., Chen B., Zhou X., Chen P., Chen K., Song Z., Cai M. Impact of intensive mariculture activities on microplastic pollution in a typical semi-enclosed bay: Zhanjiang Bay. *Mar. Pollut. Bull.* 2022, 176, 113402.
- (133) Banik P., Hossain M. B., Nur A.-A. U., Choudhury T. R., Liba S. I., Yu J., Noman M. A., Sun J. Microplastics in Sediment of Kuakata Beach, Bangladesh: Occurrence, Spatial Distribution, and Risk Assessment. *Front. Mar. Sci.* 2022, 9.
- (134) Rakib M. R. J., Hossain M. B., Kumar R., Ullah M. A., Al Nahian S., Rima N. N., Choudhury T. R., Liba S. I., Yu J., Khandaker M. U., Sulieman A., Sayed M. M. Spatial distribution and risk assessments due to the microplastics pollution in sediments of Karnaphuli River Estuary, Bangladesh. *Sci. Rep.* 2022, 12 (1), 8581.
- (135) Sanchez-Hernandez L. J., Ramirez-Romero P., Rodriguez-Gonzalez F., Ramos-Sanchez V. H., Marquez Montes R. A., Romero-Paredes Rubio H., Sujitha S. B., Jonathan M. P. Seasonal evidences of microplastics in environmental matrices of a tourist dominated urban estuary in Gulf of Mexico, Mexico. *Chemosphere.* 2021, 277, 130261.